OCS Study
BOEM 2020-039

Radar Interference Analysis for Renewable Energy Facilities on the Atlantic Outer Continental Shelf

US Department of the Interior
Bureau of Ocean Energy Management
Office of Renewable Energy Programs

BOEM
Bureau of Ocean Energy Management

OCS Study
BOEM 2020-039

Radar Interference Analysis for Renewable Energy Facilities on the Atlantic Outer Continental Shelf

August 2020

Authors
Russell J. Colburn
Christian A. Randolph
Chelsea Drummond
Michael W. Miles
Frank C. Brody
Christian D. McGillen
Andrew S. Krieger
Rachel E. Jankowski

Prepared the Department of the Interior,
Bureau of Ocean Energy Management
under BPA No. 140M0118A0002.
Call Order 140M0119F0015
By

Booz Allen Hamilton
8283 Greensboro Drive
McLean, VA 22102

US Department of the Interior
Bureau of Ocean Energy Management
Office of Renewable Energy Programs

BOEM
Bureau of Ocean Energy Management

DISCLAIMER

Study concept, oversight, and funding were provided by the US Department of the Interior, Bureau of Ocean Energy Management (BOEM), Environmental Studies Program, Washington, DC, under Contract Number 14M0119C0004. This report has been technically reviewed by BOEM, and it has been approved for publication. The views and conclusions contained in this document are those of the authors and should not be interpreted as representing the opinions or policies of the US Government, nor does mention of trade names or commercial products constitute endorsement or recommendation for use.

REPORT AVAILABILITY

To download a PDF file of this report, go to the US Department of the Interior, Bureau of Ocean Energy Management Data and Information Systems webpage (http://www.boem.gov/Environmental-Studies-EnvData/), click on the link for the Environmental Studies Program Information System (ESPIS), and search on 2020-039. The report is also available at the National Technical Reports Library at https://ntrl.ntis.gov/NTRL/.

CITATION

Colburn R., Randolph C., Drummond C., Miles M., Brody F., McGillen C., Krieger A., Jankowski R., Aug. 2020. Radar interference analysis for renewable energy facilities on the Atlantic outer continental shelf.. McLean, VA: US Department of the Interior, Bureau of Ocean Energy Management. OCS Study BOEM 2020-039. 189 p.

OCS Study
BOEM 2020-039

Final Report

Radar Interference Analysis for Renewable Energy Facilities on the Atlantic Outer Continental Shelf

Authors

Russell J. Colburn
Christian A. Randolph
Chelsea Drummond
Michael W. Miles
Frank C. Brody
Christian D. McGillen
Andrew S. Krieger
Rachel E. Jankowski

Prepared the Department of the Interior,
Bureau of Ocean Energy Management
under BPA No. 140M0118A0002.
Call Order 140M0119F0015
By

Booz Allen Hamilton
8283 Greensboro Drive
McLean, VA 22102

U.S. Department of the Interior
Bureau of Ocean Energy Management
Office of Renewable Energy Programs
August 2020

BOEM
Bureau of Ocean Energy Management

CONTENTS

LIST OF ABBREVIATIONS AND ACRONYMS

ACK	Radar code for Nantucket, MA
ACY	Radar code for Atlantic City, NJ
ADS-B	Automatic Dependent Surveillance Broadcast
AFB	Air Force Base
AGU	American Geophysical Union
AMDAR	Aircraft Meteorological Data Relay
ARSR	Air Route Surveillance Radar
ASC	Action Script Communication
ASR	Airport Surveillance Radar
BOS	Radar code for Boston, MA
BOEM	Bureau of Ocean Energy Management
C&I	Correlation and Interpolation
CFAR	Constant False Alarm Rate
CHH	Radar code for Chatham, MA
CHS	Radar code for Charleston, SC
CODAR	Coastal Ocean Dynamics Applications Radar
CNS/ATM	Communications, Navigation, Surveillance/Air Traffic Management
COP	Construction and Operations Plan
CPI	Coherent Processing Interval
DoD	Department of Defense
DOI	Department of the Interior
EIS	Environmental Impact Statement
EM	Electromagnetic
ES	Executive Summary
ESRI	Environmental Systems Research Institute
EWIR	Electronic Warfare Integrated Reprogramming
FAA	Federal Aviation Administration
FEKO	**FE**ldberechnung für **K**örper mit beliebiger **O**berfläche
FFT	Fast Fourier Transform
FM/CW	Frequency-Modulated Continuous Wave
FMH	Radar code for Falmouth, MA
FOL	First Order Line
GIB	Radar code for Gibbsboro, NJ
GIS	Geographic Information System
GPS	Global Positioning System
GRIB	Gridded Binary
HF	High Frequency
HRRR	High-Resolution Rapid Refresh
IEEE	Institute of Electrical and Electronics Engineers
IET	Institute of Engineering and Technology
IFF	"Identification, Friend or Foe"
JGR	Journal of Geophysical Research
KBOX	Radar code for Boston, MA
KDIX	Radar code for Mt. Holly, NJ
KDOX	Radar code for Dover, DE
KEWR	Radar code for Newark, NJ
KISP	Radar code for Islip, NY
KJFK	Radar code for Jasper, NY
KOKX	Radar code for Upton, NY

KPHL	Radar code for Philadelphia, PA
KPVD	Radar code for Warwick, RI
LFM	Linear Frequency Modulation
LIDAR	Light Detection and Ranging
LOS	Line of Sight
MF	Medium Frequency
MHX	Radar code for Morehead City, NC
MTD	Moving Target Detector
MTI	Moving Target Indicator
MUSIC	Multiple Signal Classification
MW	Megawatt
NEPA	National Environmental Policy Act
NEXRAD	Next Generation Weather Radar
NLFM	Non-Linear Frequency Modulation
NM	Nautical Mile
NOAA	National Oceanic and Atmospheric Administration
NWS	National Weather Service
OCS	Outer Continental Shelf
OEM	Original Equipment Manufacturer
OTH	Over-the-Horizon
PAT	Plot Amplitude Thresholding
PCR	Pulse Compression Ratio
PD	Pulsed Doppler
PRF	Pulse Repetition Frequency
PRI	Pulse Repetition Intervals
QVH	Radar code for Riverhead, NY
RAG	Range Azimuth Gating
RCS	Radar Cross Section
RI/MA	Massachusetts/ Rhode Island Cumulative Scenario
RPM	Rotations Per Minute
SF	South Fork
SIUL	Self-Initiated Upward Lightning
SME	Subject Matter Expert
SNR	Signal-to-Noise Ratio
STC	Sensitivity Time Control
SRTM-2	Shuttle Radar Topography Mission-Level 2
TDWR	Terminal Doppler Weather Radar
TRL	Technology Readiness Level
UTC	Coordinated Universal Time
VCP	Volume Coverage Programs
VHF	Very High Frequency
VWP	VAD Wind Profile
WFO	Weather Forecast Office
WGS	World Geodetic System
WSR	Weather Surveillance Radar
WTCI	Wind Turbine Clutter/Interference
WTRIM	Wind Turbine Radar Interference Mitigation
YQI	Radar code for Yarmouth, ME

EXECUTIVE SUMMARY

Introduction

The Bureau of Ocean Energy Management (BOEM) with the U.S. Department of the Interior (DOI) is responsible for leasing portions of the Outer Continental Shelf (OCS) for renewable energy development, including offshore wind energy installations. As the lead agency for renewable energy leasing on the OCS, BOEM is also responsible for studying the potential impacts of offshore wind energy leasing, including socioeconomic impacts to other OCS users under the National Environmental Policy Act (NEPA). The presence of wind energy installations is known to impact radar systems as wind turbines consist of large metal structures that can generate a return signal to radars. Radar signals generated by objects other than the intended targets (e.g., the ground, artificial structures, wind turbines), are referred to as "clutter" or "interference," and represent a potential impact to be investigated under NEPA.

In April of 2019, BOEM engaged Booz Allen Hamilton (Booz Allen) through Call Order 140M0119F0015 to study how proposed and hypothetical future offshore wind energy installations on the Atlantic coast may impact land-based radar systems, potential mitigations for these impacts, and how an atmospheric phenomenon, known as "ducting," influences these impacts. The scope of work for this study consisted of five tasks:

- **Task 1, Project Management** – project scheduling and planning, including a Post-Award Meeting to discuss approach and methodologies with BOEM.
- **Task 2 and Task 3, Line of Sight (LOS) and Interference Analysis** – computer modeling of radar systems potentially impacted by planned and hypothetical wind farms including the severity of interference impacts.
- **Task 4, Mitigation Techniques** – discussion and analysis of potential options for mitigating radar interference from offshore wind farms.
- **Task 5, Ducting Analysis** – discussion and analysis of the likelihood of ducting events around the planned and hypothetical wind farms.

Study Scope

To define the study scope, the research team determined which wind farm scenarios, as well as which radar types would be investigated.

Wind Farm Scenarios

BOEM tasked Booz Allen with investigating radar interference impacts on nine total wind farms, seven of which were in planning stages, and two of which were based on hypothetical future scenarios developed by BOEM and Booz Allen. The planned and hypothetical wind farms were in various planning stages and ranged along the U.S. Atlantic coast from Massachusetts to South Carolina (Table ES-1).

Table ES-1. Wind Farms Investigated

Wind Farm	Location	Planning Phase	Turbine Quantity	Turbine Size (Megawatts)
Vineyard Wind	Rhode Island/Massachusetts	Construction and Operations Plan (COP) under BOEM review	106	10 MW
Bay State Wind	Rhode Island/Massachusetts	COP under BOEM review	110	15 MW
South Fork	Rhode Island/Massachusetts	COP under BOEM review	15	12 MW

Wind Farm	Location	Planning Phase	Turbine Quantity	Turbine Size (Megawatts)
Mayflower	Rhode Island/Massachusetts	Pre-COP planning	67	15 MW
RI/MA Cumulative Scenario	Rhode Island/Massachusetts	Hypothetical future scenario	1,115	10-15 MW
Empire Wind	New York	COP under BOEM review	135	18 MW
Ocean Wind	New Jersey	COP under BOEM review	138	8 MW
Skipjack	Delaware	COP under BOEM review	16	12 MW
Grand Strand	South Carolina	Hypothetical future scenario	112	15 MW

Figure ES-1 shows a map of the study area for this project, including the lease or call areas of all nine planned and hypothetical future wind farms. The Cumulative Rhode Island/Massachusetts (RI/MA) Scenario is a hypothetical future scenario that includes the actual planned layouts for Bay State, Vineyard Wind, South Fork, and Mayflower, as well as hypothetical turbines that occupy all the remaining lease areas in the RI/MA area. The RI/MA Cumulative Scenario was not developed to be a realistic future scenario, rather, it was designed as a "maximum built-out" case to compare to more realistic scenarios, such as those planned in COPs.

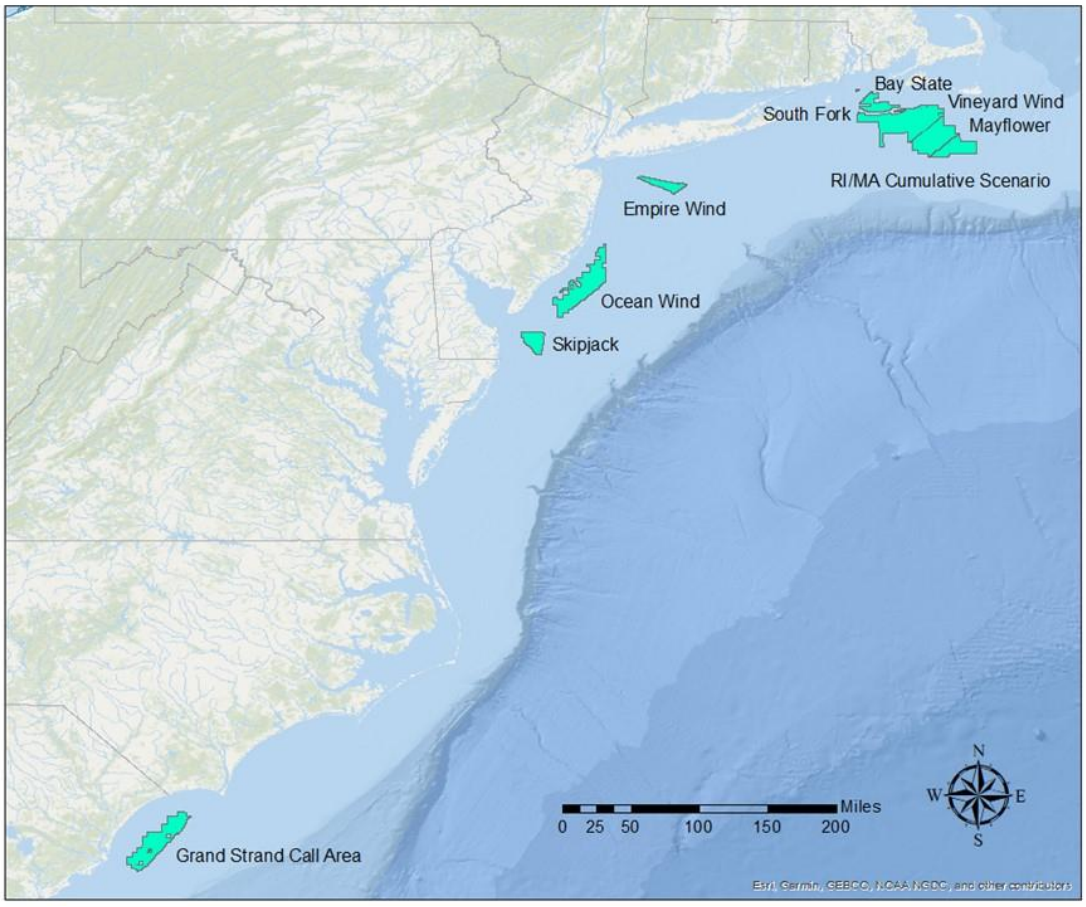

Figure ES-1. Map of Proposed and Hypothetical Wind Farm Locations

Radar Types

The research team used a radar simulation tool, WindTRx, to conduct LOS and interference analysis on the nine wind farms for four major radar types. The research team first identified which individual radar systems were within LOS of each wind farm, then analyzed severity of interference. The four major radar types investigated were:

- **Airport Surveillance Radars (ASR)** – The ASR-8 and ASR-9 series of radars are used as the primary air traffic control system for the airspace surrounding airports.
- **Air Route Surveillance Radars (ARSR) –** The ARSR-4 is a long range, L-band radar used by the Federal Aviation Administration (FAA) and Department of Defense (DoD) to monitor airspace on and around the U.S. border.
- **NEXt-generation RADars (NEXRAD) –** S-band pulse-Doppler weather surveillance radar used to support the weather assessment, forecast, and warning missions of the National Weather Service (NWS), the FAA, and the DoD.
- **SeaSonde Radars –** High frequency (HF) radar systems used to measure coastal ocean currents that can work individually or in a network with nearby systems. These radar systems are unique to the coastal environment and generally not a concern for onshore wind farms.

Key Findings

Radar Interference

The research team found that the proposed and hypothetical wind farms are within LOS of 36 radar systems, indicating that they will generate interference to these radars under normal atmospheric conditions (Table ES-2). The radar type with the most radars affected was the SeaSonde, which reflects the large number of SeaSondes along the Atlantic coast. The research team also qualitatively ranked the severity of impacts caused by each wind farm. Skipjack, South Fork, and Grand Strand were found to have low radar impacts (color coded green in the table below). Mayflower, Vineyard Wind, Bay State Wind, and Ocean Wind were found to have moderate impacts (color coded yellow), and Empire Wind was found to have higher impacts (color coded red). These qualitative scores were based both on number of radar systems impacted and severity of impact to individual systems. The RI/MA Cumulative Scenario would have higher impacts than Empire Wind, however it was not color coded because it was developed as a test case for comparison, rather than a realistic scenario like the other wind farms.

Table ES-2. Radar Systems within LOS of Modeled Wind Farms

	Number of Radar Systems within LOS				
Wind Farm	**ARSR-4**	**ASR-8/9**	**NEXRAD**	**SeaSonde**	**Totals**
Skipjack	0	1	1	5	**7**
South Fork	0	1	0	8	**9**
Grand Strand	0	0	0	2	**2**
Mayflower	0	2	0	6	**8**
Vineyard Wind	0	2	0	6	**8**
Bay State Wind	0	3	0	7	**10**
Ocean Wind	1	1	0	9	**11**
Empire Wind	1	2	2	8	**13**
RI/MA Cumulative	0	3	0	10	**13**

Wind Farm	Number of Radar Systems within LOS				
	ARSR-4	ASR-8/9	NEXRAD	SeaSonde	Totals
Total Systems Affected*	**2**	**6**	**3**	**25**	**36**

*Total radars affected per radar type may not equal the sum of each column because a single radar can be within LOS of multiple wind farms.

Mitigation Techniques

The research team used a combination of literature review and expert interviews to inform analysis of mitigation techniques available for radar interference caused by offshore wind energy installations. One unique area of concern for offshore wind energy installations is the presence of SeaSonde ocean monitoring radars, which do not operate in the terrestrial environment. Experts were interviewed from the following organizations regarding a variety of radar types:

- Wind Turbine Radar Interference Mitigation (WTRIM) Working Group/DoD
- National Weather Service (NWS)
- National Oceanic and Atmospheric Administration (NOAA)/Rutgers University
- University of Oklahoma

Mitigation techniques available for offshore wind turbines are largely informed by research and lessons learned from onshore radar interference mitigation. Table ES-3 shows a summary of major mitigation options available for the four major radar types investigated in this study.

Table ES-3. Overview of Mitigation techniques

Radar Type	Operational Mitigation	Modification Mitigation
ASR-8/9 and ARSR-4	• Passive aircraft tracking using ADS-B or signal/transponder • Increasing aircraft altitude near radar • Sensitivity time control (range-dependent attenuation) • Range azimuth gating (ability to isolate/ignore signals from specific range-angle gates) • Track initiation inhibit, velocity editing, plot amplitude thresholding (limiting the amplitude of certain signals)	• Utilizing the dual beams of the radar simultaneously • In-fill radars
NEXRAD	• Wind farm curtailment/curtailment agreement	• Potential update of radar system (long term, 20+ years away)
SeaSonde	• Data sharing from turbine operators • Wind farm curtailment/curtailment agreement	• Signal processing enhancements • Antenna modifications

Ducting Analysis

Ducting is an atmospheric phenomenon that alters how electromagnetic (EM) waves propagate through the atmosphere. Ducting events occur in the lower atmosphere and are driven by steep vertical changes in air density due to differing temperatures and moisture content with height. The density differences are typically due to strong vertical temperature inversions and/or steep vertical moisture discontinuities, especially in the lower 7,000 feet of the atmosphere. Ducting events create a refractive path that traps EM waves near the surface and causes them to propagate well beyond their intended range. An impact of ducting is that a wind turbine may be observed by a radar, when otherwise it would not, potentially causing interference with the signal (Figure ES-2)

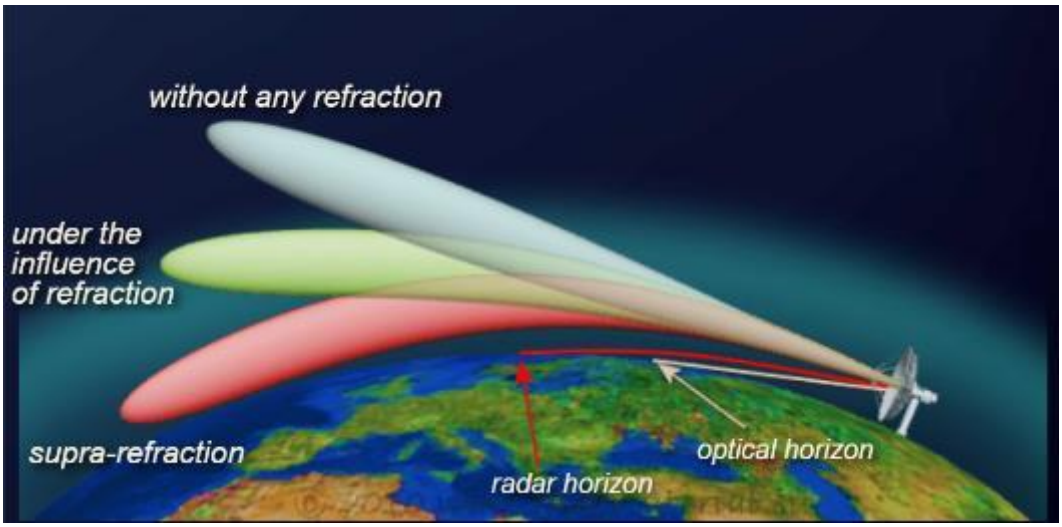

Figure ES-2 - Effects of types of refraction on radar waves

Atmospheric Vertical Profile Analyses

The primary goals of this task were to assess meteorological conditions conducive to ducting and describe probable frequency of occurrence of ducting based on these factors. A key component of understanding and assessing ducting is the vertical profile of temperature and moisture above a site or region. Meteorological sensors providing vertical profiles of the atmosphere are not available at the proposed wind farm sites. Thus, atmospheric computer model reanalysis served as a viable proxy for meteorological conditions over the proposed offshore wind farm locations. The NWS High Resolution Rapid Refresh (HRRR) model was selected for this effort. A comparison of HRRR and radiosonde data at Yarmouth, ME (YQI), Chatham, MA (CHH), Morehead City, NC (MHX) and Charleston, SC (CHS) revealed that the HRRR model provided a reliable representation of the atmosphere at the offshore wind farm locations on a monthly and seasonal basis.

Contributing Conditions

Conditions contributing to temperature inversions and thus potential ducting are listed in Table ES-4.

Table ES-4 - Meteorological Conditions Contributing to Inversions and Potential Ducting

Contributing Meteorological Condition	Seasonal Variations	Diurnal Variations
Radiational cooling	Year-round	Peaks during late night through mid-morning
Sea breeze circulations	Primarily warm season (May – Sept)	Peaks during daytime when cooler sea breeze pushes inland underneath warmer air aloft
Low-level jets	Year Round but primarily cool season (Oct – Apr)	Anytime – minor peak overnight and early morning
Subsiding/Sinking Air	Year-round	Anytime
Frontal Movement	Year-round	Anytime

Ducting Frequency

Based on assessments using HRRR atmospheric model data at the proposed wind farm sites, meteorological conditions conducive to pronounced temperature and moisture inversions - and thus potential ducting - occur 10% to 30% of the time, on average through the year. Results obtained via a literature review and from a limited qualitative analysis of coastal radiosonde data near the proposed wind farm sites showed slightly different frequencies of potential ducting. Potential ducting conditions vary on a day-to-day basis due to meteorological factors and vary seasonally due to climatological factors.

Conclusions and Recommendations

1. **Several Radar Impacts:** Proposed and hypothetical future wind farms are within LOS of several radar systems of various types along the Atlantic coast, meaning that radar interference should be of a concern for wind farm development.
2. **Unique SeaSonde Issues:** SeaSonde radars present a unique challenge for offshore wind installations because the radar systems are unique to the coastal environment and large numbers of them exist on the Atlantic coastline. SeaSondes appear to be the most heavily-impacted radar due to their prevalence; however, there may be a relatively inexpensive mitigation option available for SeaSondes that involves a software upgrade.
3. **Wind Farm Developer/Radar Operator Cooperation:** Mitigation techniques available for offshore wind farms mirror those available for onshore wind farms, with the exclusion of SeaSonde radars. Mitigation techniques available include a combination of operational mitigations and radar system modifications and upgrades. Mitigation techniques potentially involve the wind farm developers and operators and actions they could be required to take including coordination in the planning stages of wind farm development.
1. **Frequency of Ducting:** Atmospheric ducting is not unique to the coastal environment. However, some atmospheric conditions, such as the presence of moisture over the ocean and inversion layers, make ducting more common in coastal environments than onshore. Atmospheric conditions that lead to ducting occur along the U.S. Atlantic coast approximately 10-30% of the time with both seasonal day-to-day variations due to meteorological factors. As such, radars that are not in LOS of offshore windfarms under normal atmospheric conditions can become impacted during ducting conditions.
4. **BOEM COP Review:** As BOEM reviews wind farm COPs, they should consider conducting LOS analysis on nearby radar systems to determine whether major radar systems may be impacted by the proposed wind farm. Due to the common occurrence of ducting conditions, specifying the exact layouts or turbine sizes that would narrowly avoid LOS of radar systems under normal atmospheric conditions will not always result in the turbines avoiding detection in the offshore environment.
5. **Curtailment Agreements:** BOEM should consider establishing curtailment agreements among offshore wind farms and radar operators. These curtailment agreements would include specific conditions under which wind farm operations might be curtailed to allow for unimpeded radar operations. These agreements would be informed by site-specific LOS and interference analyses. Additionally, for those developments where radars are expected to be impacted, BOEM should consider drafting agreements with wind farm developers and operators to:
    a. Share real-time data-sharing for radar signal processing modifications
    b. Require In-fill radar placements where impact is significant

1 INTRODUCTION

The Bureau of Ocean Energy Management (BOEM) within the U.S. Department of the Interior (DOI), is responsible for managing all energy and mineral resources on the Federal Outer Continental Shelf (OCS). This jurisdiction includes conducting OCS lease sales as well as monitoring and mitigating environmental impacts associated with resource development. In 2005, the Energy Policy Act (EPAct) amended Section 388 of the Outer Continental Shelf Lands Act, giving the Secretary of the Interior discretionary authority to issue leases, easements, or rights-of-way for renewable energy projects on the OCS. Under this authority, BOEM issues leases on the OCS for potential renewable energy projects including wind energy.

Offshore wind energy is a developing industry in the United States, and to comply with the National Environmental Policy Act (NEPA) and other relevant laws, BOEM's renewable energy regulations require the description of coastal and marine uses that could be affected by the proposed activities, such as military activities, vessel traffic, and existing coastal and offshore infrastructure. Because various types of radar systems used by the Department of Defense (DoD), Federal Aviation Administration (FAA), and National Ocean and Atmospheric Administration (NOAA) can be affected by offshore wind facilities, the intent of this study is to provide information on the likelihood of interference, the consequences and severity of potential radar interference, the applicability and utility of currently available mitigation techniques, and how the frequency of ducting events may have an impact on radar systems.

In April of 2019, BOEM engaged Booz Allen Hamilton (Booz Allen) to study potential radar interference from offshore wind turbines in federal offshore wind leases and planning areas. The scope of work for this study consisted of five tasks:

- **Task 1, Project Management** – project scheduling and planning, including a Post-Award Meeting to discuss approach and methodologies with BOEM.
- **Task 2 and Task 3, Line of Sight (LOS) and Interference Analysis** – computer modeling of radar systems potentially impacted by planned and hypothetical wind farms including the severity of interference impacts.
- **Task 4, Mitigation Techniques** – discussion and analysis of potential options for mitigating radar interference from offshore wind farms.
- **Task 5, Ducting Analysis** – discussion and analysis of the likelihood of ducting events around the planned and hypothetical wind farms.

This Final Report presents our detailed methodology in Section 2, then results and discussion from each of the major analyses are presented in Section 3. Radar modeling is addressed in Section 3.1, Mitigation techniques in Section 3.2 and ducting analysis in Section 3.3 Conclusions and Recommendations are found in Section 4. The report also includes References (Section 5) and Appendix A with all LOS plots developed as part of the radar interference analysis.

2 METHODOLOGY

The research team used a variety of methods for this study, including computer modeling, literature review, expert interviews, and weather data analysis. This section provides detailed descriptions of study methodologies beginning with development of wind farm scenarios, then computer modeling efforts, and closing with our evaluation of mitigation techniques and atmospheric ducting events.

2.1 WIND FARM SCENARIO DEVELOPMENT

As part of defining the scope of this study, Booz Allen worked closely with BOEM to determine which wind farms would be modeled and considered in the analyses. Based on BOEM needs and available resources, the research team selected nine wind farms – some of which were currently in planning phases

and had available documentation to describe potential designs, others of which were hypothetical future scenarios based on reasonable assumptions made by the research team. The selection of the scenarios was also informed by a search for radars of concern, described in Section 2.2. BOEM's goal was to select wind farms for investigation that would have the most concern for radar interference, based on a screening-level search for nearby radar systems.

In order to conduct modeling analyses under Tasks 2 and 3, the research team collected turbine size, number, and layout (i.e., individual turbine coordinates) for each wind farm. Because the modeled wind farms were at different stages of planning during the generation of this report, various source documents were used to obtain the required information (see Table 1). Three primary methods were used to gain layouts and turbine coordinates for the study wind farms:

1. If a Construction and Operations Plan (COP) was available with specific turbine coordinates, this information was used, and was considered the most accurate and reliable information source. Coordinates were either available in COP documents or were provided by BOEM via shapefiles. Where COPs offered multiple layout scenarios, the layout with the greatest number of turbines was selected to be conservative with respect to the interference analysis.
2. If specific turbine coordinates were not available, the research team searched for high-quality maps with turbine layouts (e.g., ArcGIS maps) in documents such as COPs, pre-COP planning decks, Environmental Impact Statements (EIS) or other available documentation. These maps were georeferenced in ArcMap to generate reasonably accurate coordinates for the purposes of scenario development.
3. For hypothetical future scenarios where no planning information existed, the research team used reasonable assumptions, including expected turbine capacity (e.g., 12 MW) and typical layout rules (e.g., 1 nautical mile [NM] between turbines) to generate hypothetical future scenarios. All hypothetical turbines were placed within existing BOEM leases or planning areas.
    a. The RI/MA Cumulative Scenario was developed to simulate the maximum radar interference impacts that could result if the entire leasing area was built out to maximum capacity. The scenario consists of the four planned projects within the RI/MA lease areas (Bay State, South Fork, Vineyard Wind and Mayflower Wind) with hypothetical turbines filling out all other lease areas. For hypothetical turbines, a spacing rule of 1 NM was used.
    b. The Grand Strand scenario was developed based on the Grand Strand Call Area in South Carolina. The Call Area was further refined by placing hypothetic turbines within the portion of the call area nominated by both Fisherman Energy and U.S. Wind because this area received two nominations whereas other portions of the Call Area received only one. For the hypothetical turbines, a spacing rule of 1 NM was used.

The WindTRx model required the following information to accurately model the wind farms: turbine coordinates, turbine height, rotor size and diameter, cardinal direction of the turbine, blade rotation rates and radar cross section (RCS). All coordinate information was viewed, assessed, and generated using Environmental Systems Research Institute's (ESRI) ArcMap Geographic Information System (GIS) software. COP information for South Fork is publicly available on BOEM's State Activities web page, where Booz Allen was able to locate coordinate information in Appendix F of the COP. For Bay State, BOEM provided a GIS shapefile directly to Booz Allen where coordinate information could easily be extracted. Four out of the nine wind farms modeled for this project were georeferenced in ArcMap to acquire their coordinate information, including Vineyard Wind, Empire Wind, Ocean Wind and Skipjack. Source information for all layouts is listed in the Table 1 below.

Table 1 - Wind Farm Scenario Parameters and Data Sources

Wind Farm	Lease/Call Area	Data Source	Turbine Quantity	Megawatts (MW)	Turbine Spacing (NM)
Vineyard Wind	OCS-A-0501	EIS Alternate D2 layout, Figure 2.1-5	106	10	1
Bay State Wind	OCS-A-0500	BOEM-provided shapefile from COP	110	15	0.5-1
South Fork	OCS-A-0486	COP, Appendix F	15	12	0.8
Mayflower	OCS-A-0521	Georeferenced from map on Mayflower website	67	15	1
RI/MA Cumulative Scenario	OCS-A-0486 OCS-A-0487 OCS-A-0500 OCS-A-0501 OCS-A-0520 OCS-A-0521 OCS-A-0522	Bay State, Vineyard Wind, South Fork, Mayflower, and hypothetical	1,115	10-15	1
Empire Wind	OCS-A-0512	Pre-COP presentation, slide 51	135	18	1
Ocean Wind	OCS-A-0498	COP, Figure 4.1-1 and 4.1-2	138	8	0.5-1
Skipjack	OCS-A-0519	COP, Figure 2.1-2	16	12	1
Grand Strand	Grand Strand Call Area	Hypothetical	112	15	1

2.2 RADARS OF CONCERN

In addition to gathering information on the turbine layouts for the nine wind farms, Booz Allen also conducted research on potential radars of concern to define which radars should be included in this study. As part of the effort to identify which hypothetical wind farm areas would be the most relevant to model, Booz Allen investigated which radars exist in relative proximity to the proposed hypothetical wind farms. In collaboration with BOEM, Booz Allen identified the following states and/or regions for the hypothetical wind farms: New York, the Mid-Atlantic (New Jersey, Delaware, and Maryland), and the Carolinas (North Carolina and South Carolina). The radar types to be evaluated included ASR, ARSR, NEXRAD, and SeaSondes.

Booz Allen began by researching the BOEM's State Activities web page to identify a reasonable assumed location for proposed hypothetical wind farms. When choosing coordinates to represent the hypothetical wind farm, conservative estimates were assumed and those lease site blocks with coordinates that appeared closest to the coastline were chosen over site blocks within the wind farm that were further away from shore. These represent approximately the closest portion of the wind farm to the land-based radars. If a state activity page did not include GIS files, Booz Allen used other available PDF maps to determine an approximate location of the wind farm by entering the coordinates into Google Maps. This was only necessary for Delaware, as all other state activity pages included GIS resources to identify wind farm locations.

The next step involved a comprehensive internet search for publicly available source documents with information on the various radar types and their approximate locations. Most radar locations are not provided to the precision of a defined geospatial coordinate. The exact locations of some radars were not publicly-availably, in which case estimates were made based on available information (e.g., an ASR assumed to be located at the center point of an airport). Using available online resources, Booz Allen evaluated which radar locations of each type (ASR, ARSR, NEXRAD, and SeaSonde) appeared closest to

the wind farm areas and should therefore be examined to determine whether they are within LOS. Using Google Map's "Measure Distance" feature, the team evaluated which radars were within an approximately 120-kilometer range (a conservative range for radars that may be within line of sight). Any radar that appeared within this range from the hypothetical wind farm was presumed to be a potential radar of concern. Distances were rounded to the nearest significant figure and are approximate.

2.3 LINE OF SIGHT MODELING

To conduct the LOS analysis and model radar interference, Booz Allen used a radar simulation computer model called WindTRx. The WindTRx model computes a radar's non-anomalous (no atmospheric ducting) LOS using a spherical Earth model, a standard 4/3 radar refractivity index and digital terrain data. For this effort, the model used high-resolution terrain data from the Shuttle Radar Topography Mission-Level 2 (SRTM-2) obtained from the National Geospatial-Intelligence Agency. For illustrative purposes, the model was used to create LOS plots for each wind farm/radar combination at every 1 degree radial centered at the radar for three different heights for each wind farm: the height to the bottom of the blade, the height to the turbine hub, and the height to the max blade height. As shown in Figure 1, the inner red-shaded region is where the radar will see the entire wind turbine (mast, nacelle, hub and blade). This region will see the most interference from the turbine, as it will receive both the returns from the stationary part of the turbine (mast & nacelle) and the returns from the blades (both receding and approaching blade flashes). The middle orange-shaded region is where the radar will only see returns from part of the mast, the nacelle, the upper half of the blade sweep and part of the lower half of the blade sweep. The outer yellow-shaded region is where the radar will only see part of the upper half of the blade sweep. In this region, the radar cannot see any stationary part of the turbine and will only experience interference from the blade flash. In the yellow-shaded region, the radar can only see the top half of the turbine blades above the nacelle.

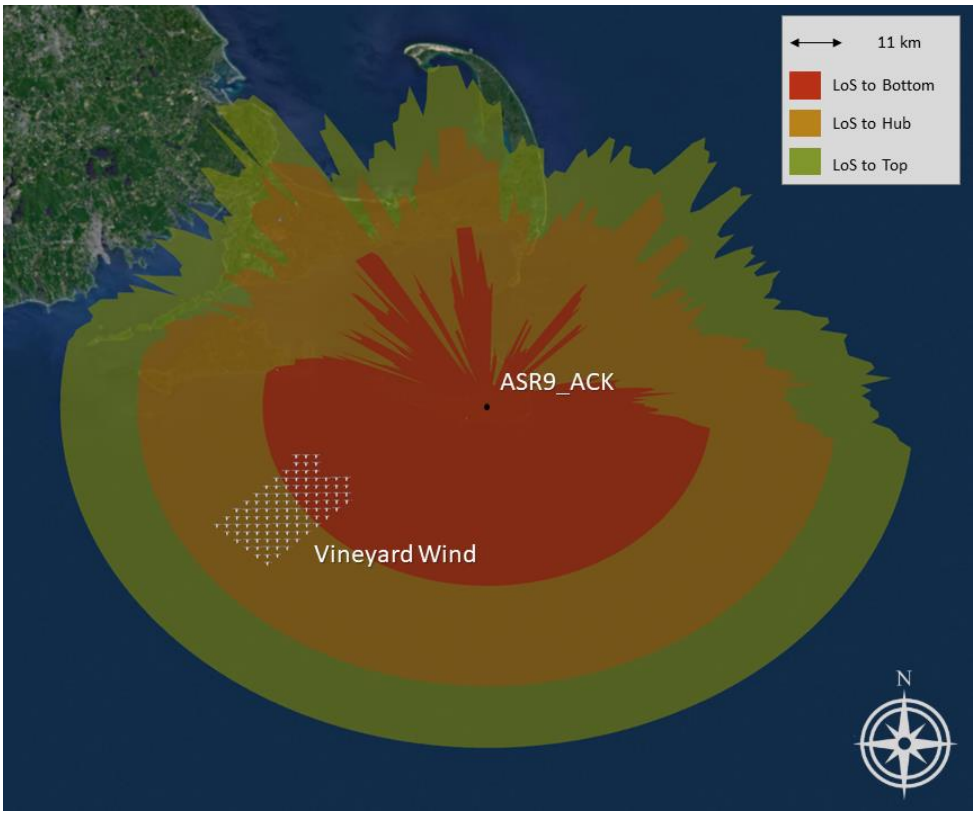

Figure 1 - Sample Line-of-Sight Plot

2.4 RADAR INTERFERENCE MODELING

Booz Allen used the WindTRx model to perform LOS analyses and determine interference levels of proposed wind farms as viewed from fixed land-based radars. WindTRx provides a sufficient fidelity radar (parameters to create a signal-to-noise-based model such as transmit power, antenna gain, transmit frequency, pulse length) and environment construct (terrain, radar propagation, clutter) to evaluate both radar LOS and radar performance, provided adequate data can be ascertained to model the radar of interest appropriately.

WindTRx generates signal returns from the wind turbine blades and structures to accurately simulate the interference the wind farm will present to the radar. WindTRx uses a WGS-84 earth model and digital terrain elevation data terrain information to accurately place each turbine with respect to the radar of interest.

Within WindTRx, the wind turbine is modeled as a user-defined number of rotating scatterers, with radar cross section data from tests and high-fidelity electromagnetic simulations. The upper right portion of Figure 2 shows a graphical example of the blades and structure models as scatterers in WindTRx. Each turbine blade is modeled using the manufacturer-specified size and rotation rate to accurately match the returns of the turbines as seen by the radar. Each individual scatterer is fully characterized in the signal environment and contributes unique power, phase, Doppler, and range/time.

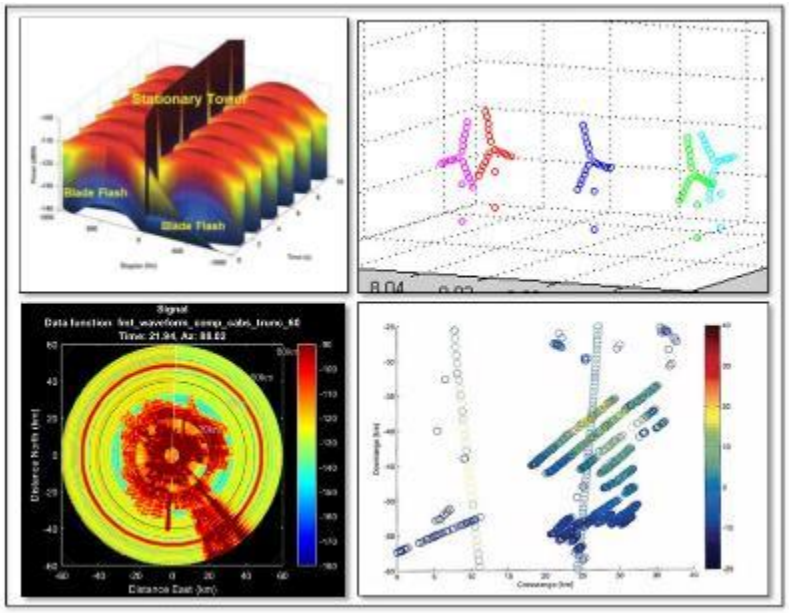

Figure 2 - WindTRx capabilities. Clockwise from top left: wind turbine Doppler versus power displays; initial wind turbine models; historical radar data used for model validation; and representative operator PPI scopes showing the effects of a radar's anti-clutter system.

A single wind turbine, as defined above, is instantiated multiple times to model a wind facility to perform detailed modeling of the scenario. As the simulation is executed within the WindTRx environment, thousands of signals will be generated with different amplitude, phase, and frequency from each wind turbine scatterer. Processing this data yields an understanding of the electromagnetic environment of the proposed wind farms as presented to the radar of interest. The returns of the individual turbines are informed by measurements, modeling in finite element electromagnetic simulation software (FEKO), and analyses of rotorcraft.

Using the radar parameters and signal processing components of the radar of interest the anticipated level of impact on the radar's performance can be assessed. This impact will compare the interference generated by the wind farm to the existing background environment.

2.4.1 RCS Modeling

WindTRx uses a semiempirical model to approximate the dynamic nature of the RCS of wind turbines. WindTRx models each blade of the turbines as a series of point scatterers which rotate about a hub for each turbine (Figure 3). These scatterers have a dynamic RCS which is based upon the rotation angle of

the blade and the geometry between the LOS vector and the plane of rotation of the turbine blades. This dynamic RCS is designed to capture the 'blade flash' and the changing Doppler spectrum of the spinning blades.

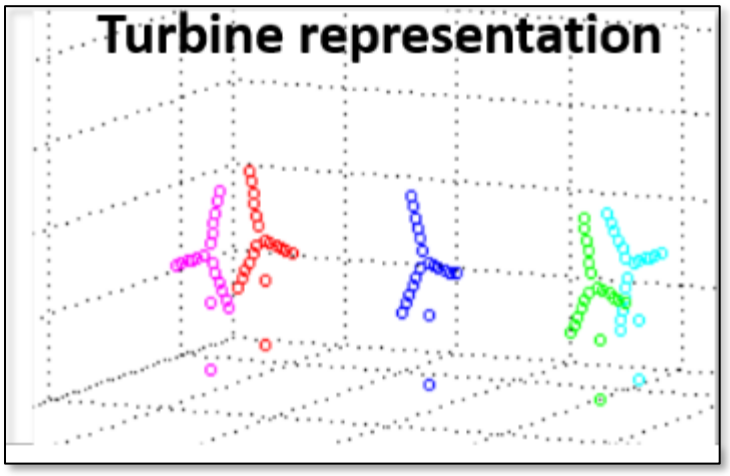

Figure 3 – Picture of WindTRx turbine model scatterers.

Due to lack of information on the measured RCS values of the large offshore turbines that were analyzed, the research team used information from studies to scale up the RCS parameters of the model which should be representative of the offshore turbines. Due to the large size of wind turbines, they will have a very large RCS which is computationally intensive to compute and beyond the scope of WindTRx. Booz Allen chose the parameters of the turbine RCS in WindTRx to have an RCS of the non-moving parts of the turbine (mast/nacelle) to be 45 dBsm. The blades will in general have an RCS that is much lower than the mast, except in certain blade geometries where it can be on the same scale as the mast or greater in what is commonly known as a "blade flash." In WindTRx, blade flashes will occur when the blade is rotated to be near perpendicular in its rotation to the LOS vector from the radar to the turbine. During a flash, the RCS of the scatterers will be scaled to the same order of magnitude as the mast. The following sources were used to compute or measure various onshore turbines that were used to scale up to the larger offshore turbines:

- "Wind Farms Impact on Radar Aviation Interests" (Poupart, 2003)
- "Modeling the Effects of Wind Turbines on Radar Returns" (Ohs, Skidmore, & Bedrosian, 2010)
- "Dynamic Radar Cross Section and Radar Doppler Measurements of Commercial General Electric Windmill Power Turbines Part 2 – Predicted and Measured Doppler Signatures" (Buterbaugh & al., 2008)
- "Stealth technology for wind turbines" (Pinto, Matthews, & Sarno, 2009)

Output from WindTRx of the RCS of a wind turbine is shown below in Figure 4 for a turbine with 100 m blades spinning at 15 rpm with the ARSR-4 radar model.

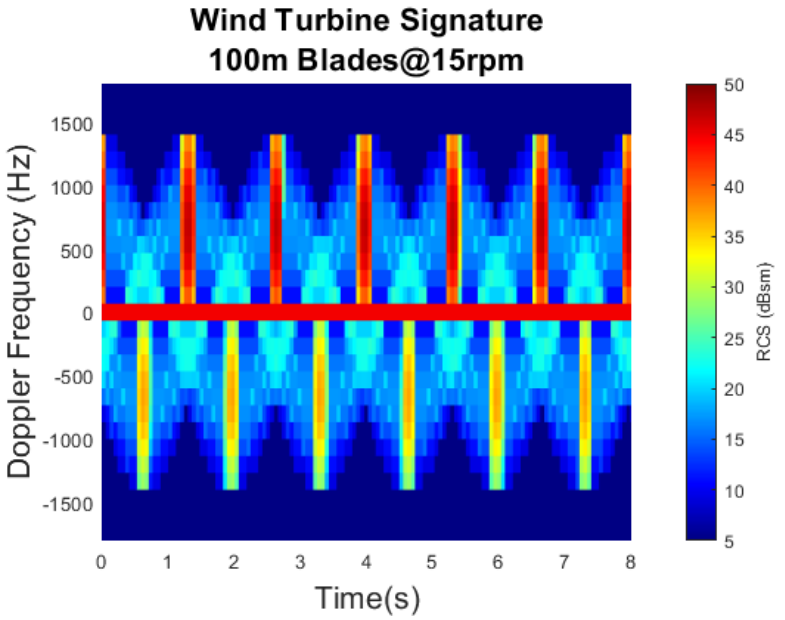

Figure 4 - Dynamic RCS of wind turbines as modeled in WindTRx

2.4.2 ARSR-4 Radars

The ARSR-4 series of radars is used in U.S. air traffic control and air defense roles. The ARSR-4 is a long range, L-band radar that is used by the FAA and DoD to monitor airspace on and around the U.S. border. This system uses a dual-stacked beam to cover 360° in azimuth and -1° to 30° in elevation with the capability of extending the coverage down to -10° with the addition of a lookdown beam where required. The system is capable of detecting targets out to 250 NM (460 km). A picture of the ARSR-4 on Cape Cod is shown in Figure 5.

The ARSR-4 also has a mode to measure weather conditions near the site. The research team did not model this mode of the ARSR-4 and is focusing on the air surveillance mode of the system.

Figure 5 - ARSR-4 at North Truro

The ARSR-4 uses dual stack transmit and receive beams when in operation. WindTRx only simulates the lower beam since the wind turbines will be at low elevation angles relative to the radar and well outside the position of the upper beams. The upper stack covers in elevation from ~5° to 30° which is well outside the elevations of the wind farms under consideration in this study.

The antenna is modeled in WindTRx as a simple sin(x)/x gain pattern. The ARSR-4 series has a dual antenna beam; a high beam and a low beam. Due to considering the low elevation beams, only the low-beam will be discussed further. The peak gain is 37.7 dB with a beam width of 1.4° and 2.6° in azimuth and elevation respectively. The full pattern used in the model is seen in Figure 6, the azimuthal slice in Figure 7, and elevation slice in Figure 8 below. The back plane of the antenna pattern is set to a constant of -10 dB in the model.

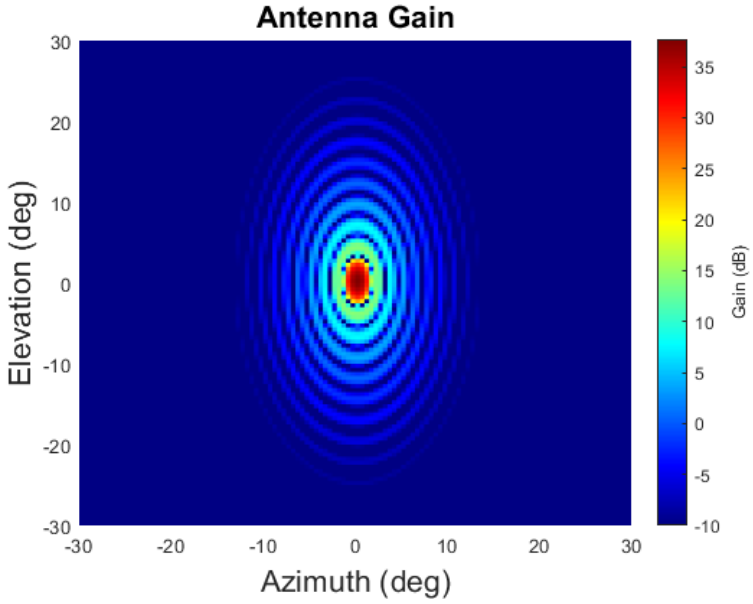

Figure 6 - Full pattern used in WindTRx for the low beam of the ARSR-4

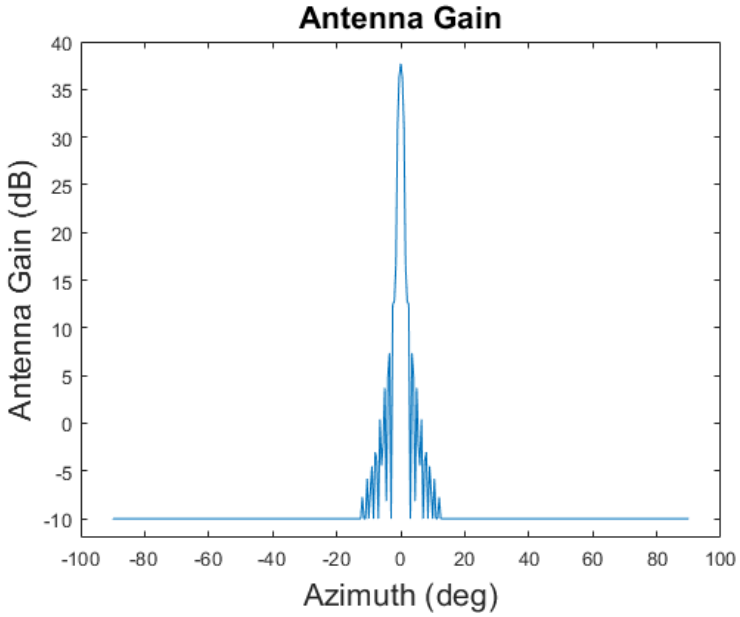

Figure 7 - Azimuth slice of the gain for the low beam antenna

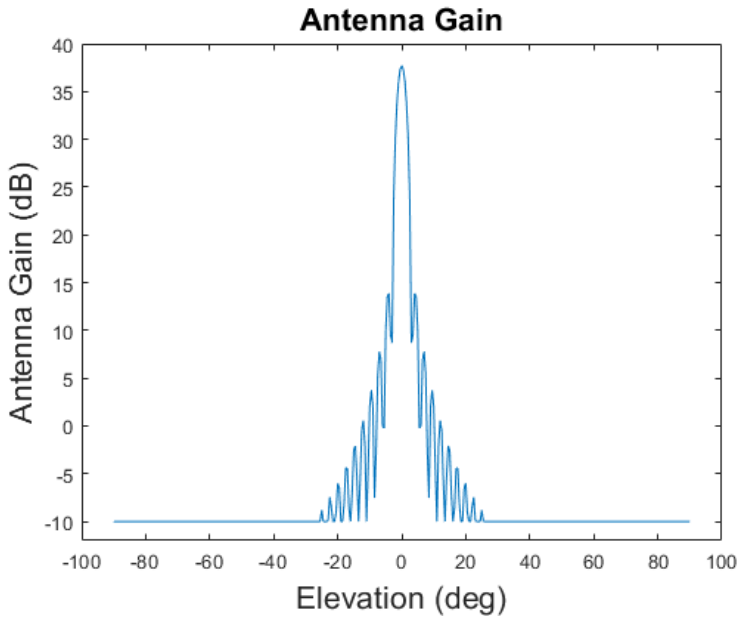

Figure 8 - Elevation slice of the gain for the low beam antenna

The radar parameters of the ARSR-4 are shown in Table 2 below. These values were taken from a government database. The radar was calibrated to have a detection range of 455 km for a 0 dBsm target.

Table 2 - Radar parameters for ARSR-4

Parameter	Data
Pedestal Rotation Rate	5 RPM
Low-Stack Antenna Gain	37.7 dB
Low-Stack Beam Width	1.4° Az, 2.6° El
Antenna Height	~23 m
Antenna Mechanical Tilt	±3°
Frequency	1.2-1.4 GHz (modeled 1.3 GHz)
Modulation	1.3 MHz bandwidth NLFM
Pulse Width	60 or 90 µs (modeled 90 µs)
Peak Power	68 kW
Max Range	250 NM (460 km)

The low-stack beam transmits eight pulses with staggered pulse repetition intervals (PRIs) for the low-stack beams. The pulses have a non-linear frequency modulation (NLFM) which has a 1.3 MHz upchirp. An integration gain of 6.9 dB for the low-stack beam is also applied to signals. The ARSR-4 model in WindTRx uses a 90 µs pulse width which will have a corresponding pulse compression ratio (PCR) of 90 after pulse compression of the signal. The pulse compression sidelobes are also modeled. This system is also capable of using a 60 µs pulse with a PCR of 60 which is not used in the model.

The ARSR-4 can uses a moving target indicator (MTI) to reject clutter signals. This processing attenuates returns with low Doppler, removing them from the signal. This is an important process to capture as it will attenuate the slowest moving parts of the blades and the mast signatures but will allow

the faster moving parts of the blades to make it through this processing. The MTI used in the ARSR-4 model sends signals through a 3-pulse delay line canceller.

The ARSR-4 performs a range-cell averaged constant false alarm rate (CFAR). In WindTRx, this is done by setting a threshold value using one guard cell on either side of the cell under test and averaging the ten cells on both sides of the guard cells. A diagram of the cell averaging is shown in Figure 9. The threshold for detection is then taken to be 13 dB greater than the value of the averaged cells.

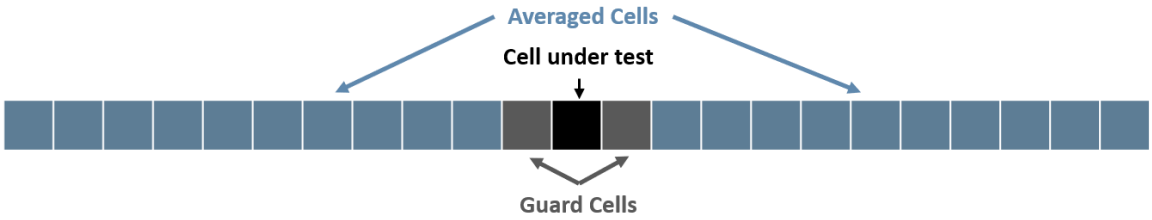

Figure 9 - CFAR used in the WindTRx model for the ARSR-4

2.4.3 ASR-8 and ASR-9 Radars

The Airport Surveillance Radar (ASR)-8 and ASR-9 series of radars are used as the primary air traffic control system for the airspace surrounding airports. The ASR-8 and ASR-9 are S-band surveillance radars. The primary radar performs surveillance approximately 60 NM around airports, providing 2-D (range and azimuth) information to air traffic control. The ASR-8 is an analog precursor to the ASR-9. The two radar types are fairly similar and for portions that are modeled the same in WindTRx it will be noted that the methodology applies to both.

The ASR-8 and ASR-9 additionally have a secondary radar that performs interrogations on aircraft transponders using "identification, friend or foe" (IFF), however this secondary radar is not being considered in this analysis because it is likely to be impacted by the presence of wind turbines.

Figure 10 - Example of an ASR-8

Figure 11 below provides an overview of the modeling of the ASR-8 and ASR-9 in WindTRx. The modeling specifics of major components will be detailed in the following section.

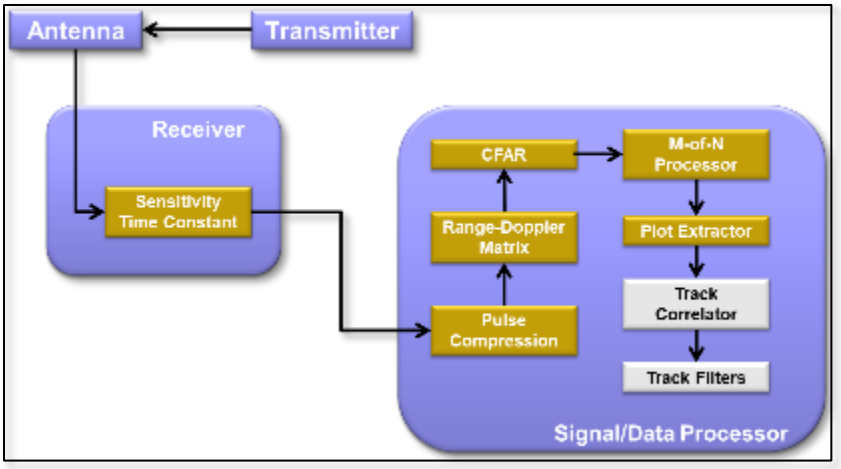

Figure 11 - Overview of ASR-8/9 WindTRx models

2.4.3.1 *Antenna*

The ASR-9 is a 2-D radar, tracking in range and azimuth only, with a single elevation beam. The antenna is a rotating parabolic dish antenna. The most probable scan period for the ASR-9 is 13 rotations per minute (RPM), which equates to a scan period of 4.62 seconds. For the ASR-8, WindTRx models the first scan mode, which operates at 12 RPM, for a complete azimuth scan in 4 seconds.

The ASR-9 antenna is modeled in WindTRx as a cosecant-squared gain pattern with a peak gain of 34 dB. The 3-dB beam width is 1.3° and 4.8° azimuth and elevation respectively. The full pattern used in the model is seen in Figure 12, the azimuthal slice in Figure 13, and elevation slice in Figure 14 below. The back plane of the antenna pattern is set to a constant of -10 dB in the model.

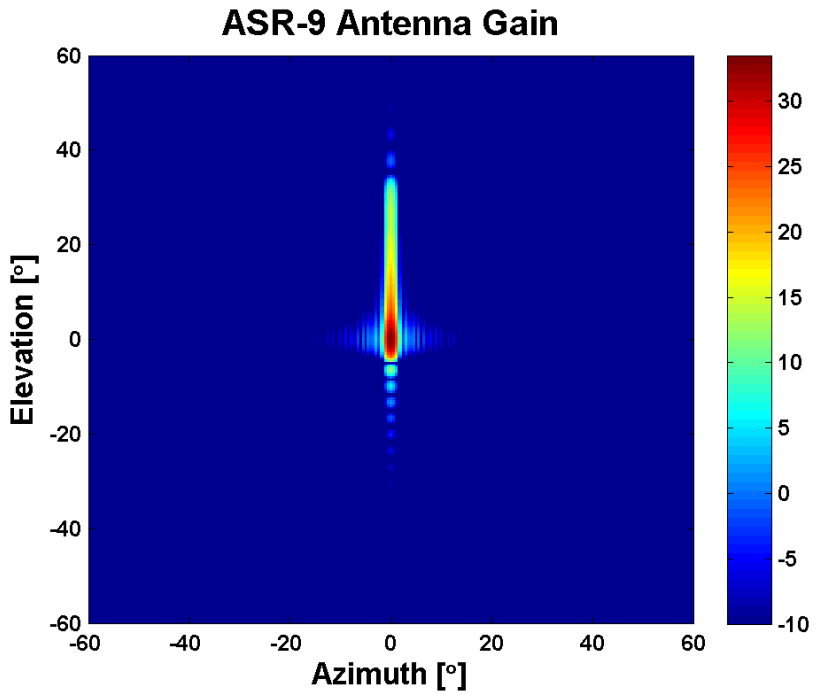

Figure 12 - ASR-9 Antenna Gain

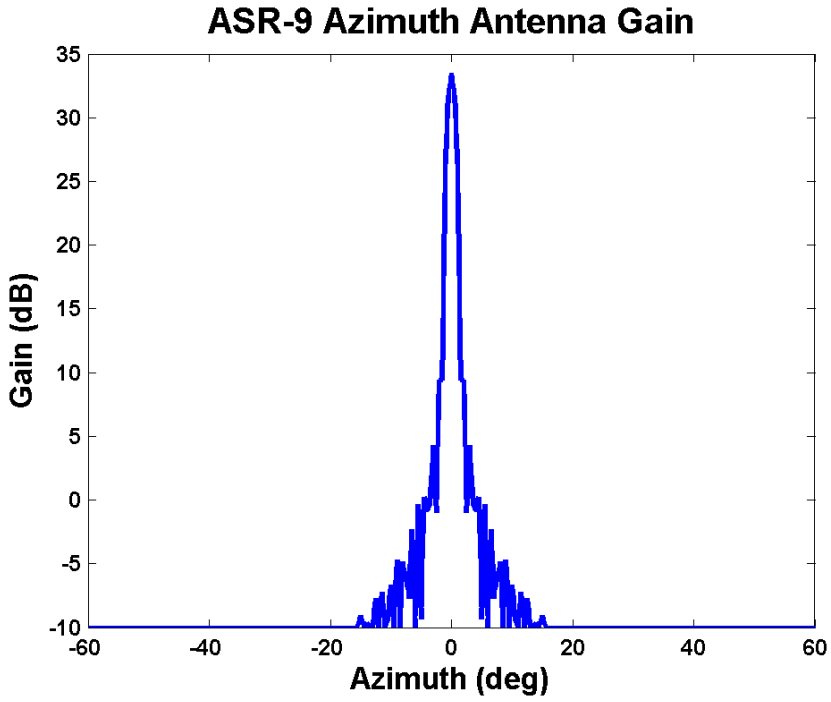

Figure 13 - ASR-9 Azimuth Cut

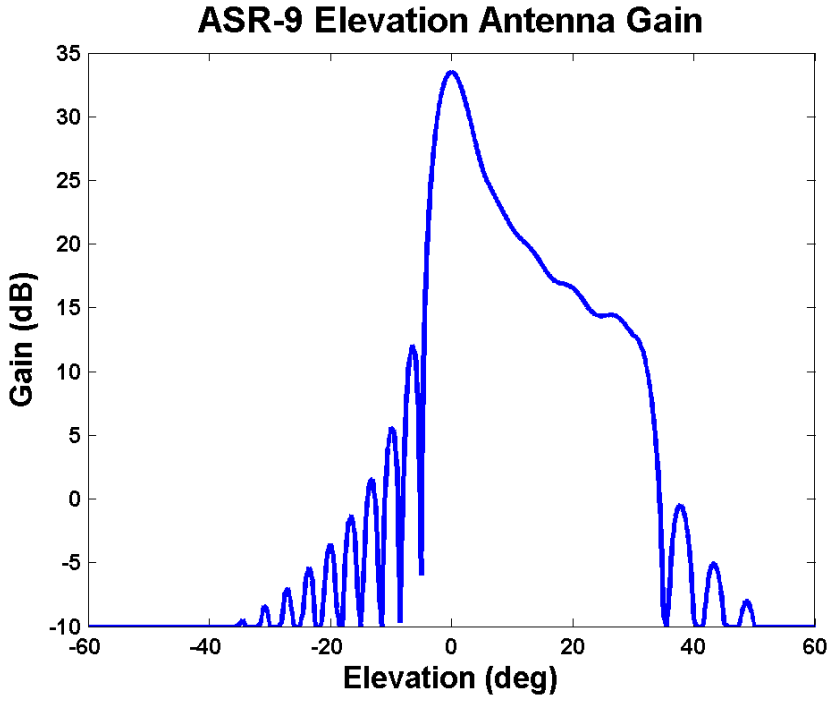

Figure 14 - ASR-9 Elevation Cut

The ASR-8 antenna is very similar to the ASR-9. It is also modeled in WindTRx as a cosecant-squared gain pattern. The elevation beam width is identical; however, the peak gain is 33.5 dBi with a wider azimuth 3 dB beam width of 1.7°. The full pattern used in the model is seen in Figure 15, the azimuthal slice is shown in Figure 16, and elevation in Figure 17.

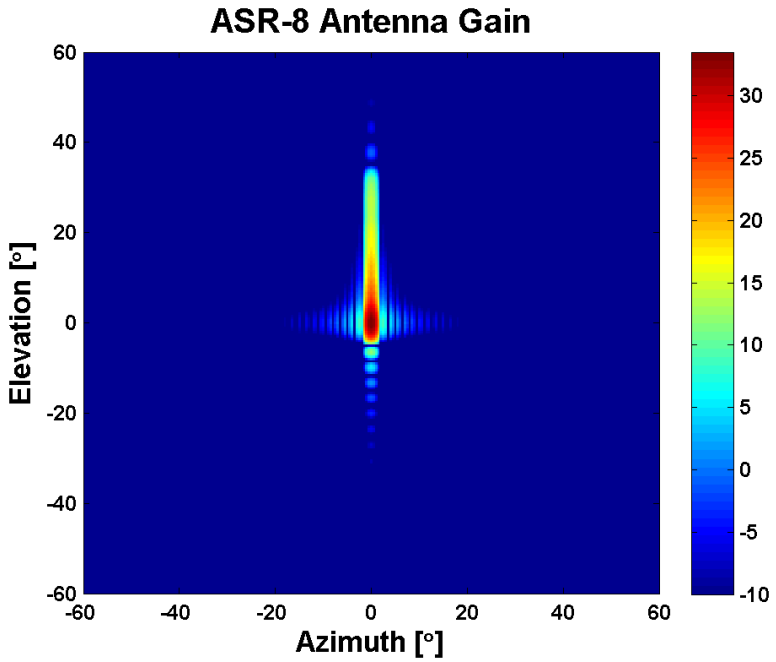

Figure 15 - Full WindTRx ASR-8 Antenna Pattern

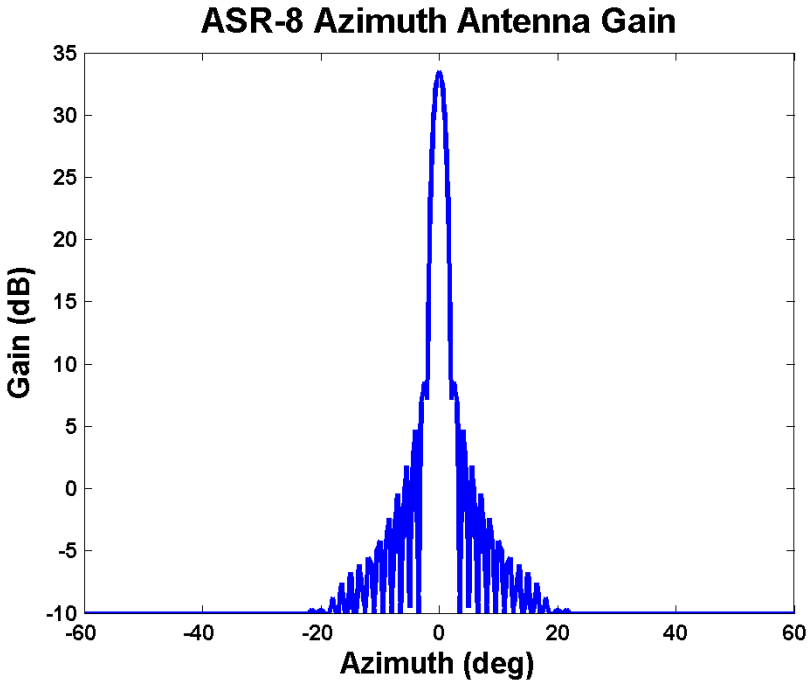

Figure 16 - ASR-8 Azimuth Cut Gain

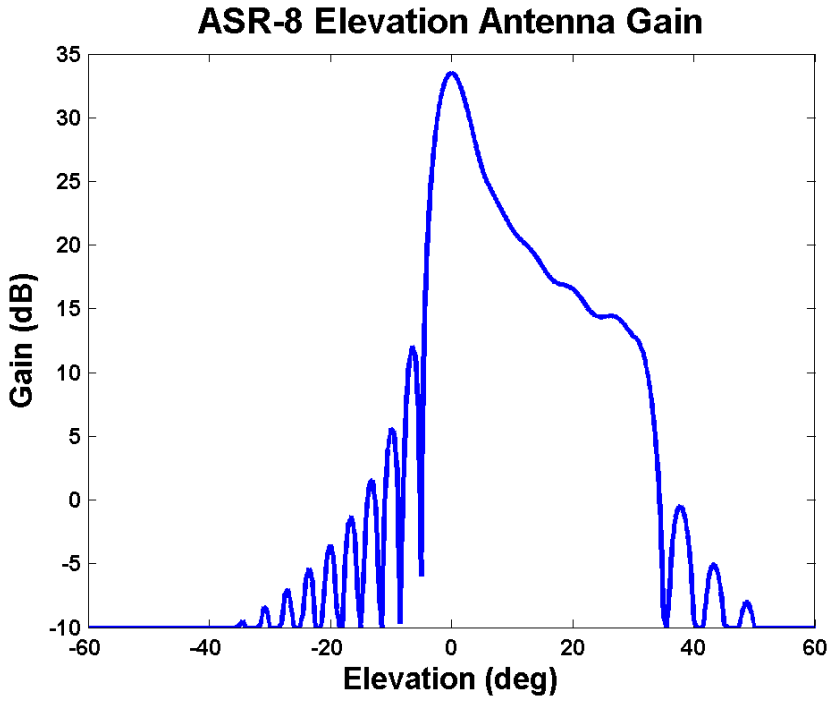

Figure 17 - ASR-8 Elevation Cut

2.4.3.2 *Radar Parameters*

The primary radar parameters of the ASR-8 are shown in Table 3 and Table 4 below. The ASR-8 transmits a pulse doublet with a short pulse and long pulse, designated below as P1 and P2, respectively. These values were taken from a government database. The WindTRx model of the ASR-8 radar is calibrated to have a detection range of 111 km (60 NM) for a 0 dBsm target.

Table 3 - Radar parameters for ASR-8

Parameter	Data
Pedestal Rotation Rate	12 RPM
Peak Antenna Gain	33.5 dBi
3dB Beam Width	1.7° Az, 4.8° El
Antenna Height	~25.6 m (varies based on tower height)
Antenna Mechanical Tilt	-1^{o} to $+5^{o}$ (modeled at 2.5^{o})
Frequency	2.7-2.9 GHz (modeled 2.8 GHz)
Modulation	Unmodulated
Pulse Width	1.03µs
Pulse Repetition Interval (PRI)	PRI 1: 830 µs PRI 2: 876 µs PRI 3: 961 µs PRI 4: 1177 µs

Parameter	Data
Peak Power	1400 kW
Max Range	60 NM (111 km)

The primary radar parameters of the ASR-9 are shown in Table 4 below. The ASR-9 transmits an unmodulated pulse with a two PRI sequence. The Electronic Warfare Integrated Reprogramming (EWIR) database gives ranges for PRI limits and the middle value in both PRI 1 and PRI 2 was used in WindTRx. The two PRIs modeled in WindTRx are set as 792 µs and 1,028 µs. These values were taken from a government database. The radar was calibrated to have a detection range of 134 km (72 NM) for a 0 dBsm target.

Table 4 - Radar parameters for ASR-9

Parameter	Data
Pedestal Rotation Rate	13 RPM
Peak Antenna Gain	34 dBi
3dB Beam Width	1.3° Az, 4.8° El
Antenna Height	Modeled at 26.4m (varies based on tower height)
Antenna Mechanical Tilt	-1^{o} to $+5^{o}$ (modeled at 2.4^{o})
Frequency	2.7-2.9 GHz (modeled 2.8 GHz)
Modulation	Unmodulated
Pulse Width	1.03µs
PRI	PRI1: 737µs - 847µs (modeled as 792µs) PRI2: 980µs - 1077µs (modeled as 1028µs)
Peak Power	1400 kW
Max Range	72 NM (134 km)

2.4.3.3 *Sensitivity Time Control (STC)*

The WindTRx ASR-8 model currently uses a fixed (non-adaptive) sensitivity time control (STC) schedule with a maximum attenuation range set to 30 km. The STC attenuator is controlled in 6 dB steps and has a minimum attenuation of -40 dB. Figure 18 shows the STC attenuation as a function of range.

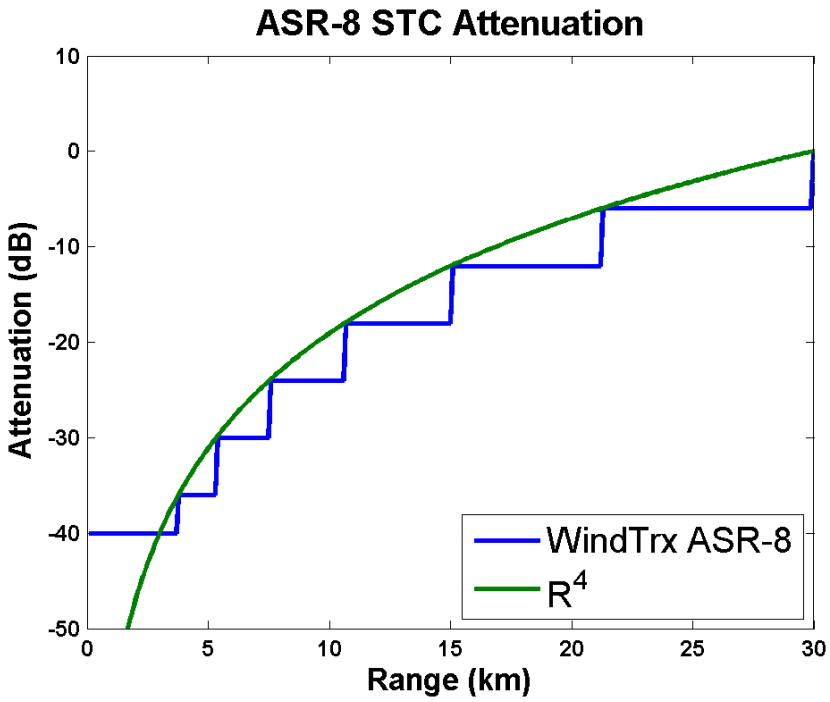

Figure 18 - ASR-8 STC Attenuation Curve

The WindTRx ASR-9 model uses a similar fixed (non-adaptive) STC. The ASR-9 contains an STC attenuator controlled in 1 dB steps and the plot below in Figure 19 shows the STC attenuation as a function of range within WindTRx with a minimum attenuation is -60 dB.

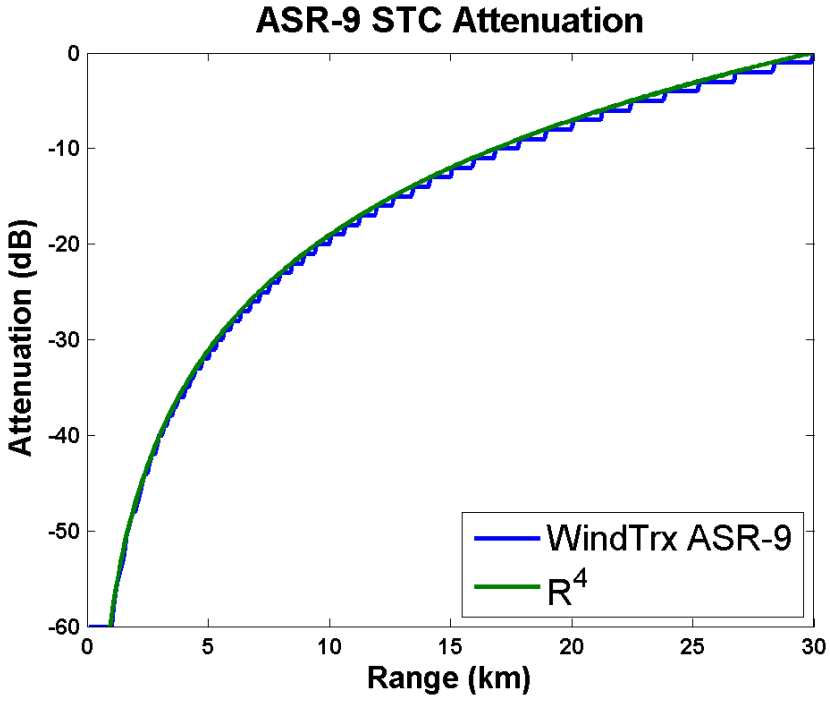

Figure 19 - ASR-9 STC Attenuation Curve

2.4.3.4 *Range-Doppler Matrix*

For both radars the return signals are placed into a range-doppler matrix. The ASR-8 and ASR-9 range gate width is 1/16 NM (115.75 m) with no overlap. There is a maximum of 977 range bins. Additionally, the current transmit pulse repetition frequency (PRF) is divided into 5 Doppler filters varying from 170Hz to 240Hz spacing for the ASR-8 and 195Hz to 253Hz for the ASR-9. The Doppler filters are modeled as attenuators with a Gaussian limited roll-off.

2.4.3.5 *Constant False Alarm Rate (CFAR)*

In WindTRx, the ASR-8 performs a range-cell averaged CFAR independently for each Doppler filter. The target input data is then fed through a 16 range-cell wide sliding window accumulator. The average of the 16 cells below and above the guard cell around the cell under test are averaged. The greater of the before and after moving clutter thresholds are determined to be the moving clutter threshold. The higher side is then compared to the cell under test. A diagram of the cell averaging is shown in Figure 20. The threshold for detection is then taken to be 13 dB greater than the signal of the averaged cells.

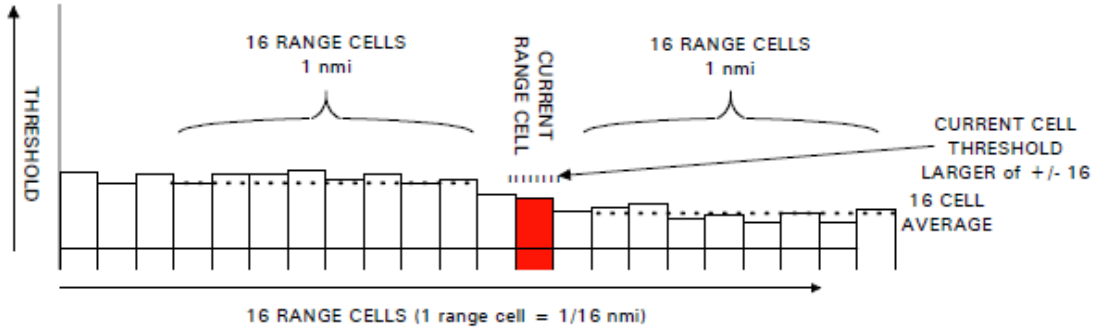

Figure 20 - Picture of the ASR-8 CFAR in WindTRx

The WindTRx ASR-9 performs a range-cell averaged CFAR independently for each Doppler filter. The sliding range window technique used is based on a CFAR description provided in (Elkin, 2001) as a sliding 14 gate window on in front of the target and behind the target. The cell under test, a guard cell next to the cell under test as well as the largest cell within the leading or trailing window and its adjacent neighbor are removed from the threshold calculation. The remainder of the leading cells are averaged as well as the separate averaging of the trailing cells. These leading and trailing windows are then compared and the largest being selected for the final threshold comparison.

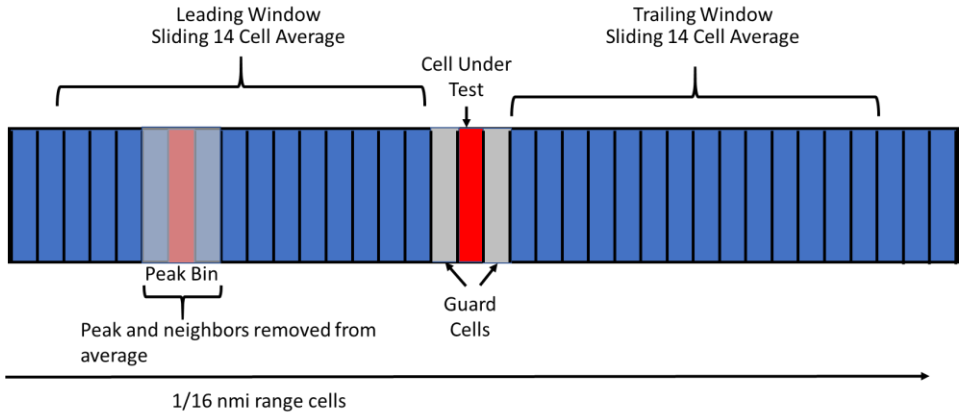

Figure 21 - ASR-9 CFAR

2.4.3.6 *Detection and Correlation:*

For both the ASR-8 and ASR-9, the CFAR output is put through an M-of-N process for each range bin to declare targets. If two or more of four coherent processing intervals (CPI) declare a detection, the integrator output is declared true and put through a detection correlator to form plots.

2.4.4 NEXRAD Radars

The Weather Surveillance Radar (WSR)-88D, also known as NEXRAD, is a powerful S-band pulse-Doppler weather surveillance radar to support the weather warning and forecast missions of the National Weather Service (NWS), FAA, and DoD (NOAA, 2017). The radar system uses advanced signal processing algorithms to digest raw radar data and notify meteorologists of hail, severe storms, tornadic circulations, downburst and gust fronts (NSSL, 2019). The radar uses a mix of waveforms to measure reflectivity and velocity within the volumetric scan using pre-programmed volume coverage programs (VCP) that can be adjusted as needed based on the current weather conditions. A picture of a WSR-88D NEXRAD is shown in Figure 22.

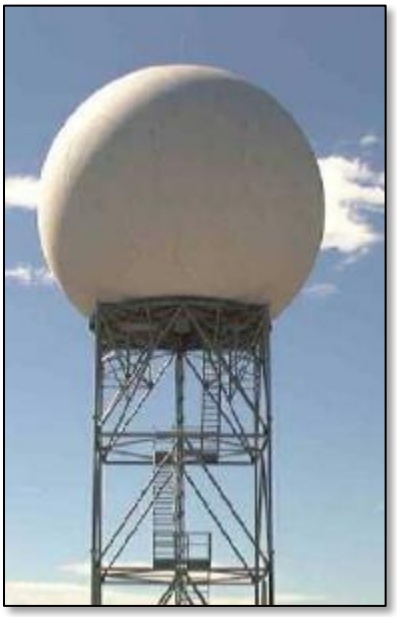

Figure 22 - WSR-88D Weather Surveillance Radar

The WSR-88D VCPs can be categorized into two main categories: clear-air mode and precipitation mode. The clear-air mode is a slower, more-sensitive scan that covers approximately 5° in elevation in 10 minutes. The precipitation mode is designed to scan higher in the atmosphere, approximately 20° in elevation, to enable meteorologists to analyze the vertical structure of storms. As such, it uses a faster scan to refresh the volumetric data in five minutes. Due to the heightened sensitivity of potential interference from wind farms during storms, one of the precipitations VCPs was developed in the WindTRx model for analysis.

The WindTRx NEXRAD radar model is not a comprehensive model of the entire radar and signal processing chain that is used to create products for weather analysts. The WindTRx model includes the basic radar features required to predict the interference posed by wind turbines onto the radar. The WindTRx model computes the returns from the wind turbines and performs basic signal processing (range-Doppler processing) to estimate the interference imposed by the turbines on the radar.

The NEXRAD uses a parabolic dish antenna to emit a pencil beam that scans the volume around the radar per the operational programmed scan. The WindTRx antenna model uses a theoretical circular pattern that matches the peak gain (45.5 dB), beam width (0.925°), and first sidelobe (-29 dB) of the NEXRAD antenna. The full pattern used in the model is seen in Figure 23 below. The back plane of the antenna pattern is set to a constant -10 dB in the model.

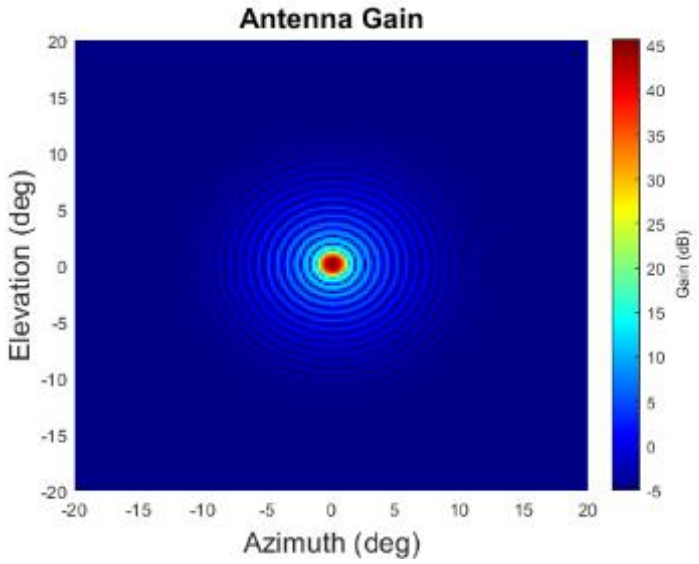

Figure 23 - WindTRx NEXRAD Antenna Pattern

The radar parameters for the WSR-88D are shown in Table 5 below. These values are taken from the NOAA websites listed previously and other available government radar databases.

Table 5 - Radar Parameters for WSR-88D

Parameter	Data
Pedestal rotation rate	16 – 26 deg/sec (varies in VCP for each elevation scan)
Antenna gain	45.5 dB
Antenna height	24.7 m
Frequency	2700 – 3000 MHz
Pulse width	1.57 µsec (for modeled VCP)
Peak power	700 kW

The WSR-88D uses two primary pulse repetition interval sequences during its volume sweep. The first sequence type, contiguous surveillance, uses longer PRIs to provide unambiguous long-range reflectivity coverage. This sequence is used for the lower elevation angle cuts of the VCP. The second sequence type, contiguous Doppler, uses shorter PRIs to provide reduced velocity ambiguous coverage. This sequence type is used at lower elevation angles to provide mean radial velocity and spectral-width weather data. When used at higher elevation angle, this sequence also provided shorter-range reflectivity data. Depending on the VCP, the radar may also combine the two primary types at various elevation angles to provide both long-range reflectivity data and mean radial velocity and spectral-width weather data.

2.4.5 SeaSonde Radars

SeaSondes are designed as a low cost, simple instrument to measure coastal ocean currents, where much of the complexity is in the signal processing. Capable of performing ocean current monitoring, oil spill tracking, vessel tracking, and other tasks while operating remotely, these systems can work together or in a network with nearby systems. They operate in the high frequency (HF) band between 5-50 MHz. For the specific frequency of each SeaSonde, there is a corresponding Bragg frequency that is used to extract sea parameters. These systems are also capable of over-the-horizon (OTH) propagation by using the HF band over the conducting sea to propagate via a surface wave as opposed to more traditional radar propagation through the atmosphere.

2.4.5.1 *Sea Clutter Modeling*

Bragg scattering occurs when the sea waves off which the radio waves scatter are spaced at half wavelength intervals which causes constructive interference in the reflected signal from multiple waves. The velocity of ocean waves will be directly related to their wavelength (λ), where g is the acceleration due to gravity in the following manner,

$$v = \sqrt{\frac{g\,\lambda}{2\pi}} \tag{1}$$

The sea clutter is modelled currently as only the Bragg peaks. The backscatter coefficient for Bragg peaks for HF radar is taken as $\sigma_0 = 0.02\ m^{-2}$ for waves following the Phillips spectrum for a fully developed sea (Barrick, First-Order Theory and Analysis of MF/HF/VHF Scatter from the Sea, 1972). This is the value that Booz Allen is using to derive the energy present in the Bragg peaks. The scattered energy will be spread between forward-moving and backward-moving ocean waves and for what follows, the backward-moving waves were assumed to be 1% of the total Bragg spectrum.

In WindTRx the Bragg signals are generated for each range bin and each azimuth cell, each of which can have a different ocean current velocity. Within each range bin the transmission attenuation and area illuminated will be "integrated" by generating a signal every two wavelengths in range and summing them over the range bin to generate one signal at the center of the bin to speed computation while still capturing the signal at a higher resolution. The signal strength of each azimuth bin in range will be identical (Booz Allen is assuming a full developed sea at all ranges) and computation is reduced by using the same signal strength in all azimuth bins at a given range. Each azimuth bin will however have a different velocity profile for the ocean currents present and thus have different Doppler frequencies.

Once the signals are generated, they are then passed through the range and Doppler filters to generate a range-Doppler matrix. The range filters are generated by doing a 512-point fast Fourier transform (FFT) over a hamming window to simulate the effects of the first stage of the double FFT processing of the SeaSondes. This will correspond to fast-time sampling to be 512 Hz for the long-range SeaSondes, 1,024 Hz for the medium-range SeaSondes, and 2,048 Hz for the short-range SeaSondes. The Doppler filters are generated in a similar manner with a 1,024-point FFT over a hamming window to simulate the second FFT with a slow-time sampling rate of 1 Hz for the long-range SeaSondes, 2 Hz for the medium-range SeaSondes, and 4 Hz for the short-range SeaSondes. The filters used for the long-range SeaSondes are shown below in Figure 24.

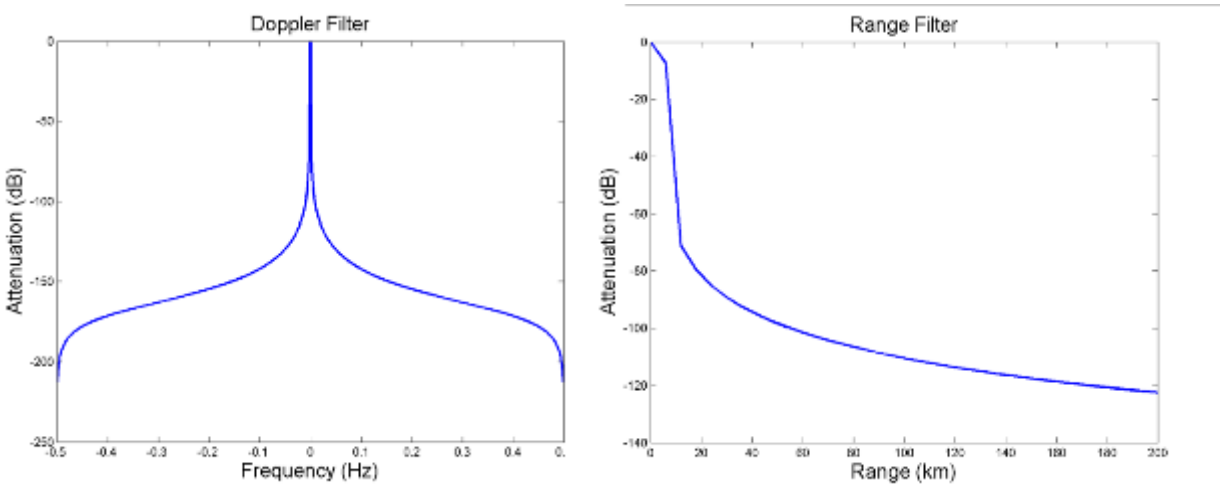

Figure 24 - WindTRx Doppler (left) and range (right) filter responses for the long-range SeaSondes

An example of the Bragg clutter returns is shown in Figure 26 and Figure 27 below. Ocean currents were added as shown in Figure 25. The choice of using 100 cm/s, which is an extreme current for the east coast (typical currents are between ~0-30 cm/s), for the choice of currents present in simulation was due to being able demonstrate interference over a larger range of currents than are typically encountered in operation. The choice of currents running parallel to the coast was due to the simplicity of interpretation and to provide a large range of radial current velocities.

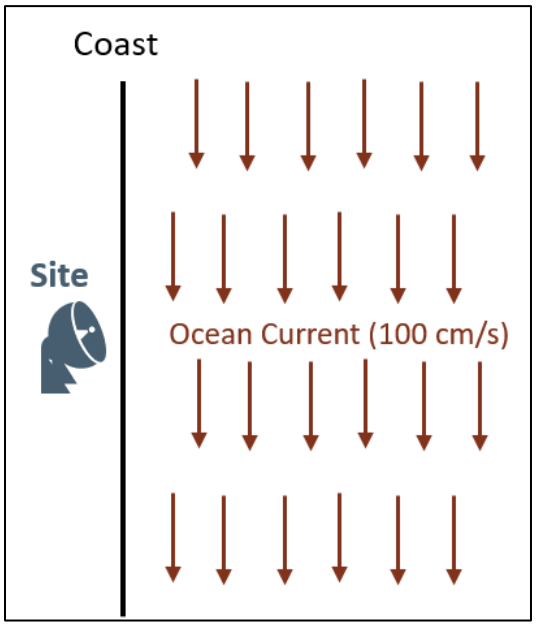

Figure 25 - Illustration of ocean currents added in example of clutter generation

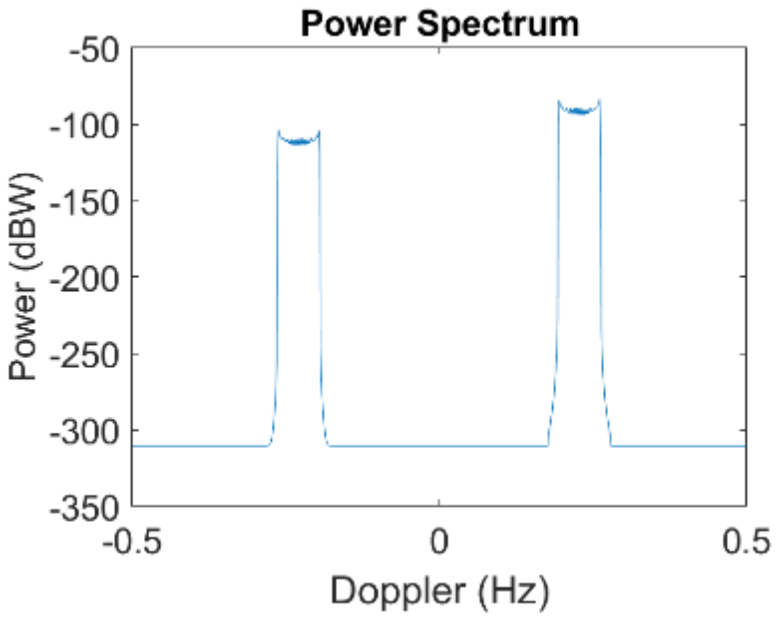

Figure 26 - Plot of the Bragg scatter power in range bin 5 (centered at 30 km). The negative Doppler Bragg peak is set to contain 1% of the total power in Bragg scattering for a fully developed sea. An ocean current of 100 cm/s tangential to the coast is also added into the spectrum.

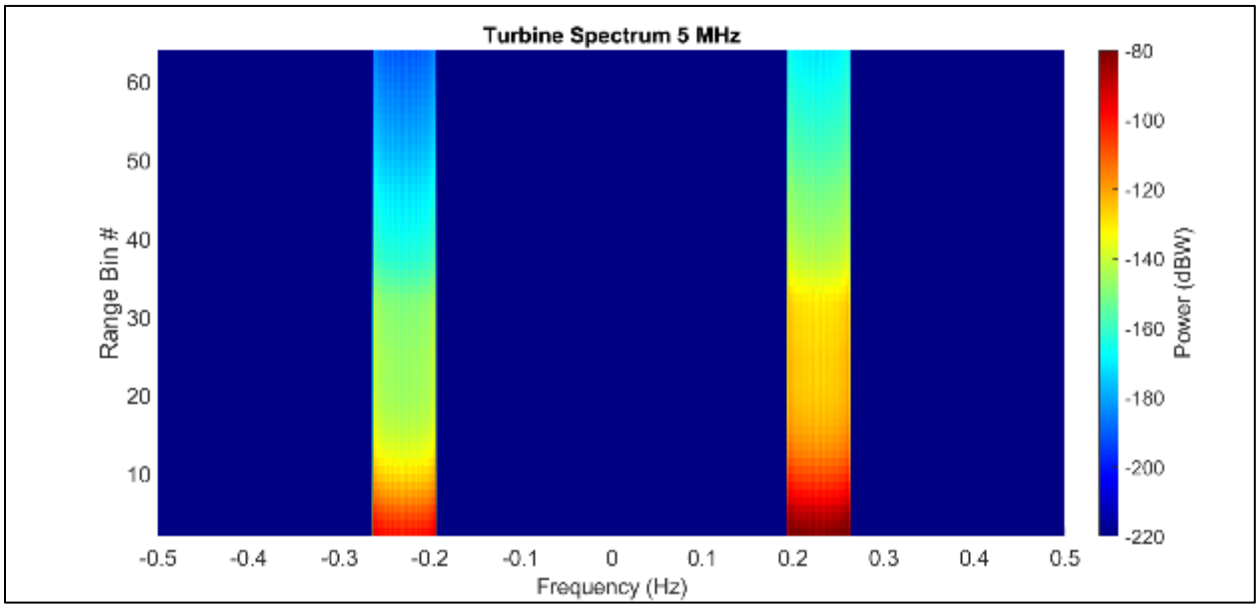

Figure 27 - Plot of the Bragg scatter power in the range-Doppler matrix. The negative Doppler Bragg peak is set to contain 1% of the total power in Bragg scattering for a fully developed sea. An ocean current of 100 cm/s tangential to the coast is also added into the spectrum.

In the modeling of sea clutter, Booz Allen did not simulate higher order sea clutter which includes higher order effects such as multiple scattering or interactions between waves of different wavelengths.

2.4.5.2 *Propagation Modeling*

The propagation of HF radio waves over a conducting surface can propagate via a surface wave which can allow for OTH capability. This mechanism occurs by electric currents induced on the surface of the Earth which will cause the radio wave to follow the curvature. The nature of the ground will determine the amount of attenuation that occurs with good conductors, such as seawater, being capable of transmitting for long distances. Due to the ground not being a perfect conductor these ground waves will be attenuated as they propagate along the surface. The amount of attenuation that occurs in this propagation mode is strongly dependent on the radio frequency used with higher frequencies being more greatly attenuated. This mode of propagation will also quickly attenuate horizontally polarized waves, so vertical polarization is needed for systems utilizing this propagation mode. Figure 28 below shows attenuation of ground wave propagation for various frequencies.

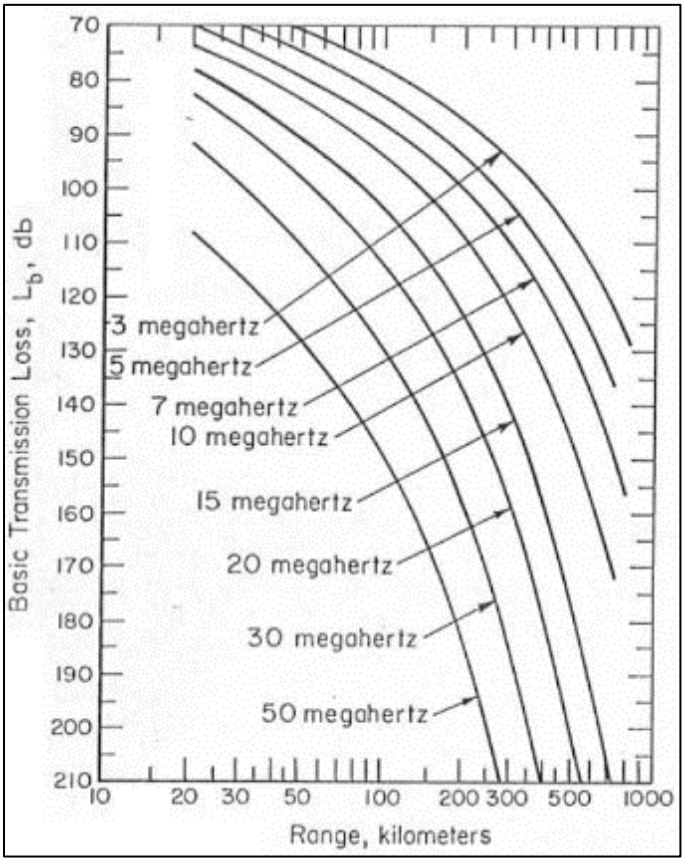

Figure 28 - One-way basic transmission loss of ground wave propagation. This is assuming a 4/3 scale Earth and a water conductivity of 4 $\Omega^{-1}m^{-1}$. (Barrick, Theory of HF and VHF Propagation Across the Rough Sea, 2, Application to HF and VHF Propagation Above the Sea, 1971)

To model this form of radio wave transmission, Booz Allen used a lookup table to compute the transmission loss. In modeling this propagation, Booz Allen ignored extra attenuation due to the surface roughness which can cause an additional few dB of loss. Effects of transmission to an elevated target were ignored as opposed to one on the ground which will have a minor impact for the heights of the turbines (Barrick, Theory of ground-wave propagation across a rough sea at dekameter wavelengths, 1970)

Modeling the turbines for the SeaSondes is done in WindTRx using the same method as for the other types of radar that were considered. After generating the turbine signals, they were run through the double FFT processing which is done by the SeaSonde systems to generate a range-Doppler map.

The waveform that is used by the SeaSonde systems is a pulsed linear frequency modulated (LFM) with a 50% duty cycle. The pulse duration of the SeaSondes is very long (on the order of ~1s) and relies on the LFM to conduct the ranging of the system.

The processing of signals in the SeaSonde systems use a double FFT processing method to generate range and Doppler of signals. The received signals are mixed with a replica of the transmitted signal and sent through a low-pass filter to generate a dechirped signal. The phase of this dechirped signal will have the following form,

$$\phi_{dechirp} = \phi_T(t) - \phi_T(t - t_d), \tag{3}$$

where $\phi_T(t)$ is the transmitted signal's phase at time t, $t_d = \frac{2R(t)}{c}$ is the time delay for a signal at range R. The transmitted signal's phase at time t is

$$\phi(t) = \omega_c t + \pi k t^2, \tag{4}$$

with k being the slope of the LFM, and ω_c being the carrier angular frequency. The first FFT will extract the range of the signal and is done over samples within the LFM sweep. The second FFT will be then done over multiple of these samples to extract Doppler. In doing this processing the system relies on the phase changing rapidly due to the slope of the LFM chirp for returns at different ranges while the Doppler contributions to the phase change being much slower. This is valid for SeaSonde systems. For more information see (Barrick, FM/CW Radar Signals and Digital Processing, 1973).

The model generates fast-time, slow-time samples. After the fast-time, slow-time matrix is generated, each column and row are convolved with a hamming window to better mirror the SeaSonde processing. The model uses 512 fast-time samples for each type of SeaSonde which are modeled. After doing the first FFT to generate the range bins the negative range bins are removed. Figure 30 shows the range-Doppler matrix at the sampling rate of 512 Hz for a single turbine in a 5 MHz system. The slow-time sampling rate is at 1 Hz and has 1024 samples.

Figure 29 and Figure 30 compare the signals from the RCS that the WindTrx model generates for a 12 rpm turbine to a report from BOEM on turbine impacts to Coastal Ocean Dynamics Applications Radar (CODAR) systems (Trockel D, 2018). The same frequencies occur in the range-Doppler map for the turbine signatures, though there is a difference in overall signal level. This difference is due to the difference in RCS phenomenology used between the two models. Figure 31 shows the RCS spectrum for a turbine spinning at 5.2 rpm, which is used throughout our results section and is displayed here for reference. Table 6 lists parameters that are used in our model.

Table 6 – SeaSonde Parameters

Frequency	LFM Bandwidth	Sweep Period	Sampling Rate	Range Bin Size	Number of slow-time samples
5 MHz	25 kHz	1.0 s	512 Hz	6000 m	1024
15 MHz	50 kHz	0.5 s	1024 Hz	3000 m	1024
25 MHz	150 kHz	0.25 s	2048 Hz	1000 m	1024

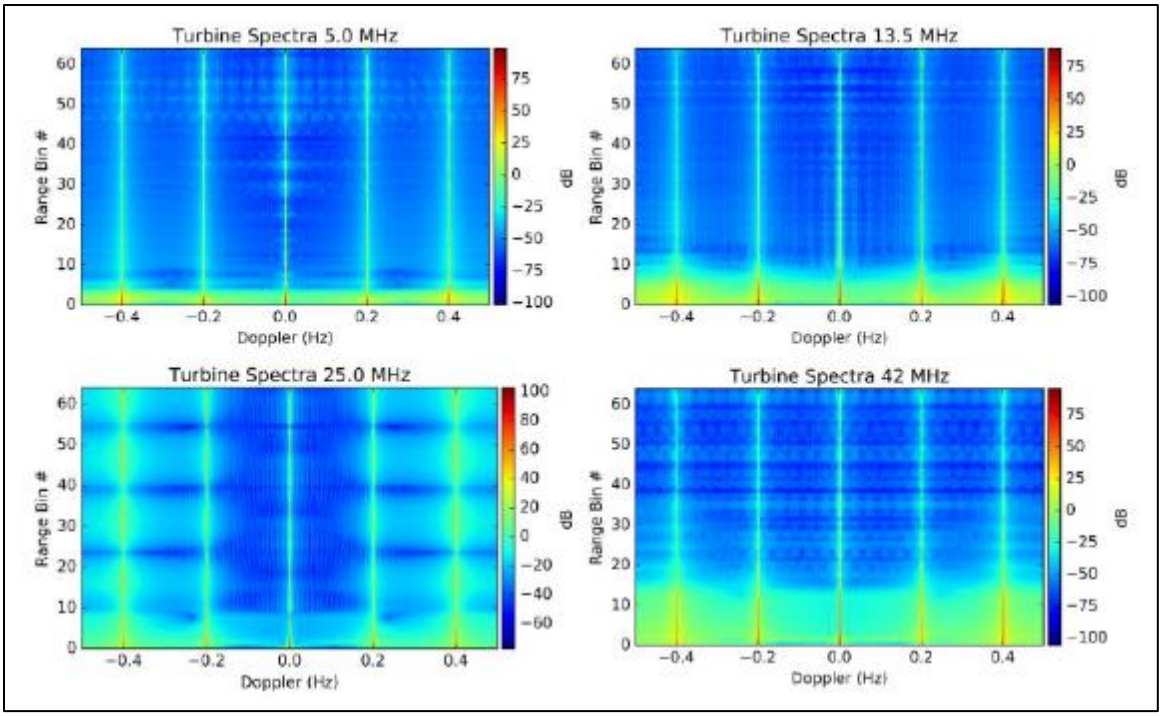

Figure 29 – This shows the range-Doppler matrix of the turbine spectrum from the simulations used in (Trockel D, 2018). Figure take from (Trockel D, 2018).

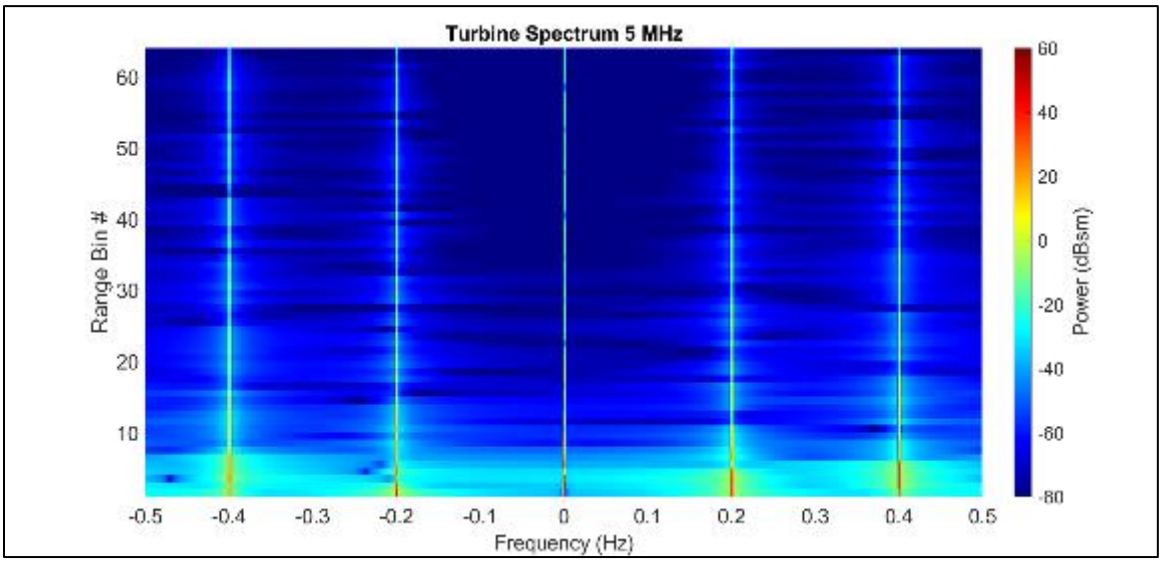

Figure 30 – Turbine spectrum coming out of a 5 MHz SeaSonde in WindTRx with a fast-time sample rate of 512 Hz. Single turbine at 6 km spinning at 12 rpm.

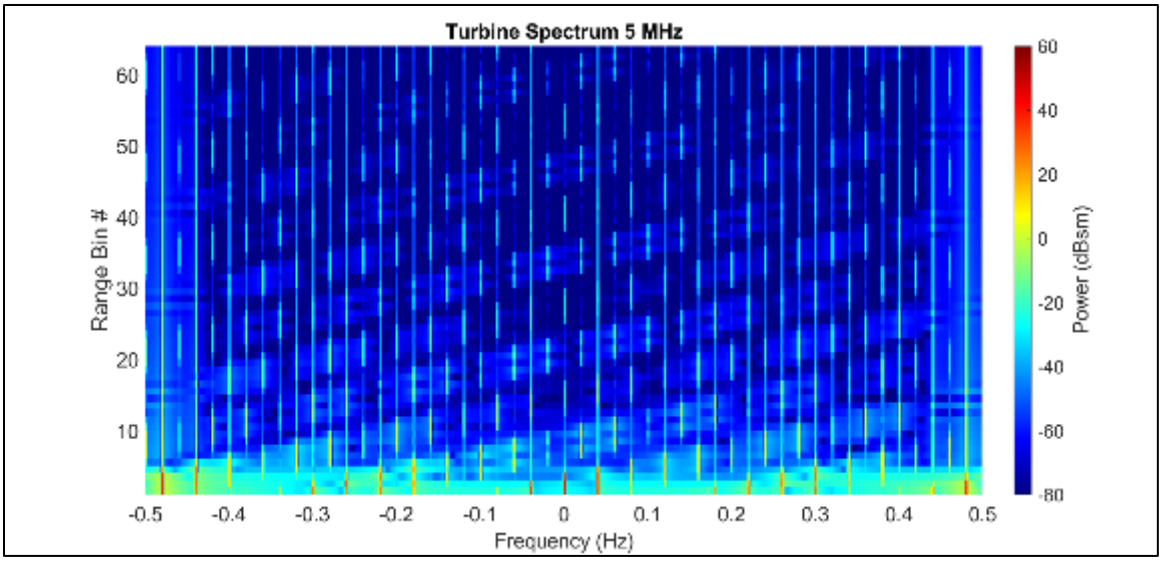

Figure 31 – Turbine spectrum coming out of WindTRx with a fast-time sample rate of 512 Hz. Single turbine at 6 km spinning at 5.2 rpm.

Since Booz Allen did not have access to information on system losses/noise figures for the SeaSondes and are not simulating second order sea scatter, the analysis was restricted as a comparison between relative strength of the first order sea return and the turbine signals. This means that the magnitudes of the power returns in actual operations will differ from the values presented in this report for the SeaSondes. The relative magnitudes of the turbine to the first order echo are the metrics that are being used for this analysis.

The SeaSondes being modeled use three co-located antennas, one whip and two loop antennas oriented perpendicular to each other, to resolve direction of arrival of signals. The model generated signals for all three antennas. For this analysis the ideal case for SeaSonde antenna patterns was considered for all systems due to lack of measured patterns for the various sites of interest near wind farms.

Once the signals are generated for each of the three antennas, they were combined for the cross spectra for the turbines. These cross spectra will form a 3×3 matrix will have elements denoted as,

$$V_{ij} = V_i V_j^*, \tag{5}$$

where V_i is the complex voltage return from the ith antenna, with antenna 1 being the omnidirectional antenna and antennas 2 and 3 being the two loop antennas. From this cross-spectra the boundaries of the Bragg region were then selected out at first order which are called first order lines (FOL). Once the FOL has been determined the angle of arrival for each range-Doppler bin in the FOL is found used to compute the surface current for each angle.

The modeled sea returns only included first order returns and did not generate second order returns which would be necessary to duplicate the FOL selection for SeaSonde systems. Booz Allen instead modeled the FOL selection with a stand-in technique to select FOL regions because second order returns were not generated. In selecting the FOL region, a CFAR-like technique was used to select the edges of the Bragg region. Our method for FOL selection is used on each range bin independently of other range bins. This method is not the method that is used in the SeaSonde systems but should only provide an estimate of what the systems would select in the presence of turbines.

The method that is used in the WindTRx model uses two tests when determining the FOL and are shown visually in Figure 32. The cells being tested start at the Doppler bin which contains the Bragg frequency for the radar of interest and becomes the cell under question. The algorithm then checks to see if the cell

has passed both tests used to determine the FOL, and if it does not satisfy both conditions, the algorithm then moves onto the cell to the right (left) to determine the upper (lower) edge of the FOL. The first test checks if the averaged power of the cell under question and adjacent bins is 13 dB above the averaged power of the 5 bins to the right (left) when determining the upper (lower) edge of the FOL. The 13-dB threshold choice is a standard CFAR threshold used in radar operations which is the reason it is used in this application. The second test is to ensure that cell under question is five times that of any of the cells to the right (left) used in finding the upper (lower) edge of the FOL. This was done to ensure a sufficiently strong return was not averaged out in the first test and prematurely find the edge of the FOL region. Once both tests have succeeded, the edge of the FOL is declared as the current cell under question. An example of the results of this method for selecting the FOL region is shown in Figure 33 where in addition to the Bragg scatter, a single turbine spinning at 12 rpm was added to demonstrate possible induced errors.

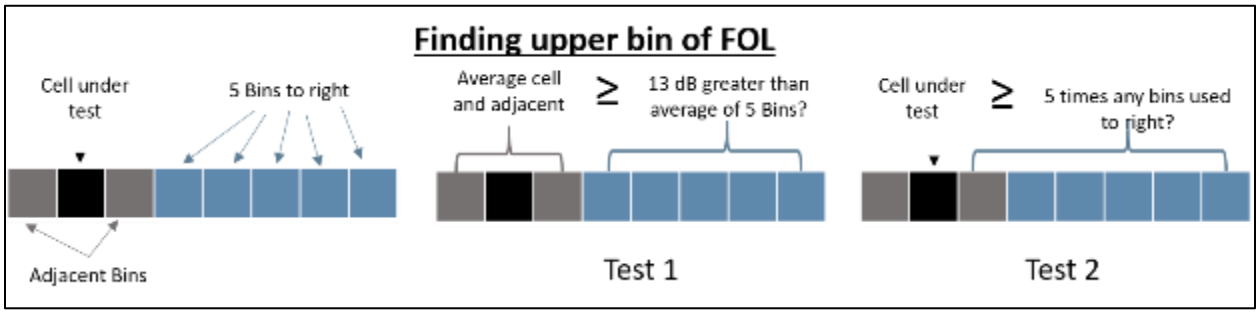

Figure 32 - Pictorial representation of the tests done for finding the upper bin of the FOL of one of the Bragg peaks. The first cell that succeeds both tests is declared to be the upper bin of the FOL.

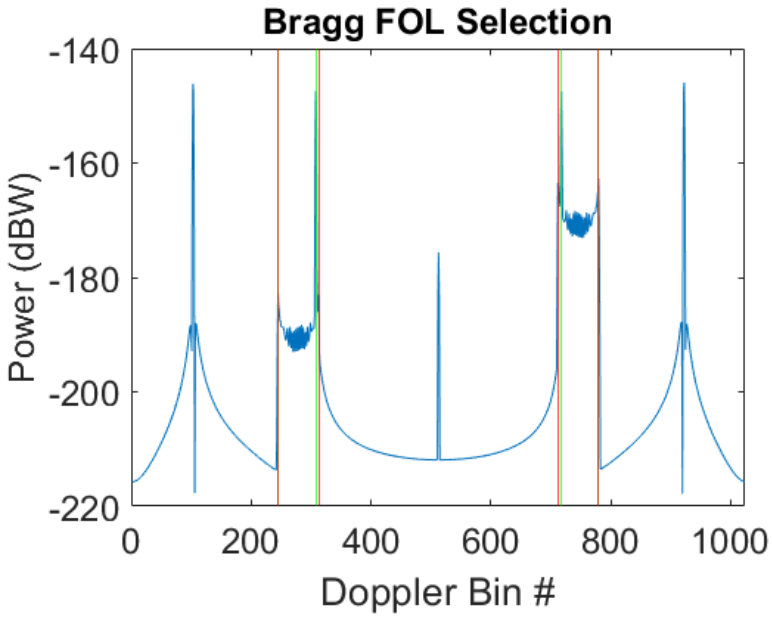

Figure 33 - Bragg FOL selection for the case with Bragg clutter returns and returns from a single turbine spinning at 12 rpm. The red vertical lines are showing where the selection algorithm is choosing the FOL lines to be in the absence of turbine interference, while the green line is where the algorithm selects the region with the addition of turbine interference.

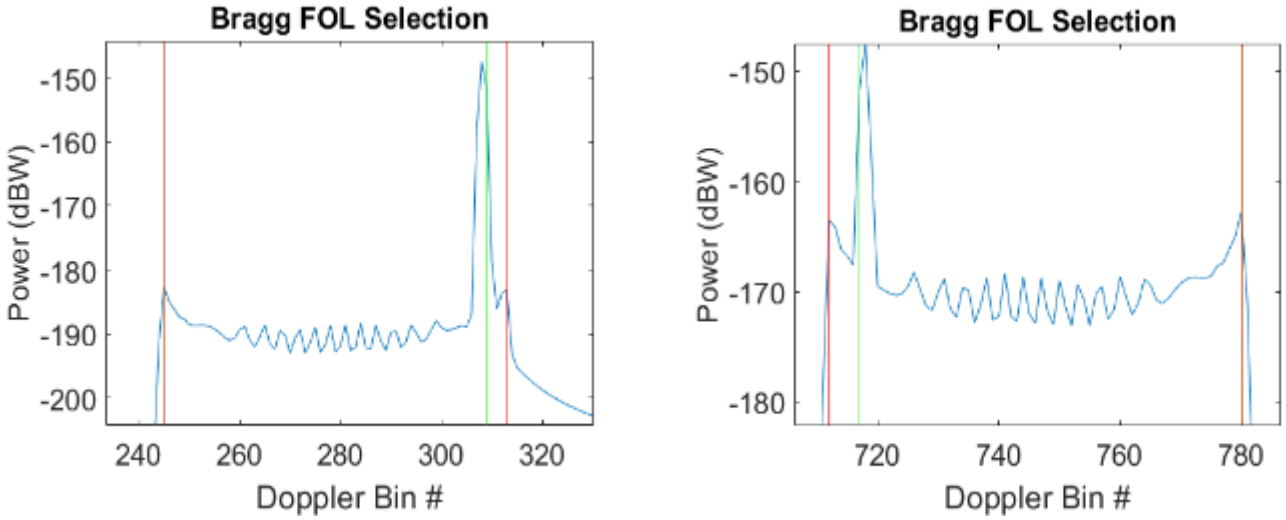

Figure 34 - Zoomed in cross-sections of Figure 33. The turbine interference is removing bins from consideration in the Bragg region.

Once the FOL regions have been selected, the SeaSondes would then perform processing to determine the angle of arrival for each Doppler bin in the FOL. The CODAR SeaSonde systems utilize the MUltiple Signal Classification (MUSIC) algorithm, which uses an eigenfunction analysis to produce both single- and double-angle solutions (Lipa, Nyden, Ullman, & Terrill, 2006). The model used simple geometry of returns to determine an angle of arrival and only consider the single-angle solution.

The angle determination in WindTRx is done by comparing the V_{12} and V_{13} cross spectra. The two cross spectra should ideally be functions of the sin and cos of the angle of arrival from the two loop antennas which are oriented perpendicular to each other. Actual antenna patterns of a deployed system will deviate from the ideal pattern due to imperfections and terrain effects and would need to be measured as an input in the SeaSonde direction finding algorithms. The simple solution for finding the direction of arrival used in WindTRx is to determine the angle by the ratio of the cross spectra in each Doppler bin in the FOL. The angle of arrival (θ) is then determined as,

$$\theta = arctan\left(\frac{V_{12}}{V_{13}}\right). \quad (6)$$

Once the angle of arrival for each Doppler bin in both the positive and negative FOL are determined the angles of arrival are then placed into angular bins which are at 5° increments.

To compute the radial current velocities, Booz Allen evaluated each range-angle bin and which Doppler bins are contained within that bin. The current velocity was measured as a shift in the Doppler frequency from the center of the Bragg peaks. Each range-angle bin can have multiple Doppler bins contained within from both the positive and negative Bragg peaks and the resulting Doppler measurement offset for that bin is taken as the average of the Doppler offsets from the corresponding Bragg peak (positive or negative). This offset was then converted to a current velocity.

2.5 MITIGATION TECHNIQUES

Proposing methods to mitigate the detrimental impact of wind turbine clutter/interference (WTCI) involved not only collecting a broad catalog of existing and proposed mitigation methods, but also evaluating the potential benefit and feasibility of the methods (Figure 35). For example, a siting

modification or design change to a radar may be expected to provide some benefit to the operation of the system, but it is possible that the specific proposed technique is not feasible for other reasons, such as cost, other competing plans, or other detrimental impact to the radar capability. For that reason, the research team leveraged a number of interviews with subject matter experts (SMEs) to provide further insight and filtering of the mitigation techniques. Published documents and interviews are cited in the following paragraphs where applicable.

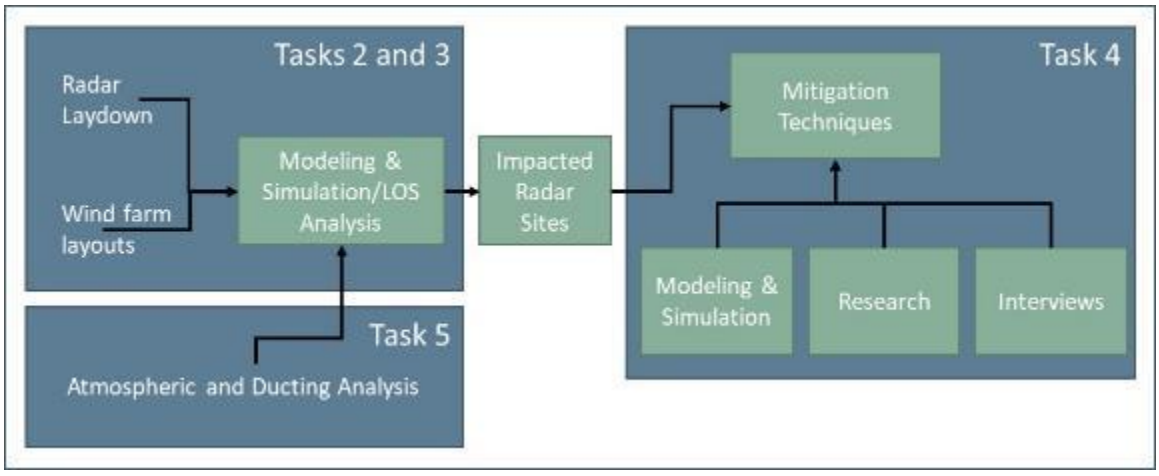

Figure 35 - Mitigation Techniques Methodology

2.6 DUCTING ANALYSIS

2.6.1 Data/Background

Radar waves propagating through the atmosphere may encounter conditions that can alter radar propagation and affect the accuracy of the radar return. Atmospheric ducting is one such scenario in the atmosphere. Ducting events, which will be explained in detail later, can effectively "trap" radar emissions in the lower atmosphere due to strong vertical density and refractivity gradients, causing radar waves to propagate differently than intended. To help assess general atmospheric conditions, including ducting, at offshore wind farms, a weather analysis was performed. The goals of the weather analysis were:

1. Identify a data source that could describe atmospheric conditions at offshore wind farms
2. Generate seasonal averages of vertical profiles at select offshore wind farm locations
3. Analyze vertical profiles to characterize frequency and proclivity of atmospheric ducting events at these locations
4. Identify real-world ducting examples from archived datasets

Accomplishing these goals supported the project effort by providing seasonal averages to assist the radar model's simulations at wind farm locations by incorporating prevailing atmospheric conditions. In addition, an understanding of the frequency and proclivity of ducting scenarios at these locations assisted in characterizing the likelihood of wind farm interference on radars. The potential interference due to ducting would be via wind farms appearing closer to the radar than their actual horizonal distance.

2.6.2 Data Methodology

The research team identified, processed, and analyzed atmospheric weather data to characterize the vertical profiles at locations indicative of the offshore wind farms considered for this project. The team

also evaluated vertical profile data at select coastal NEXRAD locations near the offshore wind farms. These vertical profiles helped determine the proclivity and frequency of ducting events at the aforementioned locations. The team set out to identify existing data sources that could be leveraged to provide data on a resolution that was both spatially and temporally effective for representing seasonal conditions at offshore wind farms. The NWS High-Resolution Rapid Refresh (HRRR) model was selected as the data source.

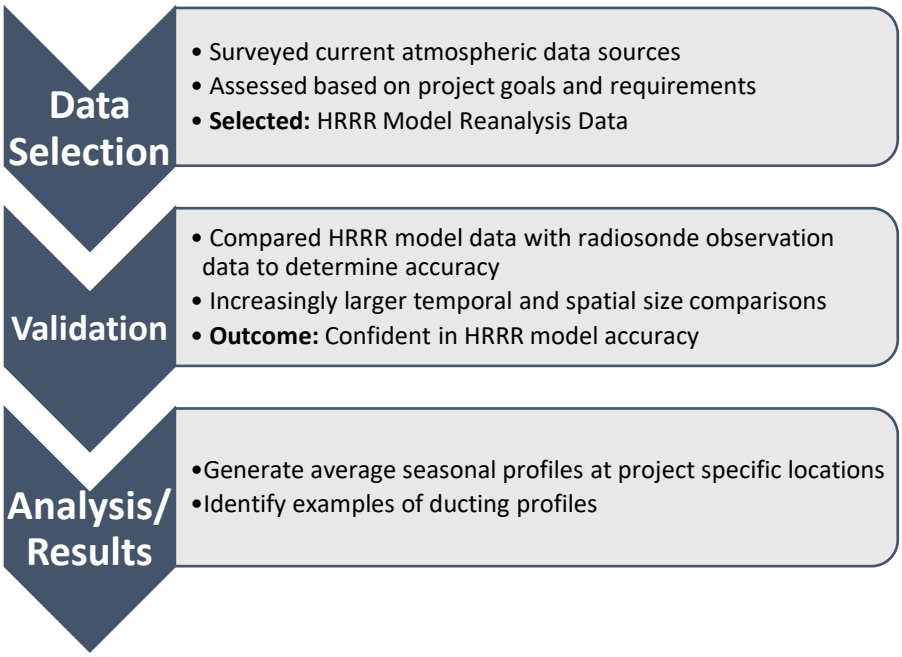

Figure 36 - Ducting Analysis Methodology

The vertical profile data from this model was then ingested, processed, and key variables were selected for analysis. Before generating final results, the team performed several validation steps to ensure the model data was appropriate and could be confidently leveraged for this effort. The validation compared the model output against observation data in order to quantify any variation. Once confidence in the model was established the team generated seasonal averages of the vertical profile data and performed an analysis of ducting frequency at project specific locations.

3 RESULTS

This section provides the results of our analyses. Section 3.1 provides the results of the radar modeling, Section 3.2 provides the results of the mitigation techniques analysis, and Section 3.3 provides the results of our ducting analysis.

3.1 RADAR MODELING

This section provides the results of our radar modeling and presents radar interference results for each of the nine wind farms. Under each wind farm section, there are subheadings for each radar type affected.

For SeaSonde results sections, most wind farms will see impacts to a larger number of SeaSondes (typically 7-10 per wind farm) with very similar results. In these instances, the results section presents a range of selected radars to "tell the story" of SeaSonde interference for that particular wind farm, without the inclusion of many additional, similar results. All LOS plots developed for this study, including all SeaSonde plots, can be seen in Appendix A.

The results for the SeaSondes are classified in terms of lettered classes due to similar levels of interference. This section provides detailed walk-throughs of one of each class of interference rather than each individual radar. Each class will have a detailed example for the first instance of that class appearing as each wind farm is discussed. Table 7 details the list of classes being used along with a short description of the class. The table is divided into three sections for each class of SeaSondes: long range 5 MHz systems (~200 km), medium range (~70-100 km) 13-16 MHz systems, and short range (~40 km) 25 MHz systems. The cumulative scenario will be discussed on its own due to the very large number of turbines.

Table 7 - Class of Interference Descriptions

Class of Interference	Description
A	Short range SeaSonde with small wind farm at long range for system
B	Short range SeaSonde with large wind farm at mid-long range for system
C	Medium range SeaSonde with small wind farm at mid-range for system
D	Medium range SeaSonde with small wind farm at long range for system
E	Medium range SeaSonde with large wind farm at short range for system
F	Medium range SeaSonde with large wind farm at mid-long range for system
G	Long range SeaSonde with small wind farm at short-mid range for system
H	Long range SeaSonde with large wind farm at short-mid range for system
I	Long range SeaSonde with large wind farm at long range for system

3.1.1 Vineyard Wind

Vineyard Wind had been proposed to BOEM in a COP when this report was written and is within LOS of one ASR-9, one ASR-8, and six SeaSonde radars. It is located in the RI/MA leasing area (lease OCS-A-0501) and has 106 10-MW turbines.

3.1.1.1 *ASR*

The ASR-9 at Nantucket (code ACK) has LOS to the Vineyard Wind farm turbines. Figure 37 below shows the LOS to the turbines. The outer edge of the red band is the LOS distance to the lowest point on

the turbine blades, the orange band shows the LOS distance to the turbine hub, and the yellow band is to the highest tip of the blades. The majority of Vineyard Wind turbines are visible from to the hub, with a few of the closest turbines having 100% visibility of the blades.

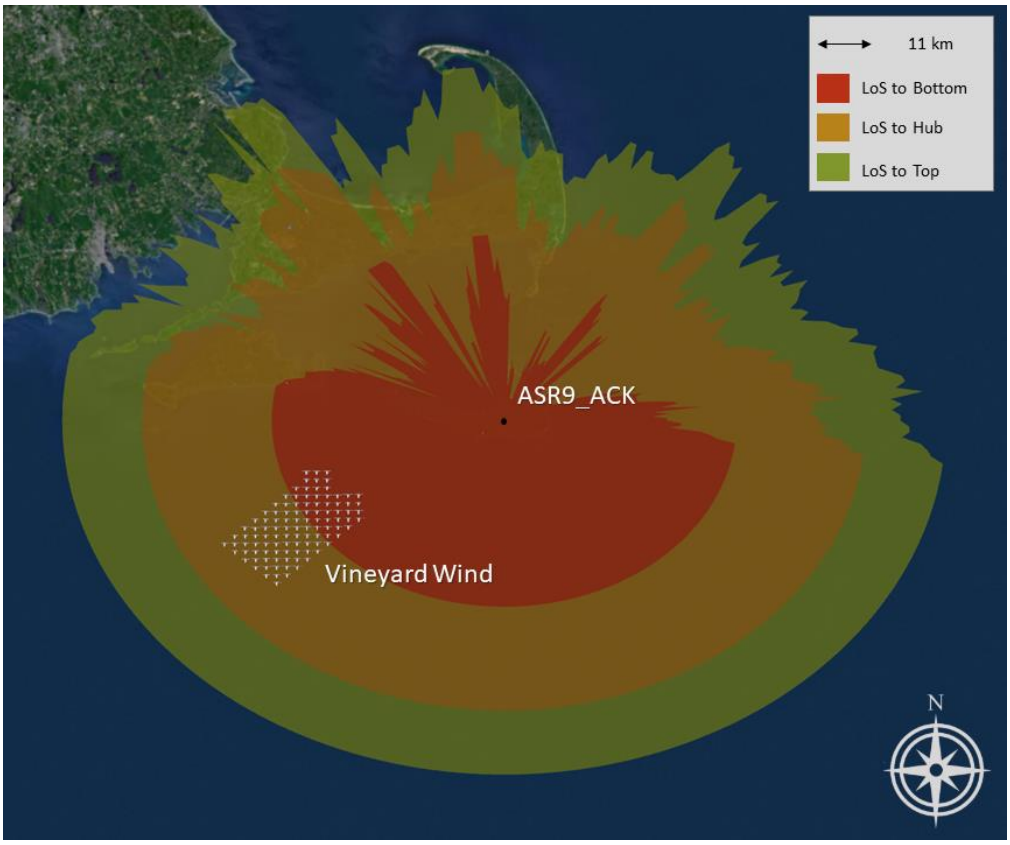

Figure 37 - Nantucket ASR-9 LOS to Vineyard Wind

There are two primary ways that the wind farm will impact the ASR-9. The first is by creating plots on the wind turbines themselves. Figure 38 shows raw detections of the ASR-9 ACK CFAR in the direction of Vineyard Wind. In the ASR-9 these detections would next be run through detection correlation algorithms to form plots and tracks. The proposed Vineyard Wind farm is short range to the ASR-9 in Nantucket. As a result of the close range (30 km to closer turbines) the signal return is large enough that the "range ring" effect is seen from sidelobe returns exceeding the CFAR threshold for detection.

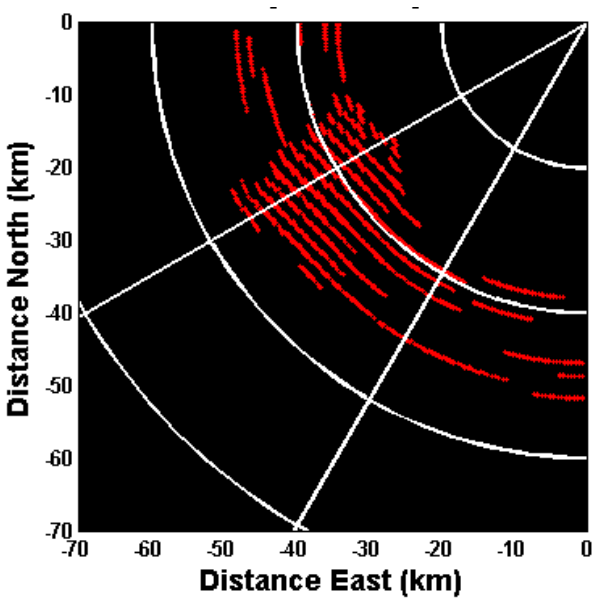

Figure 38 - ACK Raw Signal Detections from Vineyard Wind

The second impact is that the wind turbines will degrade the detections of an aircraft flying in the vicinity. Figure 39 shows the signal level required to declare a CFAR detection in the vicinity of Vineyard Wind for a small aircraft (0 dBsm) flying at 2 km altitude. The CFAR algorithm is described above in Section 2.4.3.5. The plots below should be interpreted as everywhere there is a signal to interference ratio of 13 dB or larger, a detection would be declared in that region. Range-Doppler cells around the wind turbines have a large interference level and would require a substantially larger aircraft RCS in order to achieve detection, regions below the 13 dB threshold show where the wind turbine signals are contributing to the CFAR floor and are likely to prevent aircraft in the vicinity from being detected. The subsequent figures, Figure 40 and Figure 41 show the interference for an aircraft when flying at higher altitudes, 5 km and 10 km respectively. In this case, the 10 km aircraft is flying at a high elevation relative to the 2.4° peak of the ASR-9 antenna beam. As a result, there is less aircraft signal present, making the signal to interference ratio much smaller.

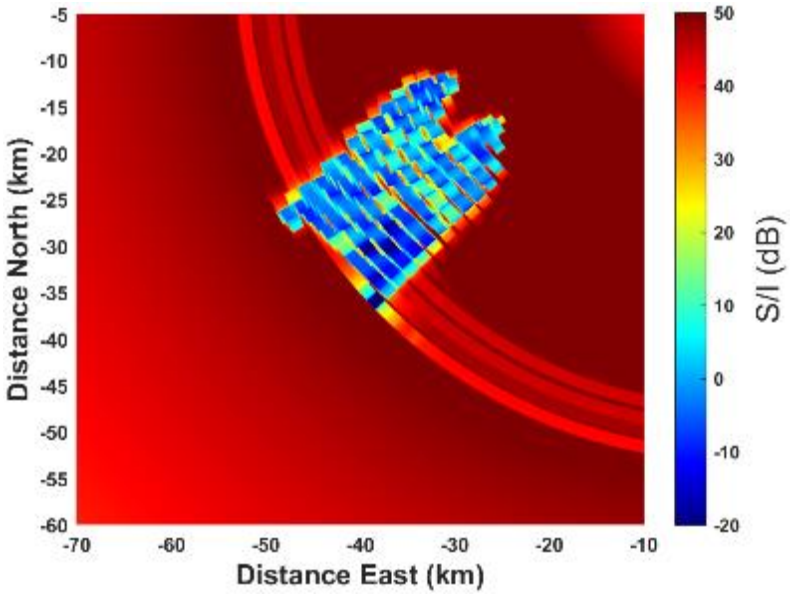

Figure 39 - Signal to Interference for a 0dBsm aircraft flying at 2km alt near ACK

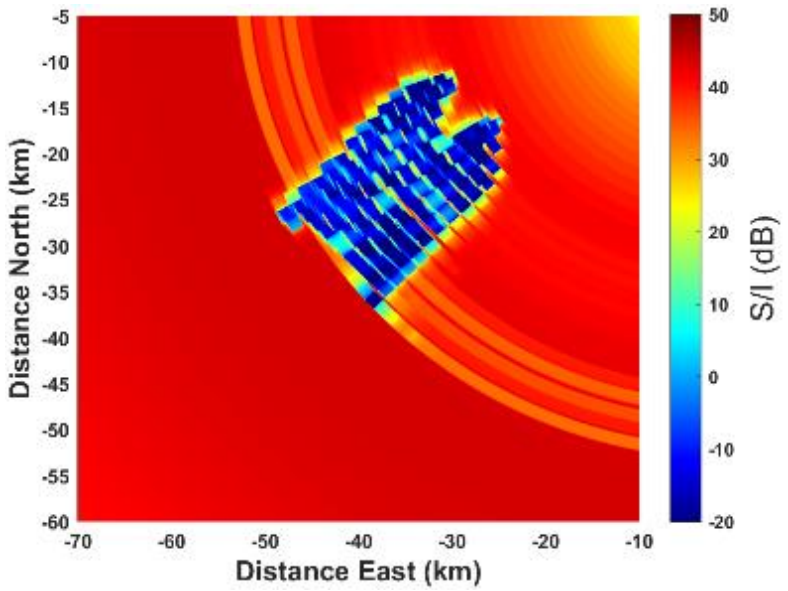

Figure 40 - Signal to Interference for a 0 dBsm aircraft flying at 5 km alt near ACK

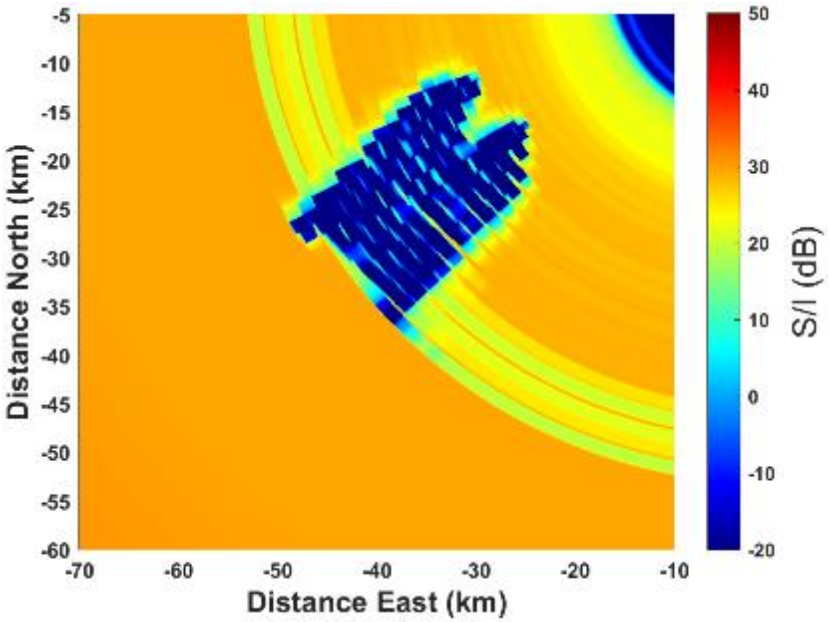

Figure 41 - Signal to Interference for a 0 dBsm aircraft flying at 10 km alt near ACK

The only other ASR within the vicinity of Vineyard Wind is the ASR-8 at Otis Airfield in Falmouth, MA (code FMH). This will have a similar level of interference as the interactions between the Bay State wind farm and the Warwick, RI (KPVD) ASR-9 discussed in more detail in the Bay State section.

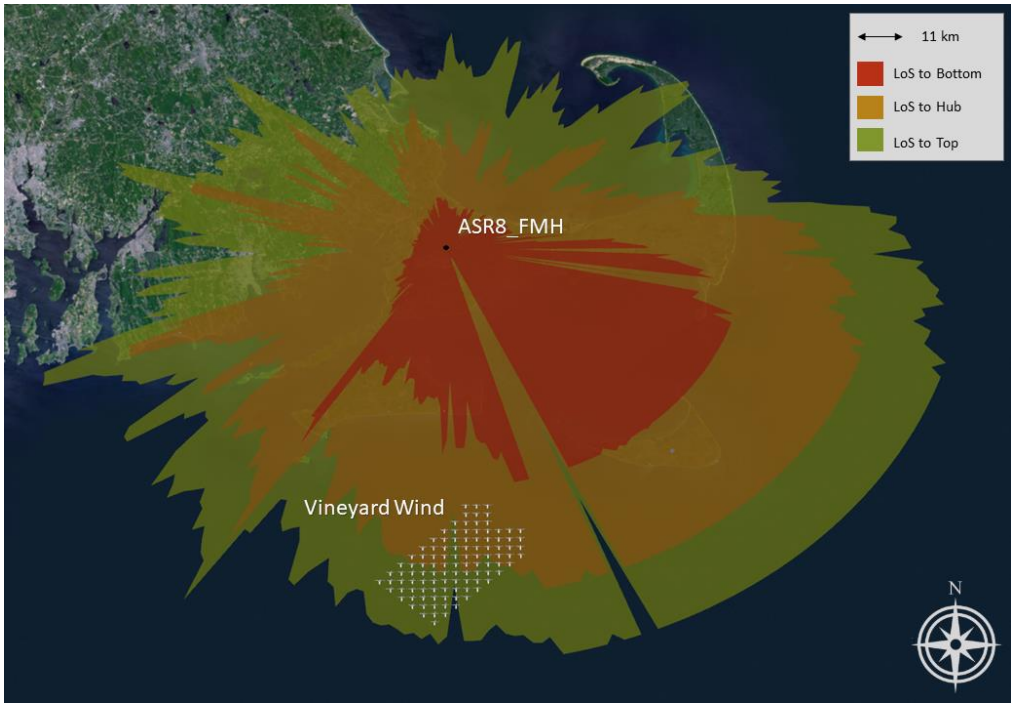

Figure 42 - ASR-8 FMH LOS to Vineyard Wind

3.1.1.2 *SeaSonde*

Table 8 - Impacted SeaSondes from Vineyard Wind

Impacted SeaSondes	Class of Interference
SQUB	B
LPWR	E
HBSR	F
NWTP	F
MVCO	H
NANT	H
AMAG	H

3.1.1.2.1 Short Range SeaSondes

There is only one short range SeaSonde that is in proximity to the Vineyard Wind farm. This is the SQUB SeaSonde located on Martha's Vineyard that is situated 30 km from the nearest turbine of Vineyard Wind. This will be class B interference which as discussed above. Since there are slightly fewer turbines (106 in Vineyard Wind vs. 110 in Bay State) and the turbines are ~10 km further away (see Figure 43), there will be less of an impact than shown above.

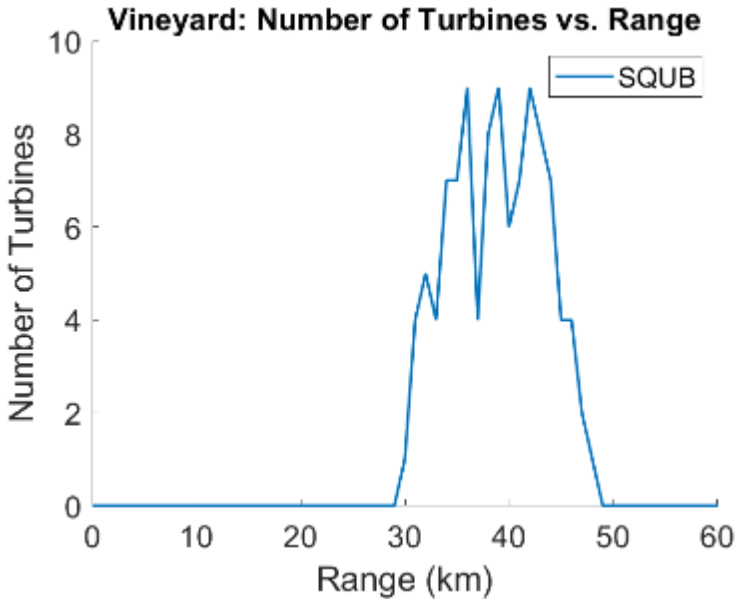

Figure 43 - Number of turbines in each range bin for the short range SeaSondes near the Vineyard Wind farm

3.1.1.2.2 Medium Range SeaSondes

There are three medium range SeaSondes in range of the Vineyard Wind farm (Figure 44). Two of these are at short range to Vineyard Wind and will fall into class E of interference where there is a large wind farm at short range. For the last SeaSonde, HBSR, the turbines will be at mid-range for the system which would place it in class F which is discussed above in the Bay State section. The HBSR system in combination with Vineyard Wind will have the turbines at further ranges than the example of this class of interference detailed in the Bay State section and thus will have less interference.

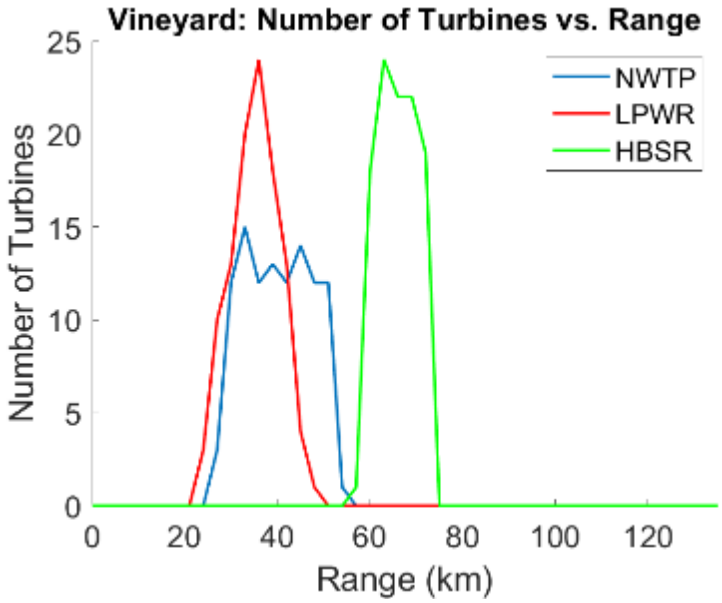

Figure 44 - Number of turbines in each range bin for the medium range SeaSondes near the Vineyard Wind farm

3.1.1.2.3 Long Range SeaSondes

There are three long range SeaSondes which are within range of the Vineyard Wind farm. All three of these, MVCO, NANT, and AMAG, are in class H for SeaSonde interference and will have results like what was presented above in the Bay State section for class H of interference.

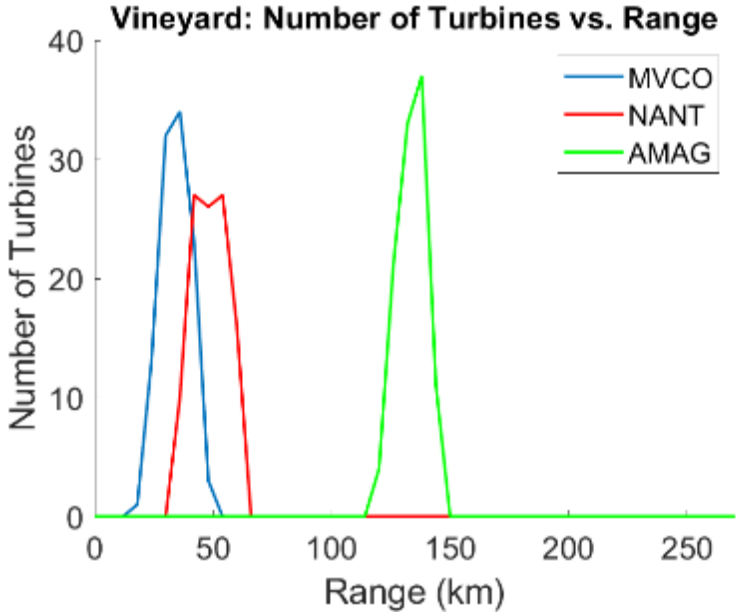

Figure 45 - Number of turbines in each range bin for the long range SeaSondes near the Vineyard Wind farm

3.1.2 Bay State Wind

Bay State Wind had been proposed to BOEM in a COP when this report was written and is within LOS of two ASR-9s, one ASR-8, and seven SeaSonde radars. It is located within the RI/MA lease area (lease OCS-A-0500) and has 110 15-MW turbines.

3.1.2.1 *ASR*

There are three ASRs near the Bay State Wind farm that were within LOS. There are two ASR-9s and one ASR-8 with potential line-of-sight, the ASR-9 at Nantucket, MA (ACK), the Providence/Coventry Tower ASR-9 in Warwick, RI (KPVD), and the ASR-8 at Otis Airfield in Falmouth, MA (FMH).

As shown in Figure 46, the ASR-9 ACK has LOS to all the Bay State Wind turbines. The outer edge of the red band is the LOS distance to the lowest point on the turbine blades, the orange band shows the LOS distance to the turbine hub, and the yellow band is to highest tip of the blades. The figure shows that the majority of Bay State Wind turbines are visible from the upper blade tip to the hub.

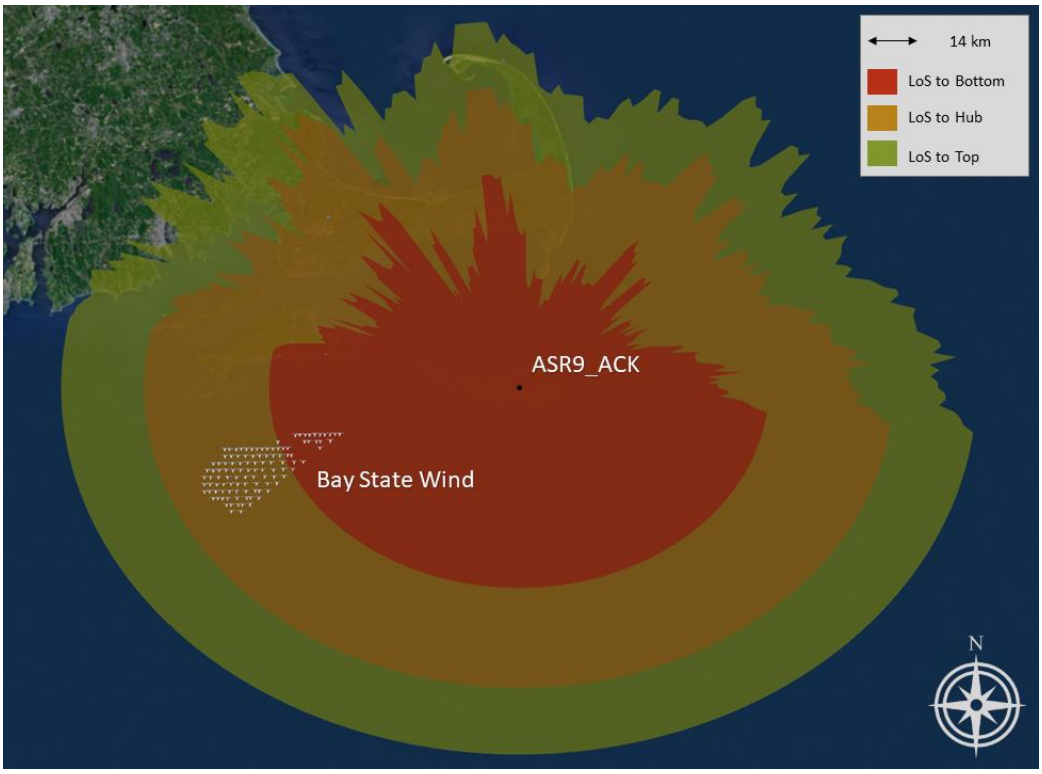

Figure 46 - Nantucket ASR-9 LOS to Bay State Wind

The Bay State Wind turbines are proposed to range from 8-MW to 15-MW capacity. Should a smaller turbine (10-MW) be selected, the impact will be similar to Vineyard Wind (Section 3.1.1). Figure 48 through Figure 53 below show the range of signal interference in the CFAR range-Doppler bins of ACK with the larger turbine size (15-MW) at Bay State Wind.

There are two primary ways that the wind farm will impact the ASR-9. The first is by creating plots on the wind turbines themselves. Figure 47 shows raw detections out the ASR-9 ACK CFAR in the direction of Bay State Wind. In the ASR-9 these detections would next be run through detection correlation algorithms to form plots and tracks. Although not all turbines may present as tracks after processing, it shows the difficulty the ASR-9 may have of maintaining an aircraft track in this field of false plots from the wind turbines.

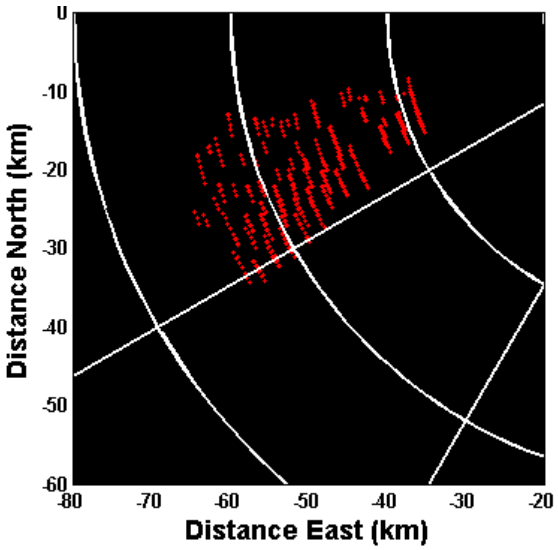

Figure 47 - ACK Raw Detections of Bay State Wind Turbines

Figure 48, Figure 50 and Figure 52 all show that at altitudes of 2 km, 5 km and 10 km, a smaller aircraft would be unlikely to be detected in the region of the turbines. The additional interference from the wind turbines at Bay State would make CFAR detections of a smaller aircraft highly unlikely.

Figure 49 and Figure 51 show that for larger aircraft (20 dBsm) the signal-to-interference ratio is high enough that CFAR detections of the aircraft would occur as it flies through the wind farm. Figure 53 shows the results of the WindTRx analysis for a 20 dBsm target at 10 km altitude the aircraft is also close to the CFAR threshold of 13 dB for a majority of the wind farm and suggests that ACK would have difficulty declaring CFAR detections for larger aircraft as well at 10 km altitude. Flight altitudes higher than 10 km would be further outside the elevation beam of the ASR-9 antenna and detection would be further impacted.

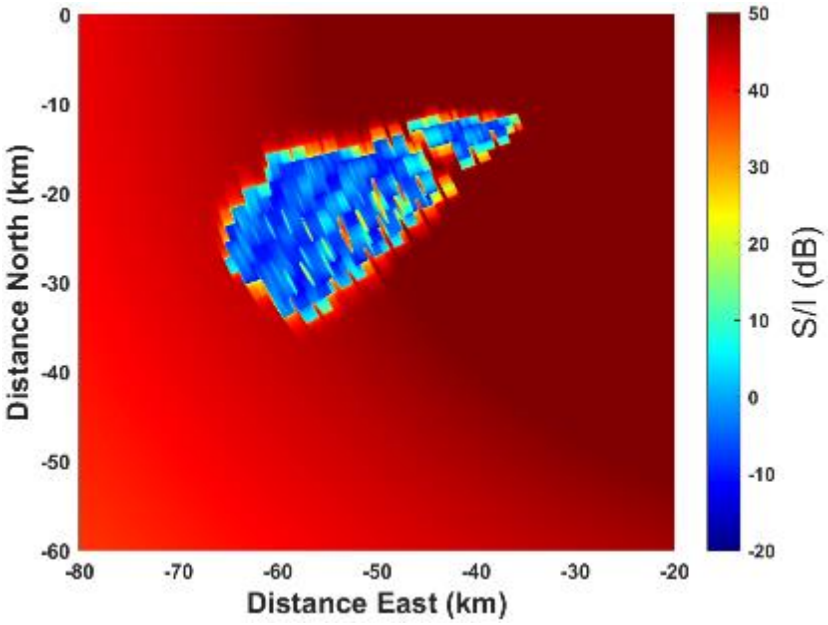

Figure 48 - Bay State Signal-to-Interference Ratio at ACK for a 0dBsm Aircraft at 2km Altitude

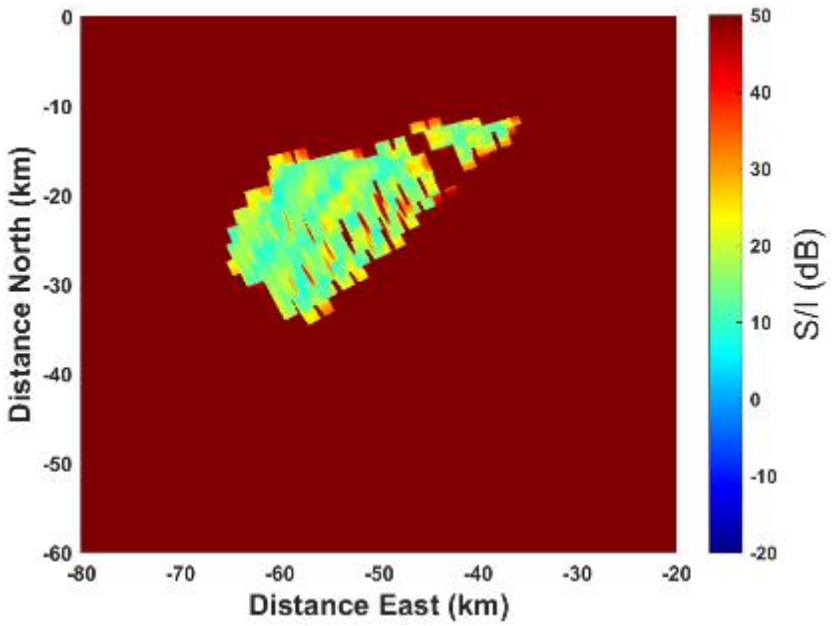

Figure 49 - Bay State Signal-to-Interference at ACK for a 20 dBsm Aircraft at 2 km Altitude

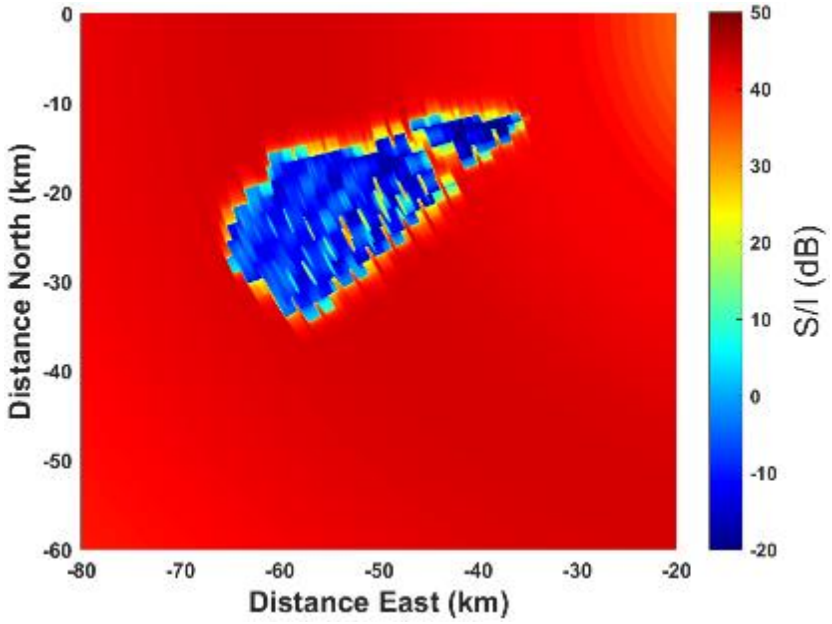

Figure 50 - Bay State Signal-to-Interference at ACK for a 0 dBsm Aircraft at 5 km Altitude

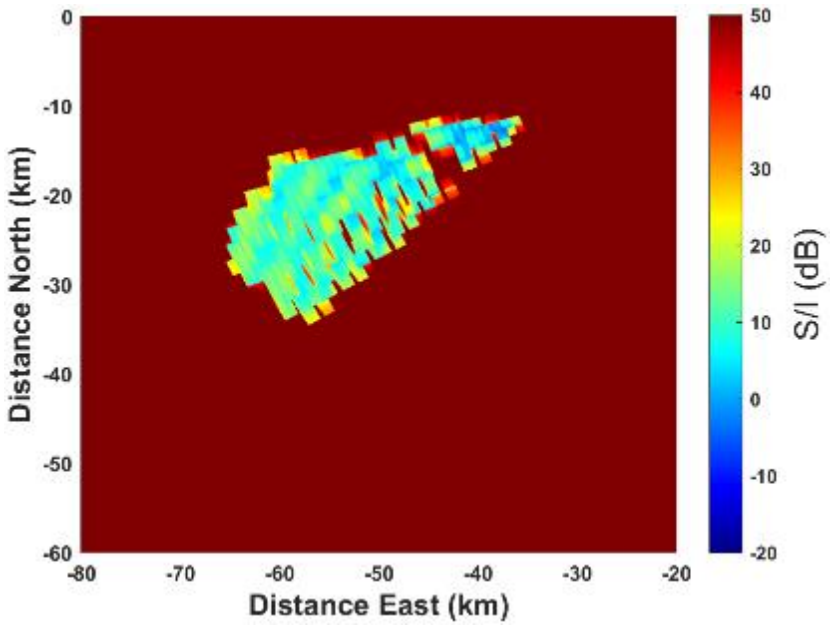

Figure 51 - Bay State Signal-to-Interference at ACK for a 20 dBsm Aircraft at 5 km Altitude

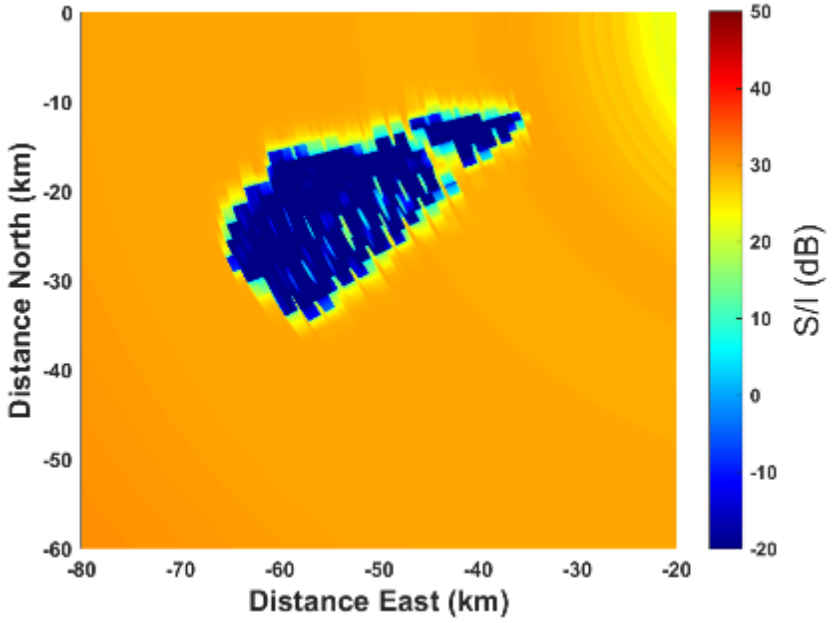

Figure 52 - Bay State Signal-to-Interference at ACK for a 0 dBsm Aircraft at 10 km Altitude

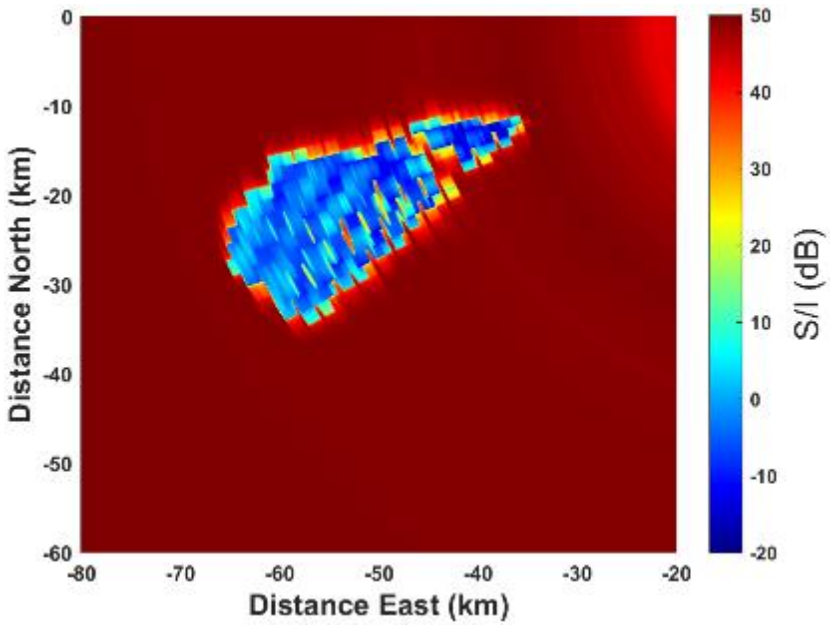

Figure 53 - Bay State Signal-to-Interference at ACK for a 20dBsm Aircraft at 10km Altitude

Figure 54 shows the ASR-9 in Warwick, RI in relationship to Bay State Wind. The majority of the turbines will have the upper portion of the blade within the LOS to KPVD.

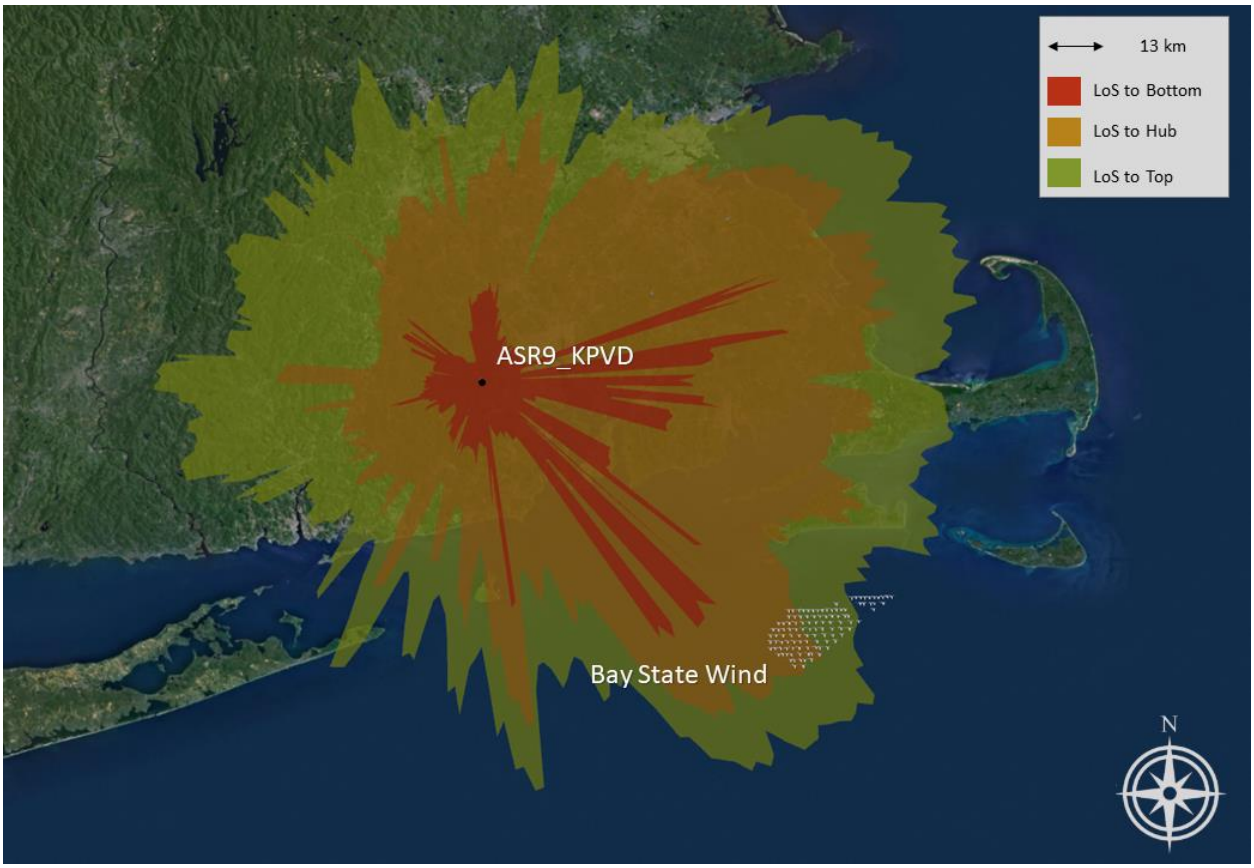

Figure 54 - ASR-9 KPVD LOS to Bay State Wind

Figure 55 below shows the WindTrx raw detections out of the KPVD CFAR process. Bay State Wind is 100 – 120 km away from KPVD, however there is still LOS to the turbines and with the large RCS of the turbines (see Section 2.4.1) the signal returns are still detectable even at this farther range. In Figure 56-Figure 58, the signal to interference ratio is shown for a 0 dBsm target at three different altitudes from which it is seen that there is a degradation of the radar performance over a section of the wind farm as opposed to the entire wind farm as with the ACK radar discussed above. The turbines near the edge of (but within) LOS do not have as large of an impact on the interference level and will require that the highest blade be closest to vertical to be seen as the radar sweeps past that azimuth which can lead to more or less interference as the radar rotation and blade angle coincide.

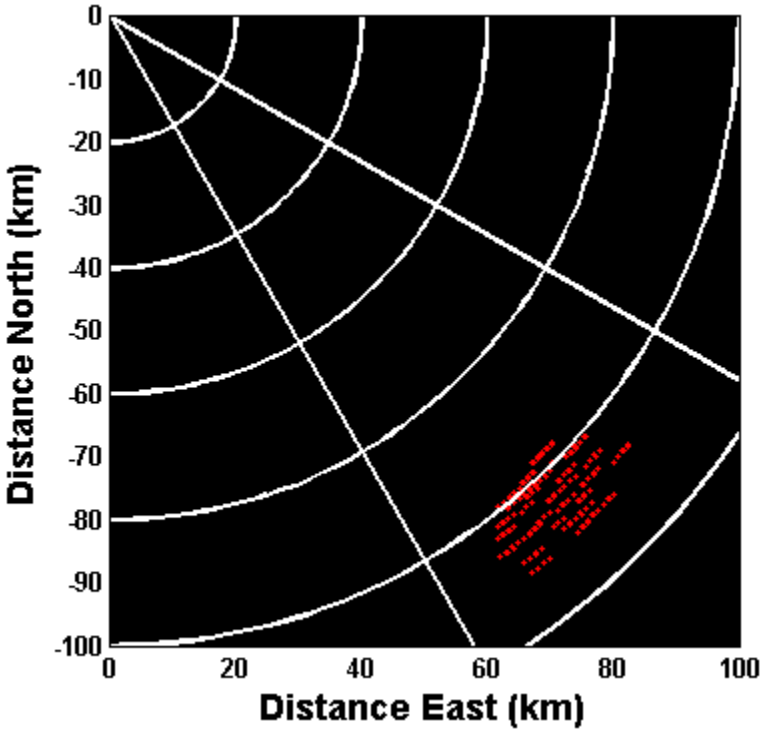

Figure 55: KPVD Raw CFAR Detections of Bay State Wind Turbines

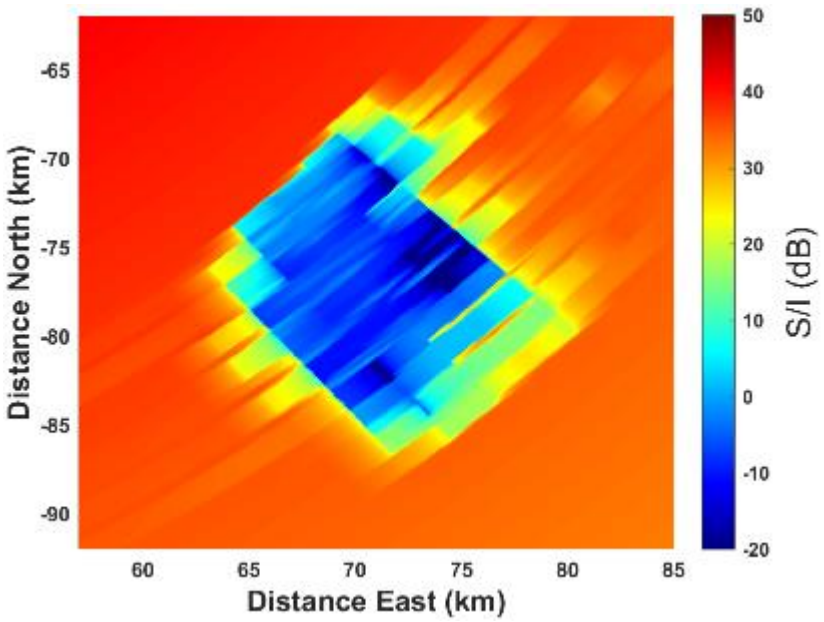

Figure 56 - Signal to Interference for a 0 dBsm aircraft flying at 2 km altitude near KPVD

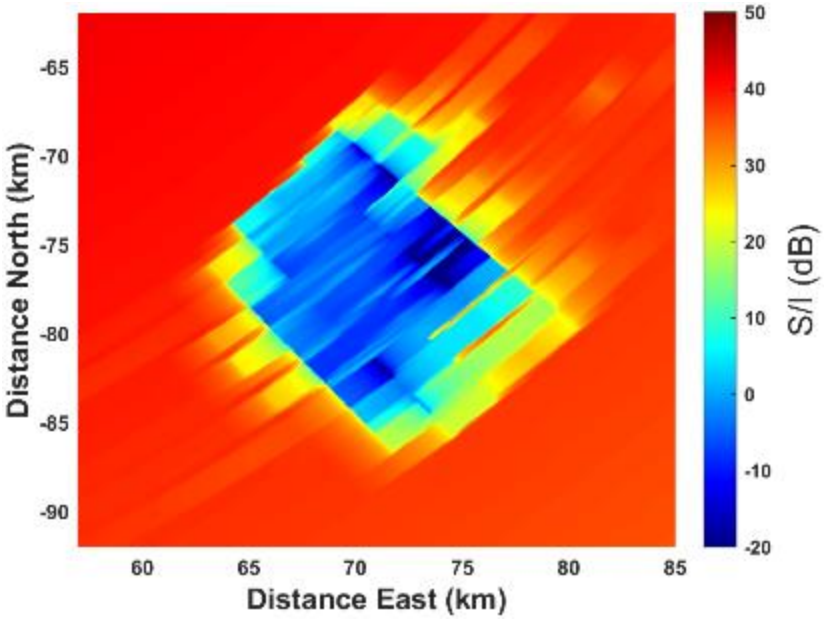

Figure 57 - Signal to Interference for a 0 dBsm aircraft flying at 5 km altitude near KPVD

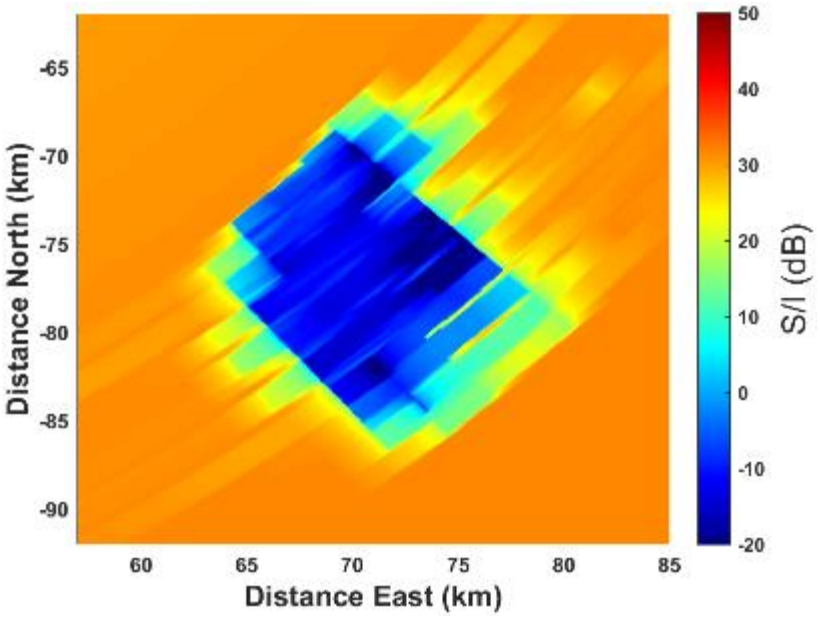

Figure 58 -Signal to Interference for a 0 dBsm aircraft flying at 10 km altitude near KPVD

The only other ASR within the vicinity of Bay State Wind is the ASR-8 FMH. Figure 59 shows the portion of the turbines that FMH will have line-of-sight. The impact on FMH will be comparable to the findings for Mayflower Wind on ACK in Section 3.1.4.1 due to the similar portion of the wind farm turbines visible to the radar.

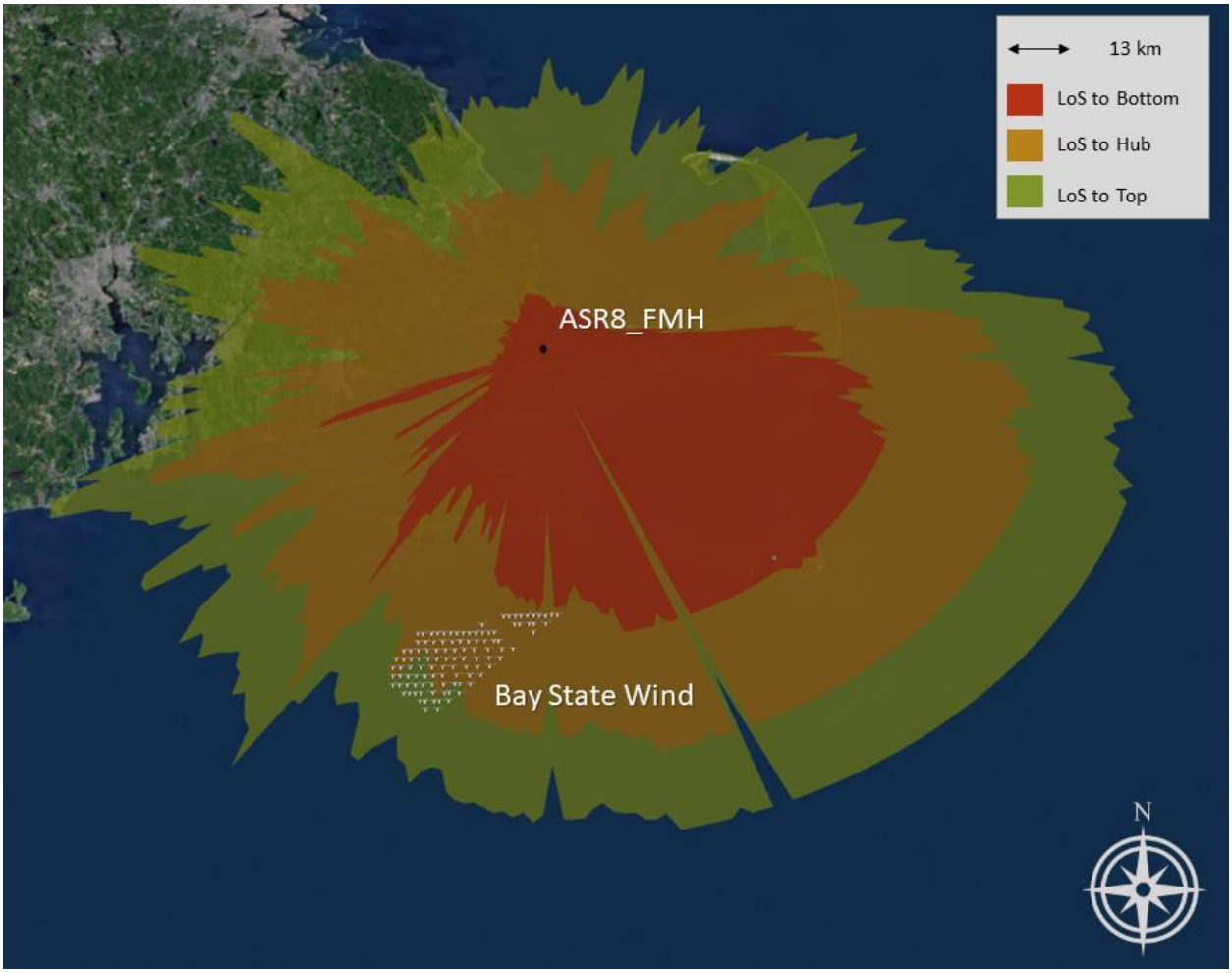

Figure 59 - ASR-8 FMH LOS to Bay State Wind.

3.1.2.2 *SeaSonde*

Table 9 - Impacted SeaSondes from Bay State Wind

Impacted SeaSondes	Class of Interference
SQUB	B
LPWR	E
HBSR	F
NWTP	F
MVCO	H
NANT	H
AMAG	H

3.1.2.2.1 Short Range SeaSondes

There is one short range SeaSonde that will be impacted by turbines from the Bay State wind farm. This is the SQUB SeaSonde located on Martha's Vineyard. Turbines from the Bay State wind farm will be placed in ranges from 20-40 km from the SeaSonde site location which will span the mid to long range capability of the system (Figure 60). This is a large wind farm with 110 turbines and will be categorized as a type B interference where there is a large wind farm in mid to long range of a short range SeaSonde.

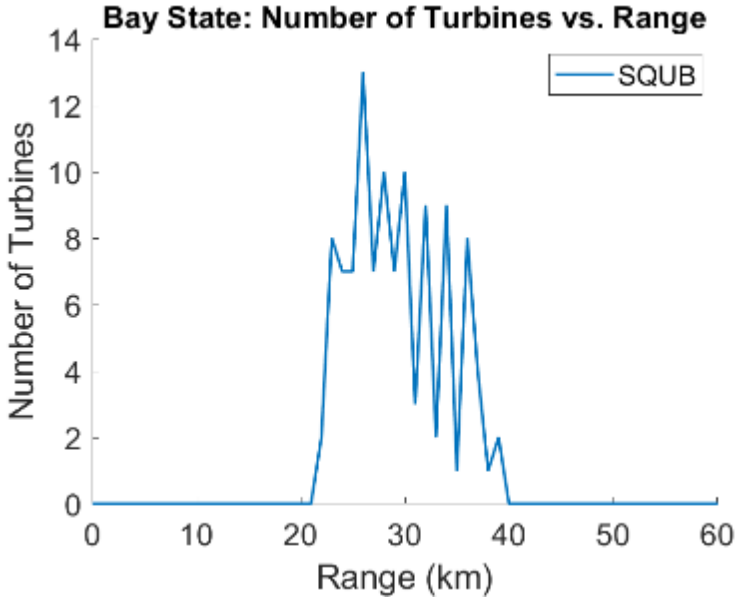

Figure 60 - Number of turbines in each range bin for the short range SeaSondes near Bay State.

This class of wind turbine interference can have a large impact due to the number of turbines present, even in the mid-range and long range. Comparing this scenario to the class A, the presence of many more turbines results in much more interference. Figure 64 shows a top-down view of the SQUB LOS with the Bay State wind farm as context for locations. Figure 61 shows the range-Doppler map of the SQUB SeaSonde and the Bay State wind farm and there is interference over the entire range of turbines present. Comparing Figure 61 to Figure 85 in the common turbine range bins (30-35 km), the larger wind farm has a greater amount of interference. This is due to both more turbines in those range bins with the larger wind farm and spillover from other FFT range bins containing turbines.

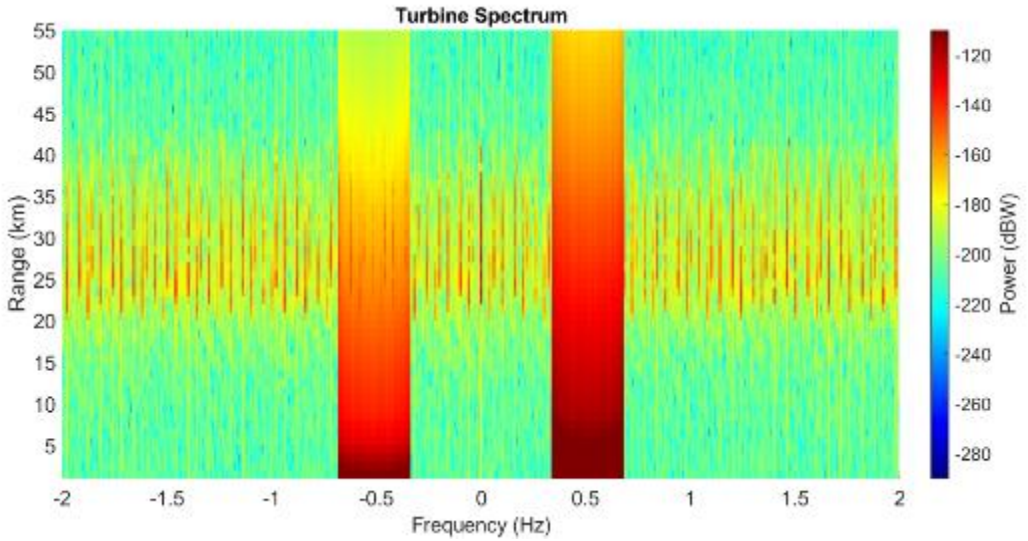

Figure 61 - Range Doppler matrix for the SQUB SeaSonde located on Martha's Vineyard with turbine interference from the Bay State. There are 110 total turbines spinning at 5.2 rpm.

The presences of the turbines in this scenario will produce both errors in identifying the FOL and in angle determination with the large number of turbines. Figure 62 shows the power spectrum of the range bin centered at 29 km (roughly middle of wind farm) with the FOL selection with (green) and without (red) wind turbine interference. In both the positive and negative Bragg peak selection, interference toward the edge of the FOL is causing additional Doppler bins to be added to the FOL used for current measurements. While the current Bragg spectrum contains 1% of the spectrum in the negative Bragg peak, even with a more even split in the Bragg energy, the turbine spectrum would still be comparable and produce similar problems.

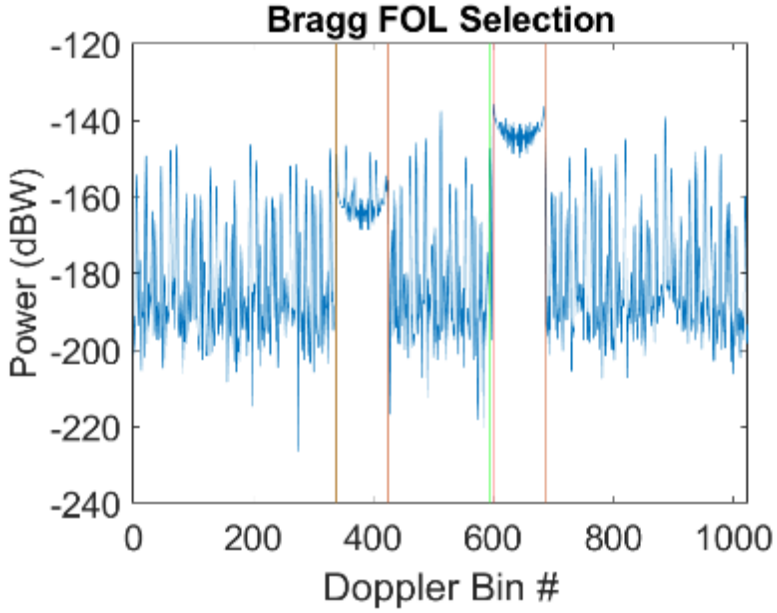

Figure 62 - Power spectrum in the 29 km range bin for the SQUB SeaSonde located at Martha's Vineyard with turbine interference from Bay State. Red lines are the FOL selection with no turbine interference and the green lines are the FOL selection with the turbine signals.

Figure 63 shows the current measurement errors induced upon the SQUB SeaSonde in the presence of the Bay State wind farm. As can be seen in the figure, the entire extent of the wind farm is producing current measurement errors at all angles with many on the order of 100 cm/s which is large as the largest current measurements present in the simulation. Figure 64 shows the line-of-sight analysis results and all wind turbines from Bay State will be within the LOS of SQUB.

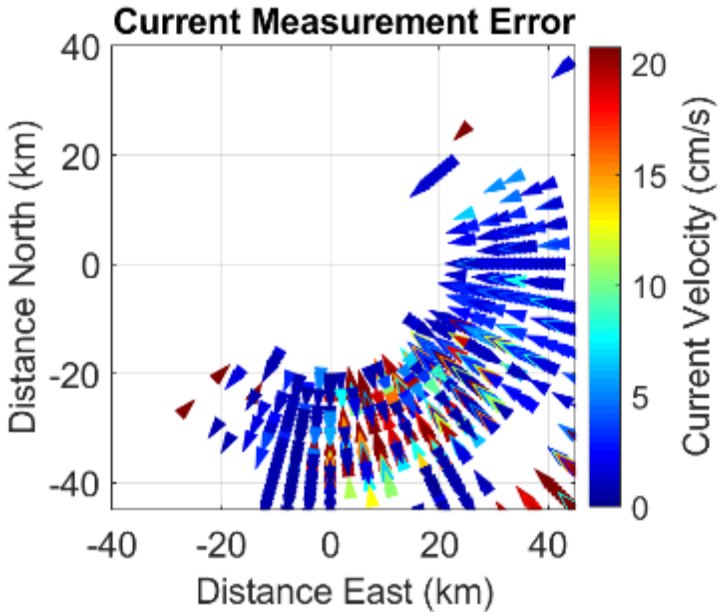

Figure 63 - Current measurement error for the SQUB SeaSonde located at Martha's Vineyard with turbine interference from the Bay State farm. Modeled sea currents were 100 cm/s running parallel to the coast.

Figure 64 - Line of Sight plot for the SQUB SeaSonde located on Martha's Vineyard with reference to the Bay State farm.

3.1.2.2.2 Medium Range SeaSondes

There are three medium range SeaSondes that were impacted by the Bay State wind farm (See Figure 65). One of these, LPWR, will have the turbines at short range for the radar, this interference is classified as class E. The HBSR and NWTP SeaSondes will have the turbines from this wind farm show up in their mid-range and have been classified as class F interference which will be discussed more below.

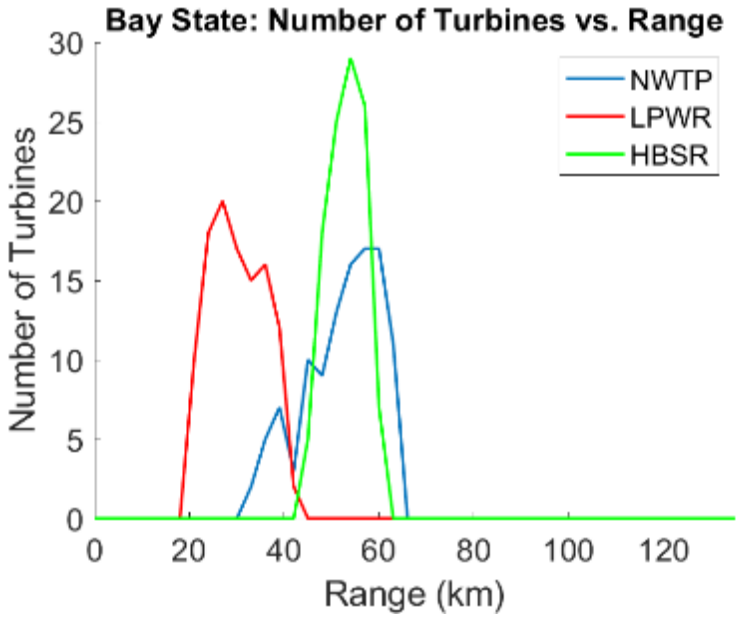

Figure 65 - Number of turbines in each range bin for the medium range SeaSondes near the Bay State wind farm

Bay State turbines will span the range from 20-40 km for the LPWR SeaSonde which will place the wind farm in short range for the system and it belongs to class E interference which will contain large wind farms in short ranges for the medium range SeaSondes. In Figure 66 below, the interference from the Bay State turbines (110 turbines) is shown in the range-Doppler map for turbines rotating at 5.2 rpm. The turbine signals bleed into range bins outside (~2-4 bins) of the range bins that the turbines themselves are within. Figure 67 shows the power spectrum in the 30 km range bin, and the turbine spectra contain spikes that are comparable in power to either of the Bragg peaks. There is also misidentification of the FOL on the negative Bragg peak where the selection without the interference is shown in red and the selection with interference is shown in green.

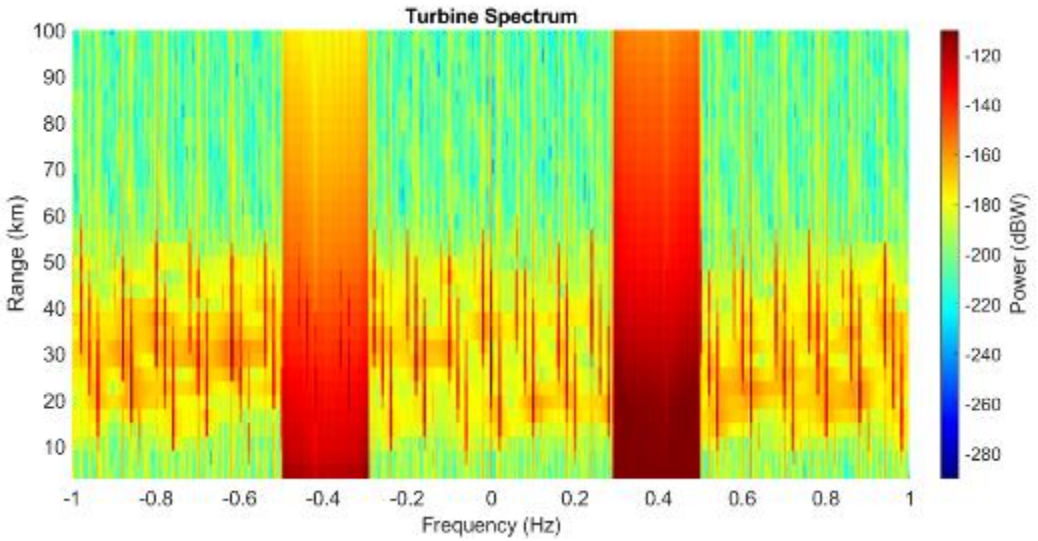

Figure 66 - Range Doppler matrix for the LPWR SeaSonde located on Martha's Vineyard with turbine interference from the Bay State farm. There are 110 total turbines spinning at 5.2 rpm.

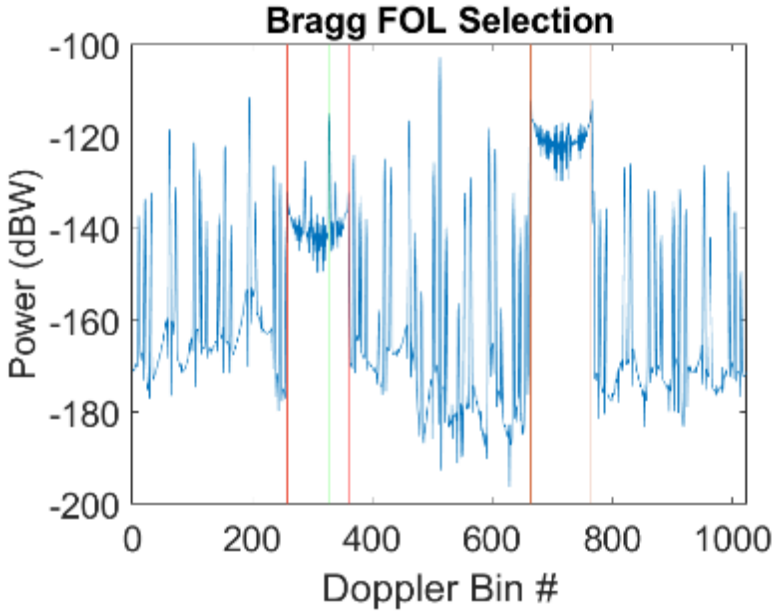

Figure 67 - Power spectrum in the 30 km range bin for the LPWR SeaSonde located at Martha's Vineyard with turbine interference from the Bay State wind farm. Red lines are the FOL selection with no turbine interference and the green lines are the FOL selection with the turbine signals.

Figure 68 below shows expected current measurement errors that are induced by the Bay State turbines. The region containing the turbines contains significant errors that will impact measurements of currents in the region of Bay State. These errors are greater in the range/angular region where Bay State sits, but smaller errors are also present outside of the physical region the wind farm occupies. Figure 69 shows the line-of-sight analysis results and all wind turbines from Bay State will be within the LOS of LPWR.

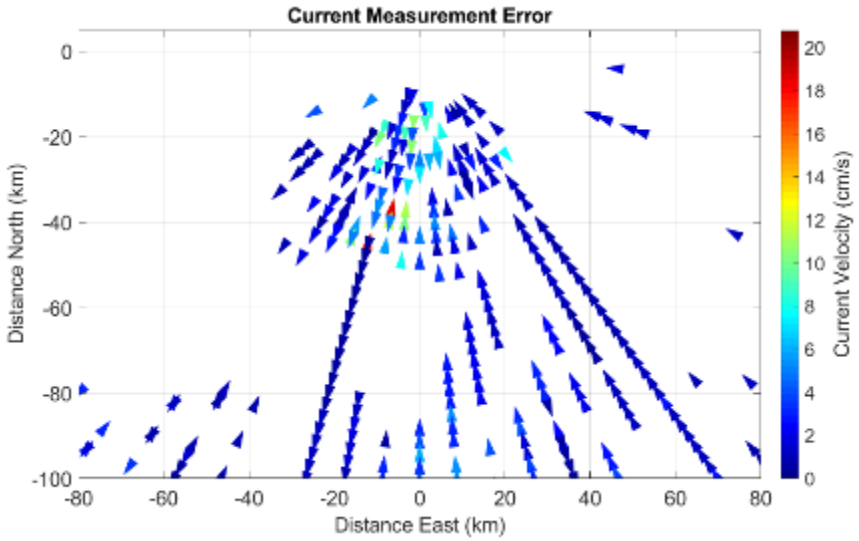

Figure 68 - Current measurement error for the LPWR SeaSonde located at Martha's Vineyard with turbine interference from the Bay State wind farm. The modeled sea currents were 100 cm/s running parallel to the coast and there are large errors in comparison to this value.

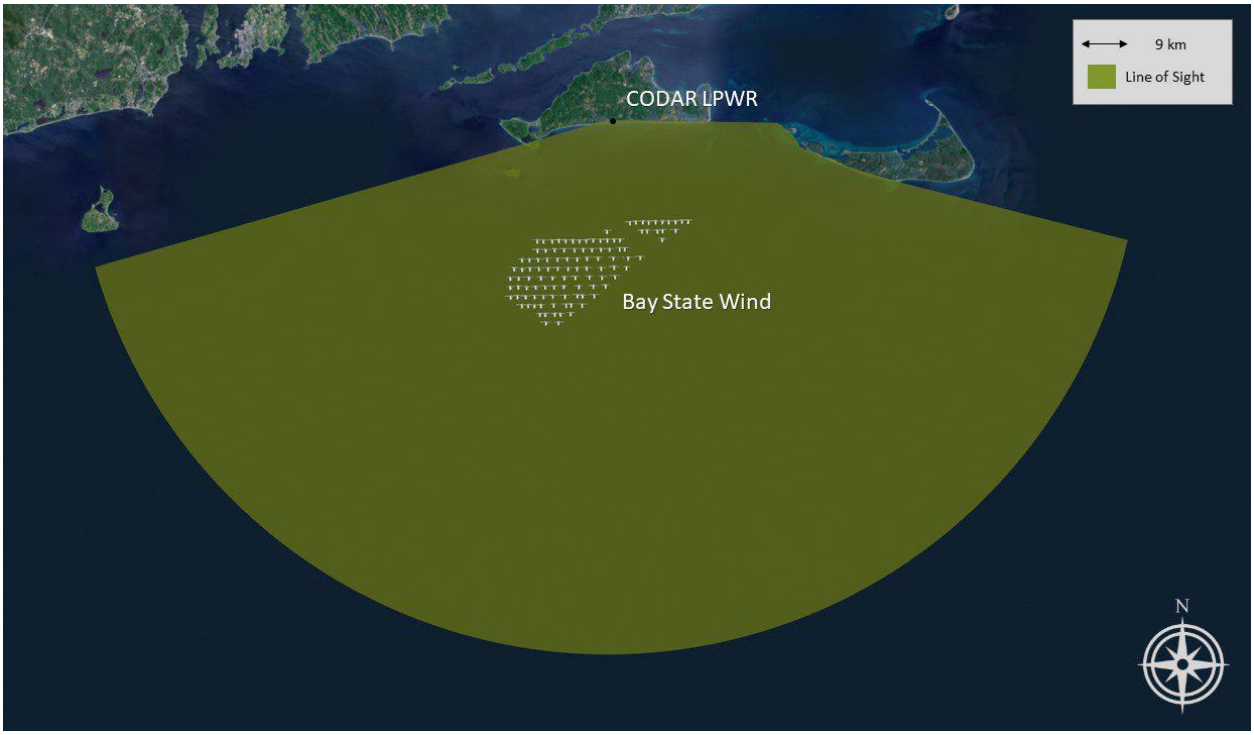

Figure 69 - Bay State, SeaSonde LPWR

The other two affect medium range SeaSondes will both see Bay State in their mid-range is in class F for medium range SeaSondes with a large wind farm at mid-range. Results from the HBSR SeaSonde are shown, which is ~40-60 km from the Bay State wind farm. Figure 70 shows the range-Doppler map with interference from Bay State. This shows a very similar phenomena as was discussed above with the LPWR and Bay State scenario with the only main difference being the relative ratios of the turbine signal strength and the signal strength of the Bragg scatters. This is shown in more detail by looking at the

power spectrum of the 54 km range bin in Figure 71 where there is a mischaracterization of the FOL region.

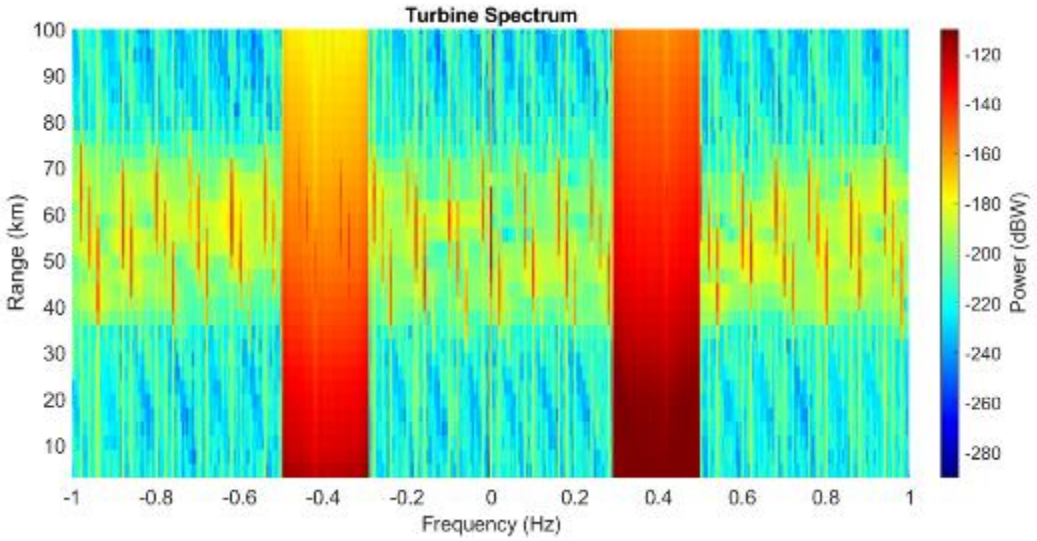

Figure 70 - Range Doppler matrix for the HBSR SeaSonde located at Horseneck Beach State Reserve, MA with turbine interference from the Bay State farm. There are 110 total turbines spinning at 5.2 rpm.

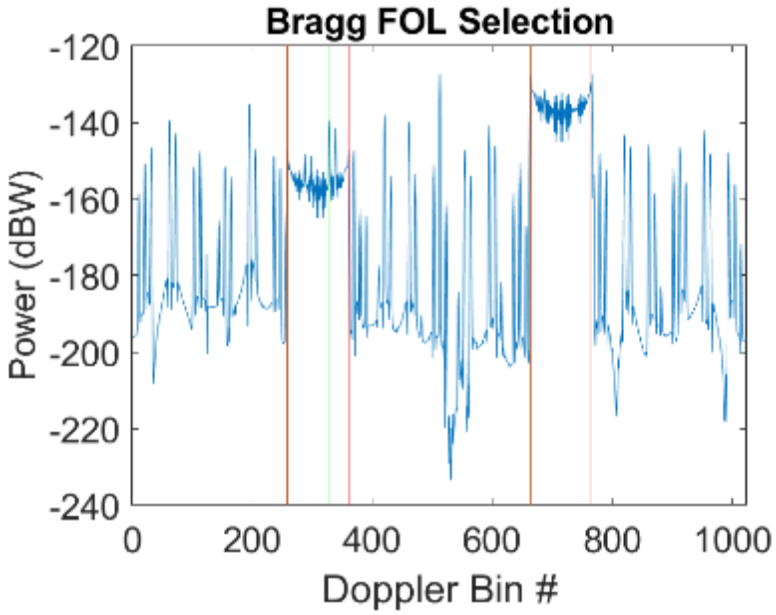

Figure 71 - Power spectrum in the 54 km range bin for the HBSR SeaSonde located at Horseneck Beach State Reserve, MA with turbine interference from Bay State. Red lines are the FOL selection with no turbine interference and the green lines are the FOL selection with the turbine signals.

The results from the short (class E) vs. mid-range (class F) differ in how localized the current measurement is impacted. Figure 72 shows that the current errors are much more localized into the radial/angular region where the Bay State turbines reside. Outside of the nearby range bins to the turbines, there is little to no impact while in the class E interference there were many current vectors

impacted outside of the range band the turbines occupy. Figure 72 shows the LOS analysis results and all wind turbines from Bay State will be within the LOS of HBSR.

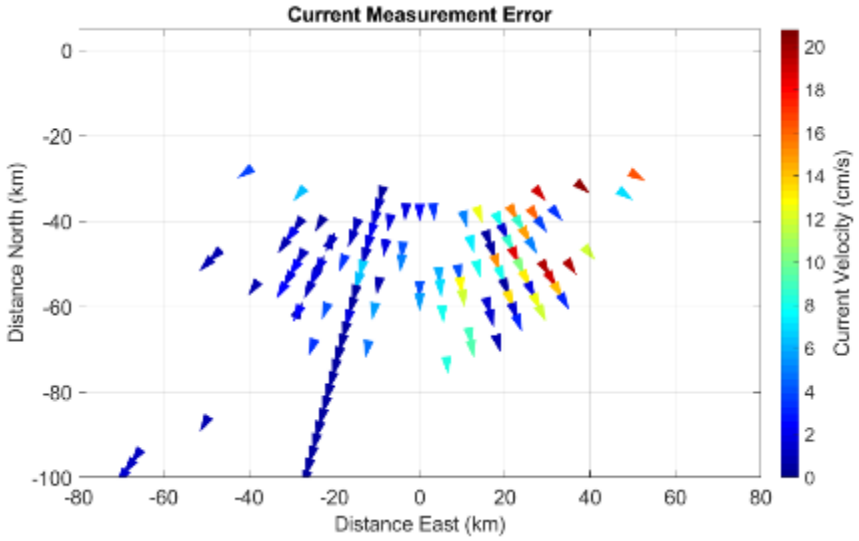

Figure 72 - Current measurement error for the HBSR SeaSonde located at Horseneck Beach State Reserve, MA with turbine interference from the Bay State farm. Modeled sea currents were 100 cm/s running parallel to the coast

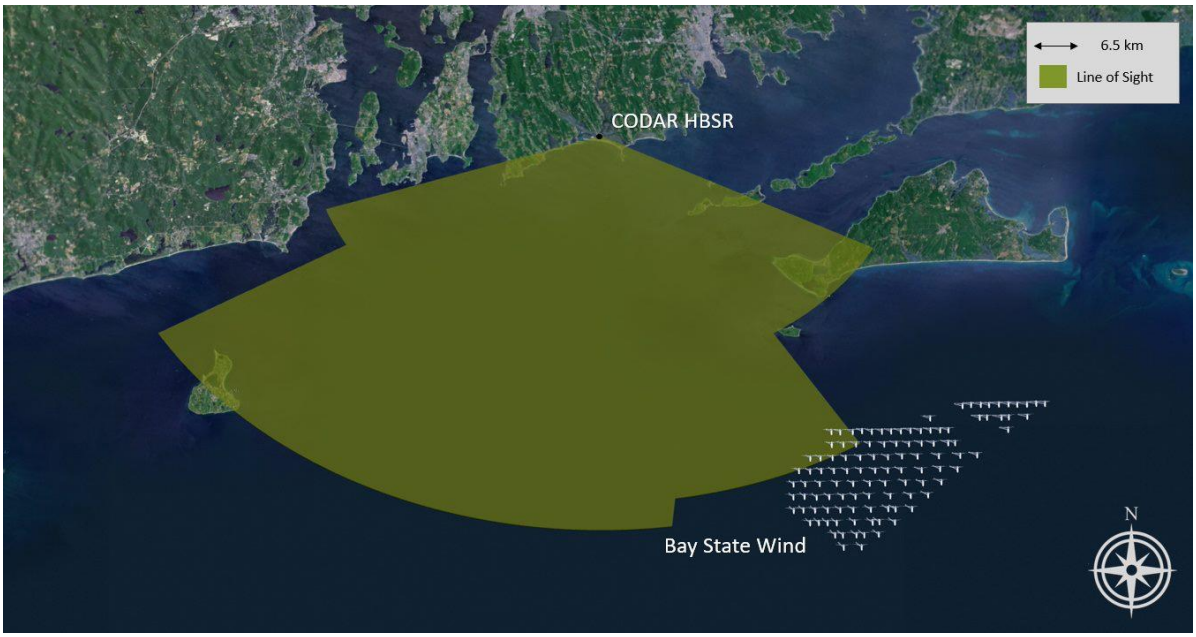

Figure 73 - Bay State, SeaSonde HBSR

The NWTP SeaSonde will be impacted similarly to the HBSR SeaSonde but will have slightly wider range distribution of affected radials due to both a wider distribution in the turbines in range and that some of the turbines will be closer to the system than those in the NBSR scenario.

3.1.2.2.3 Long Range SeaSondes

Bay State will affect the operations of three long range SeaSondes in the area. All affected SeaSondes will have the turbines show up in the short-mid range of the systems as shown in Figure 74 below. Both

systems are in class H, where there is a large wind farm within short-mid range of a long range SeaSonde. The results from the MVCO SeaSonde with Bay State are presented in greater detail below as an example of what level of interference to expect. The interference in the AMAG SeaSonde will be somewhere between the H and I classes due to the turbines being at longer ranges than the other two.

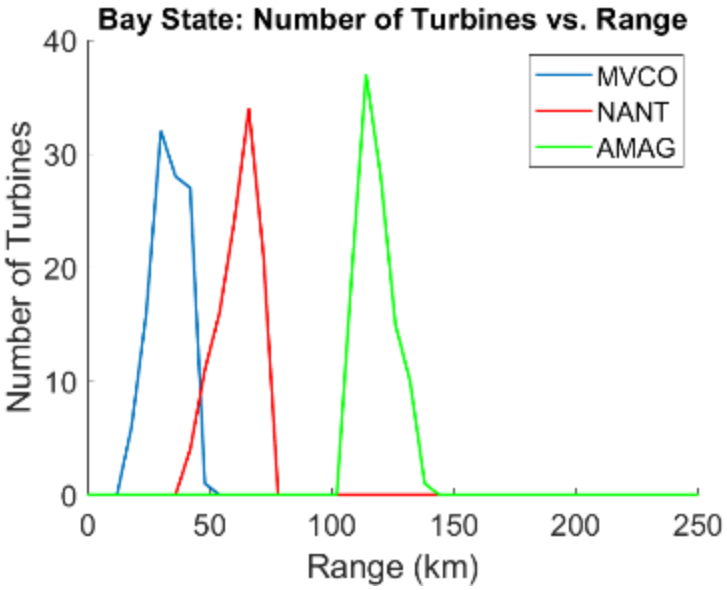

Figure 74 - Number of turbines in each range bin for the long range SeaSondes near Bay State

Bay State's turbines will be placed such that they are between 20-50 km from the MVCO turbine and the range-Doppler map is shown below in Figure 75. The interference of the turbines will impact the range bins where the turbines are located and roughly five range bins on either side of range bins containing the turbines. In Figure 76 the power spectrum of the 36 km range bin is shown. The FOL selection with (green) and without (red) the Bay State turbines is also shown and demonstrates the mischaracterization of the FOL which can occur for this class of turbine interference on SeaSondes.

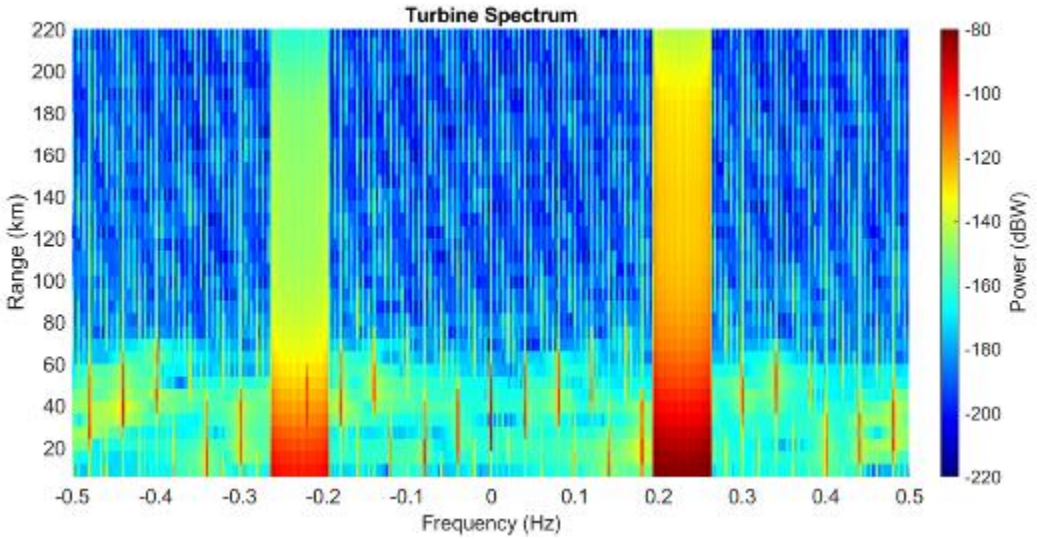

Figure 75 - Range Doppler matrix for the MVCO SeaSonde located on Martha's Vineyard with turbine interference from Bay State. There are 110 total turbines spinning at 5.2 rpm.

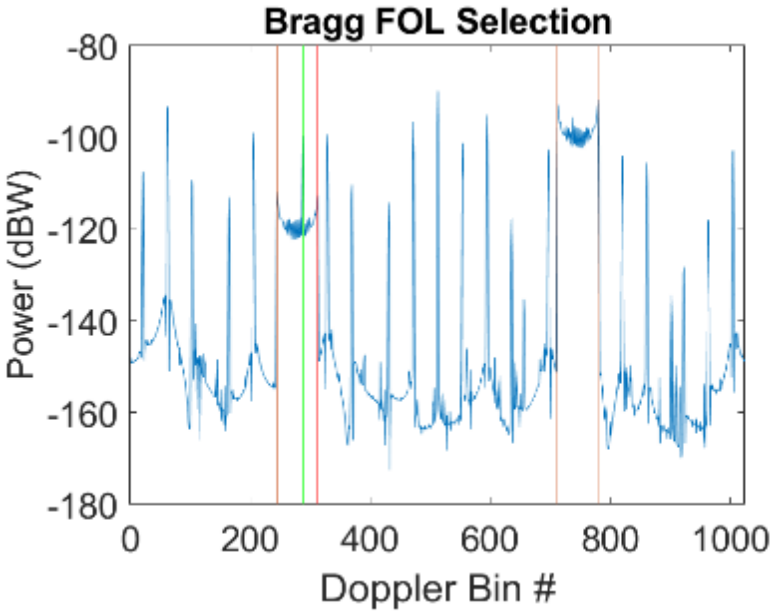

Figure 76 - Power spectrum in the 36 km range bin for the MVCO SeaSonde located at Martha's Vineyard with turbine interference from the Bay State wind farm. Red lines are the FOL selection with no turbine interference and the green lines are the FOL selection with the turbine signals.

Figure 77 shows the current measurement errors which occur with the MVCO SeaSonde and the Bay State farm. There are many changed current measurements as a result of interference from the wind farm. Current errors can be of the order of 100 cm/s, which is as large as currents which are present in the simulation. In this case, there were large errors which were not necessarily concentrated in the angular direction of the turbines. Figure 78 shows the line-of-sight analysis results and all wind turbines from Bay State will be within the LOS of MVCO.

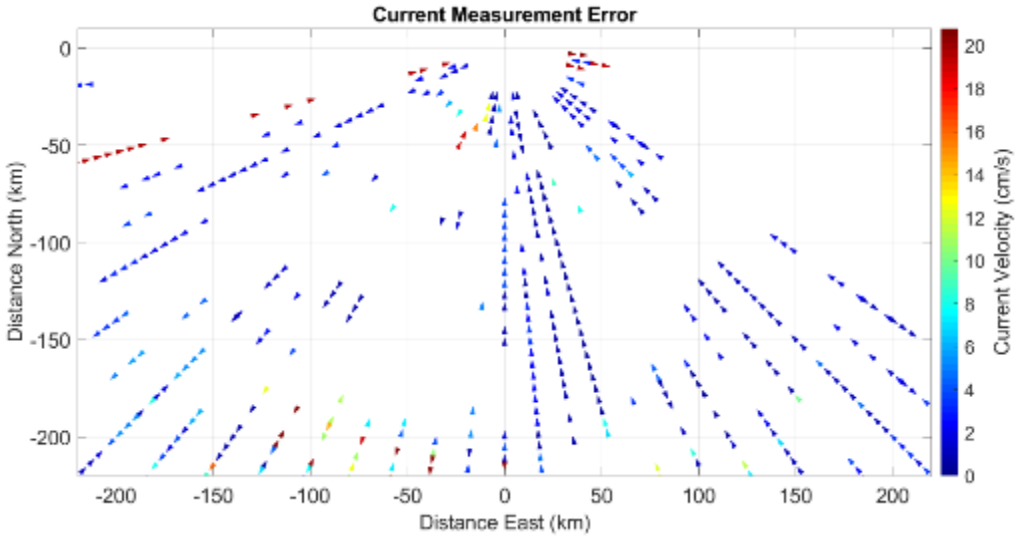

Figure 77 - Current measurement error for the MVCO SeaSonde located at Martha's Vineyard with turbine interference from the Bay State farm. Modeled sea currents were 100 cm/s running parallel to the coast.

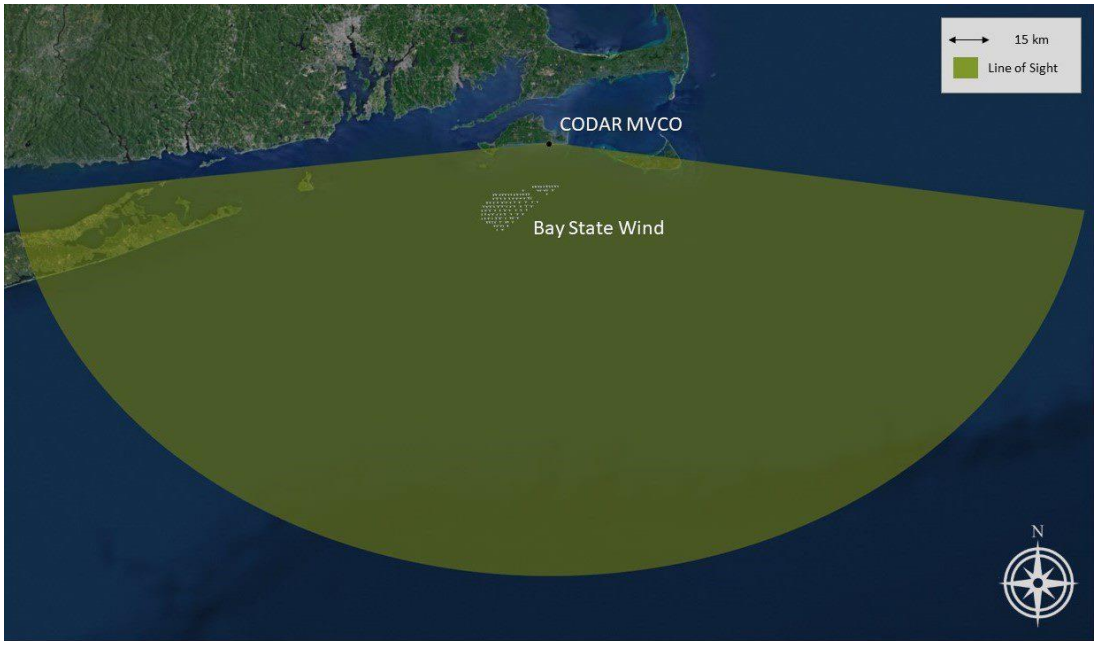

Figure 78 - Bay State, SeaSonde MVCO

3.1.3 South Fork

The South Fork wind farm had been proposed to BOEM in a COP when this report was written and is within LOS of one ASR-9 and eight SeaSonde radars. It is located within the RI/MA lease area (Lease OCS-A-0486) and has 15 12-MW turbines.

3.1.3.1 *ASR*

There is only one ASR, the ASR-9 at Warwick, RI (KPVD) in the vicinity of the South Fork wind farm. Figure 79 shows the LOS analysis results. All 15 turbines will be within the LOS of KPVD.

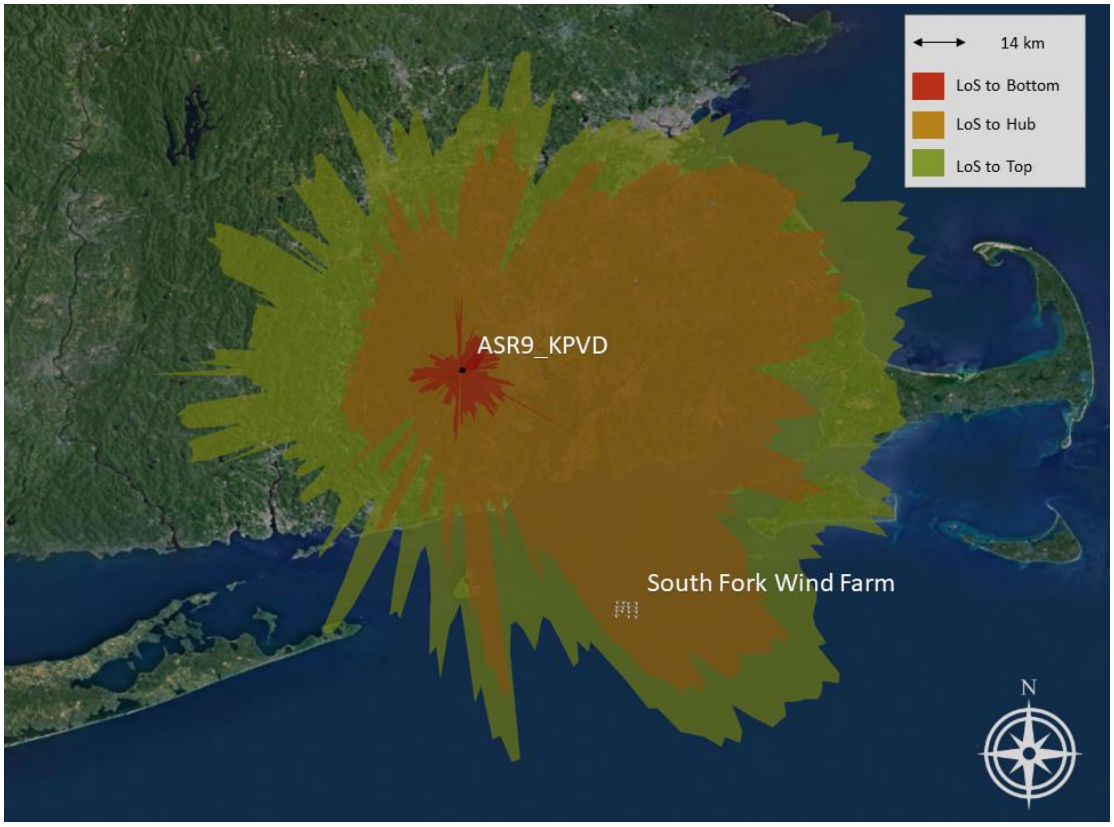

Figure 79: ASR-9 KPVD LOS to South Fork

Figure 80 shows the WindTrx ASR-9 raw CFAR detection output for the wind turbines modeled at South Fork. Using the turbine RCS modeling methodology from Section 2.4.1 the turbines return enough signal that it enters the sidelobes of the antenna, creating the appearance of a range ring of raw detections out at approximately 80 km. This is caused when the antenna is sweeping in azimuth and there is enough signal present from the returns in the azimuth sidelobes it will create a detection along its current azimuth position. Additional processing during plot correlation and tracking algorithms will likely reduce these raw detections down to fewer plots.

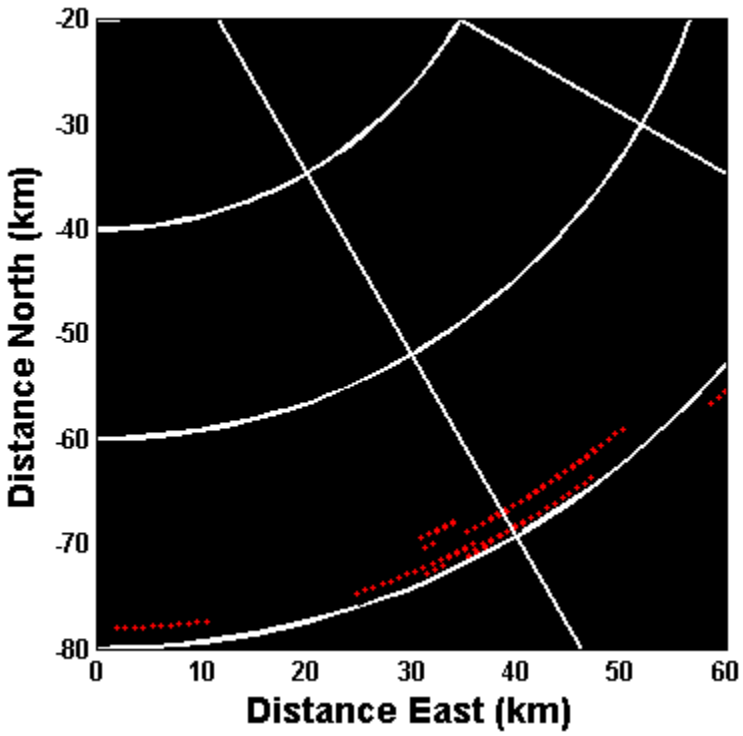

Figure 80: KPVD Raw CFAR Detections of South Fork Turbines

Figure 81, Figure 82, and Figure 83 below show the South Fork turbines' signal-to-interference for KPVD. The CFAR algorithm is described above in Section 2.4.3.5. The plots below should be interpreted as everywhere there is a signal to interference ratio of 13 dB or larger, a detection would be declared in that region. Range-Doppler cells around the wind turbines have a large interference level and would require a substantially larger aircraft RCS in order to achieve detection, regions below the 13dB threshold show where the wind turbine signals are contributing to the CFAR floor and are likely to prevent aircraft in the vicinity from being detected. Figure 81 shows that in the vicinity of South Fork there is interference that would prevent a small aircraft (0 dBsm) from being detected when flying at 2 km altitude. Figure 83 shows that as the aircraft flies above the antenna main elevation beam there is more interference (i.e., a lower signal-to-interference ratio) because the aircraft skin return will be weaker. Although the figures below show an amount of interference that would impact the ability to detect an aircraft over the turbines, the South Fork farm is only 15 turbines and the region impacted is relatively small compared with the following wind farms.

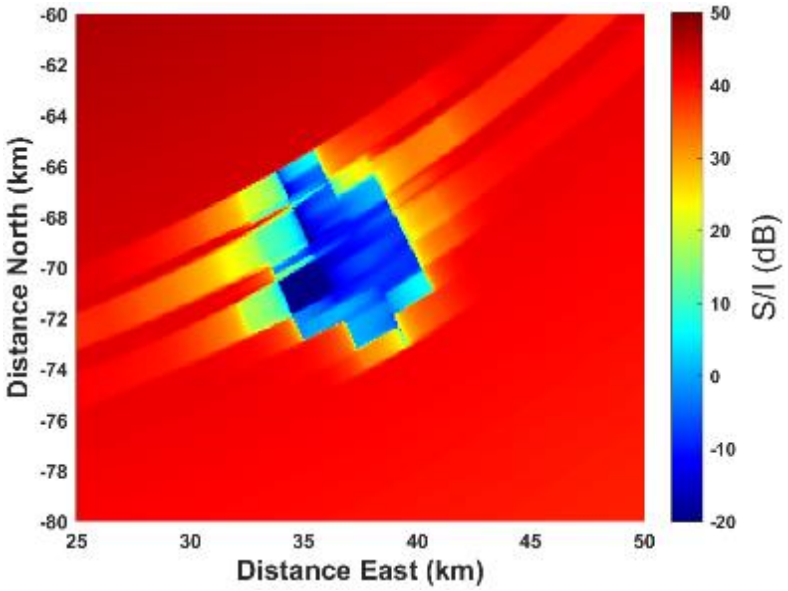

Figure 81 - KPVD Signal-to-Interference Ratio for a 0dBsm Aircraft at 2km Altitude

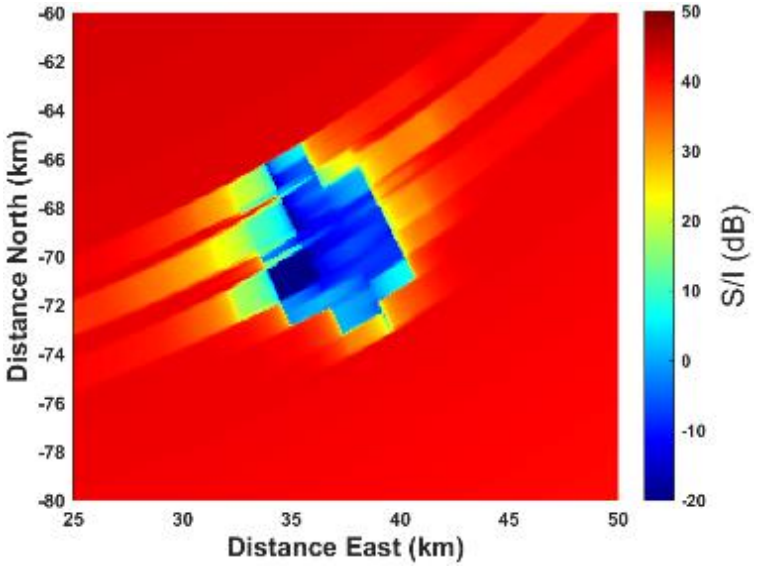

Figure 82 - KPVD Signal-to-Interference Ratio for a 0dBsm Aircraft at 5km Altitude

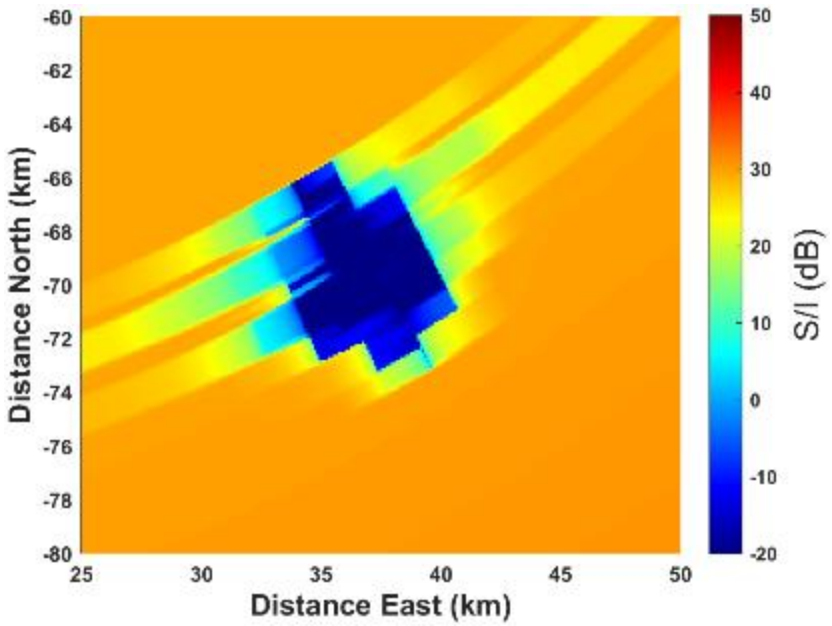

Figure 83 - KPVD Signal-to-Interference Ratio for a 0dBsm Aircraft at 10km Altitude

3.1.3.2 *SeaSonde*

Table 10 - Impacted SeaSondes from South Fork

Impacted SeaSondes	Class of Interference
BISL	A
LPWR	C
HBSR	C
NWTP	D
CPVN	C
MVCO	G
NANT	G
AMAG	G

3.1.3.2.1 Short Range SeaSondes

For the 25 MHz SeaSondes, there is only one impacted by the South Fork wind farm, which is the BISL system located at Block Island, RI. This system will see the turbines near the edge of their instrumented

range where the turbines are located ~30-36 km from the site location (see Figure 84). This is within class A for SeaSonde interference with a small wind farm (15 turbines) at long range for the system.

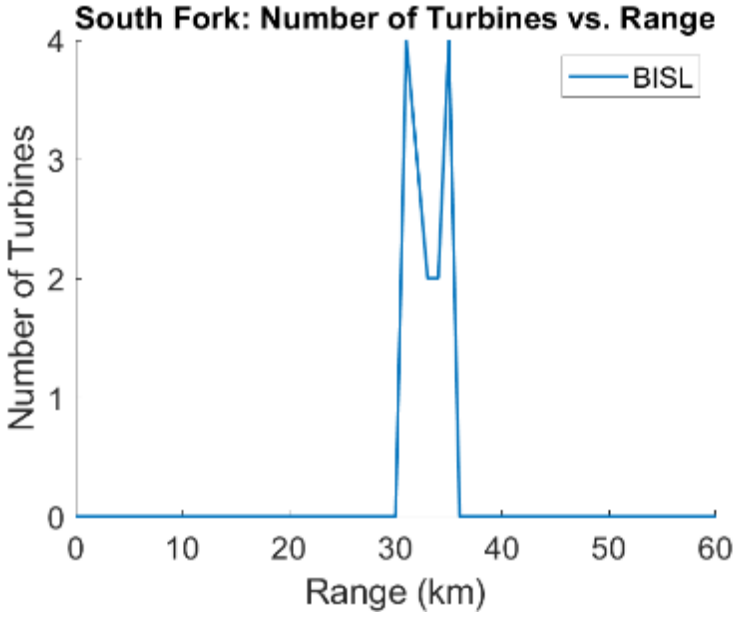

Figure 84 - Number of turbines in each range bin for the short range SeaSondes near the South Fork wind farm

Figure 85 shows the range-Doppler map of the BISL SeaSonde with turbine interference from the South Fork wind farm. The turbines were simulated to spin at 5.2 rpm. Inside the negative Bragg region, which is set to be 1% of the total Bragg signal, the turbine signal is interfering with the signal from Bragg scatter. This will degrade the measurements of the angle of arrival of the signal and affects the determination of the FOL region. Figure 86 shows the spectrum with turbine interference in the 30 km range bin the Bragg FOL selection criteria are displayed with (green) and without (red) the interference from the turbines at South Fork. On the lower Bragg peak the FOL region determination has included a few extra bins as a result of the presence of the South Fork wind farm.

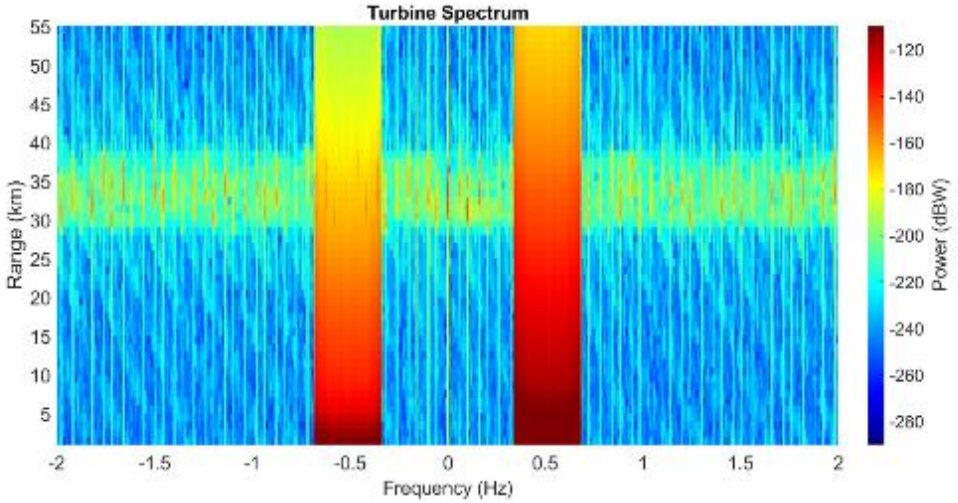

Figure 85 - Range Doppler matrix for the BISL SeaSonde located on Block Island, RI with turbine interference from the South Fork farm. There are 15 total turbines spinning at 5.2 rpm.

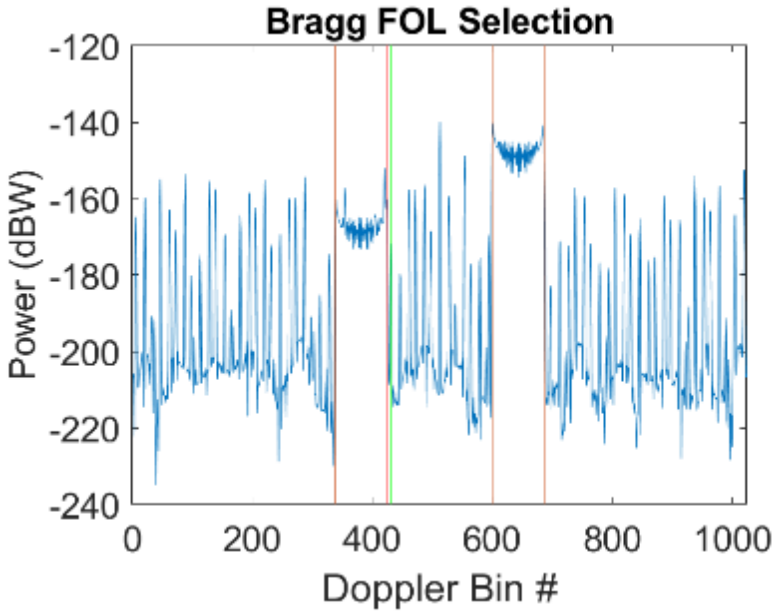

Figure 86 - Power spectrum in the 33 km range bin for the BISL SeaSonde located at Block Island, RI with turbine interference from the South Fork farm. Red lines are the FOL selection with no turbine interference and the green lines are the FOL selection with the turbine signals.

The errors in the FOL determination and angle determination lead to current measurements that are displayed in Figure 87. In the example presented here, the current was simulated at 100 cm/s running parallel to the coast (see Figure 25 in the methodology section). In the range band containing the wind farm is where most of the current measurement error is occurring and it is not necessarily isolated to just the angular region where South Fork is in relation to the SeaSonde. However, the largest errors occur in that angular direction. The maximum currents present in this simulation were 100 cm/s and there were errors as large as 31 cm/s. Figure 88 shows the LOS analysis results and all wind turbines from South Fork will be within the LOS of BISL.

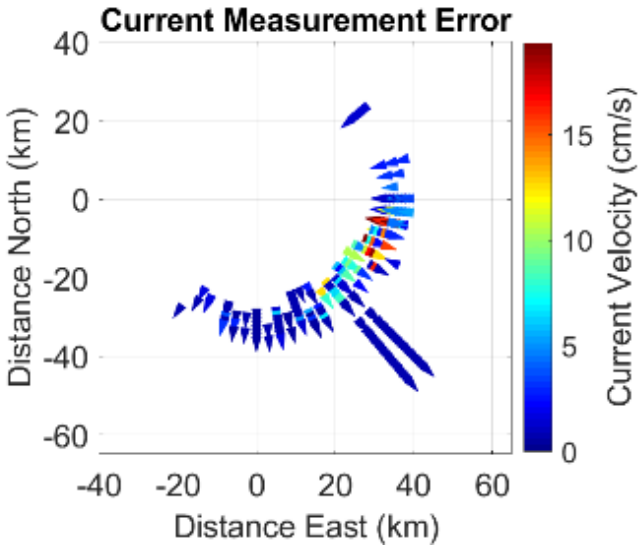

Figure 87 - Current measurement error for the BISL SeaSonde located at Block Island, RI with turbine interference from South Fork. Modeled sea currents were 100 cm/s running parallel to the coast and large errors are visible in comparison to this value.

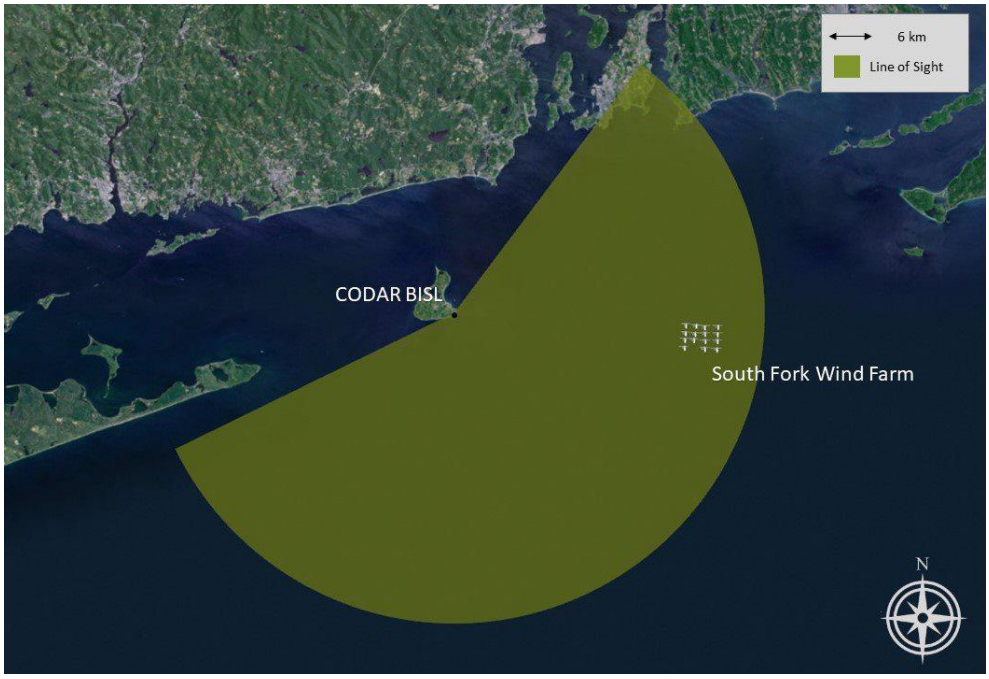

Figure 88 - South Fork, SeaSonde BISL

3.1.3.2.2 Medium Range SeaSondes

For the medium range SeaSondes, there are four that were impacted by the South Fork wind farm. The South Fork wind turbines were all in the mid-range for three of the systems, between ~35-55 km from each site location and at long range for the fourth (see Figure 89). These would all be in class C with a small (15 turbines) wind farm in the mid-range for the systems. There is also a SeaSonde that will have the turbines at long range for the system which will fall into class D.

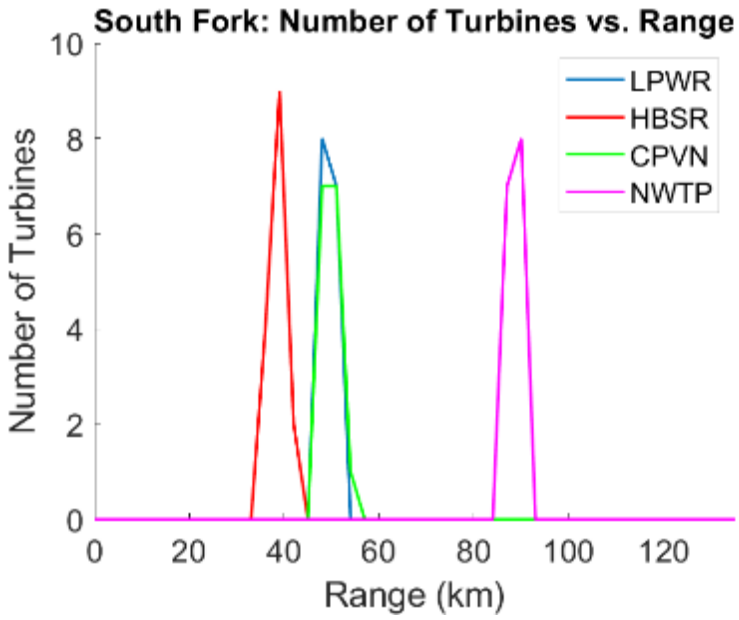

Figure 89 - Number of turbines in each range bin for the medium range SeaSondes near South Fork.

Figure 90 shows the range-Doppler map of the LPWR SeaSonde with turbine interference from the South Fork wind farm. In this plot the turbines were simulated to spin at 5.2 rpm. Inside the negative Bragg region, which is set to be 1% of the total Bragg signal. The range-Doppler map shows where the turbine signal is adding extra signal over the Bragg scatter return. This degrades the measurements of the angle of arrival of the signal in the range bins near the range bins containing the turbines. Figure 91 shows the spectrum with turbine interference in the 54 km range bin and displays the Bragg FOL selection criteria with (green) and without (red) the interference from the turbines at South Fork. For this combination of ranges and rotation rates there is no addition or subtraction of bins in the FOL region.

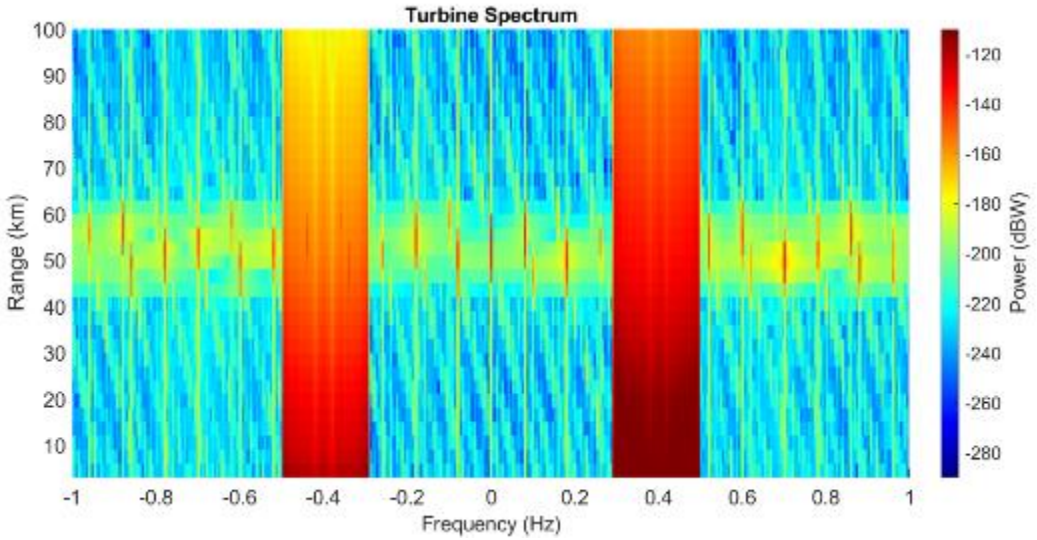

Figure 90 - Range Doppler matrix for the LPWR SeaSonde located on Martha's Vineyard with turbine interference from the South Fork farm. There are 15 total turbines spinning at 5.2 rpm.

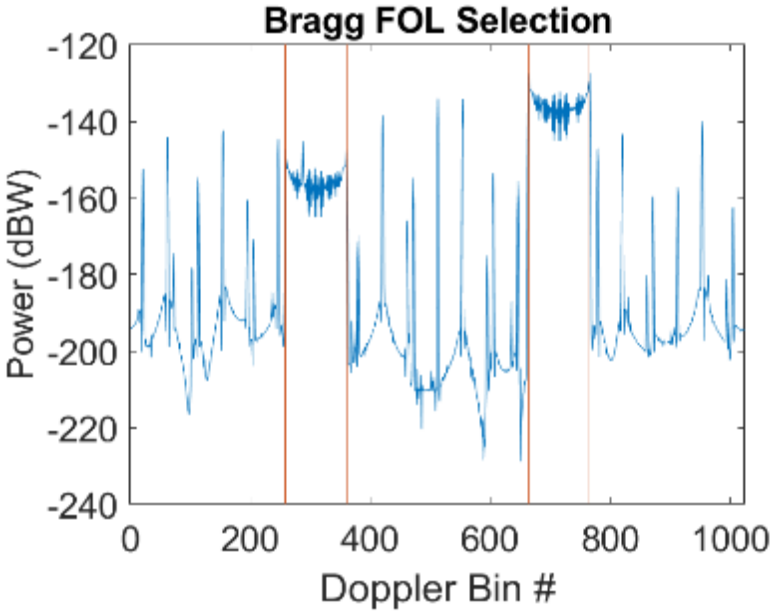

Figure 91 - Power spectrum in the 54 km range bin for the LPWR SeaSonde located at Martha's Vineyard with turbine interference from the South Fork farm. Red lines are the FOL selection with no turbine interference and the green lines are the FOL selection with the turbine signals.

The errors in the angle determination lead to current measurements which are displayed in Figure 92. In this example the current was 100 cm/s running parallel to the coast (see Figure 25 in the methodology section). In the range band containing the wind farm is where most of the current measurement error is occurring, and it is not necessarily isolated to just the angular region where South Fork is in relation to the LPWR SeaSonde, though the largest errors are in that angular direction. The maximum currents that are present in this simulation are 100 cm/s and there are errors that are as large as 18 cm/s. Figure 93 shows the line-of-sight analysis results and all 15 wind turbines from South Fork will be within the LOS of LPWR.

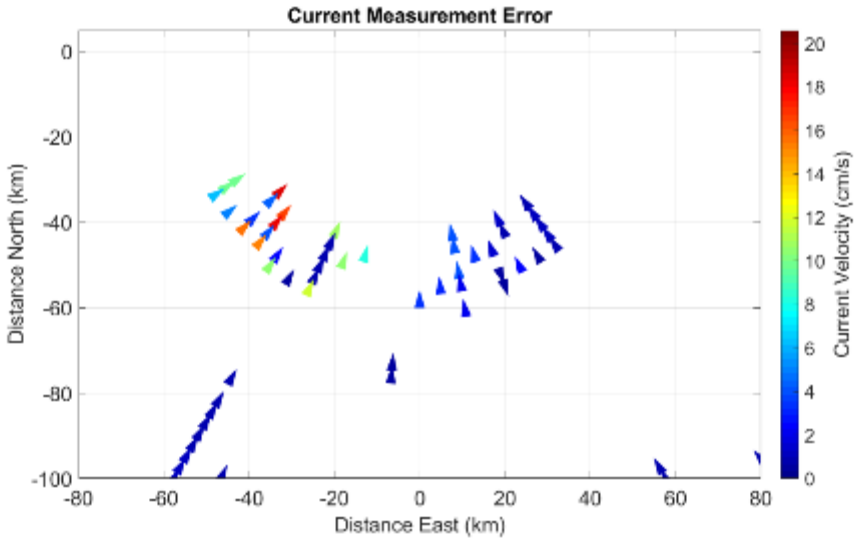

Figure 92 - Current measurement error for the LPWR SeaSonde located at Martha's Vineyard with turbine interference from the South Fork farm. Modeled sea currents were 100 cm/s running parallel to the coast.

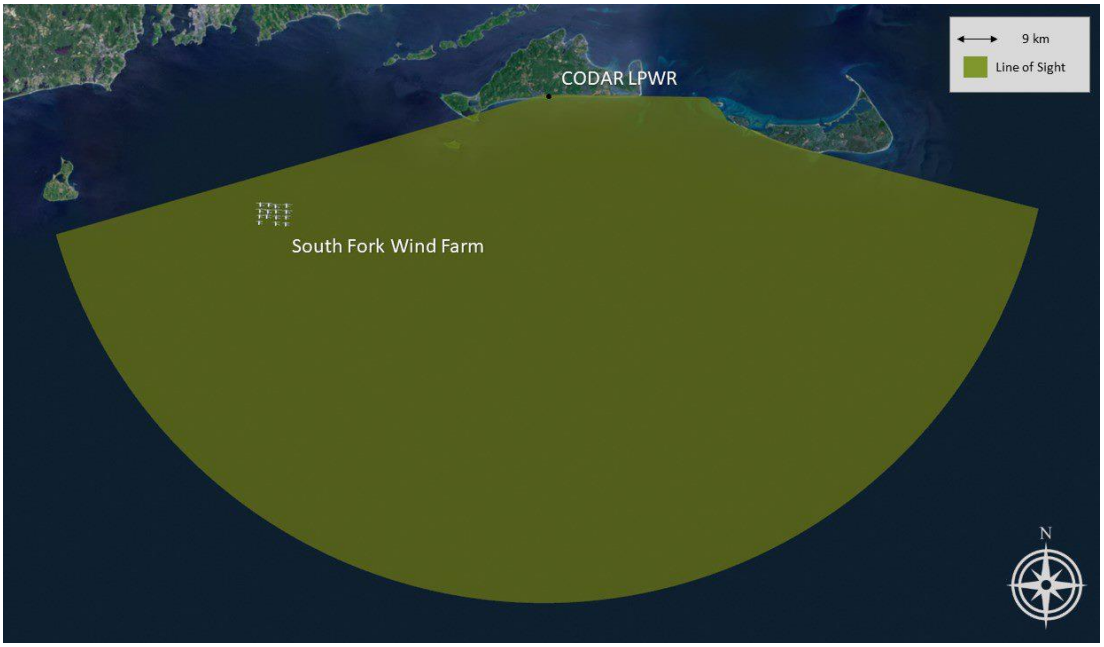

Figure 93 - South Fork, SeaSonde LPWR

The CPVN and HBSR SeaSondes will also have the same interference class as the LPWR SeaSonde and will have similar effects. The HBSR SeaSonde is situated closer to the turbines and will correspondingly have more interference.

The NWTP SeaSonde will see the Southfork wind farm near the edge of its instrumented range. Due to the small number of turbines at a long range there is minimal impact on the performance of this system. In simulations, the turbine spectrum at the far ranges in worst-case scenarios did not have a large impact on the system (see Figure 94). Some signal at the edge of the range can impact some radial current measurements at the far ranges (see Figure 95). Figure 96 shows the LOS analysis results and all 15 wind turbines from South Fork will be within the LOS of NWTP.

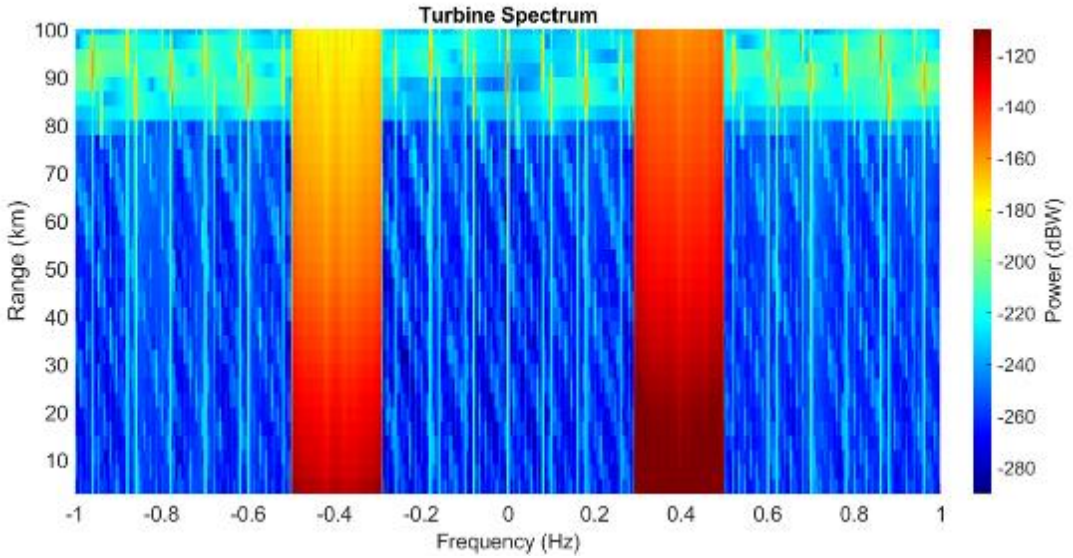

Figure 94 - Range Doppler matrix for the NWTP SeaSonde located on Nantucket, MA with turbine interference from the South Fork farm. There are 15 total turbines spinning at 5.2 rpm.

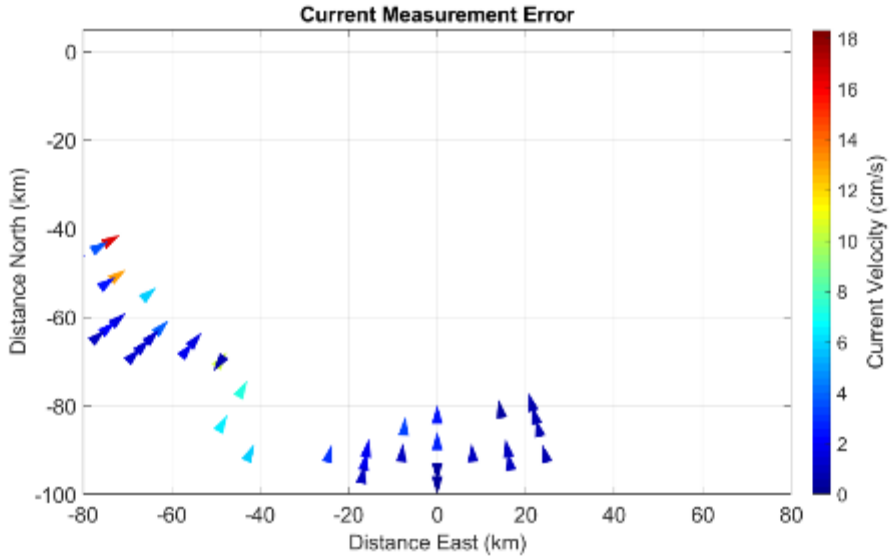

Figure 95 - Current measurement error for the NWTP SeaSonde located at Nantucket, MA with turbine interference from the South Fork farm. Modeled sea currents were 100 cm/s running parallel to the coast.

Figure 96 - South Fork, SeaSonde NWTP

3.1.3.2.3 Long Range SeaSondes

There are three 5 MHz SeaSonde systems that will be able to see the South Fork wind farm. South Fork will be at short-mid range for both long range SeaSondes affected (see Figure 97). These belong in class G of SeaSonde interference with a small wind farm at a middle range for the system which is discussed below with MVCO SeaSonde.

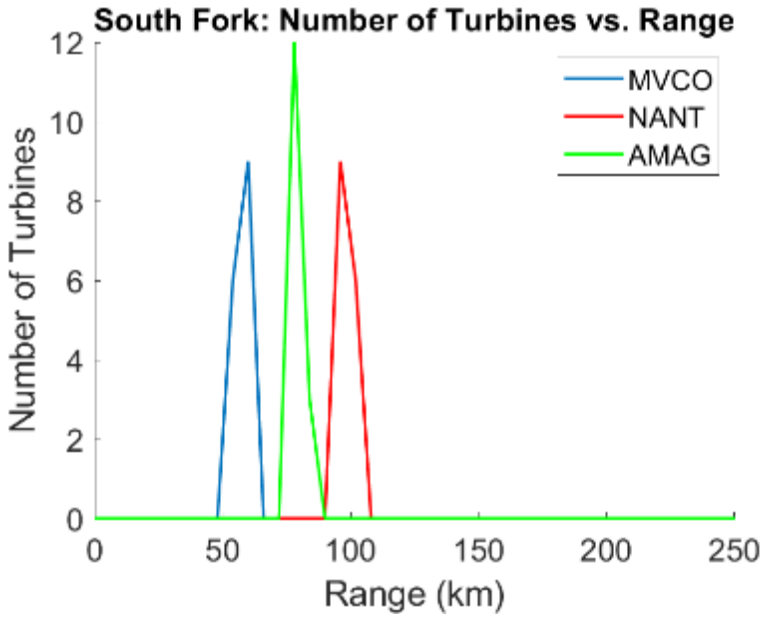

Figure 97 - Number of turbines in each range bin for the long range SeaSondes near the Southfork farm

In Figure 98, the range-Doppler map for the MVCO SeaSonde on Martha's Vineyard is shown with interference from the Southfork wind farm which contains 15 turbines that were simulated to spin at 5.2 rpm. The turbine interference is contained within the range bins that contain the turbines or adjacent bins. Also displayed in Figure 99 is the power spectrum in the 60 km range bin which is within the center

region of interference. With the rotation rate displayed, there was no change in the FOL region selection which is displayed by the red lines.

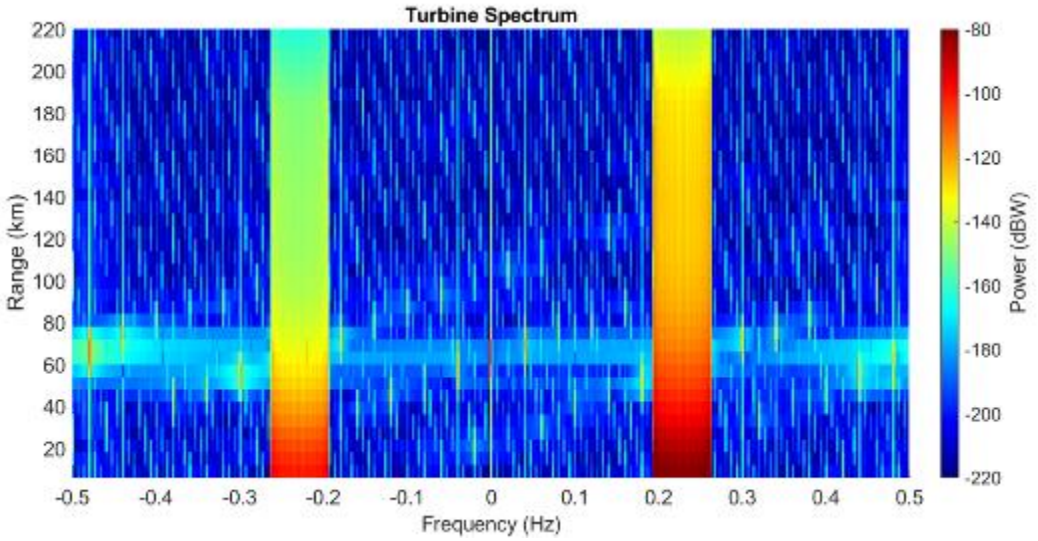

Figure 98 - Range Doppler matrix for the MVCO SeaSonde located on Martha's Vineyard with turbine interference from the South Fork farm. There are 15 total turbines spinning at 5.2 rpm.

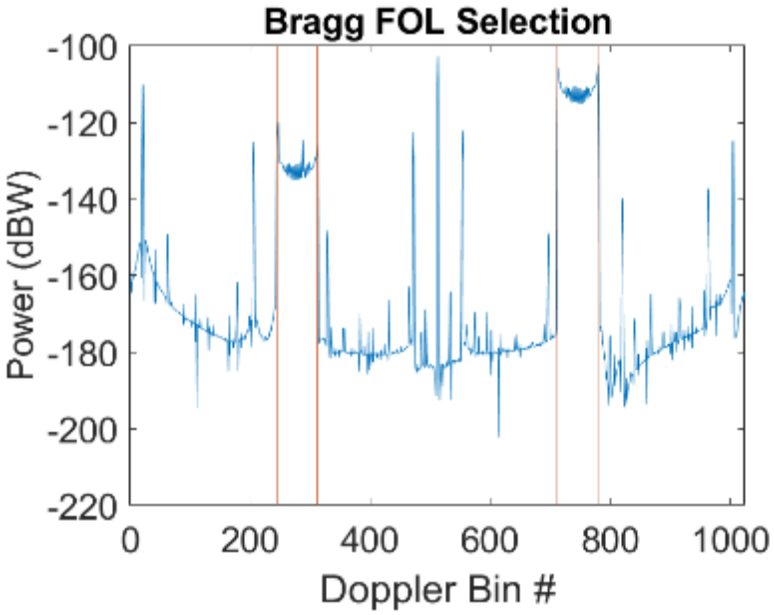

Figure 99 - Power spectrum in the 60 km range bin for the MVCO SeaSonde located at Martha's Vineyard with turbine interference from the South Fork farm. Red lines are the FOL selection with no turbine interference and the green lines are the FOL selection with the turbine signals.

The induced current measurement errors are shown below in Figure 100 and the errors are contained within the range bins near the wind farm with the largest errors in the rough direction of the Southfork wind farm. The errors in some cases are on the order of 100 cm/s, which is the largest current present in the simulation. Figure 101 shows the line-of-sight analysis results and all 15 wind turbines from South Fork will be within the LOS of MVCO.

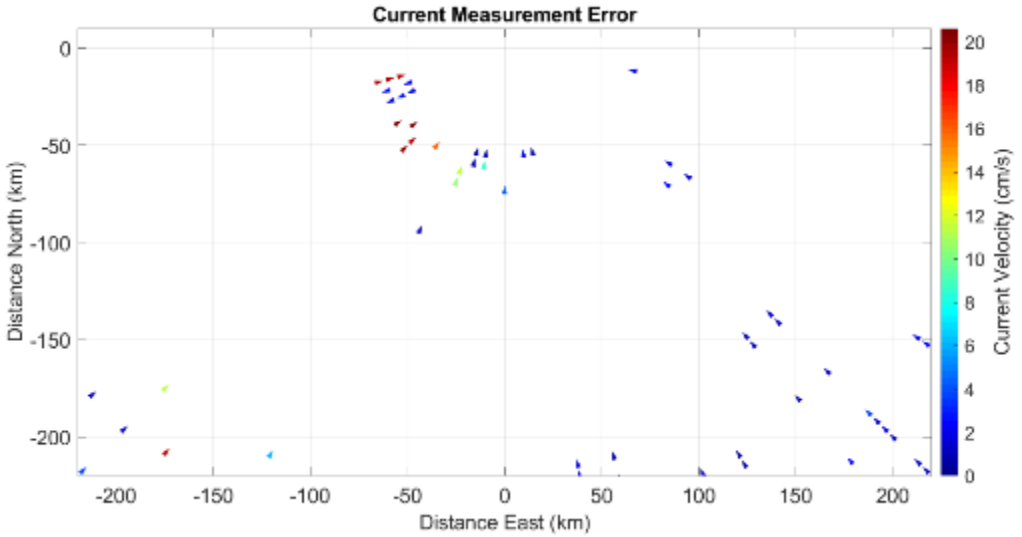

Figure 100 - Current measurement error for the MVCO SeaSonde located at Martha's Vineyard with turbine interference from the South Fork farm. Modeled sea currents were 100 cm/s running parallel to the coast.

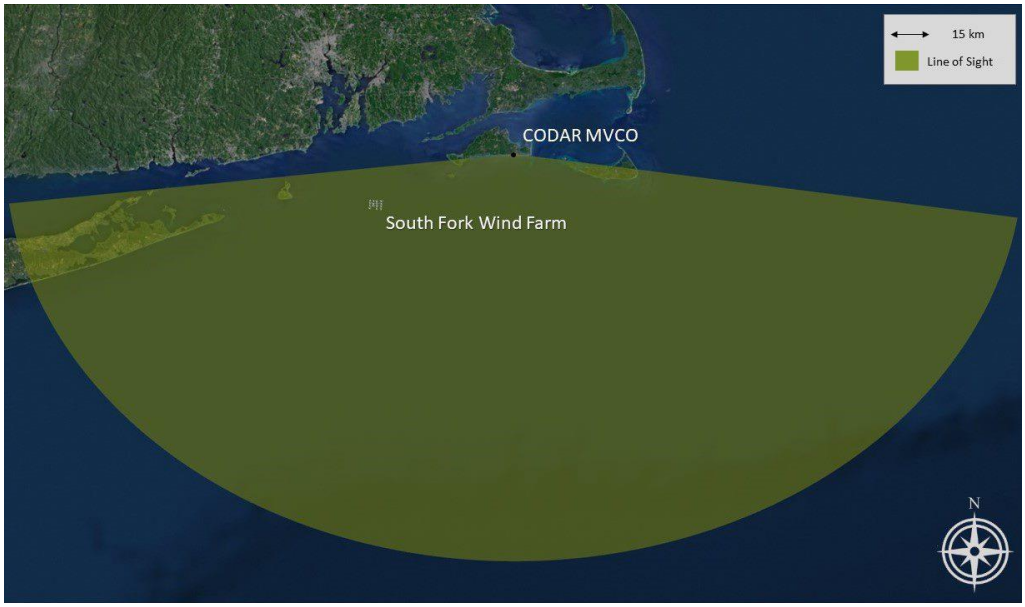

Figure 101 - South Fork, SeaSonde MVCO

The results for the NANT and AMAG SeaSondes will have similar effects and has been classified in the same class as the MVCO SeaSonde discussed above. The greater range to the turbines will mean a lesser signal return, though the long range SeaSondes will still be able to pick up the turbines at that range. The errors induced for the NANT and AMAG SeaSondes were found to still have the potential to be large but were generally more localized in range and angle than the closer MVCO SeaSonde.

3.1.4 Mayflower

Mayflower was in the early planning stages when this report was written and is within LOS of one ASR-8, one ASR-9, and six SeaSonde radars. It is located in the RI/MA lease area (Lease OCS-A-0521) and has 67 15-MW turbines.

3.1.4.1 *ASR*

There is one ASR-9 close enough to the potential Mayflower Wind farm to potentially be impacted by its development. Booz Allen conducted a LOS analysis, as shown in Figure 102. The figure shows the Mayflower Wind turbines are very similar to the Bay State Wind with respect to ACK. Therefore, the impact is expected to be consistent with the findings in Section 3.1.2.1. Figure 103 shows the WindTRx ASR-9 raw CFAR detections of the Mayflower turbines at ACK. Similar to Bay State, the turbines are expected to both produce false detections in the region of the wind farm and raise the interference for the ASR-9's ability to detect an aircraft in the vicinity, as shown in Figure 104 through Figure 109.

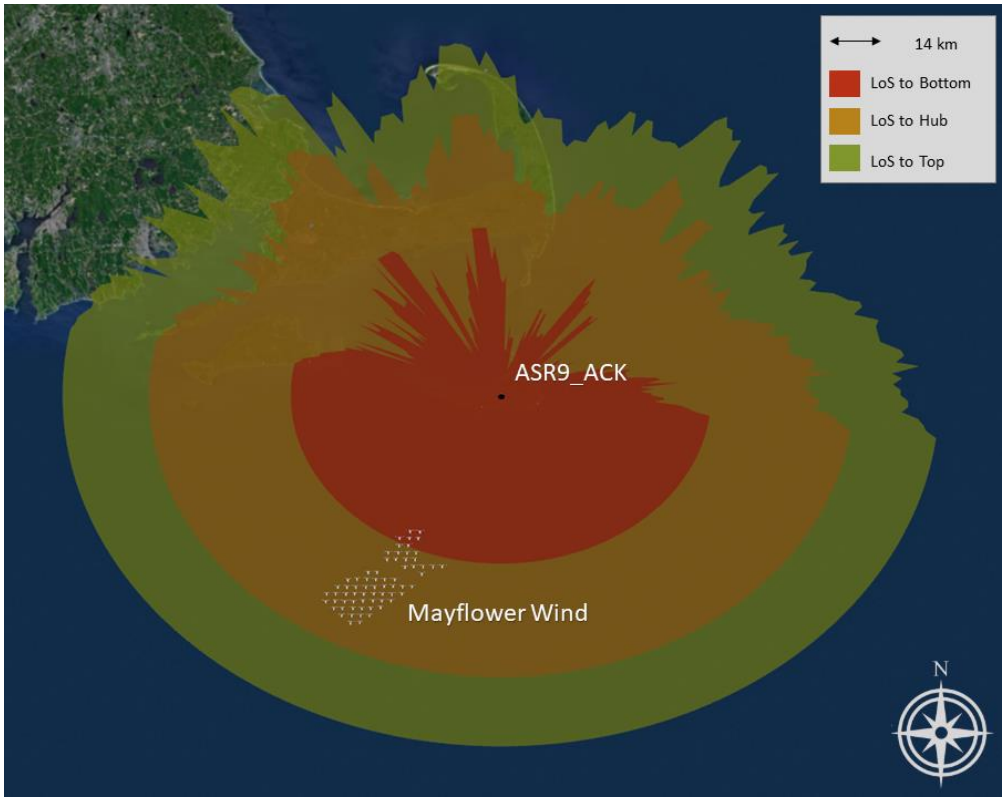

Figure 102 - ACK LOS to Mayflower Wind

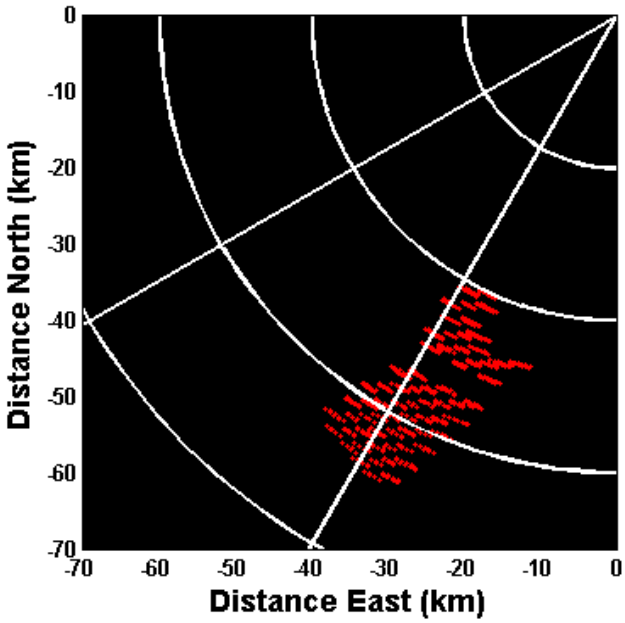

Figure 103 - ACK CFAR Detections of Mayflower Wind Turbines

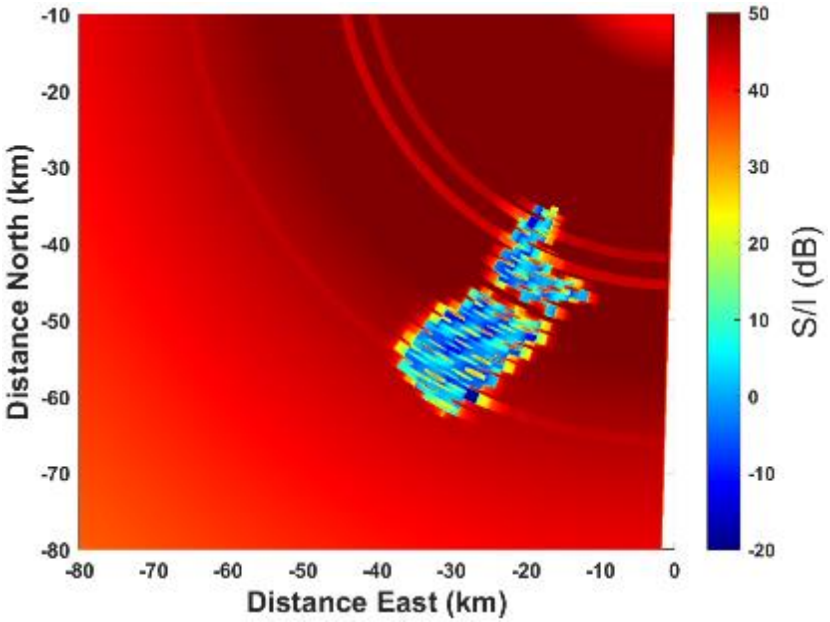

Figure 104 - Mayflower Signal-to-Interference Ratio at ACK for a 0dBsm Aircraft at 2km Altitude

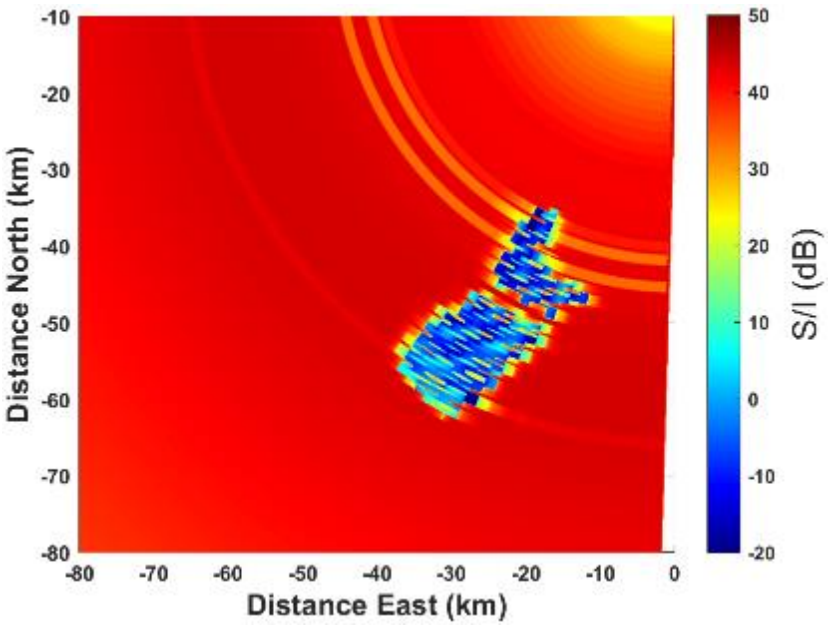

Figure 105 - Mayflower Signal-to-Interference Ratio at ACK for a 0dBsm Aircraft at 5km Altitude

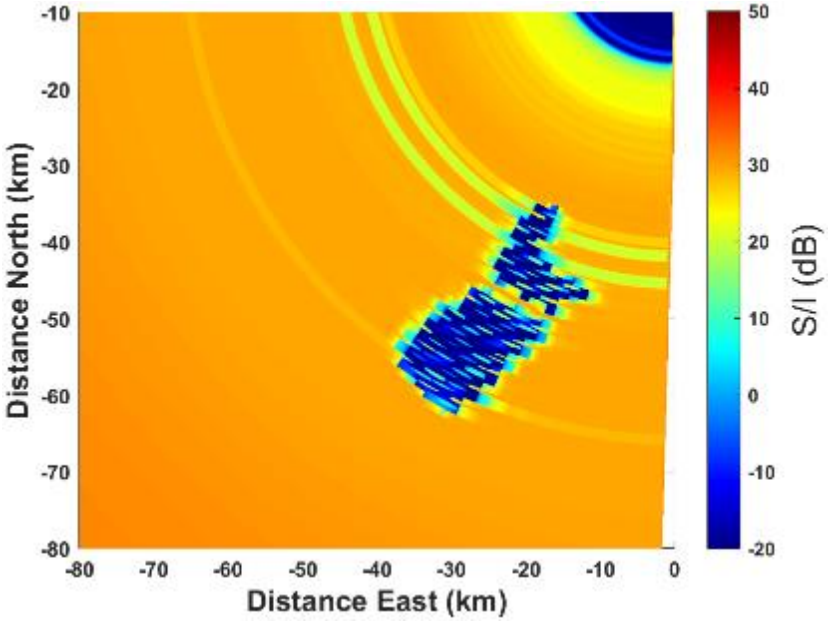

Figure 106 - Mayflower Signal-to-Interference Ratio at ACK for a 0dBsm Aircraft at 10km Altitude

The only other ASR within the vicinity of Mayflower Wind is the ASR-8 FMH. Figure 107 shows that roughly half of the turbines in Mayflower wind will be within LOS to FMH. For all the turbines that are visible, only the top half of the blades are within LOS.

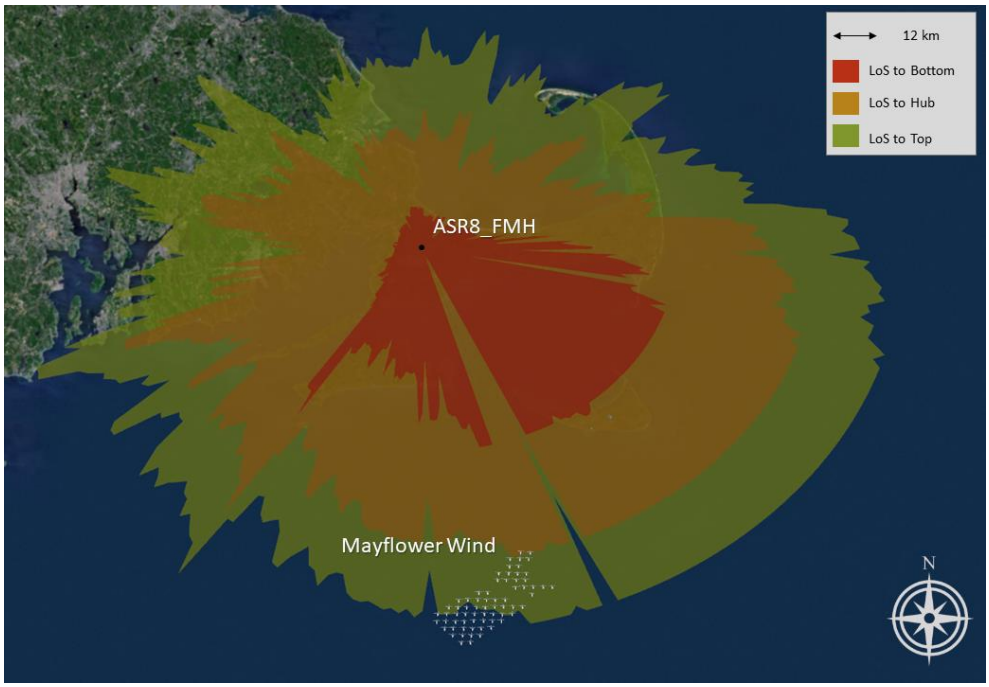

Figure 107 - FMH LOS to Mayflower Wind

3.1.4.2 *SeaSonde*

Table 11 - Impacted SeaSondes from Hypothetical Wind Farms (Mayflower)

Impacted SeaSondes	Class of Interference
NWTP	F
LPWR	F
MVCO	H
NANT	H
AMAG	H
MRCH	I

3.1.4.2.1 Medium Range SeaSondes

There are two SeaSondes that are impacted by the Mayflower wind farm with the turbines appearing at mid-range and is displayed in Figure 108. These two radars fall into class F where there is a large wind farm at mid-range which was discussed in more detail above in the Bay State section. The Mayflower wind farm is about half the size of some of the other large wind farms and thus will have less interference than others in class F.

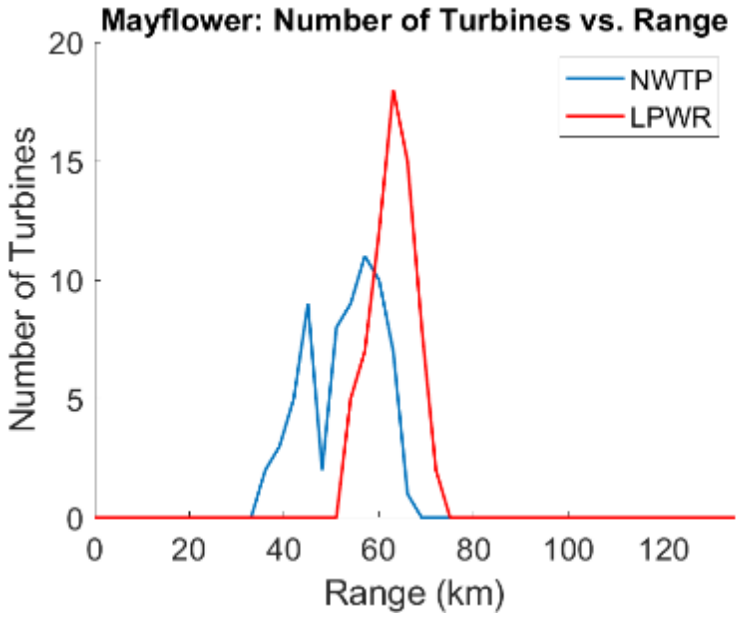

Figure 108 - Number of turbines in each range bin for the medium range SeaSondes near the Mayflower wind farm.

3.1.4.2.2 Long Range SeaSondes

Three of the long-range SeaSondes which are affected by the Mayflower wind farm, MVCO, NANT, and AMAG, will see the wind farm at mid-range (Figure 109). This classifies these systems in class H where there is a large wind farm at mid-range and is discussed in more detail under the Bay State section. While Mayflower was considered a large wind farm in this analysis, there are roughly half the number of turbines in Mayflower as in Bay State which also has this type of interference. It should be noted that this will be less of an impact than what was discussed with Bay State but will have similar interference. The last SeaSondes in range (MRCH) of the Mayflower farm will see the wind farm at extended range and it is in class I where there is a large wind farm at long range which is discussed below in the Ocean Wind section.

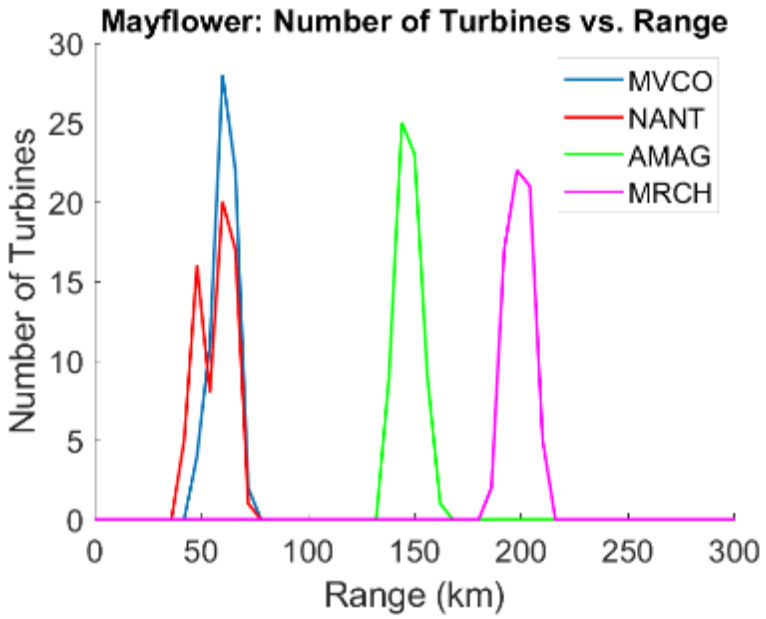

Figure 109 - Number of turbines in each range bin for the long range SeaSondes near the Mayflower farm

3.1.5 RI/MA Cumulative Scenario

The RI/MA Cumulative Scenario is intended as a "maximum case" build-out scenario for the RI/MA area. Given that BOEM anticipates that there may be a number of additional projects in the area over the next few years, the goal of this scenario was to investigate how severe radar interference could become if the maximum number of turbines were built out in this region. BOEM and the research team understand that this is a highly-unlikely build-out scenario, but stress that this hypothetical scenario was developed to investigate a "worst case" from a radar interference perspective.

The cumulative scenario consists of all the other planned wind farms in the RI/MA area (South Fork, Vineyard Wind, Bay State Wind, and Mayflower), as well as hypothetical turbines that fill out the remaining lease areas (OCS-A-0487, OCS-A-0520, OCS-A-0522).

The RI/MA Cumulative Scenario is within LOS of one ASR-8, two ASR-9s, and ten SeaSonde radars. It has 1,115 turbines that range from 10-MW to 15-MW

3.1.5.1 *ASR*

The RI/MA cumulative scenario falls within the line-of-sight of three ASR-9 radars. The ASR-8 FMH (Figure 110) and ASR-9 KPVD (Figure 111) have LOS to the northwest portion of the cumulative scenario. This will degrade the radar performance substantially in the region of their scan over the cumulative scenario similar to what will be discussed in more detail below with the ACK system below.

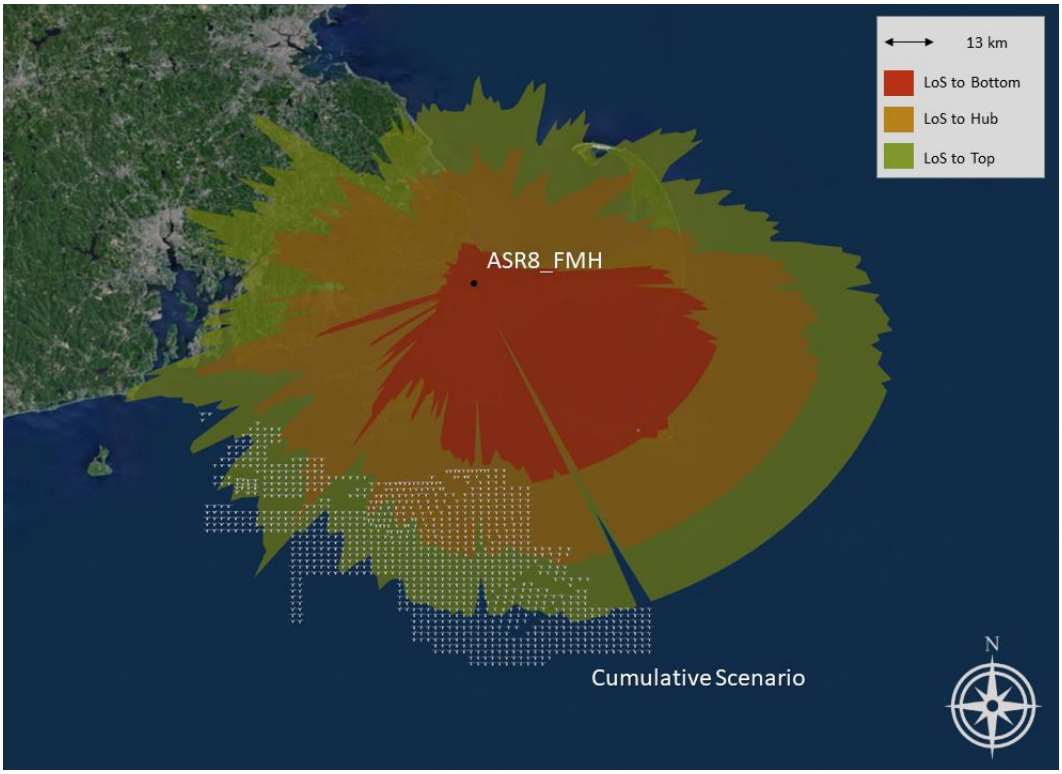

Figure 110 - ASR-8 FMH LOS to RI/MA Cumulative Scenario

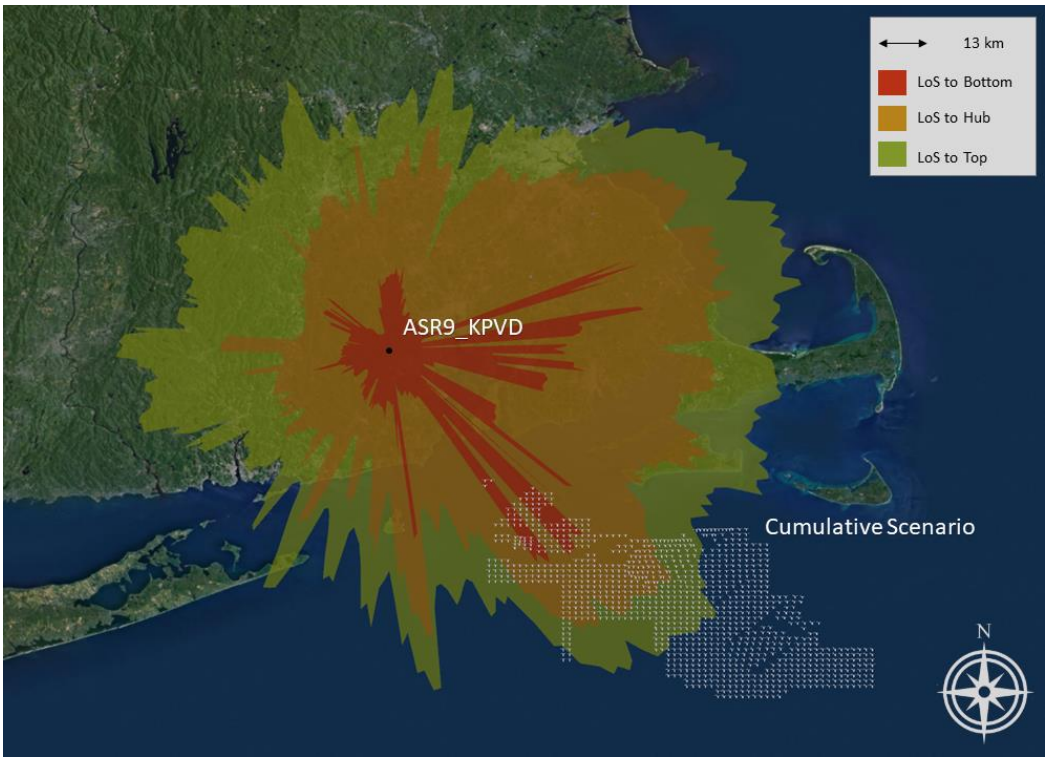

Figure 111 - ASR-9 KPVD LOS to RI/MA Cumulative Scenario

The third ASR-9 within the vicinity of the RI/MA Cumulative Scenario is ACK. Air surveillance radars have a maximum number of detections, plots and tracks they can maintain. For the purpose of showing

all the data, these limits have been removed for the following plots, however it is important to note. Should the ASR-9 start to approach these operating limits the system might lose performance and begin to ignore detections beyond some limit. This is an effect not captured here but potentially a third way a wind farm might impact the performance of a radar. The figures below show the Cumulative Scenario as presented to ACK. Figure 113 shows the raw CFAR detections if there is not a limit to the number of CFAR detections that can be declared per CPI. In Figure 114-Figure 116, the signal to interference level is shown for targets at three different altitudes for a 0 dBsm target. In addition to the many detections declared by the radar, the ability to pick out a target over the farm is degraded. Due to the size of this hypothetical scenario, this would degrade the ability to detect targets over a ~20-30 km range band in the entire southwest quadrant of the surveillance airspace.

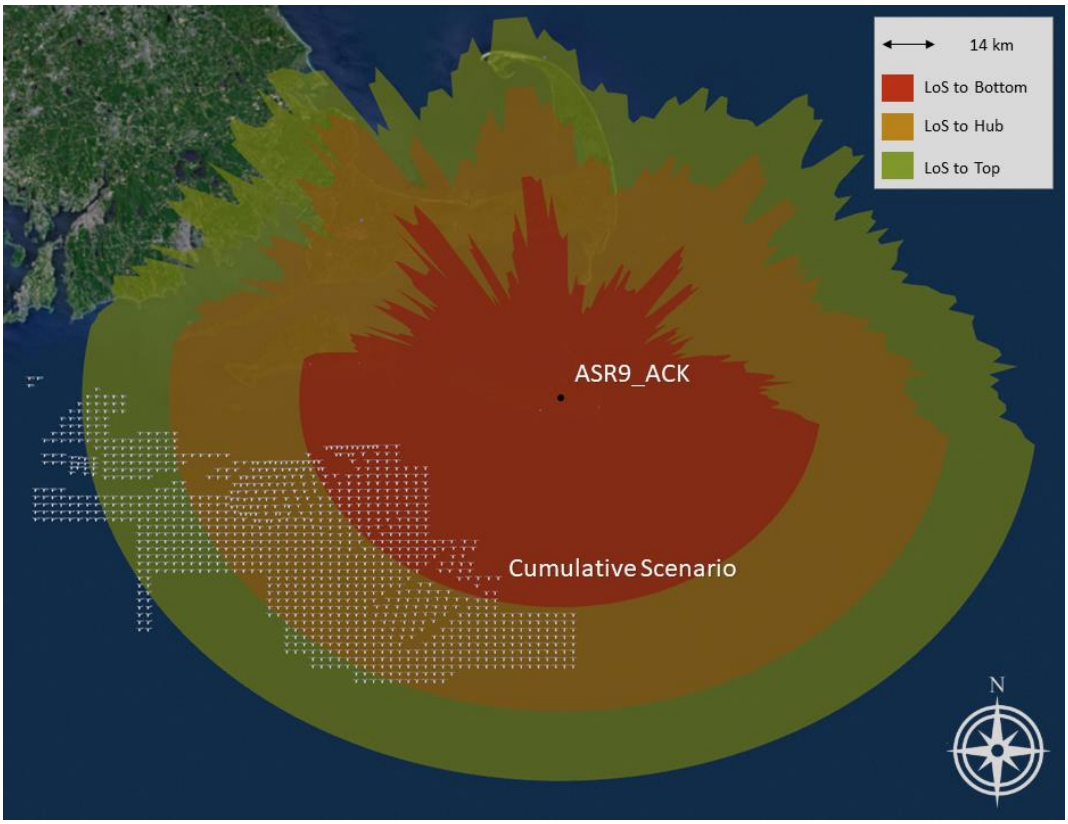

Figure 112 - ASR-9 ACK LOS to RI/MA Cumulative Scenario

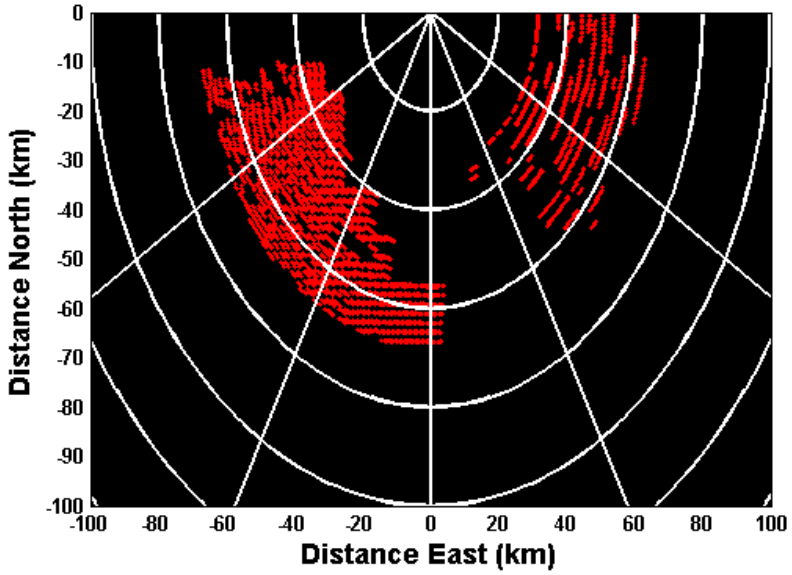

Figure 113 - ACK Raw CFAR Detections of RI/MA Cumulative Scenario Wind Turbines

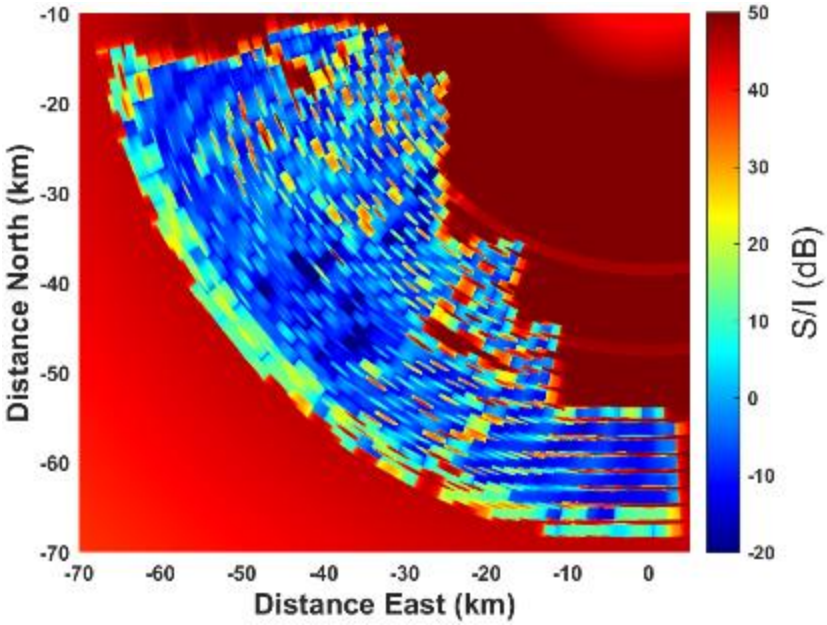

Figure 114 - Signal to Interference for a 0dBsm aircraft flying at 2 km altitude near ACK

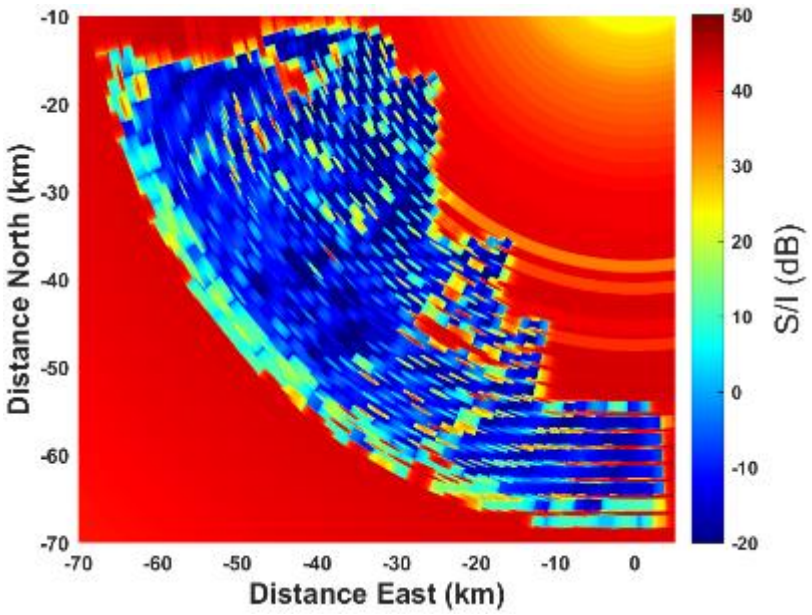

Figure 115 - Signal to Interference for a 0dBsm aircraft flying at 5km altitude near ACK

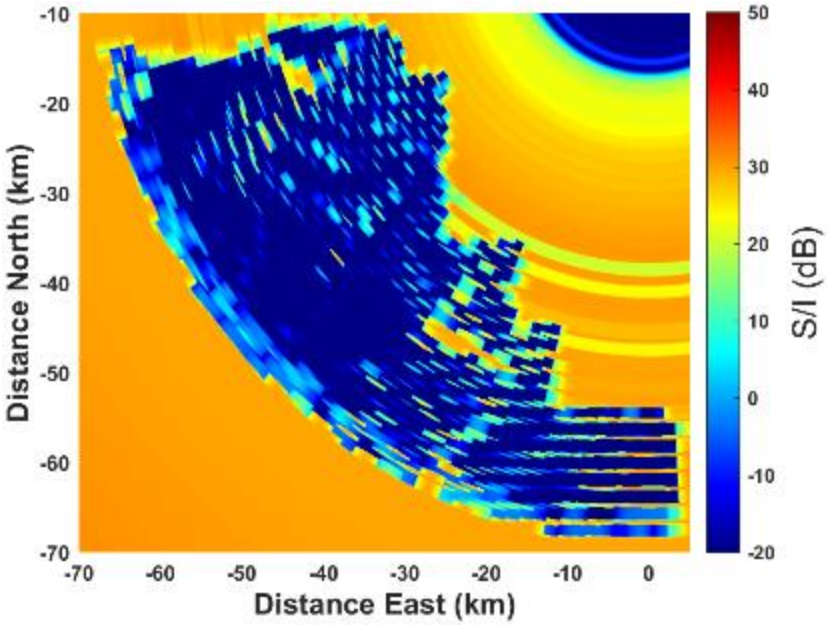

Figure 116 - Signal to Interference for a 0dBsm aircraft flying at 10km altitude near ACK

3.1.5.2 *SeaSonde*

Table 12 - Impacted SeaSondes from RI/MA Cumulative Scenario

Impacted SeaSondes
SQUB
BISL
NWTP

Impacted SeaSondes
LPWR
HBSR
CPVN
MVCO
NANT
MRCH
AMAG

3.1.5.2.1 Short Range SeaSondes

The cumulative scenario will impact two of the short range SeaSondes in the area. Both systems will see a large number of turbines starting at mid-range for the systems and extending beyond their maximum ranges as shown in Figure 117. With the very large number of turbines this scenario will not be categorized as other wind farm scenarios and the impact on the SQUB system is discussed to give an overview of the impact of this scenario.

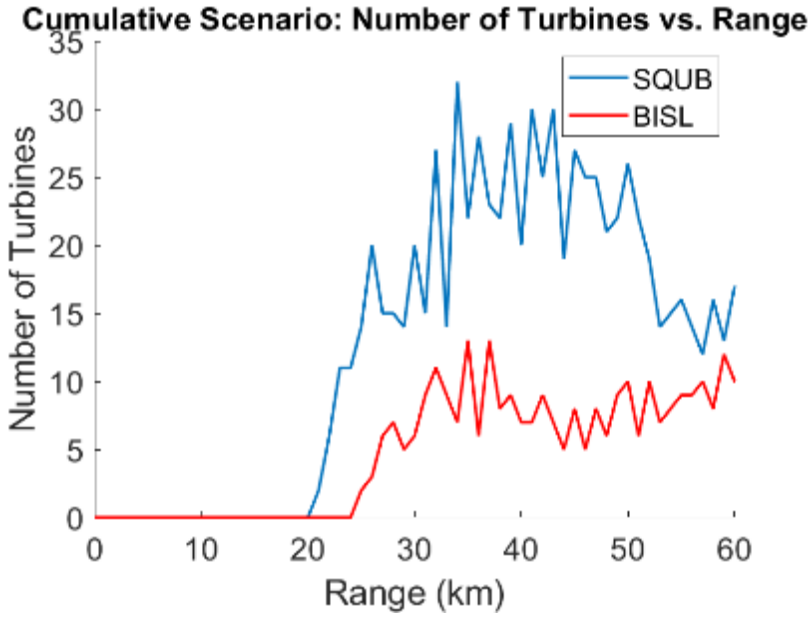

Figure 117 - Number of turbines in each range bin for the short range SeaSondes near the cumulative wind farm scenario

Figure 118 shows the range-Doppler map of the SQUB SeaSonde with interference from the cumulative scenario where there are signals from all turbines within 60 km (584 turbines) of the radar. The turbine interference extends outward from the start of the cumulative wind farm at 20 km, but the interference level starts to drop to a smaller level beyond about 40 km which is due to a rapid decrease in the propagation of the 25 MHz signal at the longer ranges. Figure 119 shows the power spectrum in the 30 km range bin and there is a strong return from the turbines that can be comparable to weaker Bragg peaks and can cause FOL misidentification as is the case in the figure.

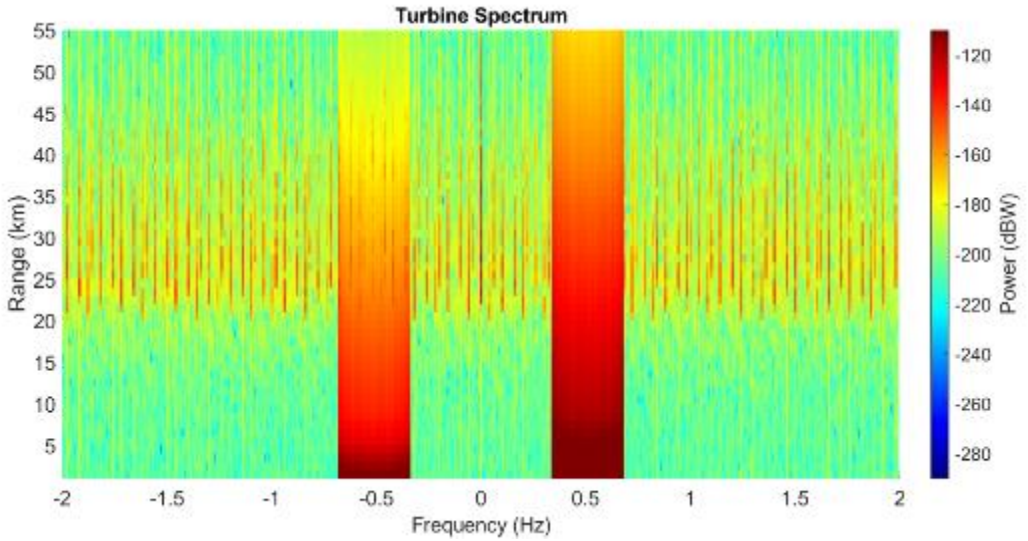

Figure 118 - Range Doppler matrix for the SQUB SeaSonde located on Martha's Vineyard with turbine interference from the cumulative scenario. There are 584 turbines spinning at 5.2 rpm located within 60 km of the SeaSonde site that were considered.

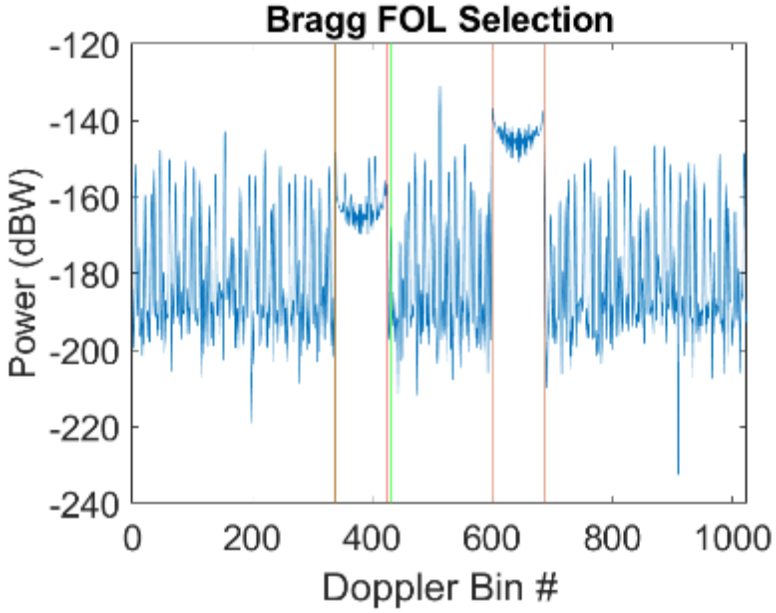

Figure 119 - Power spectrum in the 30 km range bin for the SQUB SeaSonde located on Martha's Vineyard with turbine interference from the cumulative scenario. Red lines are the FOL selection with no turbine interference and the green lines are the FOL selection with the cumulative scenario.

The effects on the current measurements in this scenario is impacted over a large radial and angular region as shown in Figure 120 which shows induced errors with turbine interference. The number of radial vectors which will see large errors will make current measurements much more difficult in the presence of this many turbines. Figure 121 shows the line-of-sight analysis results and all wind turbines from Cumulative Scenario will be within the LOS of SQUB.

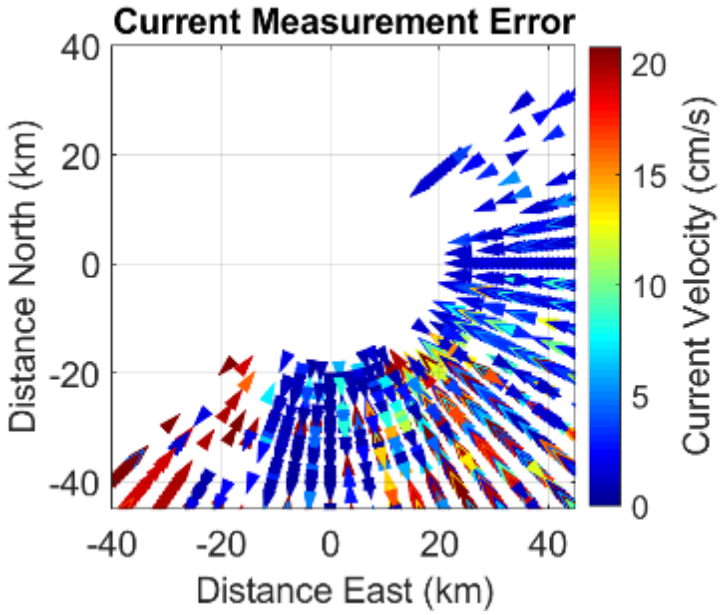

Figure 120 - Current measurement error for the SQUB SeaSonde located on Martha's Vineyard with turbine interference from the cumulative scenario. Modeled sea currents were 100 cm/s running parallel to the coast.

Figure 121 – RI/MA Cumulative Scenario, SeaSonde SQUB

The BISL SeaSonde will also be interfered with by this cumulative scenario but will not be as highly impacted. This is due to the turbines starting at 30 km away (vs. 20 km for SQUB) and having roughly half the number of turbines in the closer range as shown in Figure 117. These two effects should allow the BISL SeaSonde to perform adequately for the bulk of its instrumented range losing some efficiency in the longer ranges.

3.1.5.2.2 Medium Range SeaSondes

There are four medium range SeaSondes which will be impacted by the cumulative scenario. In Figure 122 the number of turbines that these SeaSondes will see vs. range is shown and for all but the CPVN, most of the turbines will be within the instrumented range of 100 km. Below, the LPWR SeaSonde is shown in more detail as an example of this cumulative scenario on the medium range SeaSondes in the area. The results for the LPWR will be the worst-case scenario of the impact SeaSondes due to the turbines being closest to this system, however for the other medium range SeaSondes, the impact will be similar.

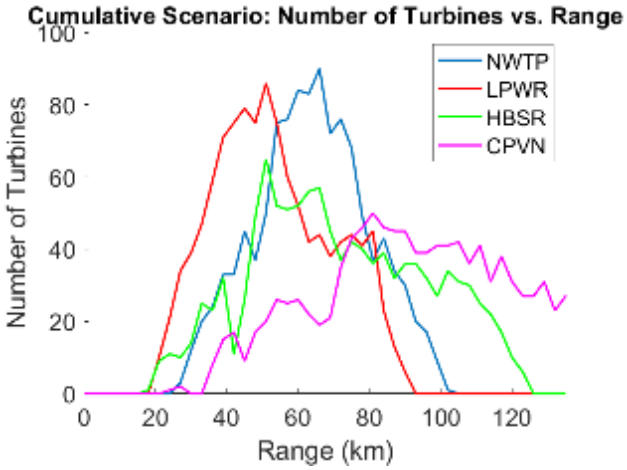

Figure 122 - Number of turbines in each range bin for the medium range SeaSondes near the RI/MA Cumulative Scenario.

The range-Doppler map for the LPWR SeaSonde with turbine interference in the cumulative scenario is shown in Figure 123. The turbines span ~20-90 km in range from LPWR and in the range-Doppler map, and the largest interference is from ~10-70 km. The turbines at longer range will have less of a signal return and the illuminated cell size of the ocean will increase making the relative interference less significant but still present. In Figure 124 the power spectrum in the 33 km range bin is shown with the FOL selection with (green) and without (red) turbine interference from the cumulative scenario. As shown, the turbine returns are on par with the returns from the Bragg scatter off the ocean which can lead to FOL misidentification and where the signal is within an FOL, strong angle misidentification.

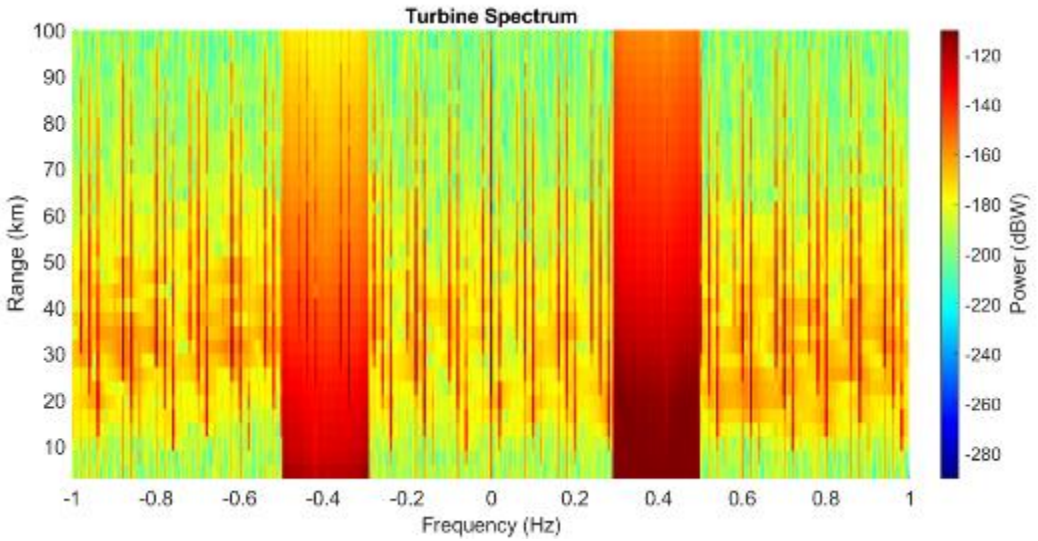

Figure 123 - Range Doppler matrix for the LPWR SeaSonde on Martha's Vineyard with turbine interference from the RI/MA Cumulative Scenario. There are 1,115 turbines spinning at 5.2 rpm.

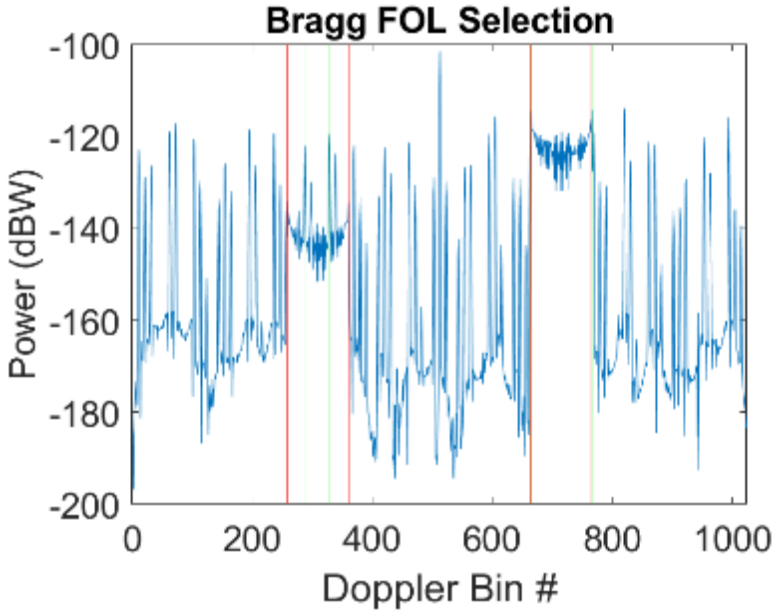

Figure 124 - Power spectrum in the 33 km range bin for the LPWR SeaSonde on Martha's Vineyard with turbine interference from the cumulative scenario. Red lines are the FOL selection with no turbine interference and the green lines are the FOL selection with the RI/MA Cumulative Scenario.

Figure 125 shows the current errors induced on the LPWR SeaSonde with the presences of the cumulative wind farm scenario. There are large errors induced over the entire region that the SeaSonde is designed to measure in the presence of the turbines with some errors being on the order of 100 cm/s, which is also the largest currents present in the simulation.

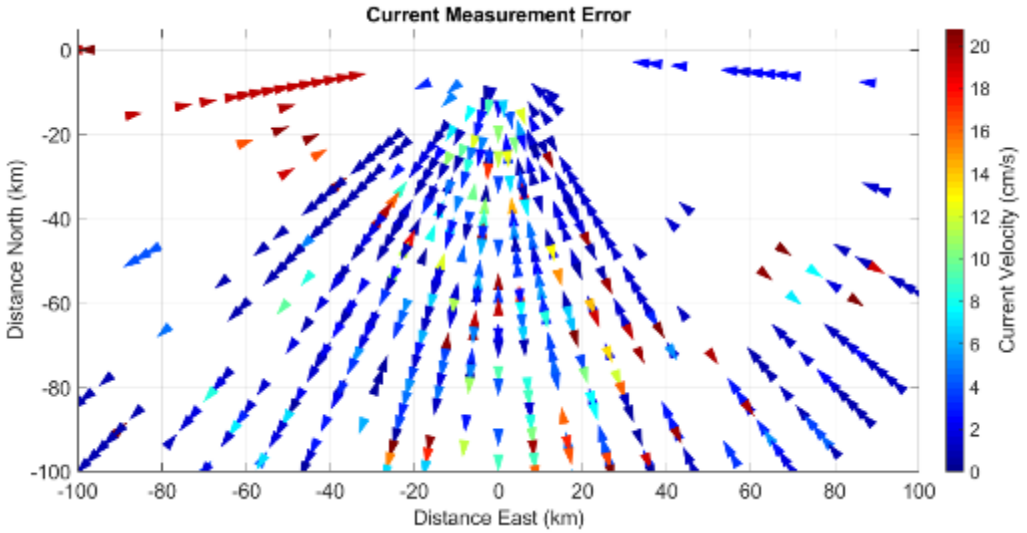

Figure 125 - Current measurement error for the LPWR SeaSonde located on Martha's Vineyard with turbine interference from the RI/MA Cumulative Scenario. Modeled sea currents were 100 cm/s running parallel to the coast.

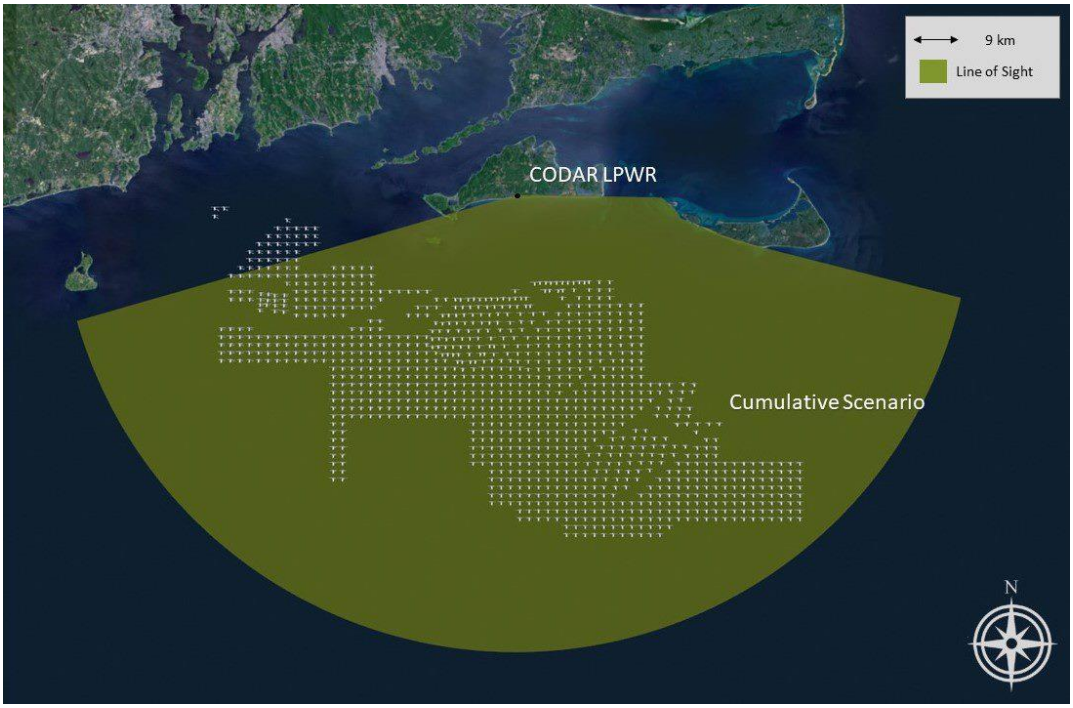

Figure 126 – RI/MA Cumulative Scenario, SeaSonde LPWR

3.1.5.2.3 Long Range SeaSondes

There are four long range SeaSondes that would be interfered with by the cumulative wind farm scenario (Figure 127). The MVCO, NANT, and AMAG SeaSondes will both be in range of nearly all the turbines of this cumulative scenario. The MRCH SeaSonde will see most of the turbines in the cumulative scenario but will see them at mid-long ranges (~120-200 km). This section provides an overview of the effects of this cumulative scenario for the MVCO SeaSonde, which will be very similar to the NANT

SeaSonde. The AMAG and MRCH SeaSondes will have less interference than either of these due to the turbines at longer ranges.

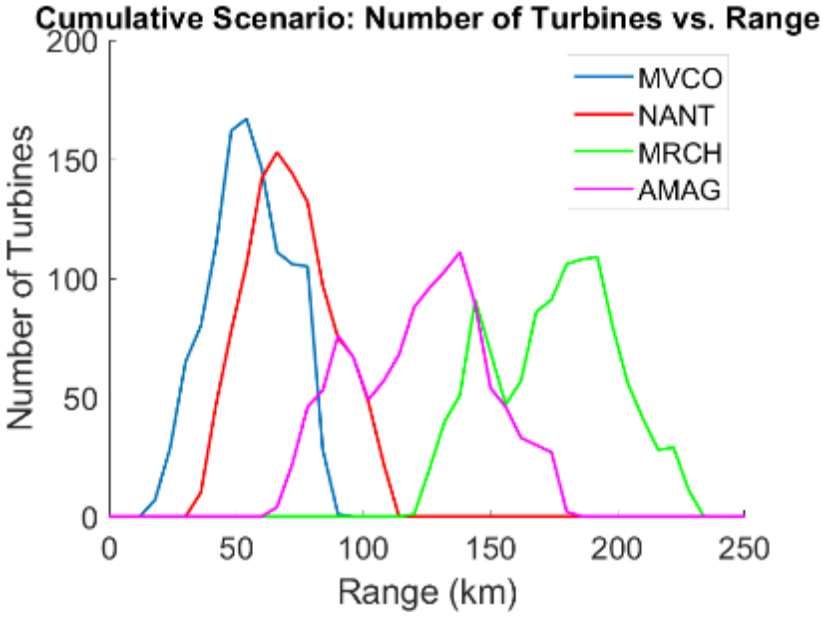

Figure 127 - Number of turbines in each range bin for the long range SeaSondes near the cumulative wind farm scenario.

The range-Doppler map for the interference of the cumulative scenario and the MVCO SeaSonde is shown below in Figure 128. The turbines span in range from ~20-100 km and in the range-Doppler map shows interference out to 100 km. The power spectrum is also displayed in Figure 129 for the 36 km range bin. The turbine returns will be of the same order as the Bragg peaks which can cause large angle errors. This can also cause FOL identification issues as well, though this is not demonstrated in the example below.

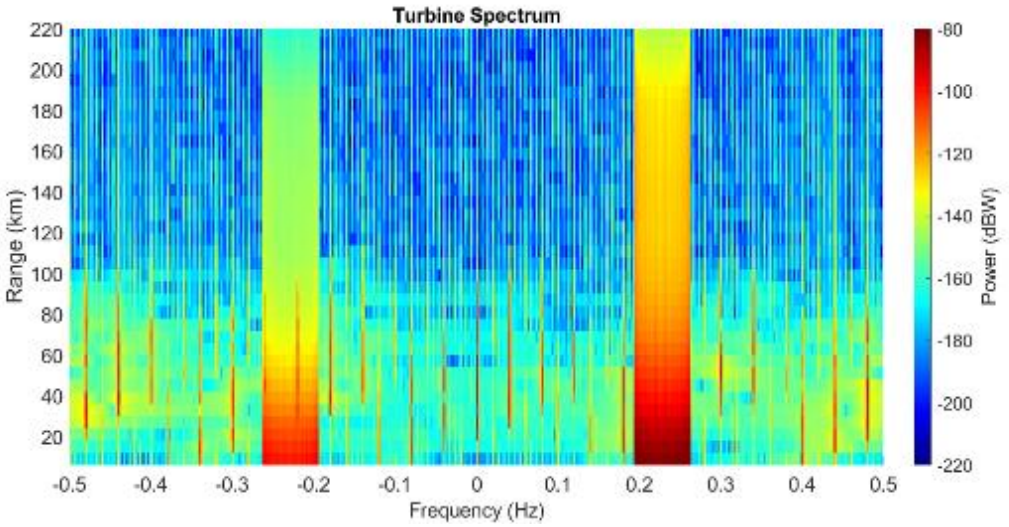

Figure 128 - Range Doppler matrix for the MVCO SeaSonde on Martha's Vineyard with turbine interference from the RI/MA Cumulative Scenario. There are 1,115 turbines spinning at 5.2 rpm.

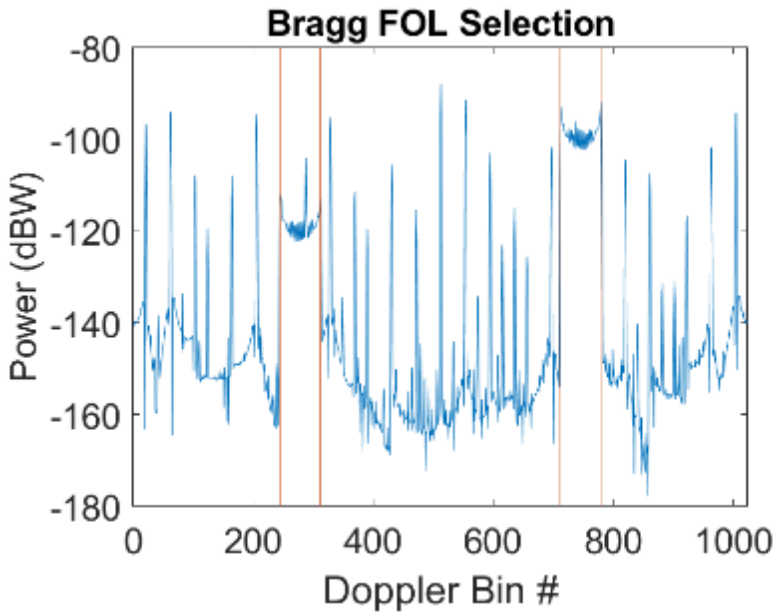

Figure 129 - Power spectrum in the 30 km range bin for the MVCO SeaSonde located on Martha's Vineyard with turbine interference from the RI/MA Cumulative Scenario. Red lines are the FOL selection with no turbine interference and the green lines are the FOL selection with the cumulative scenario.

The errors in the current measurement are shown in Figure 130. There are large errors that span most of the region that the SeaSonde is designed to measure. The largest errors present are on the order of 100 cm/s which is the same as the largest values of current present in the simulation.

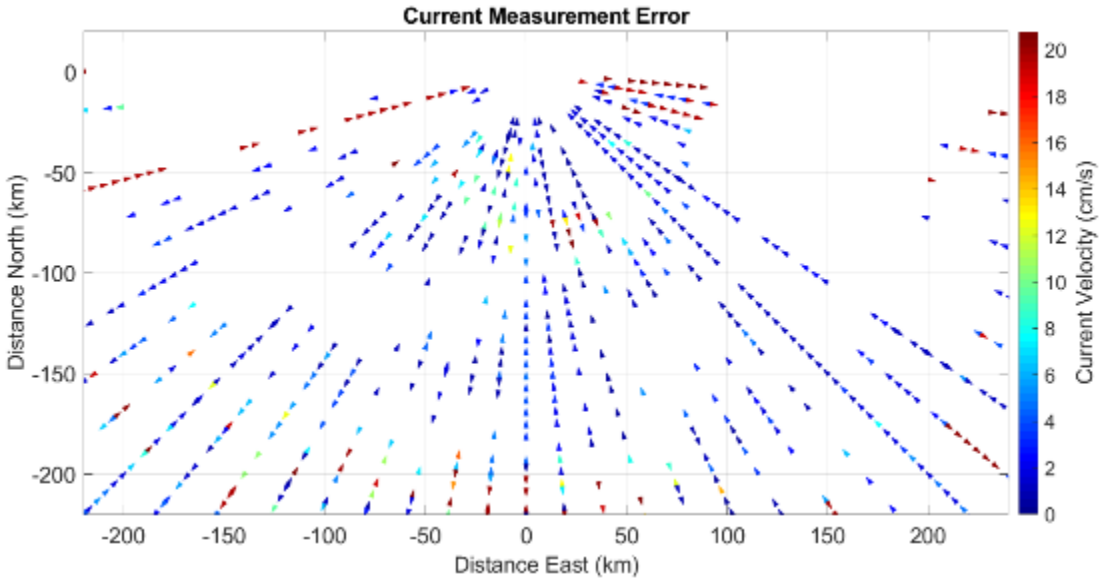

Figure 130 - Current measurement error for the MVCO SeaSonde located on Martha's Vineyard with turbine interference from the RI/MA Cumulative Scenario. Modeled sea currents were 100 cm/s running parallel to the coast.

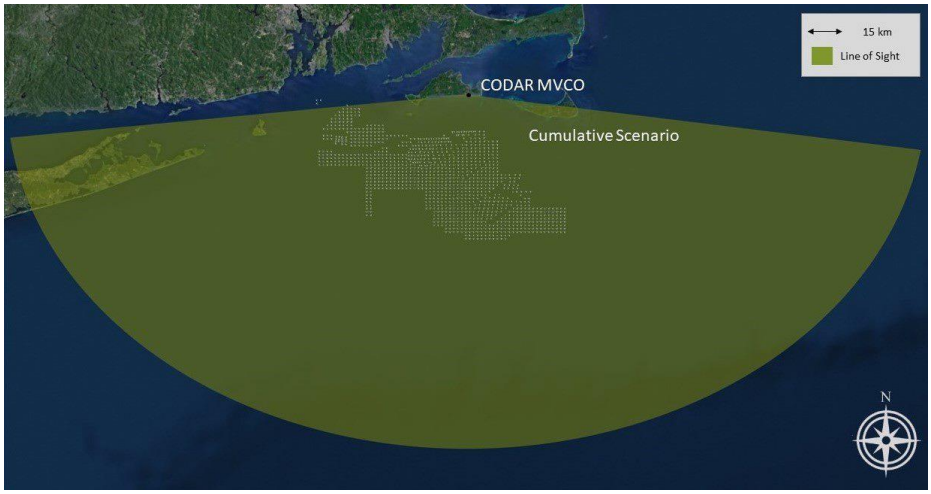

Figure 131 - RI/MA Cumulative Scenario, SeaSonde, MVCO

3.1.6 Empire Wind

Empire Wind had been proposed to BOEM in a COP when this report was developed and is within LOS of two ASR-9s, one ARSR-4, two NEXRADs, and eight SeaSondes. It is off the coast of New York and New Jersey (in the New York Bight, within Lease OCS-A-0512) and has 135 18-MW turbines.

3.1.6.1 *ASR*

Two ASR-9 are within the vicinity of Empire Wind farm. The ASR-9 in Islip, NY (code KISP) will be impacted by Empire Wind. Figure 132 shows that the ASR-9 at Islip has LOS to the turbines from the minimum of the Hub to the peak blade height. This level of impact for Empire winds on KISP will be comparable to the contribution of Vineyard Wind on ACK, detailed in section 3.1.1.1.

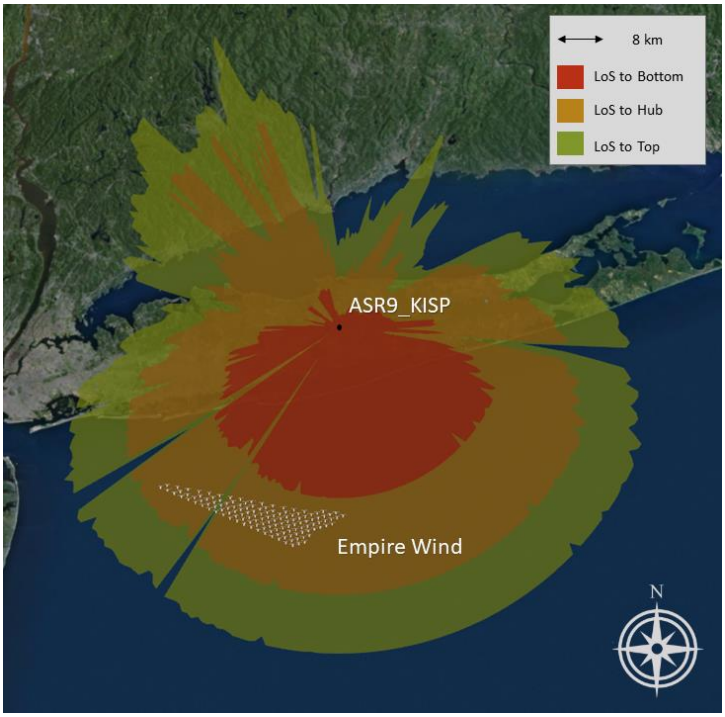

Figure 132 - KISP LOS to Empire Wind

A second ASR-9 is also in the vicinity of Empire Wind. The ASR-9 at John F Kennedy Intl Airport, Jamaica – Jasper, NY (code KJFK) will be impacted by Empire Wind. As seen in Figure 133, KJFK has LOS to nearly the entire Empire Wind farm. Figure 134 shows that aircraft surveillance in the southeast region would be impacted with wind turbine detections interfering with an aircraft flying over the vicinity of Empire Wind.

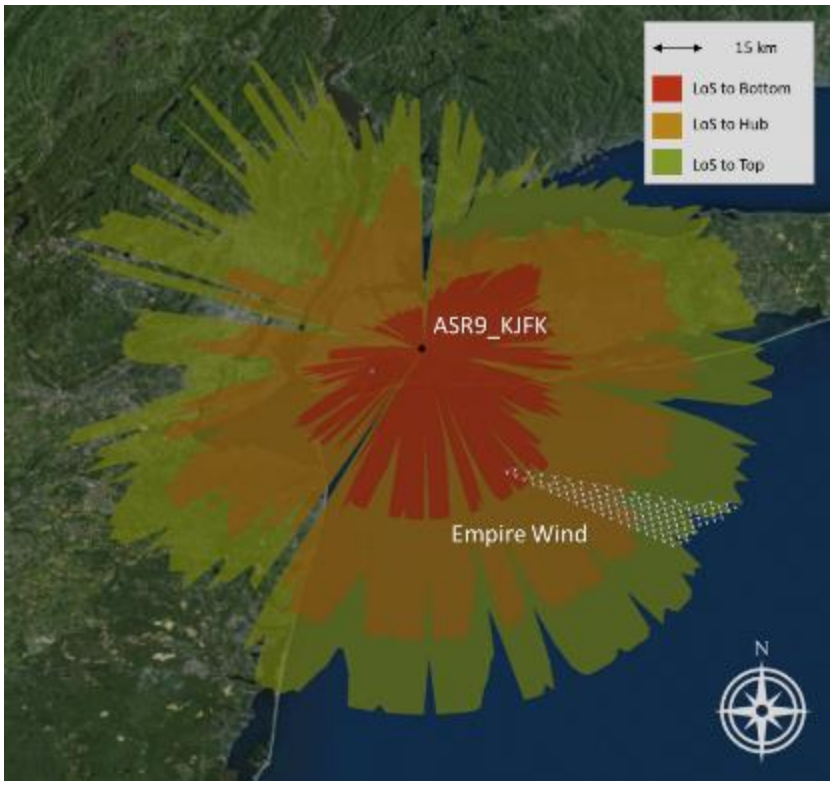

Figure 133 - ASR-9 KJFK LOS to Empire Wind

In Figure 134 the detections from the CFAR processing are shown for the turbines. In the region of the farm nearest the radar range rings can be seen where the full swept area of the blades is visible. Further from the radar there is the standard signal level drop off, but the amount of the blades within LOS is also decreasing leading to the removal of the range rings and at the far edges of the farm less detections. Figure 135-Figure 137 show the signal to interference ratio for a 0 dBsm target at three different altitudes. In these plots, the effects of the range rings on the signal to interference ratio is still visible and over much of the farm, the ability to declare a target detection is below a 13 dB threshold, except at the far edges of the farm. In the far regions of the wind farm targets are still able to be distinguished which is again due to a combination of the turbines at further ranges and less of the blades being visible to the radar.

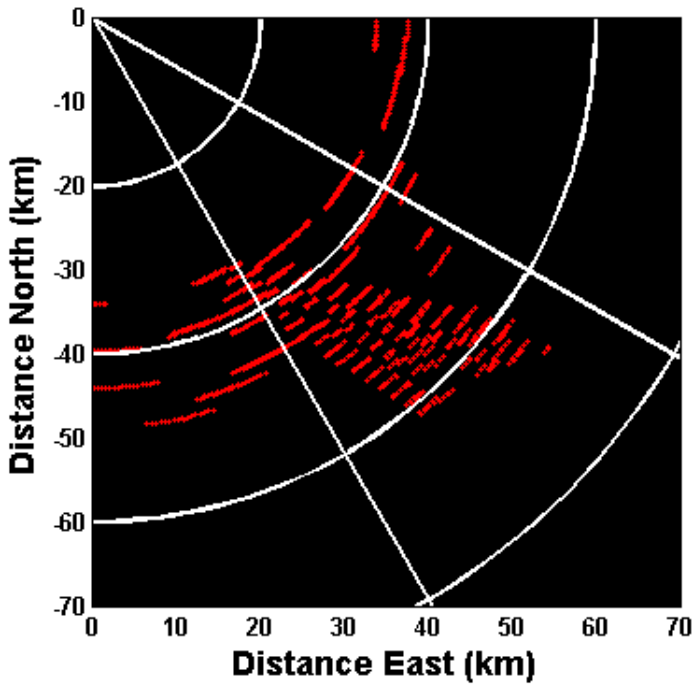

Figure 134 - KJFK Raw CFAR Detections of Empire Wind Turbines

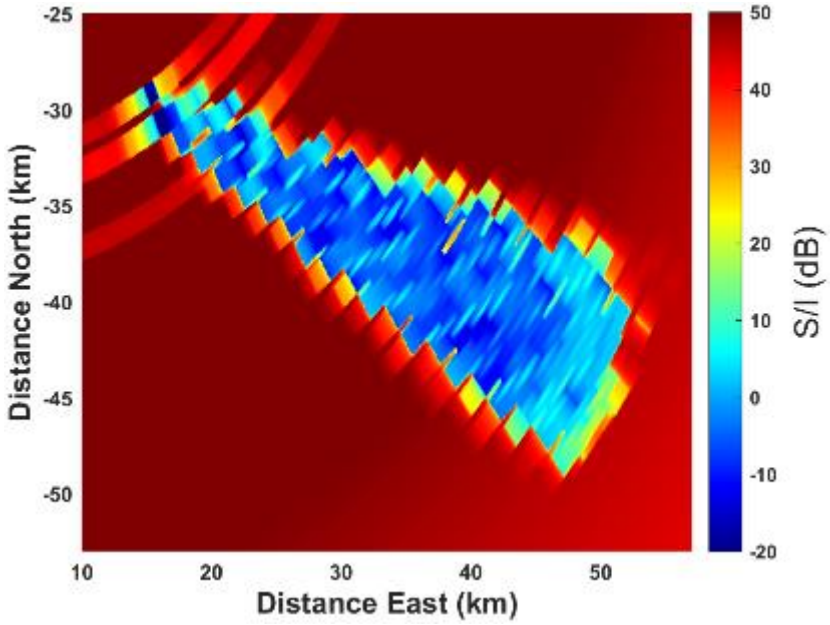

Figure 135 - Signal to Interference for a 0dBsm aircraft flying at 2 km altitude near KJFK

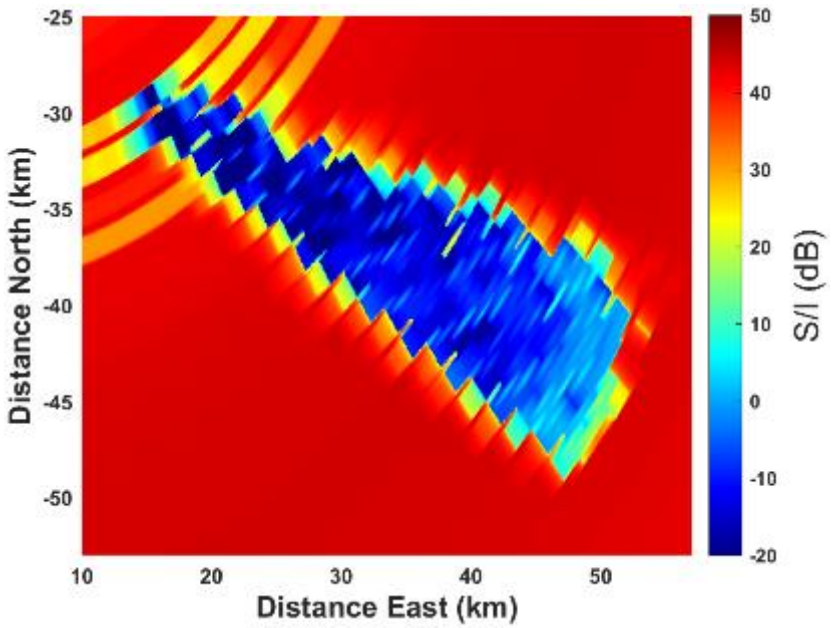

Figure 136 - Signal to Interference for a 0dBsm aircraft flying at 5 km altitude near KJFK

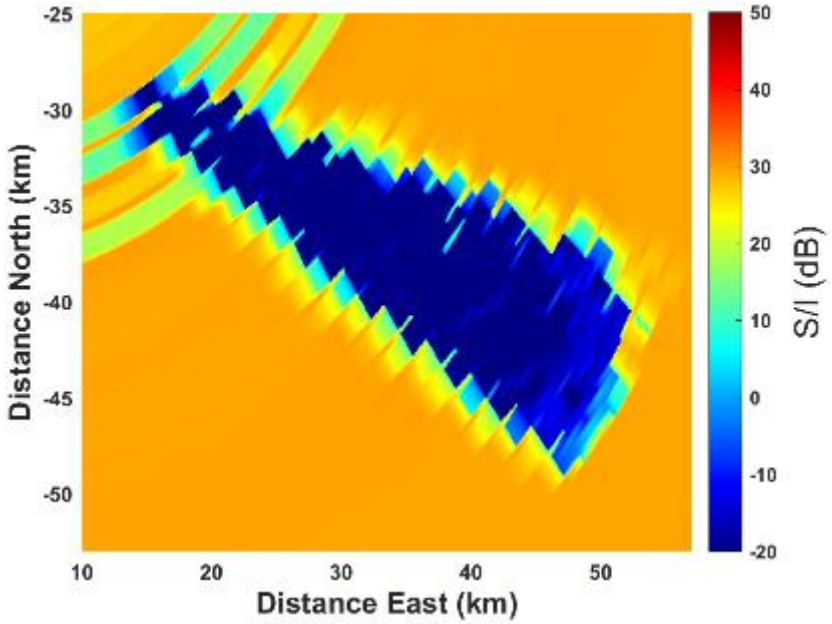

Figure 137 - Signal to Interference for a 0dBsm aircraft flying at 10 km altitude near KJFK

3.1.6.2 *ARSR*

The ARSR-4 located at Riverhead, NY (code QVH) will see impact on air surveillance over the Empire Wind farm. Empire Wind is located close enough to the ARSR that nearly all turbines have at least some part visible to the radar (Figure 138). This creates a large region that will be affected by false targets and reduced detection probability for aerial radar targets which will be discussed below.

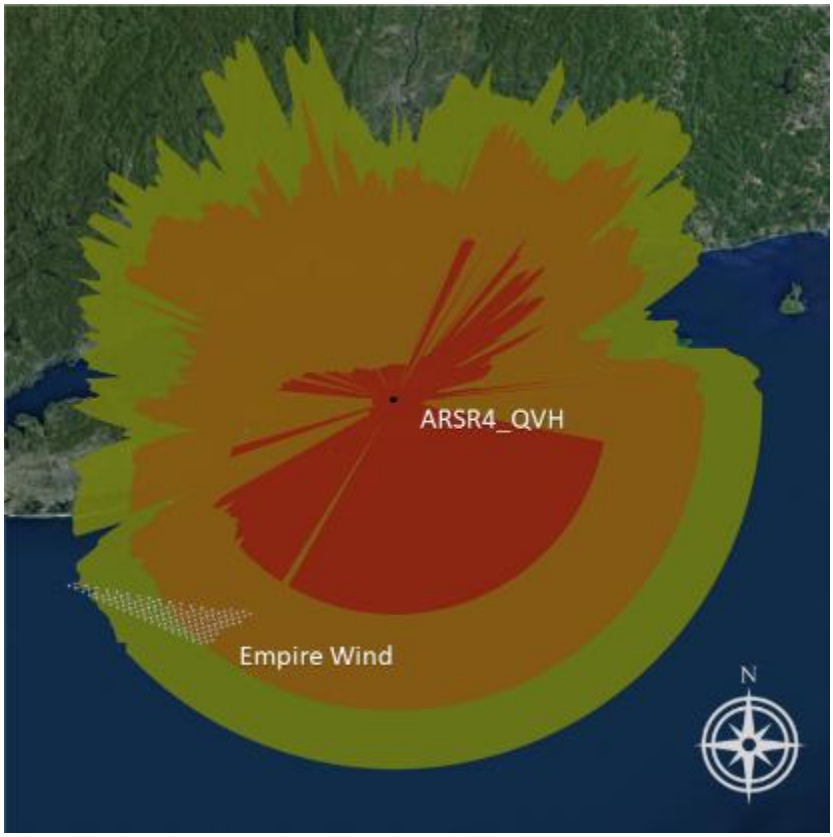

Figure 138 - LOS for the ARSR-4 at Riverhead, NY. Outer edge of the red band is the LOS distance to the lowest point of the turbine blades, edge of the orange band is the LOS distance to the turbine hub, and the edge of the yellow band is the LOS distance to the highest tip of the blades.

The result of the turbines being within the LOS of the ARSR-4 creates two main problems; false targets from the turbines and lowered detection probabilities for aircraft over the farms due to increased CFAR thresholds.

Figure 139 and Figure 140 show the signal to interference level of a small (0 dBsm, e.g., Cessna), low-flying (2,000 m) aircraft above the Empire Wind farm. For an aircraft at that altitude, over the wind farm the elevation of the target from the radar will be ~1.4°. The two plots show that for the two elevation beams that will contain the target that over the wind farm the target return does not rise above the threshold for a detection (13 dB) and does not for any other beams present so this low flying target would be lost over the wind farm.

The interference level stated here and in similar plots below is not just the wind turbine interference but is coming out of the range cell averaging of the CFAR and will include any turbine signals, noise, and pulse compression sidelobe effects of all returns.

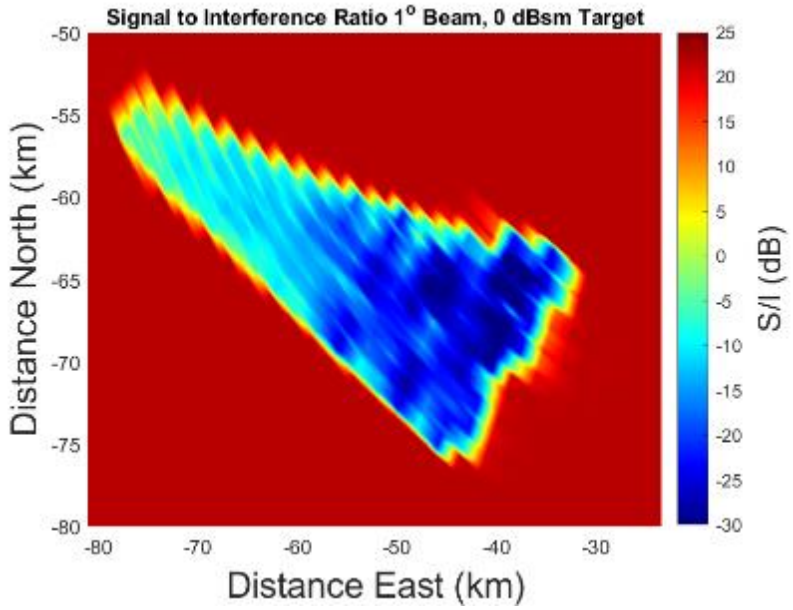

Figure 139 - Signal to interference ratio for a 0 dBsm target at 2000 m altitude over the Empire Wind farm for the ARSR at Riverhead. The elevation angle of the target is ~1.4°.

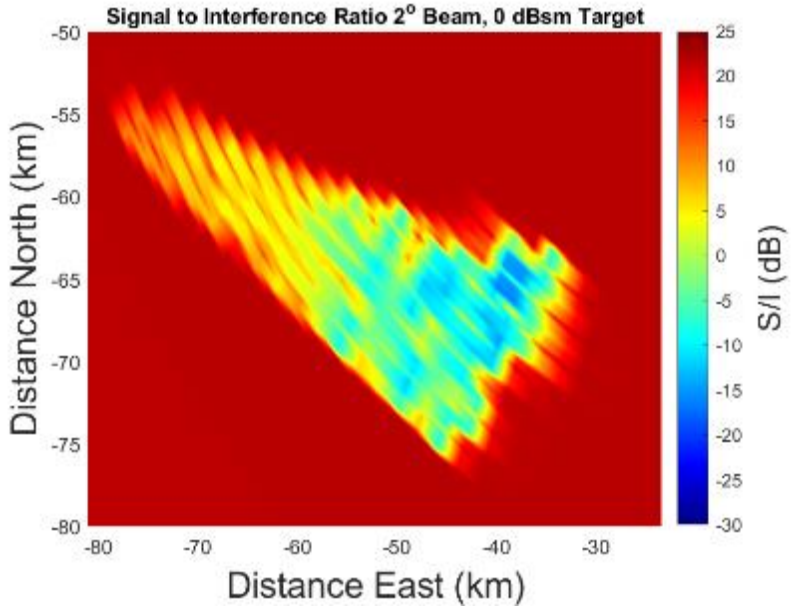

Figure 140 - Signal to interference ratio for a 0 dBsm target at 2000 m altitude over the Empire Wind farm for the ARSR at Riverhead. The elevation angle of the target is ~1.4°.

In Figure 141 and Figure 142 the signal to interference level for a large (20 dBsm, e.g., Boeing 737), low-flying (2,000 m) aircraft above the Empire Wind farm. The ARSR-4 will be able to detect this larger target over the section of the farm furthest from the radar and be able to make some detections in the 2° beam over the rest. Not pictured are signal to interference in higher beams in this scenario which will have no issues in picking out this large aircraft over the farm.

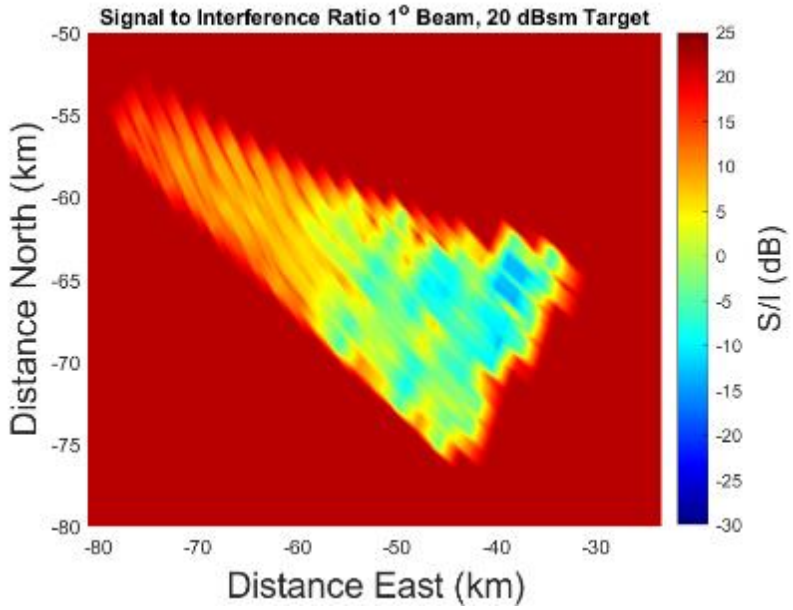

Figure 141 - Signal to interference ratio for a 20 dBsm target at 2000 m altitude over the Empire Wind farm for the ARSR at Riverhead. The elevation angle of the target is ~1.4°.

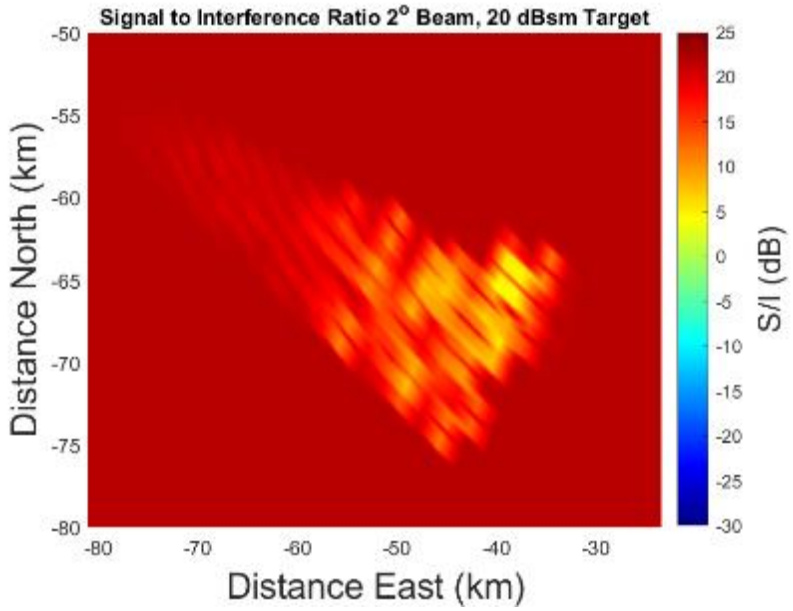

Figure 142 - Signal to interference ratio for a 20 dBsm target at 2000 m altitude over the Empire Wind farm for the ARSR at Riverhead. The elevation angle of the target is ~1.4°.

Figure 143 and Figure 144 show the signal to interference level of a small (0 dBsm) aircraft flying at 5,000 m above the Empire Wind farm for the elevation beams that will be nearest the aircraft's elevation. For an aircraft at that altitude, over the wind farm the elevation of the target from the radar will be ~3.6°. At this altitude, the nearer section of the wind farm can be seen, in both beams shown there will be issues with the detection of a 0 dBsm target and no issues picking out over the further sections of the farm. In higher beams, the signal to interference is above the CFAR threshold for detections in that beam. This can lead to errors in the elevation centroiding to determine a detection's altitude even when a target is detected.

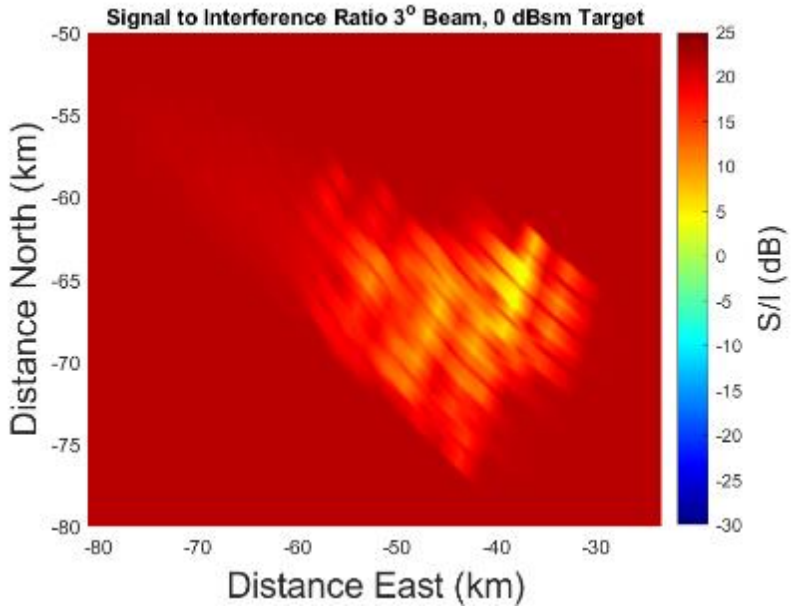

Figure 143 - Signal to interference ratio for a 0 dBsm target at 5000 m altitude over the Empire Wind farm for the ARSR at Riverhead. The elevation angle of the target is ~3.6°.

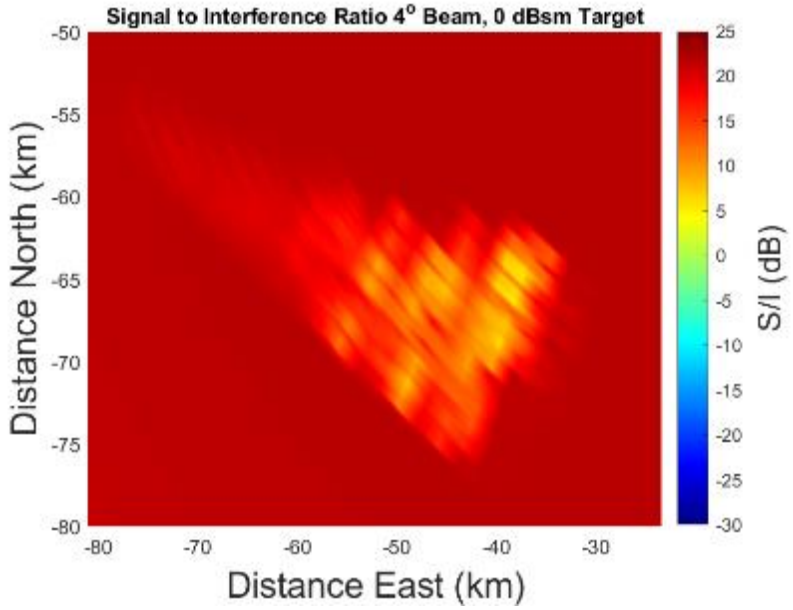

Figure 144 - Signal to interference ratio for a 0 dBsm target at 5000 m altitude over the Empire Wind farm for the ARSR at Riverhead. The elevation angle of the target is ~3.6°.

In Figure 145 the signal to interference level for a large (20 dBsm) aircraft 5,000 m above the Empire Wind farm. For the larger aircraft, the signal to interference level is well above the threshold for detection in all but the lowest beams over the wind farm, so tracking a large target at this altitude should not be a major issue for the ARSR-4.

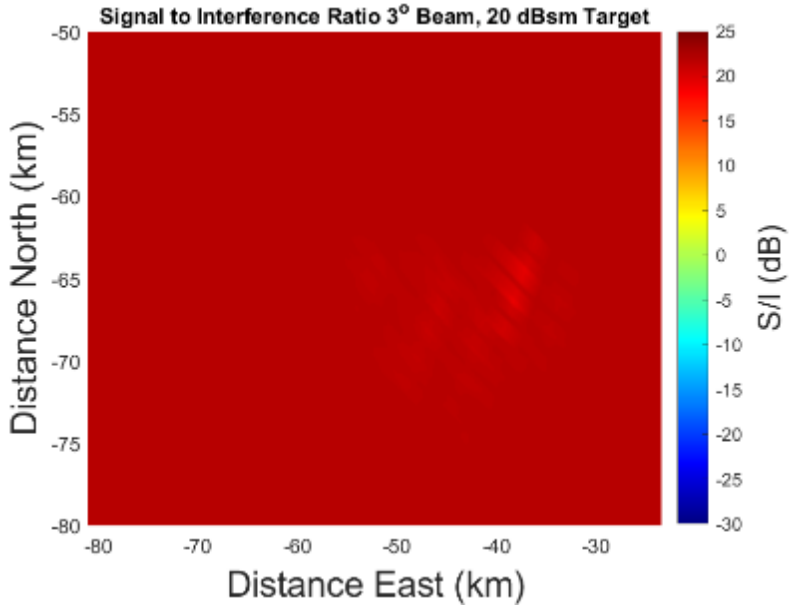

Figure 145 - Signal to interference ratio for a 20 dBsm target at 5000 m altitude over the Empire Wind farm for the ARSR at Riverhead. The elevation angle of the target is ~3.6°.

In addition to the detection degradation, there will be many false targets visible in the vicinity of Empire Wind. Figure 146 shows the declared targets of the ARSR with a 3° beam as well as false targets which appear over the entire wind farm. This can allow aircraft to hide within these false targets, making detection of an aircraft difficult while over the wind farm.

Figure 147 shows a zoomed-in version of the detections of the ARSR where there is a small (0 dBsm) target over the wind farm that is within the green circle. The small aircraft is lost due to a degraded detection from the turbines. Figure 148 shows a zoomed-in version of the detections of the ARSR where there is a large (20 dBsm) target over the farm which is within the green circle. While the target can be seen within the wind farm, there are many false targets which also exist and can potentially make distinguishing the larger aircraft difficult for an operator.

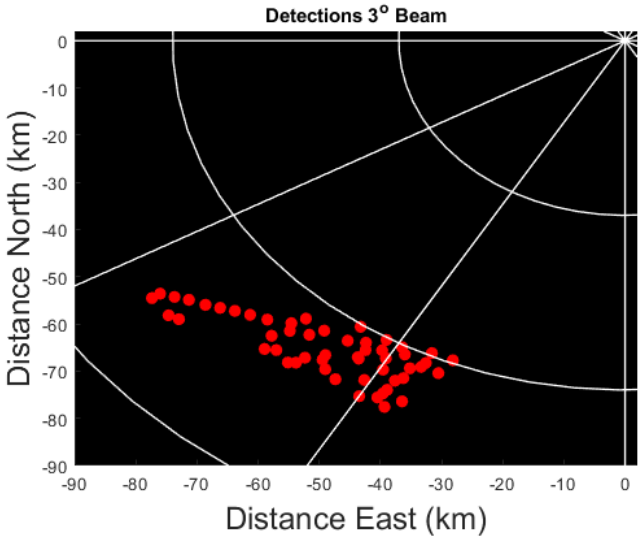

Figure 146 - Detections in the ARSR-4 at Riverhead, NY due to wind turbine interference from the Empire Wind Farm. The beam is at elevation of 3°.

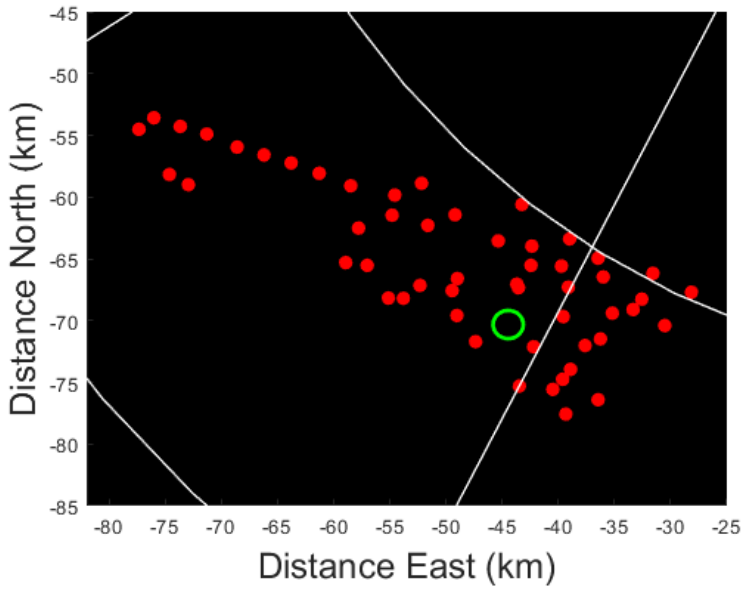

Figure 147 - Detections in the ARSR-4 at Riverhead, NY due to wind turbine interference from the Empire Wind farm. The beam is at elevation of 3°. A 0 dBsm target at an altitude of 5000 m has been simulated in addition to the wind turbines and is in the green circle. The target is not detected in this scenario.

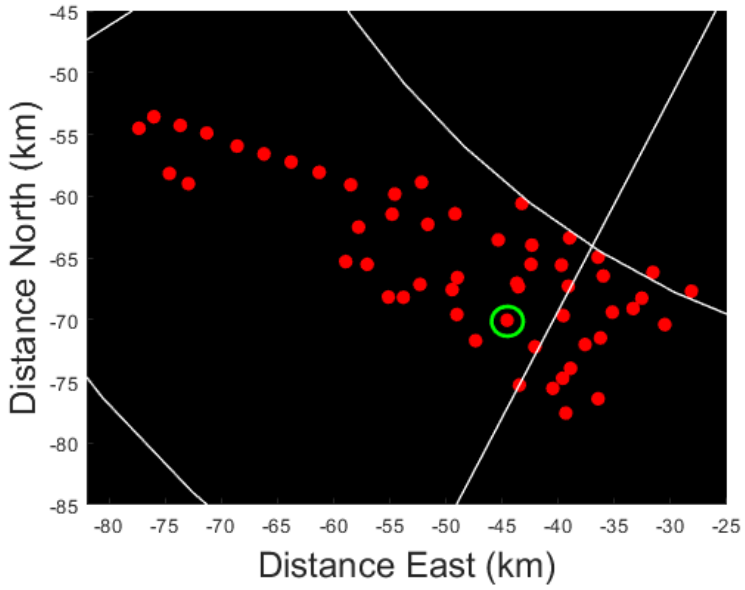

Figure 148 - Detections in the ARSR-4 at Riverhead, NY due to wind turbine interference from the Empire Wind farm. The beam is at elevation of 3°. A 20 dBsm target at an altitude of 5000 m has been simulated in addition to the wind turbines and is in the green circle. The target is detected in addition to many false targets.

3.1.6.3 *NEXRAD*

The Empire Wind turbines are within radar LOS of the WSR-88D radars located in Upton, NY (code KOKX) and Mt. Holly, NJ (code KDIX) as depicted in Figure 149 and Figure 150 below.

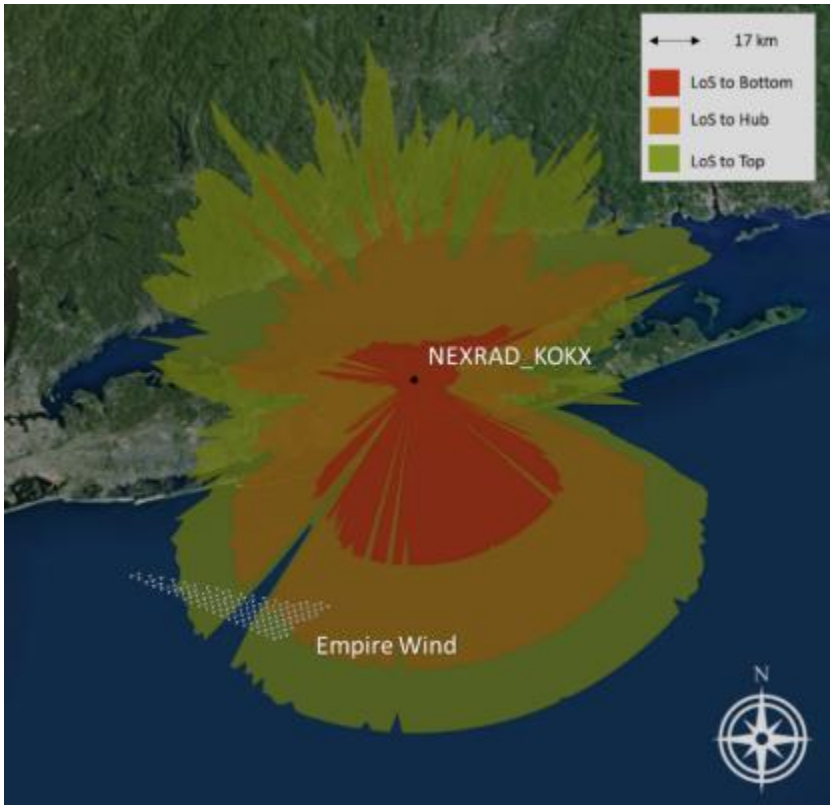

Figure 149 - WSR-88D KOKX LOS plot to Empire Wind

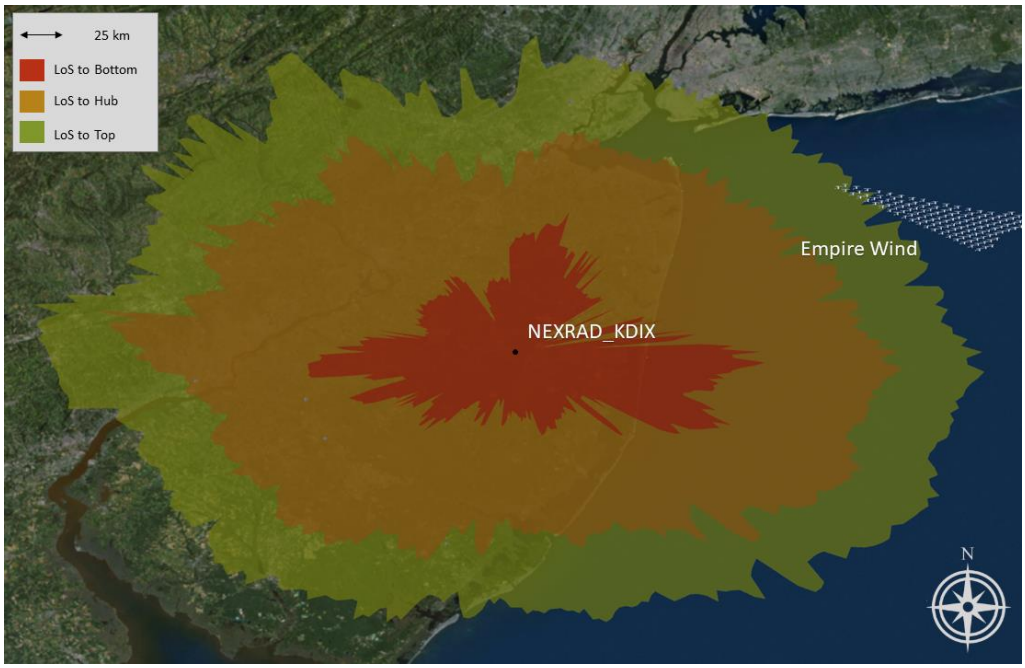

Figure 150 - WSR-88D KDIX plot to Empire Wind

When the wind turbines are within LOS of the radar, the blades interfere with the radar by presenting different Dopplers to the radar. Although WindTRx does not include the detailed weather analysis algorithms used by the NWS, the model can demonstrate the effects imposed by the wind turbine blades on the radar. Below, in Figure 151, is a plot showing where signals generated from the turbines in the

Empire Wind farm are detected by the KOKX radar. The color corresponds to the Doppler value of that is measured at the specific range bin of interest. As demonstrated in the figure, the positive and negative Doppler returns from the approaching and receding blades create Doppler discontinuities that will impact the NWS algorithms. This Doppler discontinuity is one of the methods for detecting rotation in storms that are indicative of funnel clouds and tornados. The returns from the wind farm will create false positives, similar to the interference seen by weather analysts in on-shore applications. In the section of the wind farm furthest from the radar, the radar is seeing returns from only the sections of the blade above the hub and thus only a single sign on the Doppler.

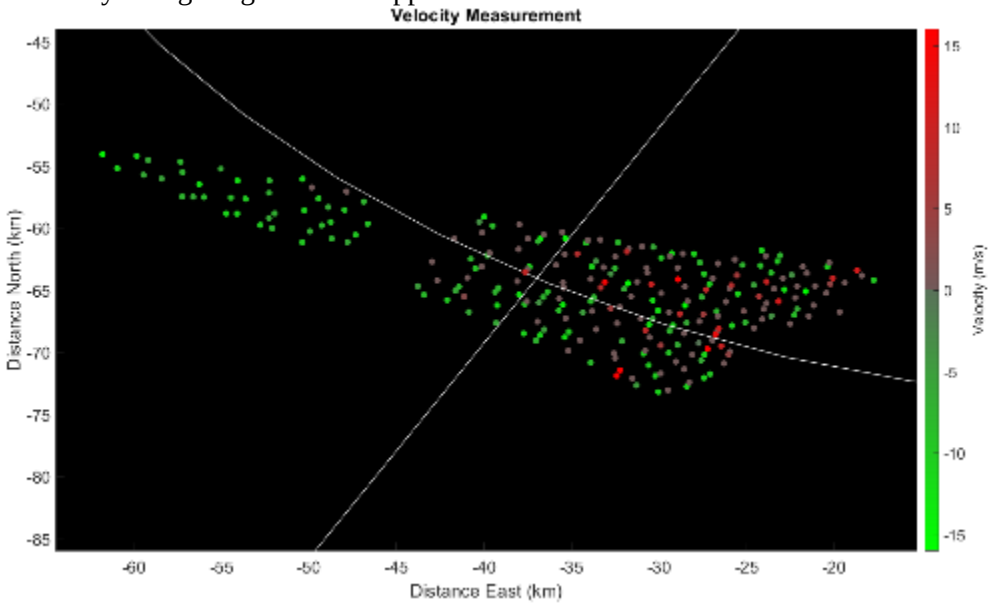

Figure 151 - Velocity measurements from the turbines in the Empire Wind farm on the KOKX NEXRAD system. The turbines in this example are spinning at 15 rpm.

During discussions with the NWS weather, one of the weather analyst's stated concerns was the impact wind turbines have as the WSR-88 scans higher in elevation. The concern is that the larger offshore turbines will impact the WSR-88D as it scans higher in elevation, negatively impacting the analyst's ability to observe the weather phenomena at altitude. Since the LOS plots show the interference to be in the two outer regions, the turbine interference should be geometrically constrained to the lower elevation angles. This constraint is verified in Figure 152, which shows the interference created by the wind turbines above the radar's thermal noise floor as a function of range and elevation.

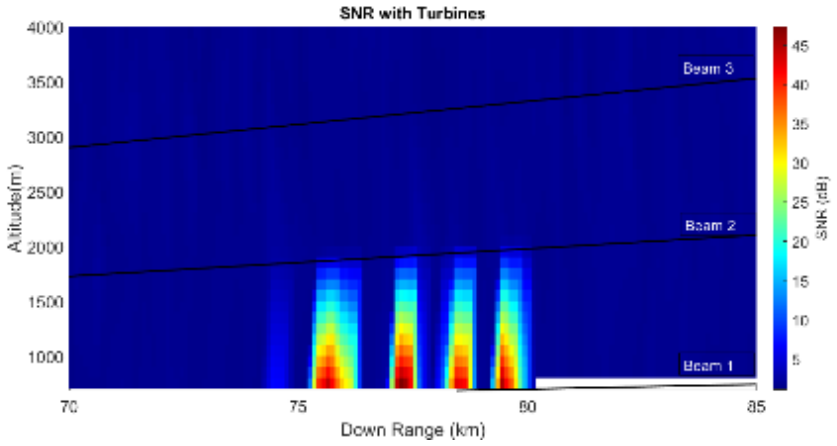

Figure 152 - Vertical slice of the signal to noise ratio (SNR) seen with the presence of the Empire Wind on the KOKX NEXRAD at a fixed azimuth. The black lines show the center of the beams at different elevations.

The KDIX radar will only see the tips of a few of the turbines from the Empire Wind farm and should have minimal interference, but still be able to see returns in a small region as shown below in Figure 153.

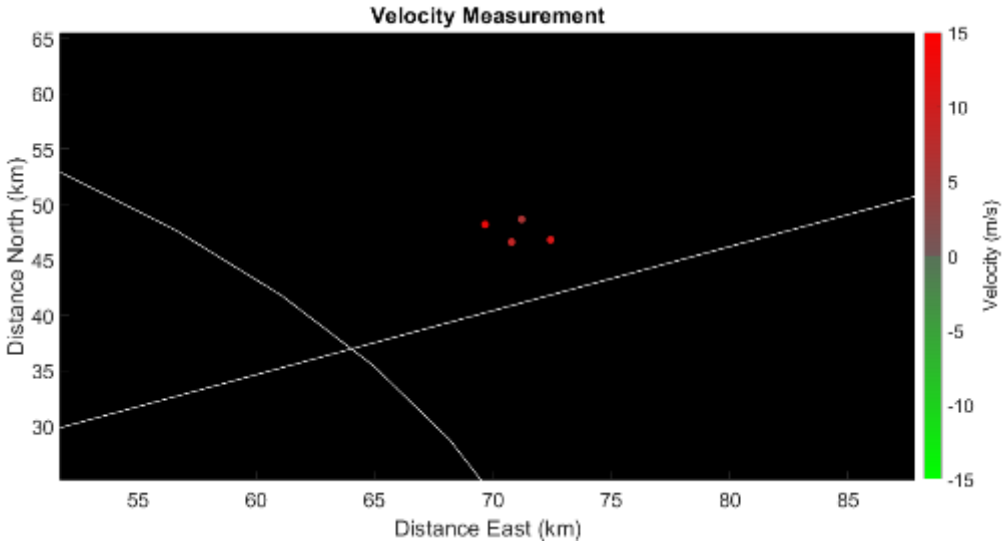

Figure 153 - Velocity measurements from the turbines in the Empire Wind farm on the KDIX NEXRAD system. The turbines in this example are spinning at 15 rpm.

3.1.6.4 *SeaSonde*

Table 13 - Impacted SeaSonde from Empire Wind

Impacted SeaSondes	Class of Interference
SEAB	F
BRAD	F
SPRK	F
MRCH	H
HEMP	H

Impacted SeaSondes	Class of Interference
HOOK	H
LOVE	H
AMAG	H

3.1.6.4.1 Medium Range SeaSondes

There are three medium range SeaSondes that are affected by Empire Wind (Figure 154). All three of these fall into class F for SeaSonde interference due to having a large farm in the mid-long range of the system which was discussed in more detail in the Bay State section above. The SPRK SeaSonde is at a greater distance from Empire Wind and will be impacted less but was found to have an overall similar effect.

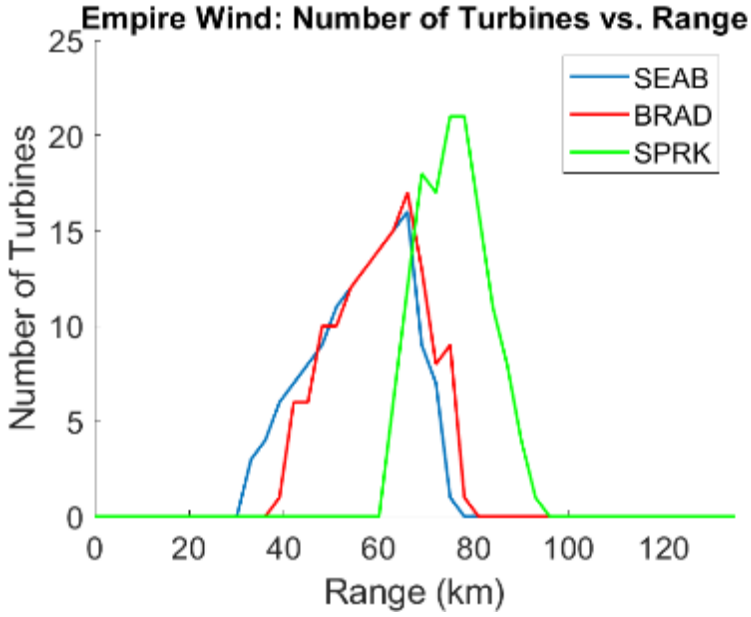

Figure 154 - Number of turbines in each range bin for the medium range SeaSondes near the Empire Wind farm

3.1.6.4.2 Long Range SeaSondes

There are five long range SeaSondes that will be affected by the Empire Wind farm. These belong to class H interference which was discussed above in the Bay State wind farm section of the report. Figure 155 shows the number of turbines through range for the four affected SeaSondes.

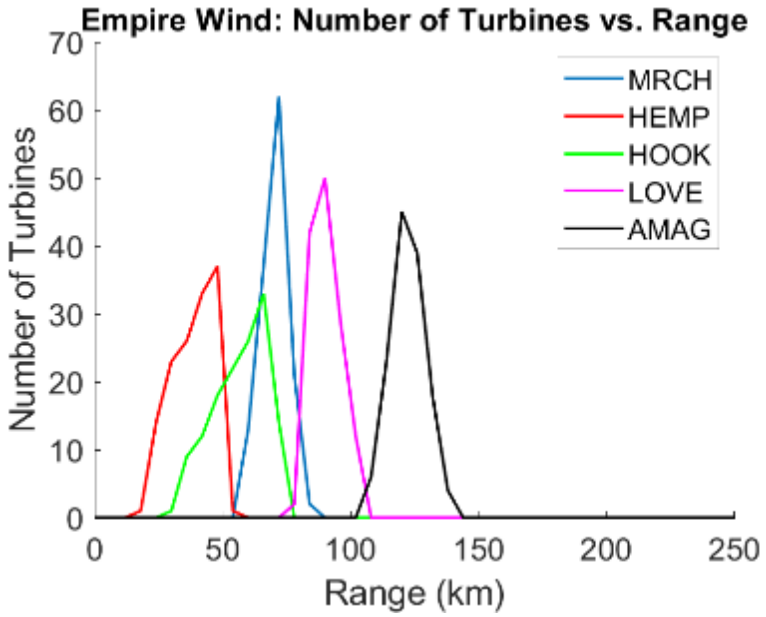

Figure 155 - Number of turbines in each range bin for the long range SeaSondes near Empire Wind.

3.1.7 Ocean Wind

Ocean Wind had been proposed to BOEM in a COP at the time this report was written and is within LOS of one ASR-9 and nine SeaSondes. It is located off the coast of New Jersey (Lease OCS-A-0498) and has 138 8-MW turbines.

3.1.7.1 *ASR*

There is one ASR that could be potentially impacted by the wind farm planned in the Ocean Wind COP. The ASR-9 in Atlantic City, NJ (code ACY) is approximately 31 km from Ocean Wind. Figure 156 below shows the LOS from ACY to the turbines proposed at Ocean Wind. The entire planned farm resides within the LOS of the ASR-9. The majority of the turbines will have, at a minimum, the top half of the blades visible, some entirely visible to the ASR. Figure 157 shows that the ASR-9 ACY is predicted to have CFAR detections of the wind turbines for the Ocean Wind farm. This will impact overflying aircraft within the 40 km to 60 km range from ACY. In Figure 158-Figure 160 the signal to interference level is shown for a 0 dBsm target flying over the farm at three different altitudes from which it can been seen that the ability to pick out an small aircraft over the farm will be extremely difficult for the radar.

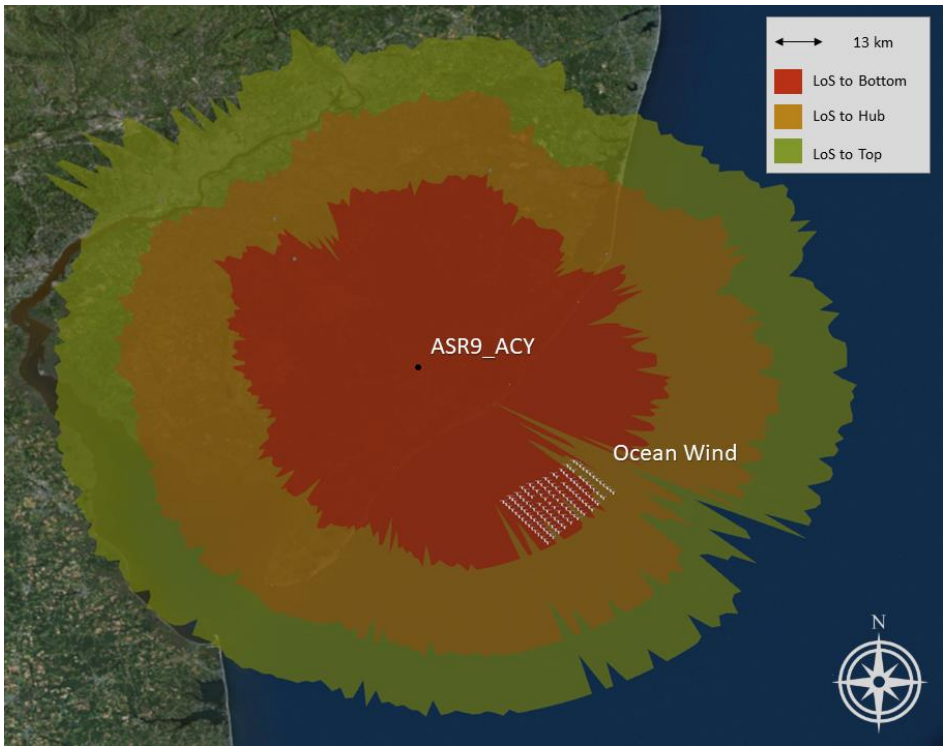

Figure 156 - ASR-9 ACY LOS to Ocean Wind

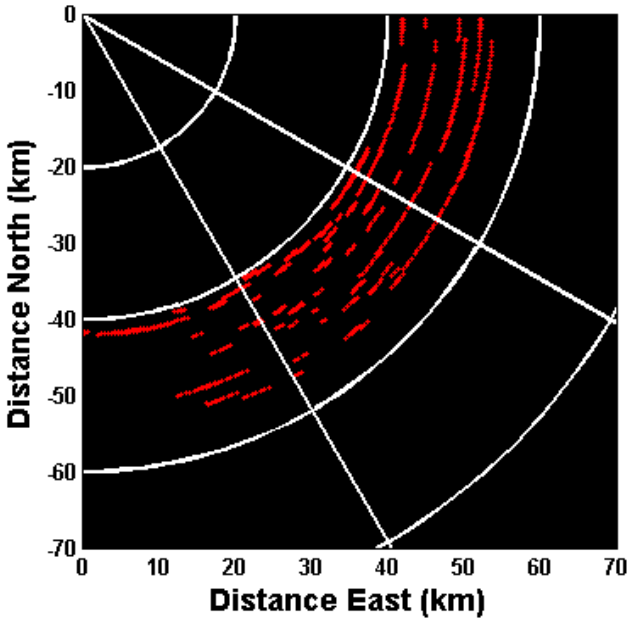

Figure 157 - ACY CFAR Detections of Ocean Wind Turbines

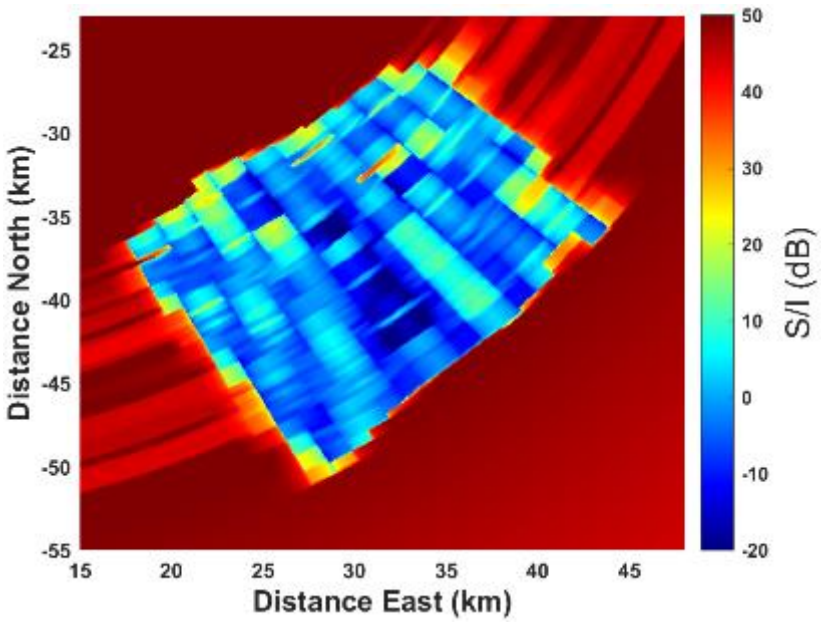

Figure 158 - Signal to Interference for a 0 dBsm aircraft flying at 5 km altitude near ACY

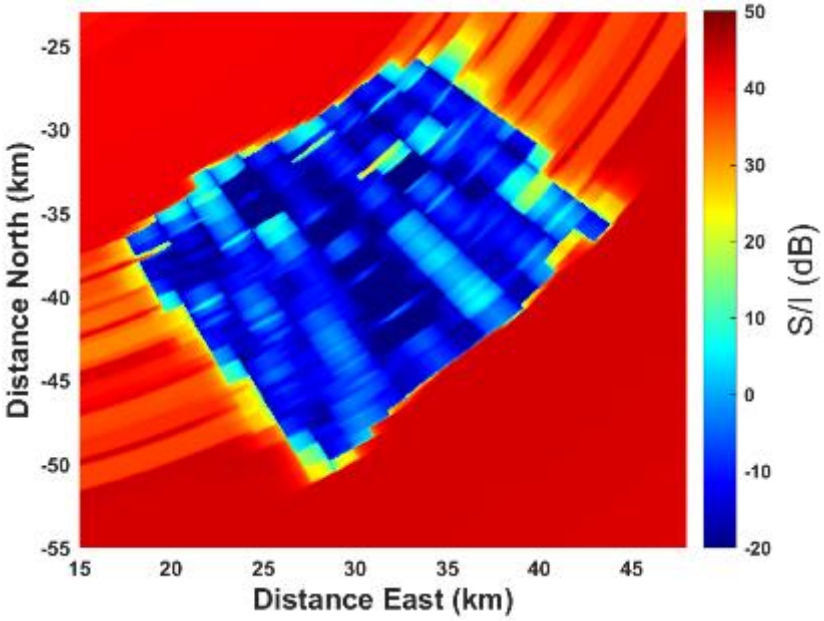

Figure 159 - Signal to Interference for a 0 dBsm aircraft flying at 5 km altitude near ACY

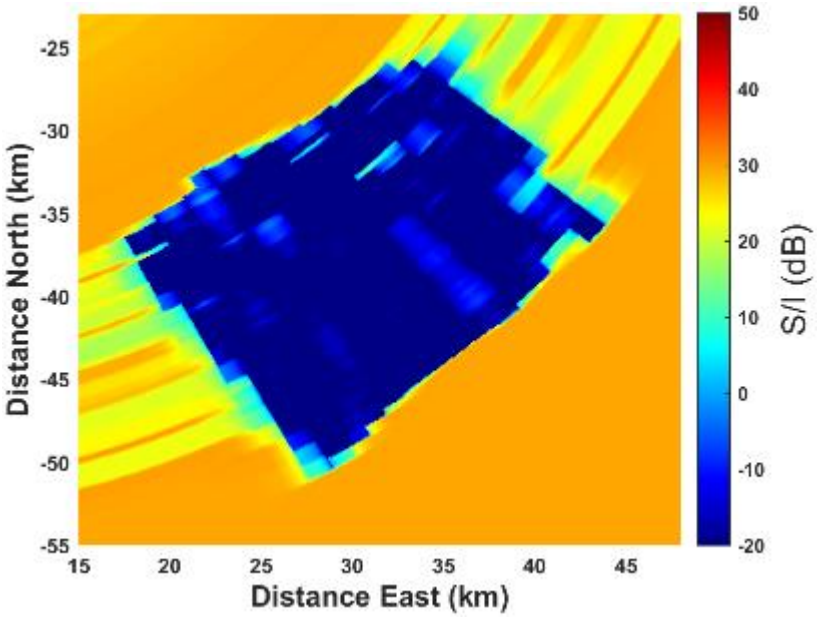

Figure 160 - Signal to Interference for a 0 dBsm aircraft flying at 10 km altitude near ACY

3.1.7.2 *ARSR*

The ARSR-4 at Gibbsboro, NJ (code QIE) has LOS to a handful of turbines on the edge of the Ocean Wind farm as seen in Figure 161. Since only the tips of a small number of turbines were visible the turbine interference on this ARSR-4 was minimal and only showed up in the lowest beams. The impact on the detection of a 0 dBsm target at 2,000 m in altitude is shown below in Figure 162 for the 0° beam and Figure 163 for a 1° beam. Over a small patch, the detection is degraded in this scenario. In cases with higher flying or larger aircraft, the interference is minimal.

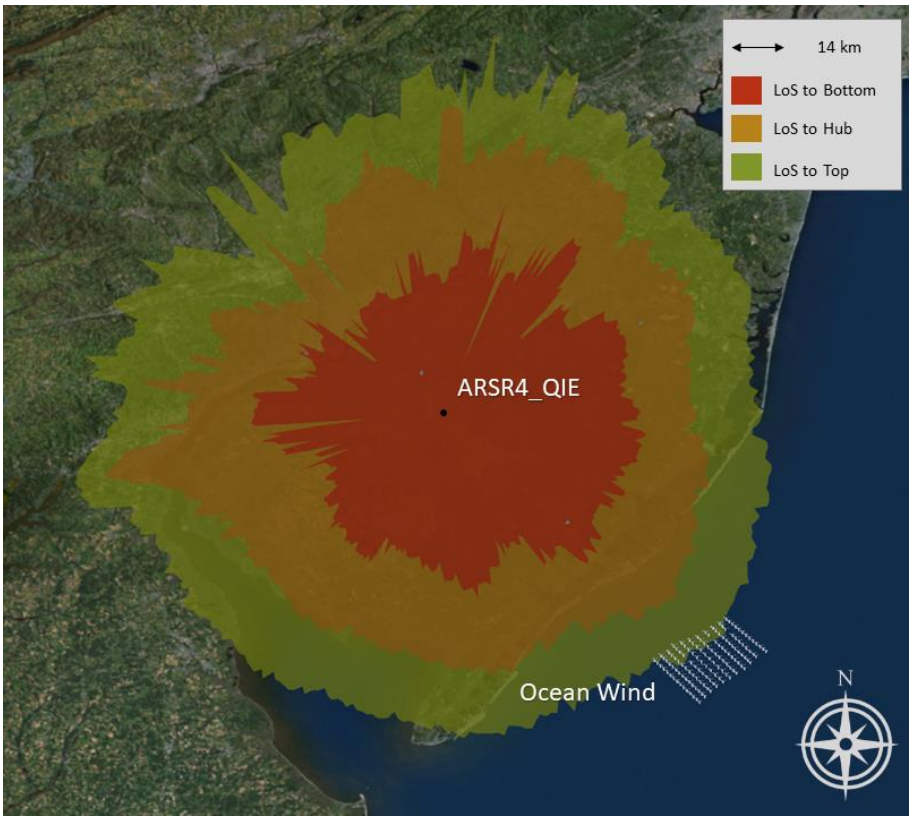

Figure 161 - ARSR-9 QIE LOS to Ocean Wind

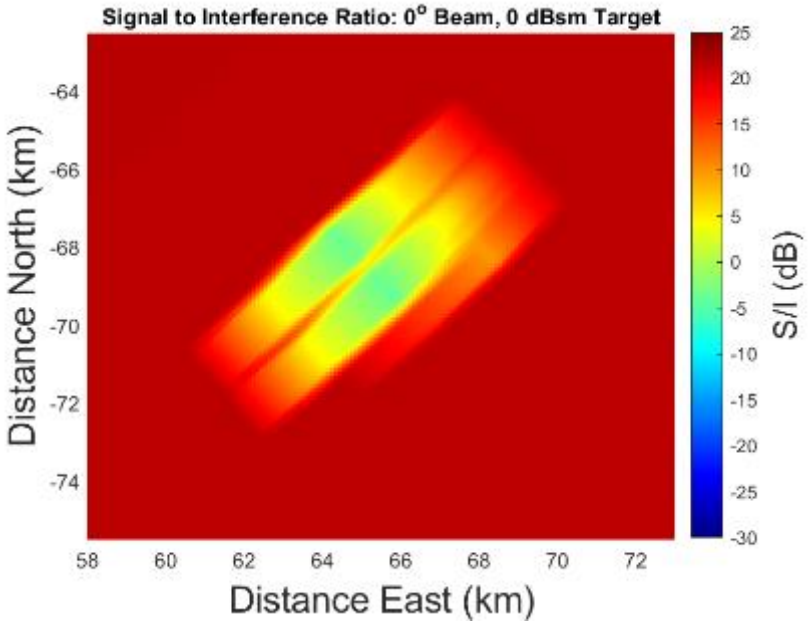

Figure 162 - Signal to interference ratio for a 0 dBsm target at 2000 m altitude over the Ocean Wind farm for the ARSR at Gibbsboro. The elevation angle of the target is ~1.2°.

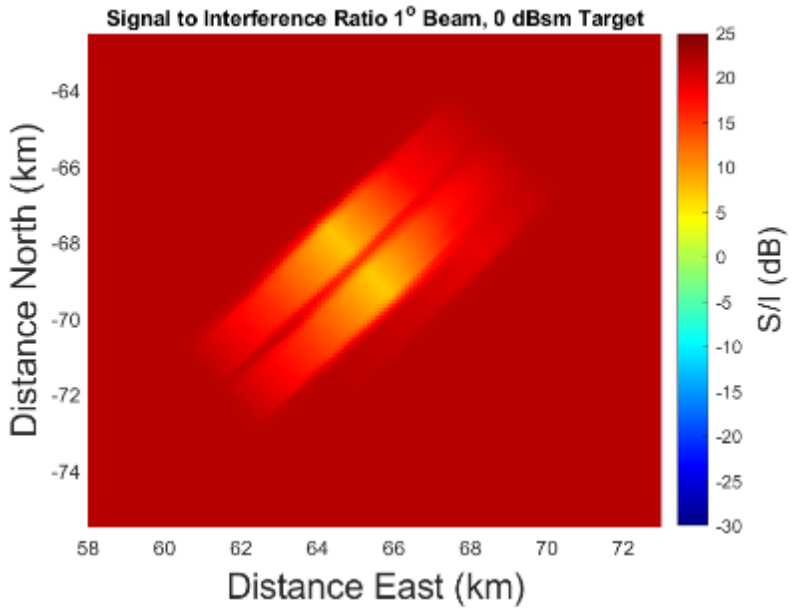

Figure 163 - Signal to interference ratio for a 0 dBsm target at 2000 m altitude over the Ocean Wind farm for the ARSR at Gibbsboro. The elevation angle of the target is ~1.2°.

3.1.7.3 *SeaSonde*

Table 14 - Impacted SeaSonde from Ocean Wind

Impacted SeaSondes	Class of Interference
SPRK	D
BRNT	F
RATH	E
WOOD	F
HEMP	I
LOVE	H
BRIG	H
WILD	H

3.1.7.3.1 Medium Range SeaSondes

There are four medium range SeaSondes within range of Ocean Wind (Figure 164). The RATH SeaSonde will see Ocean Wind as class E interference where there is a large wind farm at short range. BRNT and WOOD will both fall into class F due to the wind farm being in the mid-range of the system. The final affected system, SPRK, will see a partial wind farm due to blocking from the coast at long range, which resulted in class D interference where there is a small wind farm at long range as discussed in the South Fork section above. The effects of coastal blocking for the turbines that are significantly above the ocean's surface is a topic for further study and may modify the level of interference expected if signals from the elevated structures is not as strongly attenuated.

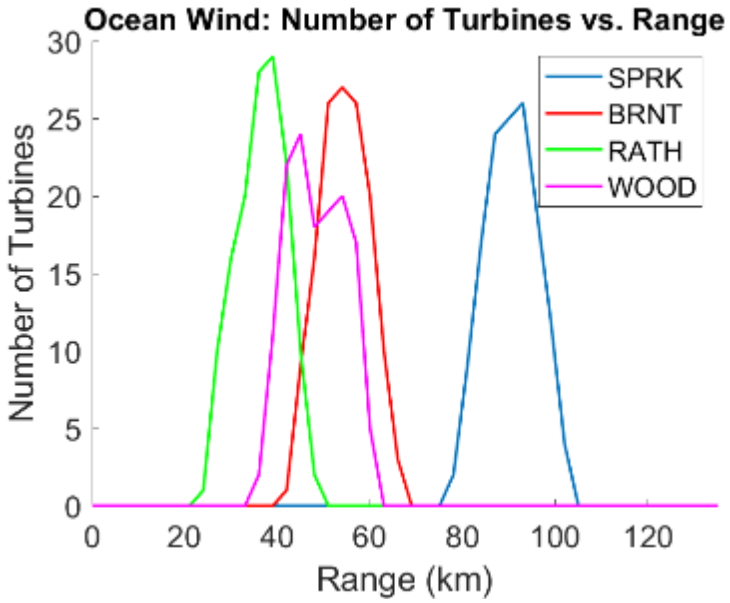

Figure 164 - Number of turbines in each range bin for the medium range SeaSondes near Ocean Wind.

3.1.7.3.2 Long Range SeaSondes

There are four long range SeaSondes that are affected by the Ocean Wind farm. LOVE, BRIG, and WILD will all fall into class H interference which is discussed above in the Bay State section of the report. Of special note is the fact that the LOVE SeaSonde will not be able to see the full wind farm due to blocking from the coast. Further study would be required to understand turbine signals from blocked turbines entering into the system. The fourth SeaSonde, HEMP, will be in class I for a large farm at long range and is discussed below. The number of turbines seen by the affected long range SeaSondes is shown below in Figure 165.

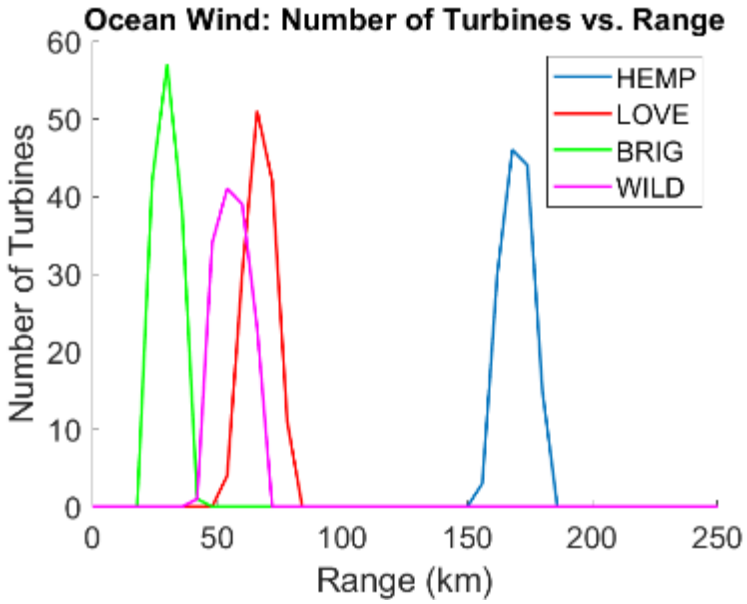

Figure 165 - Number of turbines in each range bin for the long range SeaSondes near the Ocean Wind farm

Figure 166 – Ocean Wind, SeaSonde, HEMP

The HEMP SeaSonde on Long Island will see Ocean Wind at long range for the system, which can be seen in the LOS plot, Figure 166, above. The range-Doppler map for interference from Ocean Wind is shown in Figure 167 below. The interference level at this range, even for a large farm, is minimal. This is due to less signal being returned to the radar and the area being illuminated on the ocean surface due to the large range bins. The large area illuminated will make the relative strength between the Bragg returns in that range bin and that of the farm favor the ocean return in further processing. Figure 168 shows the current errors generated in the system, and the errors are contained within a few range bins with the largest errors concentrated toward the direction of the wind farm.

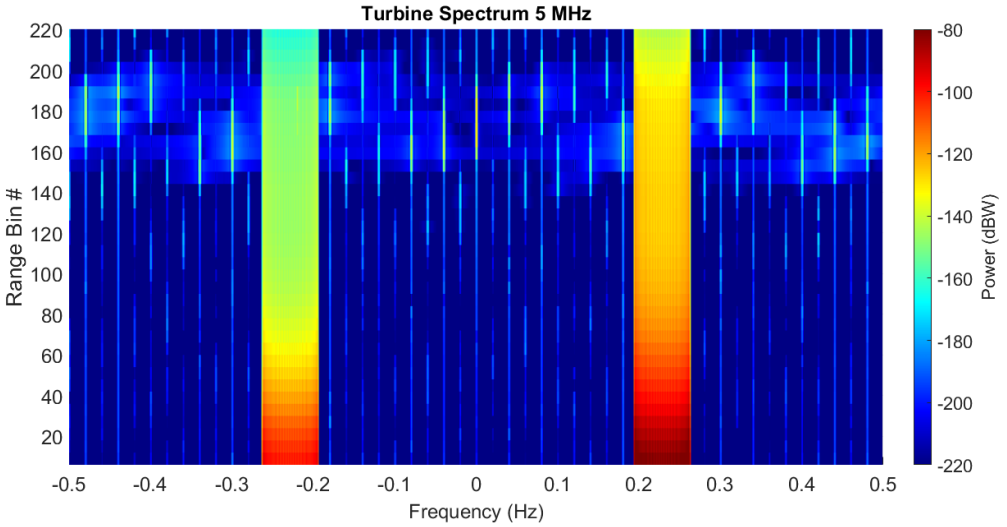

Figure 167 - Range Doppler matrix for the HEMP SeaSonde located on Long Island with turbine interference from the Ocean Wind farm. There are 138 total turbines spinning at 5.2 rpm.

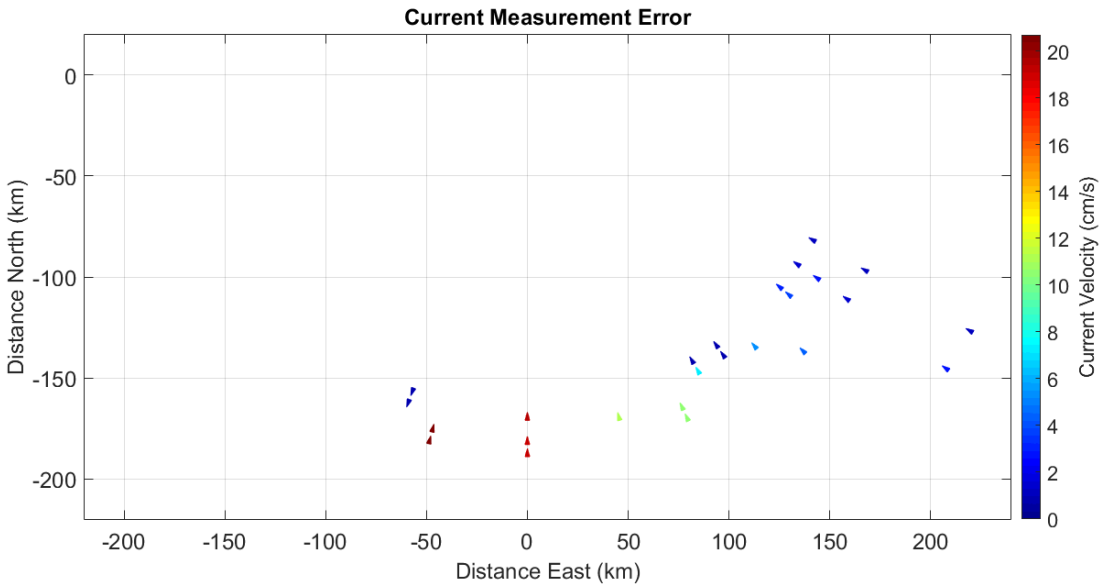

Figure 168 - Current measurement error for the HEMP SeaSonde located on Long Island with turbine interference from the Ocean Wind farm. Modeled sea currents were 100 cm/s running parallel to the coast.

3.1.8 Skipjack Wind

Skipjack had been proposed to BOEM in a COP at the time this report was written and is within LOS of one ASR-9, one NEXRAD, and six SeaSonde radars. It is located off the coast of Delaware (lease OCS-A-0519) and has 16 12-MW turbines.

3.1.8.1 *ASR*

There is one ASR-9 which is within LOS of the proposed Skipjack wind farm. The ASR-9 ACY can see the very tip of three of the turbines (Figure 169) on the edge of the farm. With the minimal amount of the blades that can be illuminated by the radar, this will have a minimal impact on the performance of the radar since only the top few meters of the blades will be visible. For the radar to see the blades, they need to be rotated such that one of the blades is near its maximum height as the radar sweeps past the farm as it spins. Even with the largest turbine configuration and worst-case orientation, there is not enough LOS to Skipjack to produce raw CFAR detections in ACY.

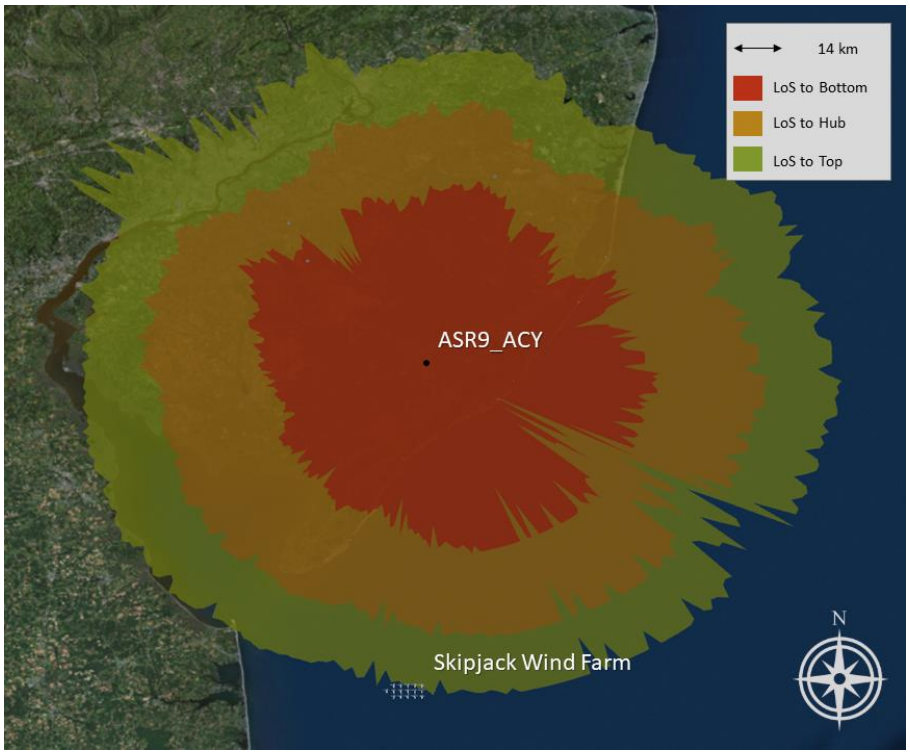

Figure 169 - ASR-9 ACY LOS to Skipjack

3.1.8.2 *NEXRAD*

The South Fork wind farm will impact the NEXRAD system located at Dover Air Force Base (AFB), DE (Figure 170). The entirety of South Fork will be visible to the radar, but since it will only see the top half of the blades and produce measured Doppler targets with a single sign over the extent of the wind farm as shown in Figure 171. As discussed above in the Empire Wind section, the interference from the turbines will only impact the lowest beams of the elevation scan, allowing the higher elevation beams to remain unaffected over the turbines.

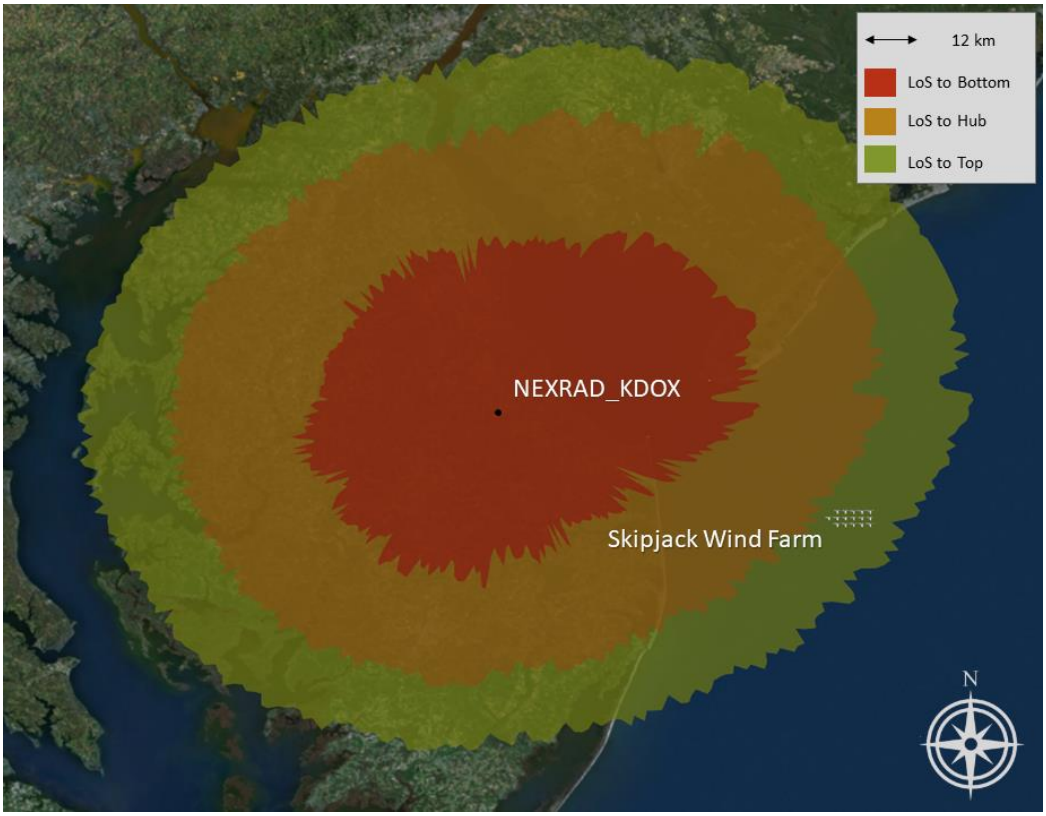

Figure 170 - WSR-88D KDOX plot to Skipjack

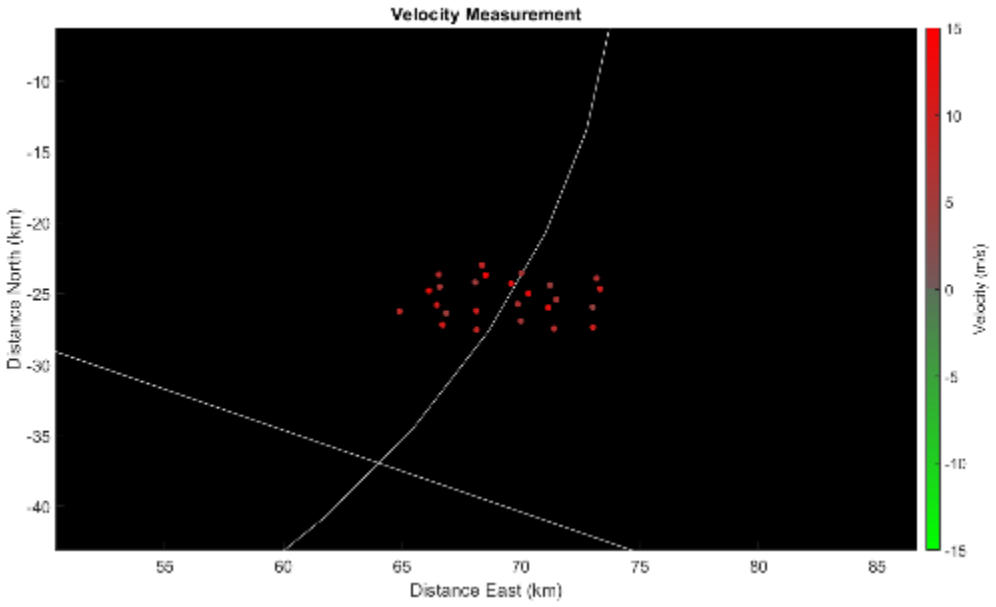

Figure 171 - Velocity measurements from the turbines in the Skipjack farm on the KDOX NEXRAD system. The turbines in this example are spinning at 15 rpm.

3.1.8.3 *SeaSonde*

Table 15 - Impacted SeaSonde from Skipjack Wind

Impacted SeaSondes	Class of Interference
RATH	C
WOOD	C
CMPT	C
BRIG	G
WILD	G

3.1.8.3.1 Medium Range SeaSondes

There are three medium range SeaSondes that are affected by the Skipjack wind farm (Figure 172). These all fall within class C interference with a small wind farm at medium range for the radars. This class of interference was discussed above in the South Fork section.

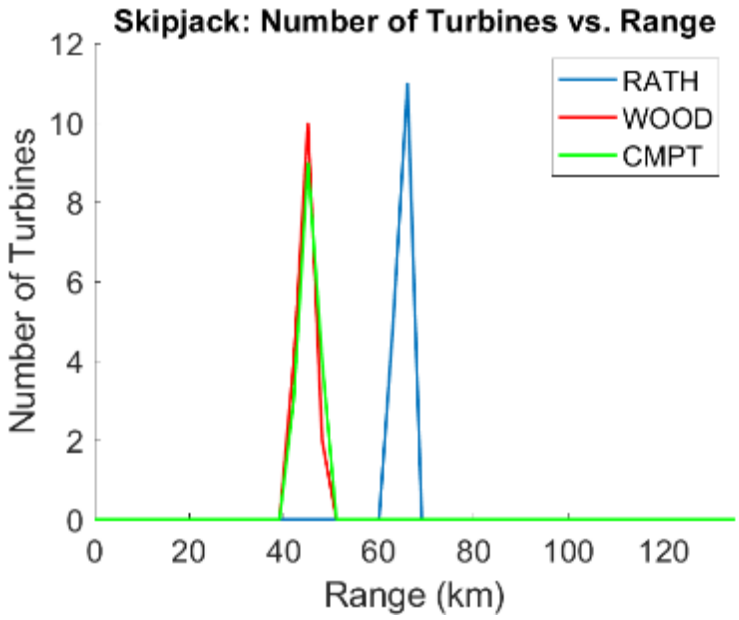

Figure 172 - Number of turbines in each range bin for the medium range SeaSondes near the Skipjack wind farm

3.1.8.3.2 Long Range SeaSondes

There are two long range SeaSondes that can see the Skipjack wind farm. Both affected systems will fall into class G, where there is a small farm at short-mid range for the system. This type of interference is discussed above in the Southfork section and has very similar results to the two systems impacted by Skipjack.

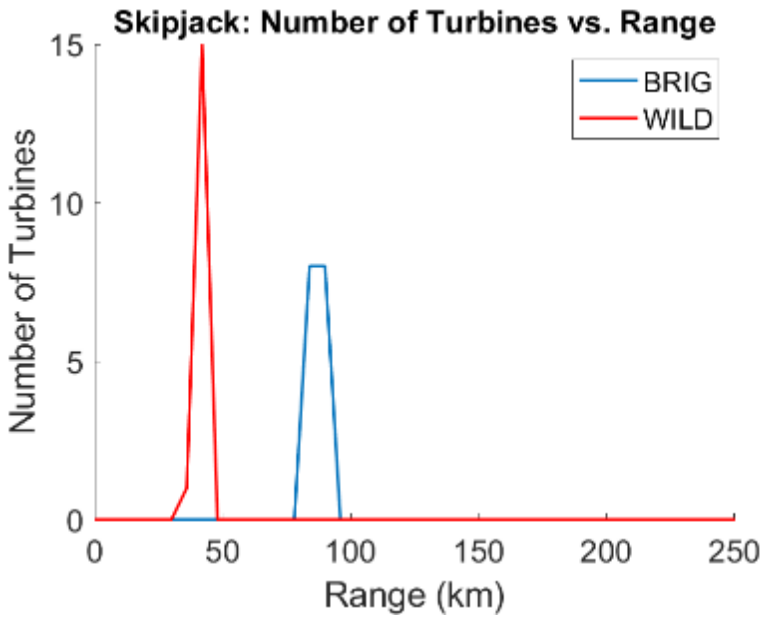

Figure 173 - Number of turbines in each range bin for the long range SeaSondes near the Skipjack wind farm

3.1.9 Grand Strand

Grand Strand is a hypothetical future scenario based on the Grand Strand Call Area off the South Carolina Coast and is within LOS of two SeaSonde radars. The Grand Strand Scenario has 112 15-MW turbines.

3.1.9.1 *SeaSonde*

Table 16 - Impacted SeaSondes from Hypothetical Wind Farms (Grand Strand)

Impacted SeaSondes	Class of Interference
CSW	H
GTN	H

3.1.9.1.1 Long Range SeaSondes

There are two long range system that are affected by the Grand Strand wind farm. Both of these systems are 8-MHz systems, which does differentiate them from the other long-range systems. This will cause minor differences but have been modeled in the simulation as the same as the 5 MHz systems. Since both systems are long range systems with a large farm at short-mid range (Figure 174), the SeaSonde interference for both systems would fall into class H for the SeaSonde interference which was discussed in more detail in the Bay State section.

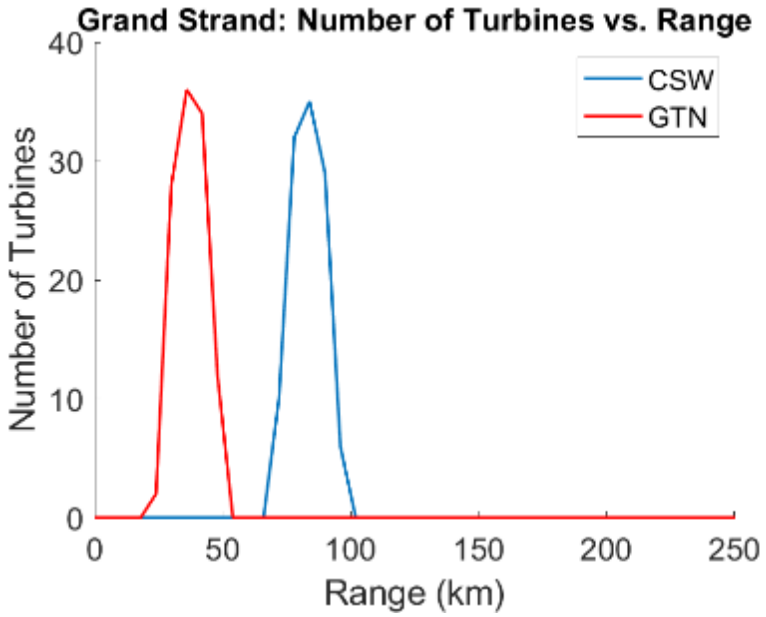

Figure 174 - Number of turbines in each range bin for the long range SeaSondes near the Grand Strand farm.

3.1.10 Discussion

The radar interference and line of sight modeling of the nine planned and hypothetical wind farms showed a total of 36 radar systems affected to some degree along the Atlantic coast (Table 17). In total, 2 ARSR-4 radars were affected, 6 ASR-8/9s, 4 NEXRADs, and 25 SeaSondes. The relatively large number of SeaSonde radars affected is largely a reflection of the prevalence of these systems along the coast.

Table 17 - Radar Systems within LOS of Modeled Wind Farms

	Number of Radar Systems within LOS				
Wind Farm	**ARSR-4**	**ASR-8/9**	**NEXRAD**	**SeaSonde**	**Totals**
Vineyard Wind	0	2	0	6	**8**
Bay State Wind	0	3	0	7	**10**
South Fork	0	1	0	8	**9**
Mayflower	0	2	0	6	**8**
RI/MA Cumulative	0	3	0	10	**13**
Empire Wind	1	2	2	8	**13**
Ocean Wind	1	1	0	9	**11**
Skipjack	0	1	1	5	**7**
Grand Strand	0	0	0	2	**2**
Total Radar Systems Affected*	**2**	**6**	**4**	**25**	**36**

*Total radars affected per radar type may not equal the sum of each column because a single radar can be within LOS of multiple wind farms.

3.1.10.1 *Qualitative Ranking of Radar Impacts*

In evaluating the degree of impact that the wind farms may have on radar systems, both the count of radar systems, as well as the severity of impacts is important. For example, for some wind farms, only the tips of a few of the turbine blades are visible to the radar under normal atmospheric conditions, meaning that the interference generated could be dealt with fairly easily by radar operators. Table 18 groups wind farms qualitatively by the severity of impacts generated to the radar systems evaluated. To generate these rankings, the research team used the LOS plots in Appendix A to estimate counts of turbines within radar LOS.

Table 18. Qualitative Ranking of Radar Impacts

Wind Farm	# of Turbines	Summary of Impacts	# Radars Impacted	Qualitative Interference Score
Skipjack	16	• Few top blades visible to ASR-9 ACY • Few top blades visible to NEXRAD KDOX • In range of 5 SeaSondes	7	Low
South Fork	15	• All turbines visible by ASR-9 KPVD • In range of 8 SeaSondes	9	Low
Grand Strand	112	• In range of 2 SeaSondes	2	Low
Mayflower	67	• Few top blades visible by ASR-8 FMH • All turbines visible by ASR-9 ACK • In range of 6 SeaSondes	7	Moderate
Vineyard Wind	106	• All turbines visible by ASR-8 FMH and ASR-9 ACK • In range of 6 SeaSondes	8	Moderate
Bay State Wind	110	• Few top blades visible by ASR-9 KPVD • All turbines visible by ASR-9 ACK and ASR-8 FMH • In range of 7 SeaSondes	10	Moderate
Ocean Wind	138	• Few top blades visible by ARSR-4 QIE • All turbines visible by ASR-9 ACY • In range of 8 SeaSondes	10	Moderate
Empire Wind	135	• All turbines visible by ARSR-4 QVH, ASR-9s KISP and KJFK • Few top blades visible by NEXRAD KDIX • Most turbines visible by NEXRAD KOKX • In range of 8 SeaSondes	13	Higher

3.1.10.2 *RI/MA Cumulative Scenario*

The RI/MA Cumulative Scenario is in a category of its own as it would have high radar impacts in the region; however, as noted previously, the purpose of this scenario was to provide a "maximum build-out case" for purposes of comparison to other, more realistic scenarios. The research team does *not* expect a wind farm the size of the RI/MA Cumulative Scenario to be developed in the near, or far future.

The RI/MA Scenario is, of course, notable for the sheer number of turbines present (1,115), making it eight times larger than the largest wind farm submitted to BOEM in a COP (Ocean Wind). While the large number of turbines would certainly lead to high impacts, it is notable that the RI/MA Cumulative Scenario does not impact significantly more *individual systems* than the much smaller, more realistic scenarios (see Table 17). For example, The RI/MA scenario impacts 13 total radar systems, similar in

scope to Empire Wind (13 systems), Ocean Wind (11 systems), and Bay State Wind (10 systems). This pattern suggests that, while a full build-out of the RI/MA leasing area would likely increase interference impacts to nearby radar systems, it would not impact a dramatically different population of systems.

Another way to view the RI/MA scenario is to walk through the progressive build out of the RI/MA area's various wind farms (starting with the smallest farm) and note which radars are successively impacted as each new wind farm is built (Table 19). Beginning with South Fork, the smallest wind farm in the area, one ASR-9, KPVD is impacted, with the radar seeing mostly just the tips of the turbines. Even looking at only South Fork, eight SeaSondes are impacted – illustrating the prevalence of SeaSonde radars and underscoring the fact that impact to a large population of SeaSondes is unavoidable with offshore wind farm development in the area. Mayflower, the next largest wind farm planned for the region impacts two additional ASR radars (ASR-8 FMH and ASR-9 ACK) and impacts only five SeaSondes – all of which are also impacted by South Fork. Adding Vineyard Wind, the next largest wind farm planned for the area adds no additional impacted ASRs (ASR-8 FMH and ASR-9 ACK were already impacted by Mayflower), and impacts seven SeaSondes, only one of which (SQUB) has not already been impacted by the previous wind farms. Building the next largest planned wind farm, Bay State, impacts no new ASRs (ASR-8 FMH, ASR-9 ACK, and ASR-9 KPVD) and no new SeaSondes. Building out to the Cumulative Scenario only adds one impacted radar to the population – SeaSonde MRCH.

Table 19. Illustration of Sequential Build-Out of RI/MA Lease Area

Wind Farm				SeaSondes								
	ASR-9 KPVD	ASR-8 FMH	ASR-9 ACK	AM AG	BI SL	CP VN	HB SR	LP WR	MV CO	NA NT	NW TP	SQ UB
1. **South Fork**	✓			✓	✓	✓	✓	✓	✓	✓	✓	
2. **Mayflower**		✓	✓	✓				✓	✓	✓	✓	
3. **Vineyard Wind**		✓	✓	✓			✓	✓	✓	✓	✓	✓
4. **Bay State Wind**	✓	✓	✓	✓			✓	✓	✓	✓	✓	✓
5. **RI/MA Cumulative**	✓	✓	✓	✓	✓	✓	✓	✓	✓	✓	✓	✓

3.1.10.3 *Individual Radar Systems*

Up to this point, this discussion section has focused on the impacts of wind farms, but another way to view the results is by investigating impacts to individual radar systems. As shown in Table 17, SeaSondes had the greatest number of systems impacted at 25. ASR-8 and ASR-9 systems were the next most commonly impacted systems, with six total systems across seven of the nine wind farms. While NEXRADs had four individual systems impacted, only Empire Wind and Skipjack impacted that category of radars. ARSR-4s were only impacted by Empire Wind and Ocean Wind.

Table 20 crosswalks all ASR-8/9, ARSR-4, and NEXRAD impacts with wind farms. Impacts of ASR-8s and ASR-9s can be seen across all wind farms. Impacts can be grouped into essentially three regions – FMH, ACK, and KPVD are exclusively impacted by RI/MA area wind farms. Moving to the New York Bight area, Empire Wind impacts KJFK and KISP, then in the Mid-Atlantic Region, Ocean Wind and Skipjack impact ACY.

There are only two ARSR-4s impacted within the study scope. Empire Wind impacts ARSR-4 QVH on Long Island and Ocean Wind impacts QIE in New Jersey.

NEXRAD and ARSR-4 radars are unique in that they feature multiple beams. For impacted systems that are capable of 3D measurements, the impact for the offshore wind farms examined in this report were greatest in the lowest beams of these systems. This is due in this case to the turbines being at longer

ranges for the systems, making them at low elevation. Since the impact on these systems is in the lower beams, they are still be able to perform most normal operations in all but the lowest beams.

It is also important to highlight the radar systems that were *not* impacted by any wind farms in the study (color coded with green rows in Table 20 and Table 21 below). Four ASR-9s, one ARSR-4, and one NEXRAD were not impacted by any wind farms (six total systems). SeaSondes are discussed separately below due to the sheer number of individual systems.

Table 20 - Radar Impacts to Wind Farms

Wind Farm	Vineyard	Bay	SF	Mayfl.	RI/MA Cumul.	Emp.	Ocn.	Skpj.	GrStnd.
ASR-8 FMH	✓	✓	✓	✓	✓				
ASR-9 ACK	✓	✓		✓	✓				
ASR-9 BOS									
ASR-9 KBDL									
ASR-9 KPVD		✓	✓		✓				
ASR-9 KEWR									
ASR-9 KJFK						✓			
ASR-9 KISP						✓			
ASR-9 KPHL									
ASR-9 ACY							✓	✓	
ARSR-4 GIB									
ARSR-4 QVH						✓			
ARSR-4 QIE							✓		
NEXRAD KBOX									
NEXRAD KDOX								✓	
NEXRAD KDIX						✓	✓		
NEXRAD KOKX						✓			

A large number of SeaSondes were impacted (a strong theme to this study's results), with relatively even numbers impacted across the wind farms. Only Grand Strand impacted fewer than five SeaSondes. Of the 31 SeaSondes reviewed as part of this study, seven systems were not impacted by any of the study wind farms (non-impacted SeaSonde rows are color coded in green).

Table 21 - Radar Impacts to Wind Farms

Wind Farm	Vineyard	Bay	SF	Mayfl.	Cumul.	Emp.	Ocn.	Skpj.	GrStnd.
SeaSonde AMAG	✓	✓	✓	✓	✓	✓			
SeaSonde ASSA									
SeaSonde BISL			✓		✓				
SeaSonde BRAD						✓			

Wind Farm	Vineyard	Bay	SF	Mayfl.	Cumul.	Emp.	Ocn.	Skpj.	GrStnd.
SeaSonde BRIG							✓	✓	
SeaSonde BRNT							✓		
SeaSonde CEDR									
SeaSonde CMPT								✓	
SeaSonde CPVN			✓		✓				
SeaSonde CSW									✓
SeaSonde GCAP									
SeaSonde GTN									✓
SeaSonde HBSR	✓	✓	✓		✓				
SeaSonde HEMP						✓	✓		
SeaSonde HOOK						✓			
SeaSonde LOVE						✓	✓		
SeaSonde LPWR	✓	✓	✓	✓	✓				
SeaSonde MNTK									
SeaSonde MRCH				✓	✓	✓			
SeaSonde MVCO	✓	✓	✓	✓	✓				
SeaSonde NANT	✓	✓	✓	✓	✓				
SeaSonde NAUS									
SeaSonde NWTP	✓	✓	✓	✓	✓				
SeaSonde RATH							✓	✓	
SeaSonde SEAB						✓			
SeaSonde SILD									
SeaSonde SPRK						✓	✓		
SeaSonde STLI									
SeaSonde SQUB	✓	✓			✓				
SeaSonde WILD							✓	✓	
SeaSonde WOOD							✓	✓	

3.2 MITIGATION TECHNIQUES

3.2.1 How Modeling Results Inform Mitigation Techniques

The proposed and hypothetical wind farms modeled in this study are within the LOS[1] for a number of radars as shown in the previous modeling results. Although impact to these radars varies based upon the radar type and the specific locations of the turbines, the preceding radar analyses shows that these radars will be impacted by WTCI under normal atmospheric conditions. Ducting and other anomalous conditions may increase the frequency of the impact. This section of the report refers to these sensors as "impacted" radars. The very large rotating structures with strong RCSs from wind turbines provide a difficult problem for many radars, and certain radar attributes make the impact more difficult to mitigate. Many of the impacted radars have characteristics that make the mitigation problem quite difficult. Each of the following characteristics, and the previously mentioned atmospheric conditions, were addressed in detail in our modeling of the impact to the radars of interest. The primary characteristics that make these radars susceptible to WTCI are:

- **Fan-shaped transmission and receive beams** that illuminate the surface of the earth and ocean. Fan-shaped beams (narrow in the horizontal/azimuthal plane and broad in the vertical/elevation plane, see Figure 175) produce a measurement without any vertical content; these radars only "see" in range and azimuthal direction and are referred to as "2D" radars because they do not measure altitude. Therefore, any returns that are in this fan beam are processed without discrimination or separation in altitude or vertical extent. The ASR series are range-azimuth processing systems, although there are upgrades and an additional beam that will be discussed further.

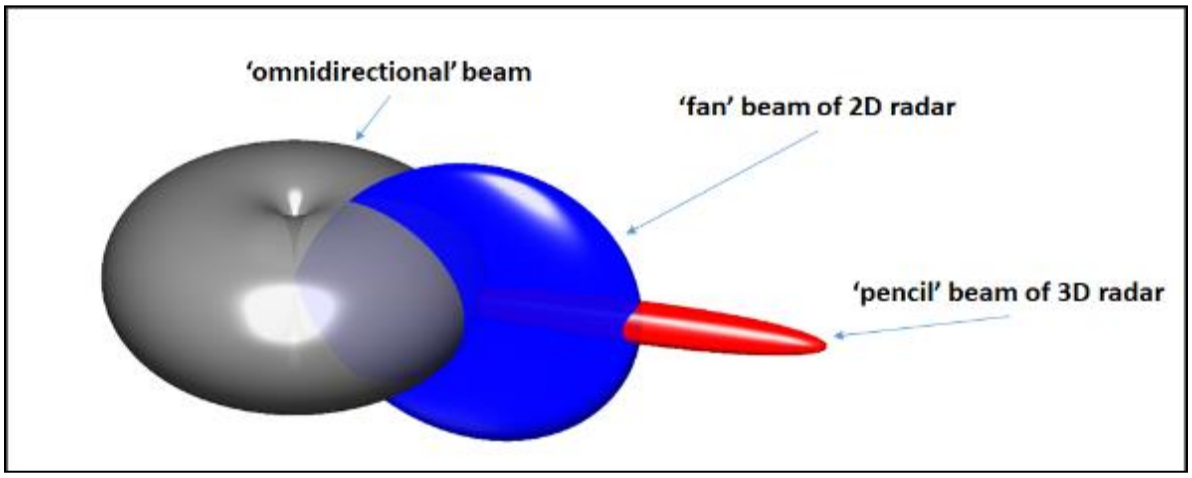

Figure 175 - Illustration of various radar beam types

- **Omni-directional beams** which illuminate the surface of the ocean. Although sophisticated processing allows for direction estimation by the SeaSonde HF ocean monitoring radars, the relatively simplistic antenna system does not provide many degrees of freedom to more precisely locate the turbines in angle or to separate angular returns. Although the transmitted waveform is propagated through an omni-directional antenna, the returns are received through a pair of loop antennas that are nearly-omni-directional but provide for more degrees of freedom than the

[1] The term LOS is something of a misnomer given that propagation effects impact the path of an electromagnetic ray from a radar to a given location in the atmosphere, and radar horizon is not geometric line of sight. Even optical LOS is not a geometric straight-line path. These LOS variations based upon atmospherics and radar frequency/polarization are addressed in Section 3.3, but for the purpose of this section LOS refers to those instances where a radar ray can propagate to a location under normal, non-anomalous atmospheric conditions.

somewhat simplistic view in Figure 175).

- **Transmitted waveforms that are not-optimized for WTCI** which can allow the turbine returns to mix in with the intended signals. These waveforms may be lower resolution than optimal for WTCI mitigation or may be ambiguous in a measurement domain (such as velocity measurement), or both low resolution and ambiguous.

3.2.2 Common Clutter Mitigation Designs

Surface-based radars have been designed over decades to reject clutter, although the term "clutter" itself is a relative term. For example, the radars designed to detect airborne returns/targets (e.g., ASR-9, ARSR-4, NEXRAD) have transmitted waveforms and signal processing to reduce the reflected returns from the ground and the sea surface. The SeaSonde radar, however, is designed to measure the sea return itself and therefore its target is what the other radars would term clutter. The waveforms and clutter rejection methodologies have historically been based upon the assumption that the surface-based clutter returns are non-moving; or very slowly moving such as tree limbs and leaves blown by the wind. Although this is not an exhaustive list, the following are common clutter rejection methods.

- **Siting Optimization.** Siting may be optimized for clutter reasons, and clutter fences (including berms and terrain features to mask a specific direction) – frequently used at radar test sites – can be placed around the radar site to reduce the illumination of clutter at certain aspects. Tower-mounting – which provides longer-range capability – also makes site modification more difficult or merely infeasible.
- **Three-Dimensional (3D) radar.** By employing a 'pencil beam' of relatively high-resolution capability, a 3D radar can point its beam above the clutter for a cleaner measurement. The NEXRAD radar and the ARSR-4 are 3D radars. Still, if measurement close to the surface is required, there is the possibility that clutter sources will be illuminated. Even if the surface is illuminated, measuring data in multiple beams – even if sequentially and not simultaneously – can provide insight into the clutter environment and allow for more rejection methods.
- **Moving target indicator (MTI).** MTI is a relatively simple and common method to mitigate clutter. The radar will transmit a series of pulses (three or four consecutive pulses, for example) and will use a series of summing circuits to delay and add the pulses together with amplitude multipliers and phase shifts applied to each pulse. If the returns are from a moving target, the phase of the signal changes from pulse to pulse, while a non-moving target has a consistent phase that – through the summing circuit – will cancel itself out and allow the moving target to pass through.
- **Pulsed Doppler (PD) or Doppler radar.** A PD radar such as NEXRAD will typically transmit a number of coherent pulses that will allow for a relatively fine Doppler measurement on the target and will allow for the processing system to ignore very low Doppler returns. A continuously-emitting (not pulsed) radar like the SeaSonde provides high resolution Doppler returns where stationary signals can be gated out effectively. However, moving turbines have Doppler returns which can get around the typical low-Doppler constraints in these radars.
- **Moving target detection (MTD).** MTD radars are a class of PD systems that typically employ a smaller number of coherent pulses than typical PD systems. The smaller number of processed pulses reduces the Doppler/velocity resolution capability of the system but still can provide significant attenuation of non-moving returns the ASR-8/9/11 and ARSR4 use MTD waveforms, but – as above – the moving turbines produce returns that avoid the clutter-mitigation filters in these radars.
- **Clutter Map.** A clutter map is produced in a radar when returns are saved and processed as follows: (1) A set of returns are identified as clutter in specific 'bins' (e.g., range, angle, Doppler) by comparing returns from multiple scans and looking for consistent returns in specific bins, or in some designs looking for specific Doppler returns. (2) Those bins are either blanked (ignored) or

the 'consistent' signal (generated by averaging multiple scans) is subtracted from the current measured signal in that bin. Blanking a bin in a system without required resolution can result in dropouts which may result in loss of measurement of a desired target; therefore, subtraction would be preferred. For example, blanking a range-angle bin in a 2D radar would result in targets flying about the clutter source being essentially invisible to the radar. However, if the blanking occurs in a Range, Angle bin but only for certain Doppler returns, the chance of missing a target of interest can be lowered significantly. Likewise, if it is a 3D radar, the map can also be beam-dependent and further reduce the chance of missing an intended target.

- **Simultaneous-beam processing.** Using multiple beams simultaneously allows for higher resolution in angle, can offer the ability to attenuate signals in angle if the radar architecture allows it. Depending upon the number of beams in either the vertical (elevation) or horizontal (azimuth) planes – or both – a radar can further separate potential interference sources in angle in addition to range and Doppler. Widely used signal processing techniques such as Digital Beam Forming and MUSIC[2] can cancel or null interference sources in angle space.
- **A-priori gating.** Having an a-priori knowledge of the location of clutter sources can allow for some mitigation. Similar to a clutter map, a radar may be able to gate out returns from a specific range-angle cell or suppress track initiation that occurs within a range-angle cell.
- A method that has been frequently proposed involves treatment - or redesign - of the turbine blades to create a low RCS, and thereby lower the signal interference. This is a somewhat unrealistic approach for a number of reasons discussed below. Because of these obstacles, it is more feasible to 'actively' address the returns of the turbines in the signal processing using real-time turbine data provided by the wind farm to the radars of interest, rather than relying upon passive 'stealth' methods.
    - **RCS varies as a function of aspect angle and frequency** (Knott, 1993)**.** RCS can be treated through structural shaping and materials application, but the effectiveness of these methods is geometry (and frequency) dependent. Even on well-controlled structures there will typically be aspects with signature levels that are not controllable. The varied – and somewhat arbitrary/uncontrollable – geometries from radars to the turbines would create aspect angles that are uncontrollable and invariably would present large returns in some cases. It is reasonable to assume that – if treatment were feasible – the lower returns could ease the signal processing mitigation demands, however. Also, because of the long wavelengths of the ocean-monitoring radars (on the order of tens of meters), physical treatments, shaping, and numerical estimation methodologies of the turbines and blades would be of a higher technical risk than higher radar frequencies.
    - **Development timeline and feasibility of turbine redesign**. Low RCS designs would require some shift of expertise from defense applications to wind turbine modifications, quite possibly a transfer of currently-protected defense technology to the commercial sector, and most probably new test facility development given the size of the turbines. Shaping and treatment would most probably also have some measurable adverse effect upon the efficiency of the blades. Additionally, cutting-edge manufacturing methods have been critical to the development of low RCS defense systems (AeroTechNews, 2017). In addition to those infrastructure obstacles, the timeline of the wind farm developments is almost certainly too early to be impacted by a turbine redesign timeline.

3.2.3 Mitigation Techniques (Generic Classification)

This section discusses mitigation techniques that are applicable to all radar systems evaluated in this report. As apparent from the above discussion, the focus on mitigating non-moving clutter implies that

[2] MUSIC is employed by the SeaSonde to provide higher resolution angle measurements.

there are shortfalls in currently deployed radar systems when the clutter has moving components such as the blades of wind turbines. Therefore, mitigation of WTCI must rely on new systems, enhancements to old systems, alternate data sources, or potentially limiting the utility of fielded systems in affected locations. For the purposes of this document, mitigation methodologies can be lumped into the following categories:

- **Operational:** Operational methods involve using the non-modified system with operational constraints. For example, re-siting a radar, using a secondary data source (i.e., Automatic Dependent Surveillance Broadcast [ADS-B], a Global Positioning System (GPS) based broadcast from an aircraft to provide its position - rather than a skin track of an aircraft), limiting altitudes of flight over the wind farm, using existing modes available on a radar, or shutting down wind farm operations during events are some examples of operational mitigation.
- **Modification:** Radar modifications could encompass hardware changes, software and signal processing changes, or potentially both (such as adding an additional signal processing and display system – typically known as a "sidecar"). Except in the case of the addition of a sidecar, it is expected the original equipment manufacturer (OEM) would be required to make the modifications to the radar. If the knowledge of the turbine states (direction, rotation rate, rotation angle) were required by the signal processing system, then data sharing from the wind farm and the associated transmission and receiving/integration equipment would also be required.
- **Addition:** Adding other secondary sensors – sensors designed to be less impacted by wind turbines – could be used to provide data in impacted regions. These proposed systems – commonly called 'in-fill' radars – would be expected to be relatively inexpensive and short range, and probably need to be deployed near or within the wind farm itself and potentially on a turbine mast, or masts. The primary impacted radar would need some modification to accept and integrate the data from the infill systems. One system – the LightWave Radar by C Speed (C Speed, LLC., 2018) is currently undergoing tests at Travis AFB (Carter, 2015). Siting of such a radar has not been accomplished offshore but C Speed has developed offshore designs. Each Lightwave Radar can support a 15NMrange of service, so multiple radars may be needed for large wind farm installations (Lyseck, 2019).
- **Replacement:** Although typically not a feasible alternative for near-term mitigation except through normal life-cycle replacement, ensuring that the next generation of radars are designed with WTCI mitigation should be a goal of the acquiring users of these radar systems.

3.2.4 Mitigation Techniques by Radar Type

Prior to installation of the wind farm(s), it will be important for each impacted radar site to make and archive recordings as a baseline reference for comparison after installation. These recordings should be spread across seasons, and across times-of-day to ensure a broad range of atmospheric conditions are addressed.

Similarly, the following agreements should also be considered prior to wind farm development:

- **Curtailment Agreements.** These agreements can be enforced by BOEM for wind farms on BOEM leases and involve conditions under which wind farms would cease operations to reduce radar interference in special or emergency circumstances. For certain radars, and in certain conditions, curtailment agreements may be beneficial. Hurricane/tropical storm or severe thunderstorm/tornadic activity, or significant oil or hazardous spills could result in scenarios where temporarily curtailing wind farm activity – or portions of a wind farm – would be in the public interest.
- **Data Sharing Agreements.** Some of the mitigation techniques offered show promise if turbine information is available to the radar signal processing system. In addition to specific turbine location, the following information may be quite helpful: turbine orientation, turbine rotation rate, and potentially turbine rotation angle in real time. The CODAR SeaSonde system currently

has a mitigation technique that requires this kind of information[3], although others have been proposed for radars on this list. Additional equipment, such as communication equipment may be required to provide turbine information to the radar processor.

3.2.4.1 *SeaSonde Radars*

There are 25 SeaSonde radars performing ocean monitoring in the vicinity of the wind farms of interest. HF radars have a variety of beneficial characteristics which has allowed an expansion of their employment and made them valuable for several uses. These are relatively low-cost, low-power systems with a small number of non-complex parts (stationary antennas with simple structures); with the complexity resident in the signal processing system, hosted on a workstation capable of performing ocean current monitoring, aid in oil spill containment, tracking vessels, and other tasks while operating remotely. These systems work both independently and in a networked manner to share data and provide additional information.

Our analysis (and reference (Trockel D, 2018)) show that wind turbine interference impacts the SeaSonde ocean current measurements by biasing the measurement of the true background noise level (affecting the sea echo identification algorithms), changing the boundaries of the sea echo peaks by allowing the turbine echoes to be processed as part of the sea echo, and changing the angular measurement for the radial current vectors by causing turbine echoes to be convolved within the sea echo. The mechanical simplicity of the system affords some mitigation constraints but also provides some upgrade capabilities. Of all the impacted radar systems in this analysis, the SeaSonde has the most opportunity for modification.

Operationally there is one primary option for mitigation. Should other mitigation options listed here not be selected, and there occur cases/events where the appropriate authority deems the ocean current measurement capability of SeaSonde of such importance (e.g., spill containment) (Roarty, 2019) that curtailment of wind farm operations is the most effective option, pursuing a curtailment agreement could be considered.

Modification of the SeaSonde, as mentioned prior, is more feasible than any of the other impacted radars. The manufacturer, CODAR, has been developing signal processing enhancements (Trockel D, 2018), although their effectiveness should be tested and validated prior to modification. Similarly, the simplicity of the SeaSonde antenna system lends itself to the addition of relatively inexpensive elements that could increase the angular capability of a single employment. At the time this report was published, CODAR Ocean Sensors was engaged with BOEM in a project to "reduce or eliminate the interference experienced by CODAR HF coastal oceanographic radar from offshore wind turbines. To accomplish this, the study will: (1) assess the impact of turbine interference, spread out in range-Doppler space, on radar-derived physical oceanographic measurements; and (2) provide to the HF radar community, within six months of this project's completion, a software package for mitigating interference that is capable of real-time integration with the existing operational SeaSonde data processing tool chain (viz. SeaSonde Radial Suite)."[4]

3.2.4.2 *The NEXRAD Radars*

Because of the infrastructure, complexity, and expense of the NEXRAD, mitigating wind turbine interference presents complex difficulties for this radar system. **Operationally**, curtailment of the wind farm(s) during critical weather events is an effective mitigation method, and Curtailment Agreements where feasible should be considered for impacted radars and specific weather events. For example, there has been at least one instance where a tornado was tracked by radar going into a wind farm, then "lost"

[3] Discussions between Russell Colburn and Hugh Roarty via telephone on November 11, 2019.
[4] Text in quotes was provided by BOEM from the study statement of work. The full study title provided was "Implementation of Mitigation for Offshore Wind Turbine Interference on High-Frequency (HF) Coastal Oceanographic Radar."

when over the wind farm, and then re-emerged as a detected tornado outside the wind farm (Schultz, 2019). **Modification** of NEXRAD radars involves an understandably rigorous process to ensure any system modification does not impact current radar capabilities and signal interpretations Because of that required rigor, and because signal processing modifications could filter or alter measured information (Palmer, 2019), there have been no offered modifications (beyond the deployed measure discussed following) to effectively mitigate wind farm clutter effects without impacting/masking base data (measured return signal). The one modification to address wind farm clutter mitigation that has been incorporated into the NEXRAD is a precipitation estimator that provides higher accuracy when applied in the vicinity of wind farms (it is more accurate than not using this enhancement around wind farms). **Replacement** of the NEXRAD is more than 20 years away (Palmer, 2019), but the research/development and acquisition process is underway. Windfarm clutter mitigation ideally should be addressed in the requirements of this next generation of weather radar, although the research team understands that currently this is not being addressed (Schultz, 2019).

3.2.4.3 *ASR-8/9/11 Series and ARSR-4*

The ASR-8s and ASR-9s which are predicted to be impacted by the wind farm developments addressed in this study have a variety of mitigation techniques available and proposed. **Operationally** available techniques may not be optimal but still provide some capability and include the use of Sensitivity Time Control (STC) (range-dependent attenuation), Range Azimuth Gating (RAG) (ability to isolate/ignore signals from specific range-angle gates) (Wait, 2019), Track Initiation Inhibit, Velocity Editing, Plot Amplitude Thresholding (PAT) (limiting the amplitude of certain signals) (Drake, 2011). The existence of the secondary signal (beacon transponder), and ADS-B allows for a passive track of those aircraft transmitting the signal. An additional operational consideration could include raising the altitude floor of aircraft flying over the wind farm to ensure they avoid the low beam of the radar and fly primarily in the upper beam. (This operational consideration would not address non-cooperative low altitude targets where they are a concern.) **Modifications** have been proposed, and in some cases integrated onto test systems or deployed on versions of the ASR series in European countries (Drake, 2011). For example, utilizing the dual beams of the radar simultaneously provides elevation data which can provide some spatial information to mitigate the clutter from wind farms, which resulted in a significant improvement in detection (Drake, 2011). The addition of in-fill radars has shown promise; recent tests at Travis AFB in California show an increase in detectability of targets (C Speed, LLC., 2012).

3.3 DUCTING ANALYSIS

3.3.1 Ducting Events

Ducting is an atmospheric phenomenon that alters how electromagnetic (EM) waves propagate through the atmosphere. Ducting events occur in the lower atmosphere and are driven by steep changes in air density from differing temperatures and moisture content with height. Ducting events create a refractive path that trap EM waves near the surface and cause them to propagate well beyond their intended range. An impact of ducting is that a wind turbine or other structure may be visible to a radar when it otherwise would not. In Figure 176 an example of a ducting event involving the ASR-9 ACY and the Skipjack wind farm is shown. The pink line in this plot shows the radar horizon in a 4/3 Earth model and the tips of a few of the turbines are barely visible. The blue line shows a ducting ray that can propagate beyond the radar horizon and into the region where the turbines are situated, allowing for the horizon masked turbines to become visible to the radar. A key study goal was to identify and characterize these ducting events at the project-specific locations. In order to do this, the team first set out to evaluate the meteorological setup and key atmospheric variables contributing to these events.

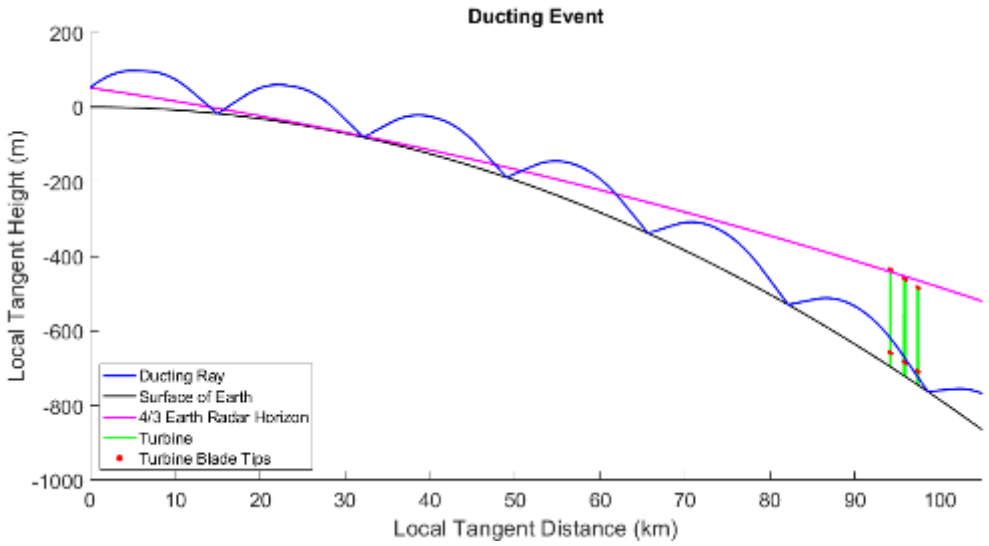

Figure 176 - Example of ducting event

3.3.1.1 *Identifying Ducting Events from a Meteorological Perspective*

Understanding the key atmospheric variables and the drivers of these variables was the first step in identifying ducting events. The research team evaluated existing studies relating to ducting probability, drivers, and identification to better understand the current state of research and guide the investigation. One such study, published by the American Geophysical Union (AGU) Journal of Geophysical Research (JGR) provided an overview of the geographic probability of ducting, included as Figure 177. The research team used this study to investigate vertical profiles at the locations with high ducting probability to better understand the atmospheres that contribute to these scenarios. The research team identified two main scenarios where ducting events occur. First, evaporation directly above the ocean's surface, enhancing the vertical gradient of moisture and leading to evaporation ducts. Second, a temperature inversion caused by warm, dry air aloft that is aligned vertically over cooler air at the Earth's surface. In the lowest layers of the atmosphere above the ocean's surface, evaporation ducts are near-permanent features. Thus, the majority of the investigation focused on identifying temperature inversions and steep negative moisture gradients.

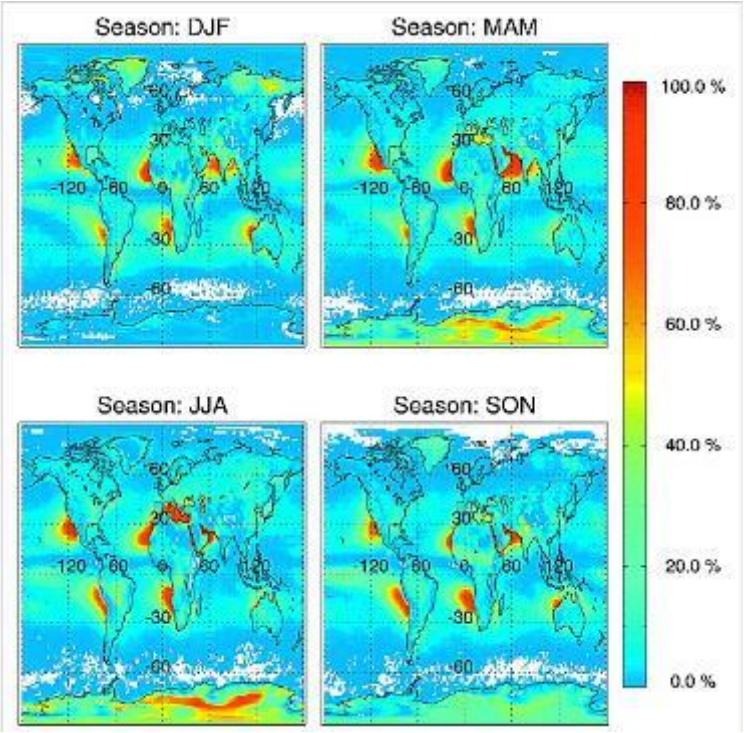

Figure 177 - Geographic probability of ducting by season

In addition, Booz Allen performed a qualitative assessment of ducting frequency on select coastal stations along the eastern seaboard. In order to refine ducting frequency occurrence in proximity to proposed offshore wind farms, NWS radiosonde data was assessed for frequency of meteorological conditions conducive to ducting. The team targeted locations near the coast with enough spatial distribution to provide separate representative atmospheres. The NWS radiosonde sites selected were Chatham, MA (CHH), Morehead City, NC (MHX) and Charleston, SC (CHS). These sites were selected due to their coastal locations and proximity to the proposed offshore wind farm locations as displayed in Figure 178. NWS radiosonde data is output at 00:00 UTC and 12:00 UTC daily and for this assessment a full year of 2019 data was used.

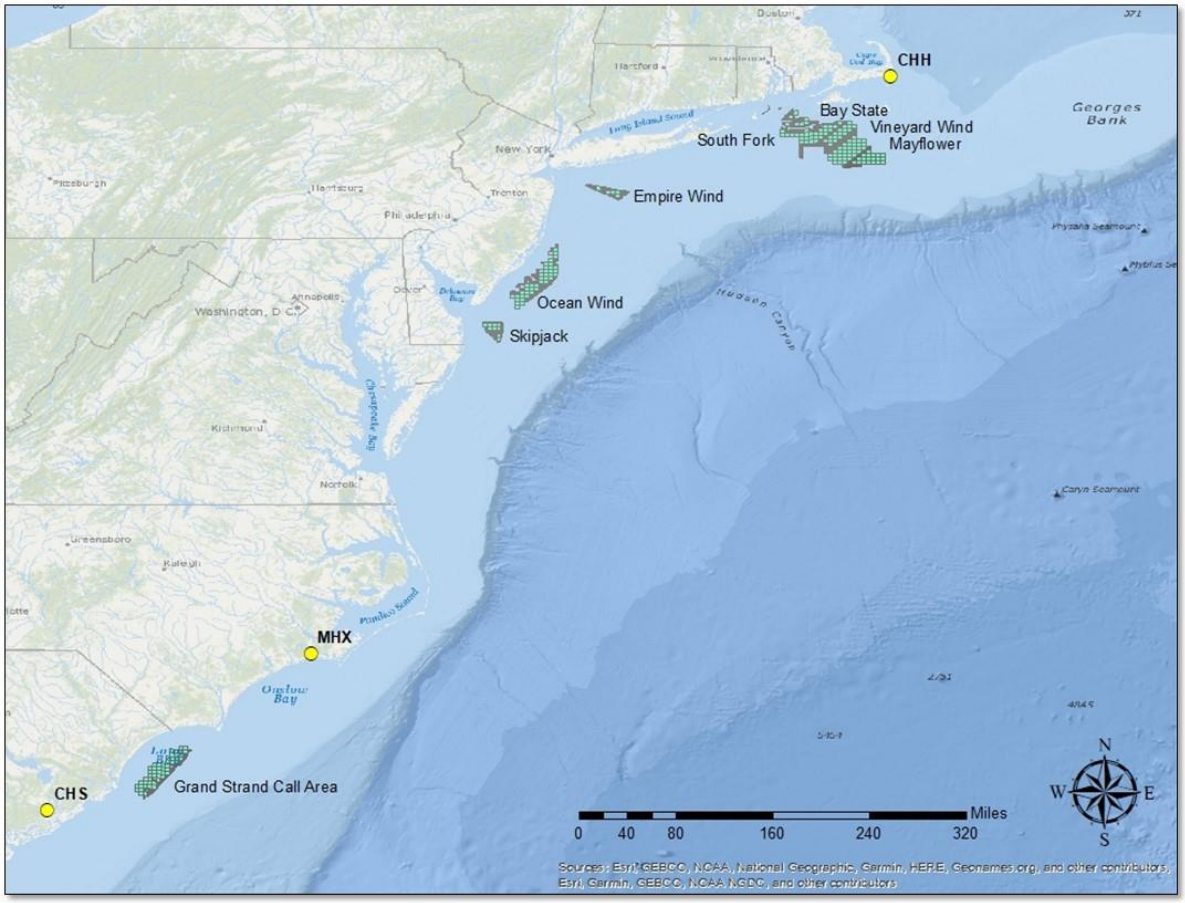

Figure 178 - Radiosonde Stations and Wind Farm Locations

The team viewed the 2019 radiosonde data and assessed the Skew-T Log P chart outputs to identify vertical profiles that would potentially lead to ducting. The team applied their subject matter expertise and findings from the literature review to appropriately identify vertical profiles that may lead to ducting events. Vertical profiles conducive to ducting are described in Section 3.3.1.2.

3.3.1.2 *Variables*

For viewing and analyzing the atmospheric variables contributing to ducting, the team used the meteorological standard Skew-T Log P diagrams, which represent the vertical profile of the atmosphere at a point-location. An example Skew-T Log P diagram is included as Figure 179. These diagrams describe how temperature and moisture variables (x-axis) change with height (y-axis). Under inversion conditions, an increase in temperature with height, radar signals may "bounce" off the inverted atmospheric layer causing them to propagate farther horizontally than would occur under typical atmospheric conditions.

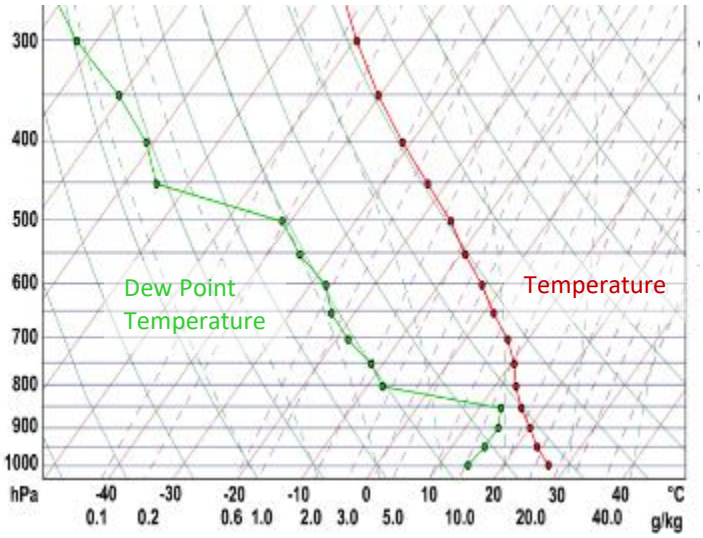

Figure 179 - Skew-T Log P diagram of typical vertical profile

A typical vertical profile is unlikely to induce a ducting event. As an example, the profile in Figure 179 exhibits a typical lapse rate or decrease in temperature and moisture as height increases, moving away from the heat source and moisture source at the surface. This behavior presents an atmosphere that would not trap or duct EM waves and would allow them to propagate as anticipated.

A vertical profile containing a temperature inversion (Figure 180) is an example in of an atmosphere that could induce ducting. This temperature inversion is characterized by the temperature increase with height as indicated by the arrow. This creates a scenario where warmer, drier air sits atop relatively cooler, moister air. These changes in the temperature and moisture conditions with height lead to a sharp density gradient and thus an increased refractive gradient. Ducting may occur due to change in refractive index and increased refractive gradients associated with sharp temperature or moisture inversions.

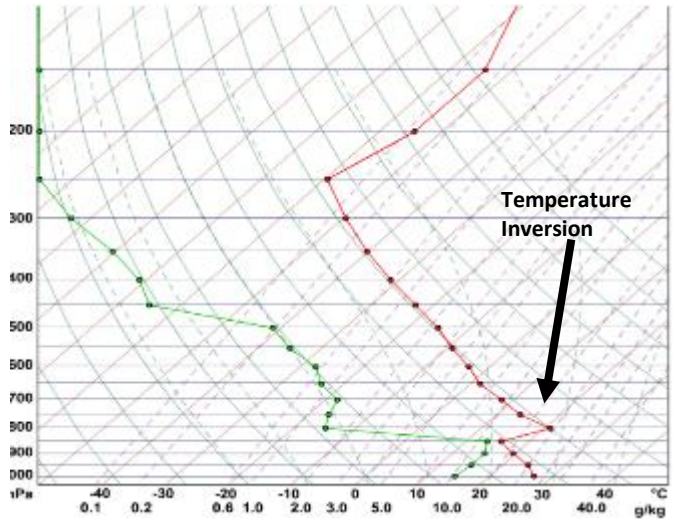

Figure 180 - Skew- T Log P diagram of a temperature inversion

3.3.1.3 *Causes of Inversions*

The team also considered the causes of these inversions and the primary drivers of the trends in atmospheric variables that lead to ducting. An overview of a few key drivers is included below:

- **Radiational cooling:** When the earth's surface emits long-wave radiation causing heat to escape to the atmosphere above. This can lead to situations where the air above the surface is warmer than the surface creating a temperature inversion. An example of this process is shown in Figure 181.

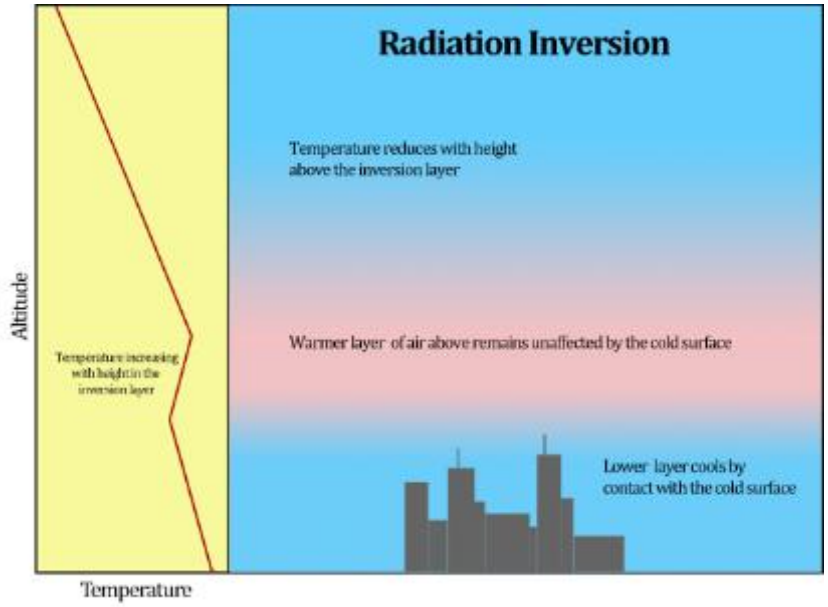

Figure 181 - Inversion from radiational cooling

- **Subsiding (sinking) air:** Typically associated with strong high-pressure systems that cause air aloft to dry out and warm up above a still-cool surface layer.
- **Frontal movement and passages:** This may occur immediately following a cold front passage when cold air is relatively "shallow" and warm air aloft still exists. This is shown in Figure 182.

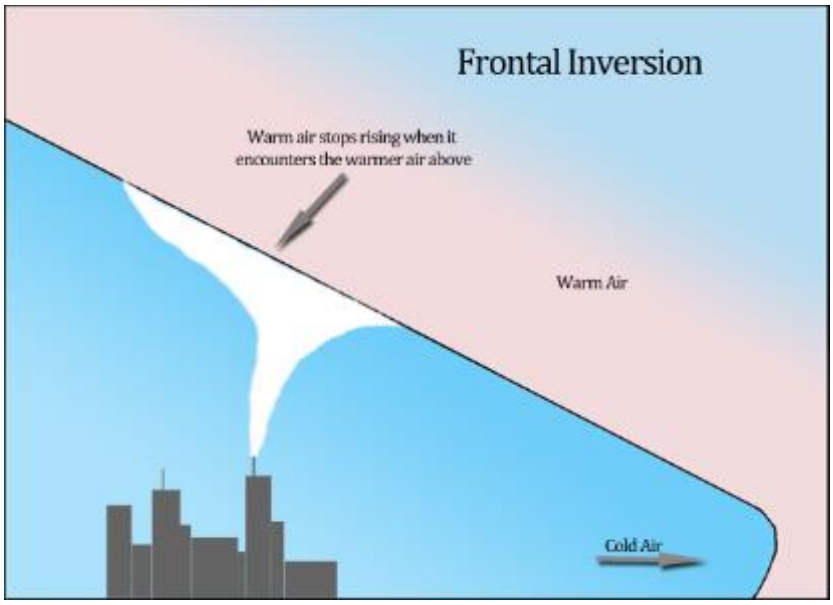

Figure 182 - Frontal Inversion

- **Warm air advection**: Warm advection occurs when warm air aloft overruns cold air near the surface due to warm front passage or regional influences (e.g., mountain ranges).
- **Seabreeze circulations**: Cooler ocean air blows inland to displace the rising warmer air inland. This helps force the warmer air upward/aloft and creates an inversion scenario. An example is shown in Figure 183.

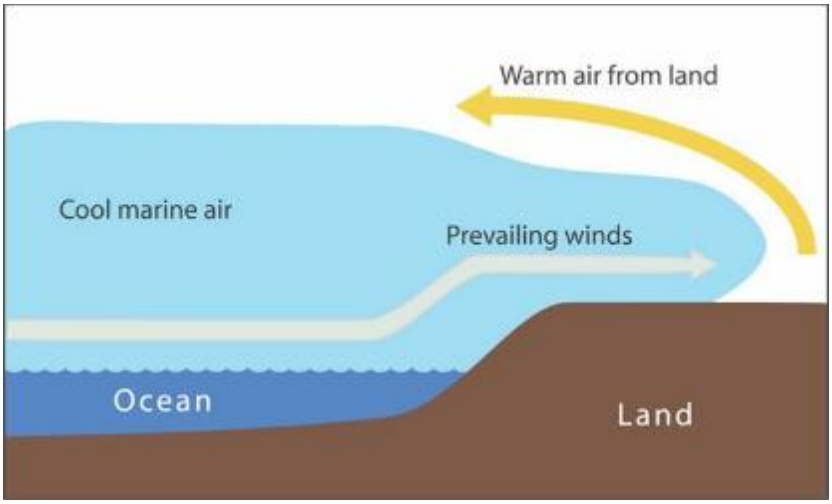

Figure 183 - Seabreeze circulation

3.3.2 Data selection

3.3.2.1 *Cataloging Available Data Sources*

Due to the remote location of offshore wind farms, identifying relevant weather observations is not straightforward. Typical routine weather observation stations are located near airports or major cities. Weather observations that provide a vertical slice of the atmosphere are even more scarce. NWS launches weather balloons twice a day from a limited amount of weather offices across the country. While some of these stations are coastal, none of them exist offshore. To identify the best data source available, Booz Allen accessed several available data sources to determine their applicability and suitability to this effort and address this data gap.

The team compiled a list of archived observation and model reanalysis data sources. Observation data was gathered from a weather sensor either in-situ or via remote sensing in real time. This data was then stored and archived to generate a historical dataset of observations. Model reanalysis data is the post-processing of a numerical weather prediction model using a suite of observations and represents a model's interpretation of the state of the atmosphere at all grid points. A list of the data sources and their applicability to the project are included in Table 22. More detail of how applicability was evaluated is in the next section (3.3.2.2).

Table 22 - Data Sources Evaluated

Description	Type	Spatial Coverage	Applicability
Land-Based Radiosondes	Profile	~10m-60km	Medium
Vertical Wind Profilers	Profile	100-5000m	Low
WSR-88D Doppler Radar VWP	Profile	250m range, gate resolution 230km range	Low
Satellite Sounder Retrievals	Profile	Varies by product	Medium
Ship-Based Radiosondes	Profile	Similar to land-based radiosondes	Medium
HRRR Reanalysis or Initialization Archives	Profile	NA/Worldwide	Medium/High

Description	Type	Spatial Coverage	Applicability
Aircraft Data/ Aircraft Meteorological Data Relay (AMDAR)	Profile	Near airports	Low
Light Detection and Ranging (LIDAR)/Ceilometer	Profile	Near Airports, or other point location	Low
Surface Observations	Surface		Low
Buoy Observations	Surface	Point locations, offshore and near offshore	Low/Medium
GOES Skew-T	Profile	Point locations, offshore and near offshore	Medium/High

3.3.2.2 *Assessing Project Applicability*

The team developed target characteristics for the data to meet overall project needs. The team then assessed the data catalogue against these characteristics. These primary drivers of applicability were based on reliability and ability to characterize ducting. Data sources were prioritized or deemed more applicable based on:

1. Ability to detect lower-atmosphere
2. Spatial resolution
3. Accuracy
4. Frequency of reporting
5. Archive period

These criteria were used given the importance of having a detailed and accurate picture of weather conditions relevant to the horizontal and vertical geography of the wind farms. These are relatively small areas at low altitude, when compared to many other applications of climatic data. This meant it was challenging to ensure the necessary detection in lower atmosphere and the high data resolution. The additional criteria of accuracy, frequency of reporting, and archive period are needed for an accurate estimate of the general seasonal conditions. A dataset without each of these criteria would have been insufficient to provide seasonal averages to assist the radar model's simulations at wind farm locations by incorporating prevailing atmospheric conditions.

3.3.3 Data Sources

The team determined that the dataset most able to fulfill the requirements was NWS's HRRR Model Reanalysis Sounding Data. This dataset is available daily over a three-year archive period and provides reliable high-resolution information about conditions within and above offshore wind farm locations

3.3.3.1 *HRRR Model*

The HRRR model reanalysis produces post-processed weather data in 3×3 km grid squares and at 50 vertical layers of the atmosphere (NOAA, 2019). The model covers the entire United States land mass as well as the offshore areas where the proposed wind farms are located for this project. Data is available for each hour of the day for an archive period of three years. The HRRR model outputs the necessary temperature and moisture variables to investigate atmospheric ducting events at the wind farm sites. A comparison of how the HRRR's characteristics meet the criteria demands for the project is described in Table 23.

Table 23 - HRRR characteristics

Dataset Criteria	HRRR Characteristic
Ability to detect lower atmosphere	50 vertical layers
Data resolution	3 km horizontal resolution
Accuracy	Radiosonde initialization
Frequency of reporting	24 model runs per day
Archive period	Archived data starting from 2016 to present

Although the HRRR model was assessed as the most appropriate for this study it has some limitations in accuracy and resolution. The HRRR model, like other atmospheric numerical models, is a multi-dimensional mathematical representation based on assimilating multiple data sources. These sources include surface observations, weather radar, radiosonde, and weather satellite data. This objective reanalysis of the atmosphere is therefore subject to small accuracy errors compared to direct measurements. In addition, micro-regional differences and atmospheric influences are not always detectable at 3 km horizontal resolution, due to the resolution of the input data and the weighting/smoothing of the reanalysis algorithms.

3.3.3.2 *NWS Radiosonde Data*

Radiosonde data from the NWS weather balloon launches were used to validate HRRR vertical profile data. The NWS weather balloons are launched twice daily at 00 UTC and 12 UTC from various stations, typically at or near NWS Weather Forecast Offices (WFOs). Some of these radiosonde sites are coastal stations relatively near the offshore wind farm locations. The vertical profile observations generated by the radiosondes were compared with the HRRR model data output at the same locations to help identify examples of ducting events in the model archive.

3.3.4 Data Processing and Validation

The HRRR and radiosonde data were collected and compared to validate the relative accuracy of the HRRR reanalysis data to meet the requirements of the project. This was done by comparing the model's output with NWS radiosonde data at four coastal stations (described in Section 3.3.4.2) near the project wind farms. These stations are YQI, MHX, CHH, and CHS. Initially, small sample sizes were used for both datasets, but increasingly larger datasets were used to ensure robust results. These results indicated that the HRRR was a reliable seasonal representation of the atmosphere at the offshore the wind farm locations.

3.3.4.1 *Data Processing*

The HRRR data archive used is maintained by the University of Utah's Center for High Performance Computing (Blaylock, Horel, & Liston, 2017). This archive was accessed via a Python script which downloaded temperature, dew point temperature (thereafter referred to as dew point) and relative humidity at each vertical level for the archive period at 12UTC and 00UTC. These observations were converted from Gridded Binary (GRIB2) to Action Script Communication (ASC) format using the NOAA Weather and Climate Toolkit. The HRRR variables were then extracted and processed using an R-script for the three validation sites and finally the wind farm areas.

The weather station radiosonde data was collected via the University of Wyoming's archive and consolidated in Excel tables (Oolman, 2020). The two datasets were then aligned at coinciding altitudes (+/- 12.5 mb) and the measurements were compared for temperature, dew point, and relative humidity

3.3.4.2 *Data Validation*

The HRRR and radiosonde data were compared by calculating the absolute difference between the measurements for each height and coincident time (00UTC and 12UTC). The percent difference was then calculated to better characterize the relative accuracy of the HRRR reanalysis data compared to the radiosonde sounding. The absolute difference was then averaged twice a day (00UTC and 12UTC) for July 24th and July 28th at YQI, July 28th-July 30th at MHX, July 26th, 27th, and July 30th at CHS, and the month of May at CHH. All dates were from 2019 and these dates were chosen due to the propensity of temperature inversions at these locations during these dates.

Table 24 below shows the absolute difference and the percent difference for the three environmental variables (temperature, relative humidity, and dew point) at three of the coastal stations selected. The absolute difference is the difference between the radiosonde output and the model output at the coinciding height level. The percent difference was calculated by dividing this difference by the radiosonde value.

Table 24 - Comparison HRRR and Radiosonde data (Daily/Monthly at GPS Point)

Variable	YQI	MHX	CHS	Average
Temperature	0.66	0.62	0.50	0.59
Temperature (%)	4.72%	2.30%	1.25%	2.76%
Relative Humidity	12.68	5.98	6.07	8.25
Relative Humidity (%)	19.02%	11.20%	4.59%	11.60%
Dew Point	2.59	1.37	0.78	1.58
Dew Point (%)	34.01%	30.58%	4.06%	22.88%
Note: The large % in dew point is primarily due to large errors at the 5000 ft. level. The model performed better than indicated in this table at lower altitudes with regards to dew point. This is shown in Figure 184.				

The initial sample and comparison at the three locations was not sufficient to form a robust statistical conclusion of the performance of the HRRR model in comparison to the radiosonde data. Specific discrepancies that arose when comparing the HRRR output to the radiosonde observation data:

1. HRRR sounding is representative of conditions within a three km square while the observation data represents a distinct point and trajectory.
2. Sounding data is not output at routine vertical intervals. Due to the weather balloon's ascent rate, data is collected at irregular height intervals. This meant that matching height levels were not always available for comparison with HRRR data. There is no known method by which the height levels can be matched between datasets, so the average in a 12.5 mb (roughly 350 feet) range was calculated.
3. HRRR struggled to replicate the precise vertical distribution of moisture in the lowest levels of atmosphere. While the actual moisture values were reasonably similar, the magnitude of steep vertical increase/decreases were not always reflected in HRRR data.

In order to deal with the limitations of this comparison, the team conducted a more comprehensive assessment to create a long-term estimate of potential errors in the HRRR data. The evaluation period

was extended from one month to the complete archive period of nearly three years, in order to increase the sample size and improve the statistical validity of the comparison. In addition, the data grid used from the HRRR expanded from 3×3 km to 9×9 km. Table 25 presents findings for three environmental variables (temperature, relative humidity, dew point) and the percent difference between the HRRR data and the radiosonde output at CHH for this increased spatial and temporal scale.

Table 25 - CHH Cross-reference of HRRR and Radiosonde data (Archive Period & 9kmx9km Grid)

Variable	CHH – Average	Winter	Spring	Summer	Fall
Temperature (%)	8.53%	24.27%	4.65%	2.57%	2.61%
Relative Humidity (%)	3.84%	4.62%	3.71%	3.70%	3.57%
Dew Point (%)	21.08%	10.70%	34.81%	11.20%	27.62%

The table summarizes the results of the average percent difference when comparing the HRRR model data and the radiosonde measurements at CHH over the three-year archive period and on a 9×9km grid.

Accounting for two of the three sources of error described above.

1. The R script was modified to use three HRRR grids cells, making a 9×9 km area rather than one 3×3 km grid. This change improved accuracy by accounting for potential misalignment between the radiosonde and the grid cell. It also smoothed micro-regional variations.
2. To help explain the larger differences in HRRR dew point performance at CHH, the HRRR model's error was looked at vertically for dew point. This made it clear that some of the model's error was attributable to errors at the highest altitude of interest (850 mb or approximately 5,000 feet), but it was more accurate at the critical lower altitudes as displayed in Figure 184.

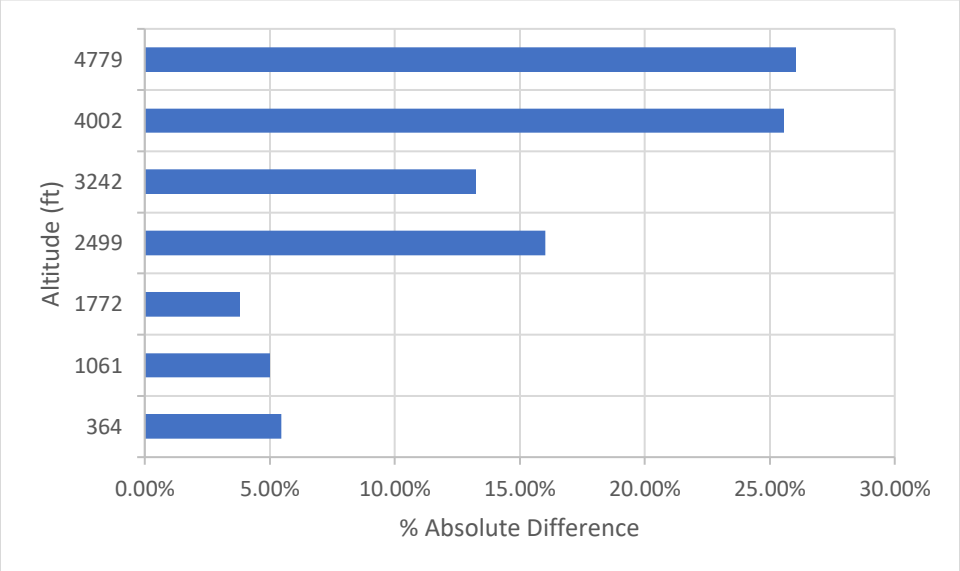

Percent differences between HRRR data and radiosonde sounding measurements based on the height of the sounding. The HRRR model matches the radiosonde data better at lower altitudes.

Figure 184 - Dew Point Difference with Altitude at CHH

3.3.5 Conclusion/Recommendation on HRRR Data

The results of the HRRR validation indicated that the model realistically represents temperature values and trends (for example, a 2.13% difference at CHH). The model reliably depicts relative humidity, as evidenced by a 1.67% difference at CHH. However, the HRRR model performs less well with regards to dew point, though it still performs reasonably well at lower altitudes. The HRRR model's accuracy is highly variable when comparing a single data point to radiosonde measurements. However, when the HRRR is averaged with a larger temporal and spatial sample size the differences in the absolute values between the HRRR model and the radiosonde observations are low enough to instill confidence in overall performance and representation of atmospheric trends. Therefore, the team concluded that the data can be used with confidence as a representative profile, especially when averaged across months or seasons, over remote areas associated with wind farms.

3.3.6 Ducting Frequency

This section provides an overview of the frequency of ducting on the eastern seaboard and nearby coastal radiosonde stations. Meteorological conditions conducive to ducting occur occasionally along the eastern seaboard. These conditions feature a strong temperature inversion (temperature warming with ascending height) coincident with a sharp change from moist to dry air aloft, typically in the lowest 7,000 feet of the atmosphere. Along the eastern seaboard and in the western Atlantic Ocean, ducting conditions occur 20% to 30% of the time, with seasonally variability.

3.3.6.1 *2019 Sounding Data Assessment*

In order to assess probable ducting frequency, vertical profile data for three coastal radiosonde stations was evaluated for the one-year period of 2019. The stations were CHH, MHX, and CHS. Primary drivers of probable ducting scenarios were identified qualitatively and included. frontal inversions, warm air advection, sea-breeze circulations, and radiational cooling.

The assessment results showed that conditions conducive to ducting occurred on average 20% of the time in 2019 at these radiosonde locations. The specific results were 19% at CHH, 25% at MHX, and 18% at CHS. This assessment also revealed some seasonal trends for 2019 as seen in Figure 185. All three locations had peak frequencies of probable ducting scenarios in the winter, with lower frequencies in the late spring and early summer. MHX had the highest count of ducting scenarios and displayed less seasonal variability than the other two sites. CHS had the highest single-month occurrence for this one-year span, in December. The AGU study (Engeln & João, 2004) included in our literature review noted similar ducting frequency along the eastern seaboard but observed different seasonal variability. Higher ducting rates were reported by the U.S. Navy during a study of ducting events at Wallops Island, VA. With some ducting events occurring on a micro-scale, the separate methods used by each study may lead to varying results. However, each study confirms the existence of ducting in offshore environments. Ducting should thus be considered when developing offshore wind farms to help mitigate turbine interference on radar systems.

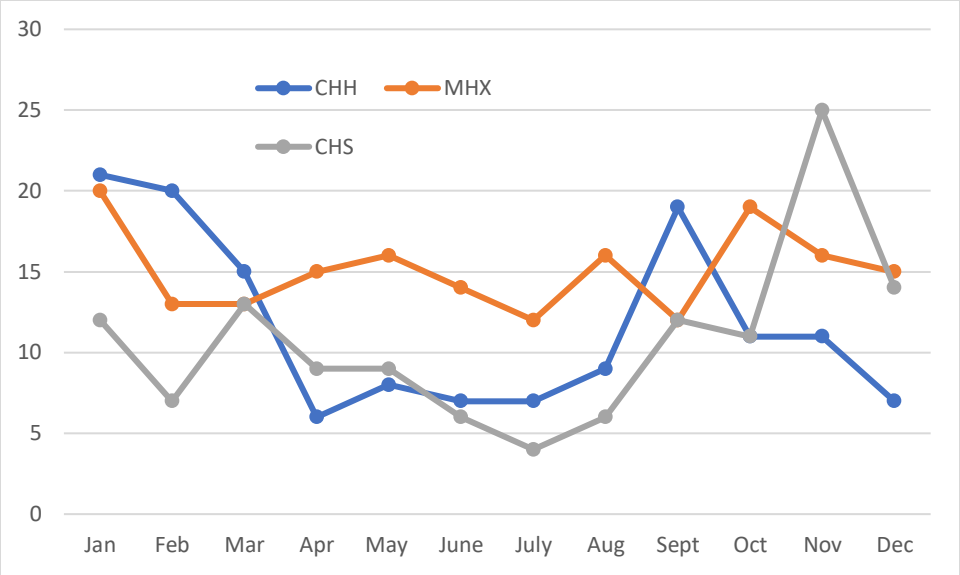

Figure 185 - 2019 Count of Pronounced Inversions and Potential Ducting Scenarios

The second part of this assessment was to use subject matter expertise and knowledge gained from the literature review to determine conditions at these locations that would contribute or generate the vertical profiles that lead to potential ducting scenarios. As noted in section (3.3.1.3), temperature inversions and moisture discontinuities may occur anywhere due to several factors. Key contributing factors for the offshore locations of this assessment are described in Table 26 below.

Table 26 - Meteorological Conditions Contributing to Inversions and Potential Ducting Scenarios

Contributing Meteorological Condition	Seasonal Variations	Diurnal Variations
Radiational cooling	Year-round	Peaks during late night through mid-morning
Sea breeze circulations	Primarily warm season (May – Sept)	Peaks during daytime when cooler sea breeze pushes inland underneath warmer air aloft
Low-level jets	Year Round but primarily cool season (Oct – Apr)	Anytime – minor peak overnight and early morning
Subsiding/Sinking Air	Year Round	Anytime
Frontal Movement	Year Round	Anytime

3.3.6.2 *HRRR Model Analysis*

Booz Allen conducted a preliminary, qualitative analysis of 2019 vertical profile sounding data to determine the frequency of potential ducting scenarios at three locations on the eastern seaboard. The NWS radiosonde locations selected were CHH, MHX, and CHS. The findings of this analysis can be found in Section 3.3.6.1. This preliminary analysis provided a limited assessment of potential ducting frequency at eastern seaboard locations.

The team expanded the temporal and spatial scale of the analysis by analyzing three years of data from 2017 to 2019 using the HRRR (Section 3.3.3.1) model reanalysis for locations that included all potential offshore wind farms. This addressed the small sample size and narrow spatial focus of the 2019 sounding data analysis. In addition, the HRRR enabled analysis of vertical atmospheric profiles offshore in the proximity of proposed wind farm locations.

The goal of this detailed analysis was to determine the frequency of ducting at the potential wind farm locations. The team did this by using HRRR model reanalysis data with an increased spatial and temporal scale and sample size. The team evaluated HRRR data based on the following parameters:

- 3-hour intervals (e.g., 13z, 16z, 19z)
- All height levels up to 600mb (~18,000 ft)
- Yearly data from 2017 to 2019
- Inclusion of all potential wind farm locations identified in this study

To identify ducting events, the radio refractivity at each HRRR data point was calculated using the following equation (N):

$$N = \frac{77.6}{T}\left(P + 4810\frac{e}{T}\right)$$

The team evaluated changes in the calculated radio refractivity with increasing height A negative change in radio refractivity with height was used to approximate the refractive gradient and would indicate a scenario where ducting could occur. The probable ducting events were compared to the complete set of HRRR-based refractive index data to determine percentages of occurrence of ducting. Probable ducting events below 200 m aloft were omitted due to the potential for the model to capture evaporation ducts, which are near permanent features over ocean areas, and could misrepresent the frequency of the more critical/impactful atmospheric ducts aloft. A global ducting frequency study based on atmospheric model data (Engeln & João, 2004) indicated that duct layers 200 m or less are considered non-critical.

The team generated probable ducting frequency percentages for the five proposed wind farm sites. The results were aggregated across the entire domain and analyzed seasonally for each site. The team found that probable ducting occurred, on average, 19.6% of the time across all sites. The seasonal findings are show in the Table 27. This table includes the averages by season and site averages.

Table 27 - HRRR Ducting Frequency Results

	Ducting Frequency (% of time)				
Location	**Fall**	**Winter**	**Spring**	**Summer**	**Average**
Vineyard Bay	22.8	9.6	12.1	30.5	**18.8**
Empire Wind	20.5	8.1	10.8	27.8	**16.8**
South Fork Wind	22.8	9.2	12.2	30.5	**18.7**
Skipjack Wind	26.0	12.5	16.3	35.0	**22.4**
Ocean Wind	24.9	11.0	14.8	34.0	**21.2**
Average	**23.4**	**10.1**	**13.2**	**31.5**	**19.6**

The observed seasonal trends were similar to ducting frequencies found in the literature review and were meteorologically consistent. For example, the observed increase in ducting frequency in the spring and summer can be partially attributed to the atmosphere aloft warming while the ocean surface remains cool. This setup increases the frequency of temperature and moisture inversions, key contributors to ducting.

Spatial trends were observed when comparing the different locations. Skipjack Wind had the highest frequencies for all seasons. Skipjack is also the most southern of the proposed wind farm locations

analyzed. Ocean Wind, the second most southern farm, has the second highest ducting frequencies. The increased frequency of warm air aloft aids in the formation of temperature inversions and subsequent ducting when compared to the more northern sites.

The HRRR-based analysis shows a more consistent and robust picture of the frequency of ducting at potential wind farms, compared to the preliminary qualitative analysis using only 2019 sounding data. Although the 2019-only and 2017-2019 analyses results were roughly similar, the 3-year study using HRRR reanalysis data showed seasonal and spatial trends more clearly. The findings also align well with the ducting frequencies calculated off the eastern seaboard in the referenced AGU study.

3.3.7 **Discussion**

The team was able to validate and produce seasonal atmospheric condition profiles of six proposed wind farm sites: Skipjack, Vineyard Wind, Bay State Wind, South Fork, Ocean Wind, and Empire Wind (Figure 178). The Vineyard Wind and Bay State Wind sites are in close enough geographic proximity to make meteorological differences negligible, so these sites were combined into a single profile. The resulting profiles from all the sites are representative of expected weather conditions off the Eastern Seaboard of the United States.

A similar research study conducted (Engeln & João, 2004) found that ducting occurs approximately 20-30% (Figure 186) of the time in these areas with seasonal variability. Therefore, the absence of ducting events from the seasonal profiles characterizing the seasonal profiles at the wind farm sites is not unexpected.

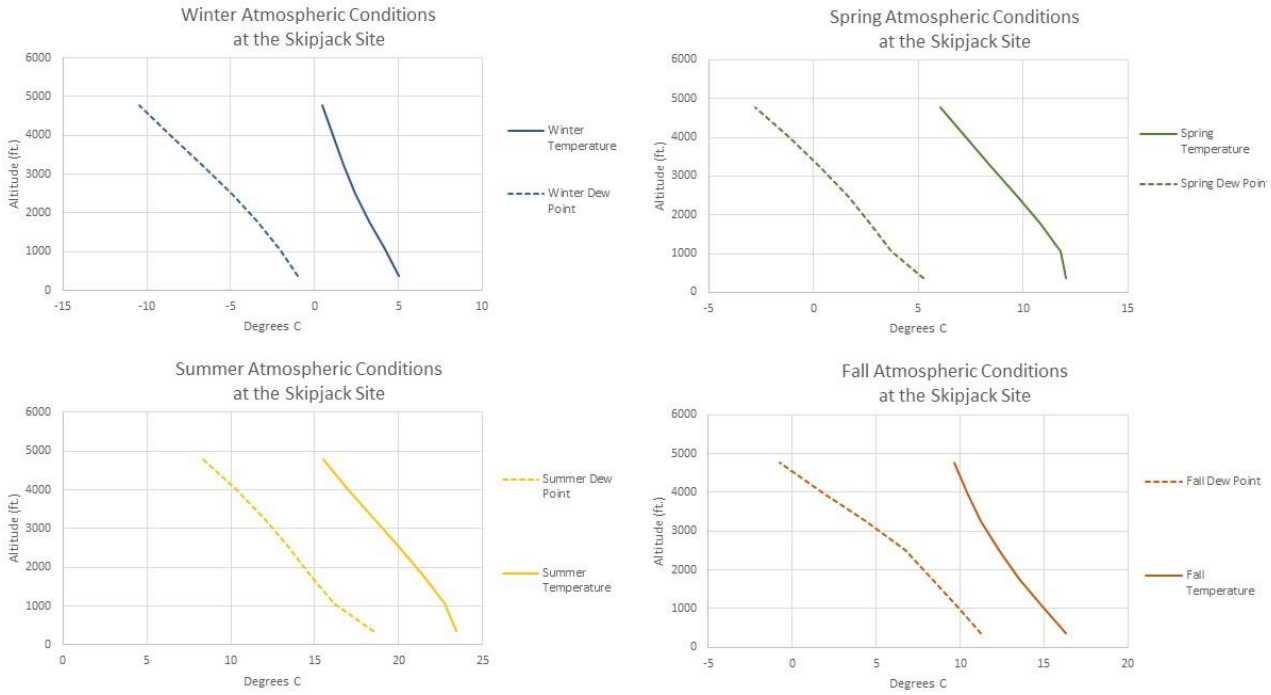

Figure 186 - Seasonal Average Vertical Atmospheric Profiles at Skipjack Site

4 CONCLUSIONS AND RECOMMENDATIONS

Booz Allen developing the following conclusions and recommendations based on this study's findings:

1. **Several Radar Impacts:** Proposed and hypothetical future wind farms are within LOS of several radar systems of various types along the Atlantic coast, meaning that radar interference should be a concern for wind farm development.
2. **Unique SeaSonde Issues:** SeaSonde radars present a unique challenge for offshore wind installations because the radar systems are unique to the coastal environment and large numbers of them exist on the Atlantic coastline. SeaSondes appear to be the most heavily-impacted radar due to their prevalence; however, there may be a relatively inexpensive mitigation option available for SeaSondes that involves a software upgrade.
3. **Wind Farm Developer/Radar Operator Cooperation:** Mitigation techniques available for offshore wind farms mirror those available for onshore wind farms, with the exclusion of SeaSonde radars. Mitigation techniques available include a combination of operational mitigations and radar system modifications and upgrades. Mitigation techniques potentially involve the wind farm developers and operators and actions they (the developers and operators) would be required to take including coordination in the planning stages of wind farm development.
4. **Frequency of Ducting:** Atmospheric ducting is not unique to the coastal environment. However, some atmospheric conditions, such as the presence of moisture over the ocean and inversion layers, make ducting more common in coastal environments than onshore. Atmospheric conditions that lead to ducting occur along the U.S. Atlantic coast approximately 10-30% of the time with both seasonal day-to-day variations due to meteorological factors. As such, radars that are not in LOS of offshore windfarms under normal atmospheric conditions can become impacted during ducting conditions.
5. **BOEM COP Review:** As BOEM reviews wind farm COPs, they should consider conducting LOS analysis on nearby radar systems to determine whether major radar systems may be impacted by the proposed wind farm. Due to the common occurrence of ducting conditions, specifying the exact layouts or turbine sizes that would narrowly avoid LOS of radar systems will not always result in the turbines avoiding detection in the offshore environment.
6. **Curtailment Agreements:** BOEM should consider establishing curtailment agreements among offshore wind farms and radar operators. These curtailment agreements would include specific conditions under which wind farm operations might be curtailed to allow for unimpeded radar operations. These agreements would be informed by site-specific LOS and interference analyses. Additionally, for those developments where radars are expected to be impacted, BOEM should consider drafting agreements with wind farm developers and operators to:
    a. Share real-time data-sharing for radar signal processing modifications
    b. Require In-fill radar placements where impact is significant

5 REFERENCES

AeroTechNews. (2017). *A Gathering of Eagles: Design Evolution of the F-22 Raptor.* Retrieved from AeroTechNews: https://www.aerotechnews.com/blog/2017/10/21/a-gathering-of-eagles-design-evolution-of-the-f-22-raptor/

Barrick, D. (1970). *Theory of ground-wave propagation across a rough sea at dekameter wavelengths.* Battelle Memorial Institute, Columbus Laboratories.

Barrick, D. (1971). Theory of HF and VHF Propagation Across the Rough Sea, 2, Application to HF and VHF Propagation Above the Sea. *Radio Science*, 527-533. Retrieved from https://doi.org/10.1029/RS006i005p00527

Barrick, D. (1972, January). First-Order Theory and Analysis of MF/HF/VHF Scatter from the Sea. *IEEE Transactions on Antennas and Propagation*, 2-10. doi:10.1109/TAP.1972.1140123

Barrick, D. (1973). *FM/CW Radar Signals and Digital Processing.* U.S. Department of Commerce. Retrieved from http://www.codar.com/images/about/1973Barrick_FMCW.pdf

Blaylock, B. K., Horel, J. D., & Liston, S. T. (2017, December). Cloud archiving and data mining of High-Resolution Rapid Refresh forecast model output. *Computers & Geosciences, 109*, 43-50. doi:https://doi.org/10.1016/j.cageo.2017.08.005

Buterbaugh, A., & al., e. (2008). *Dynamic Radar Cross Section and Radar Doppler Measurements of Commercial General Electric Windmill Power Turbines Part 2 – Predicted and Measured Doppler Signatures.* Wright Patterson AFB, Air Force Research Laboratory, Dayton. Retrieved from https://users.ece.utexas.edu/~ling/US3%20AMTA%20Wind%20Turbine%20-%20Part%202.pdf

C Speed, LLC. (2012). "Lightwave Radar Primary Surveillance Radar". Liverpool, NY.

C Speed, LLC. (2018, January). *C Speed Announces LightWave Radar Wind Turbine Mitigation and In-fill Air Surveillance Radar System Achieves TRL-9 Status.* Retrieved from http://www.lightwaveradar.com/images/LWR_PressRelease_0418_6.pdf

Carter, A. (2015, March). *Travis Tests Radar Technology*. Retrieved from Travis Air Force Base: https://www.travis.af.mil/News/Article/767933/travis-tests-radar-technology/

Drake, P. (2011). "Overview of Raytheon Wind Farm Mitigation Techniques and Test Results". *CNS/ATM Conference.*

Elkin, G. (2001). *The Radar Correlation and Interpolation (C&I) Algorithms Deployed in the ASR-9 Processor Augmentation Card (9PAC).* Massachusetts Institute of Technology, Lincoln Laboratory. Lexington: Federal Aviation Administration.

Engeln, A. V., & João, T. (2004). A ducting climatology derived from the European Centre forMedium-Range Weather Forecasts global analysis fields.

Knott, E. F. (1993). Radar Cross Section Fundamentals. In *Radar Cross Section Measurements.* Boston: Springer. doi:https://doi.org/10.1007/978-1-4684-9904-9_1

Lipa, B., Nyden, B., Ullman, D. S., & Terrill, a. E. (2006, October). SeaSonde Radial Velocities: Derivation and Internal Consistency. *IEEE Journal of Oceanic Engineering, 31*(4). Retrieved from http://www.codar.com/images/about/2006Lipa_RadVel.pdf

Lyseck, D. (2019). C Speed Radar. (B. A. Hamilton, Interviewer)

NOAA. (2017). *Radar Operations Center*. Retrieved from National Weather Service: https://www.roc.noaa.gov/WSR88D/Engineering/NEXRADTechInfo.aspx

NOAA. (2019). *High-Resolution Rapid Refresh (HRRR)*. Retrieved from Earth System Research Laboratory: https://rapidrefresh.noaa.gov/hrrr/

NOAA. (2019, July). *NOAA Weather and Climate Toolkit*. Retrieved from National Centers for Environmental Information: https://www.ncdc.noaa.gov/wct/

NSSL. (2019). *Research Tools: NEXRAD*. Retrieved from NOAA The National Severe Storms Laboratory: https://www.nssl.noaa.gov/tools/radar/nexrad/

Ohs, R., Skidmore, G., & Bedrosian, G. (2010). Modeling the Effects of Wind Turbines on Radar Returns. *Military Communications Conference (MilCom).* doi:10.1109/MILCOM.2010.5680316

Oolman, L. (2020). *Department of Atmospheric Science*. Retrieved from University of Wyoming: http://www.weather.uwyo.edu/upperair/sounding.html

Palmer, D. R. (2019, September). University of Oklahoma. (B. A. Hamilton, Interviewer)

Pinto, J., Matthews, J., & Sarno, G. (2009). Stealth technology for wind turbines. *IET Radar, Sonar and Navigation*, *4*(1), 126– 133. doi:10.1049/iet-rsn.2009.0031

Poupart, G. (2003). *Wind farms impact on radar aviation interests.* Technical Report, QinetiQ (UK). Retrieved from https://www.osti.gov/etdeweb/biblio/20414080

Roarty, H. (2019, November). NOAA. (B. A. Hamilton, Interviewer)

Schultz, J. (2019, November). National Weather Service. (B. A. Hamilton, Interviewer)

Trockel, e. a. (2018). *Impact Assessment of Offshore Wind Turbines on High Frequency Coastal Oceanographic Radar.* CODAR Ocean Systems for BOEM.

Wait, J. (2019, September). FAA. (B. A. Hamilton, Interviewer)

Warner, T. A., Lang, T. J., & Lyons, W. A. (2014, July 12). Synoptic scale outbreak of self-initiated upward lightning (SIUL) from tall structures during the central U.S. blizzard of 1–2 February 2011. *Journal of Geophysical Research*.

APPENDIX A LOS PLOTS

A.1 VINEYARD WIND

ASR

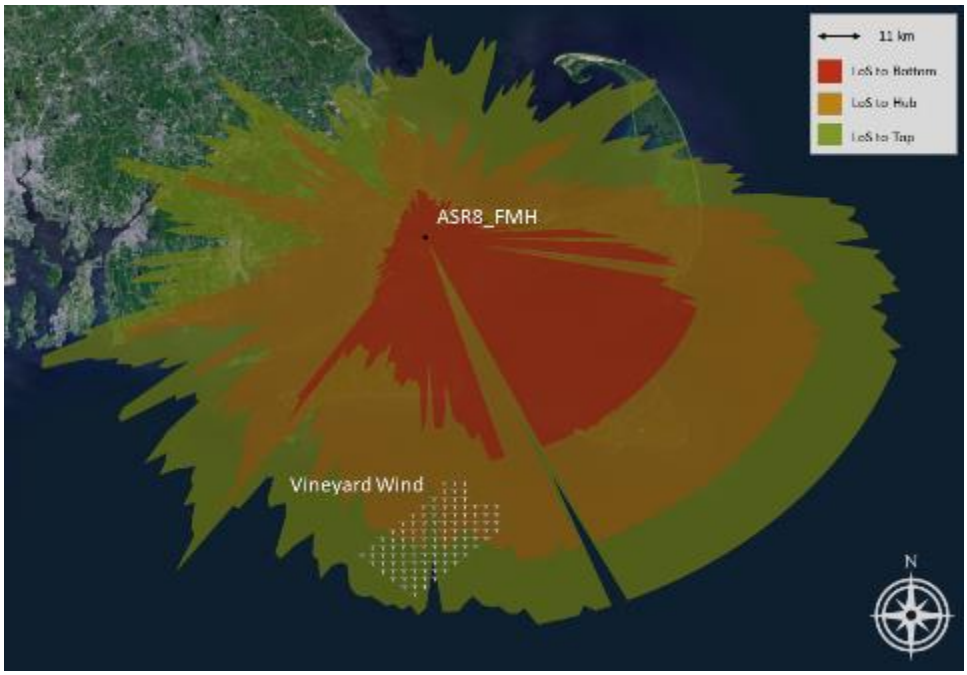

Figure 187 - Vineyard Wind, ASR-8, FMH

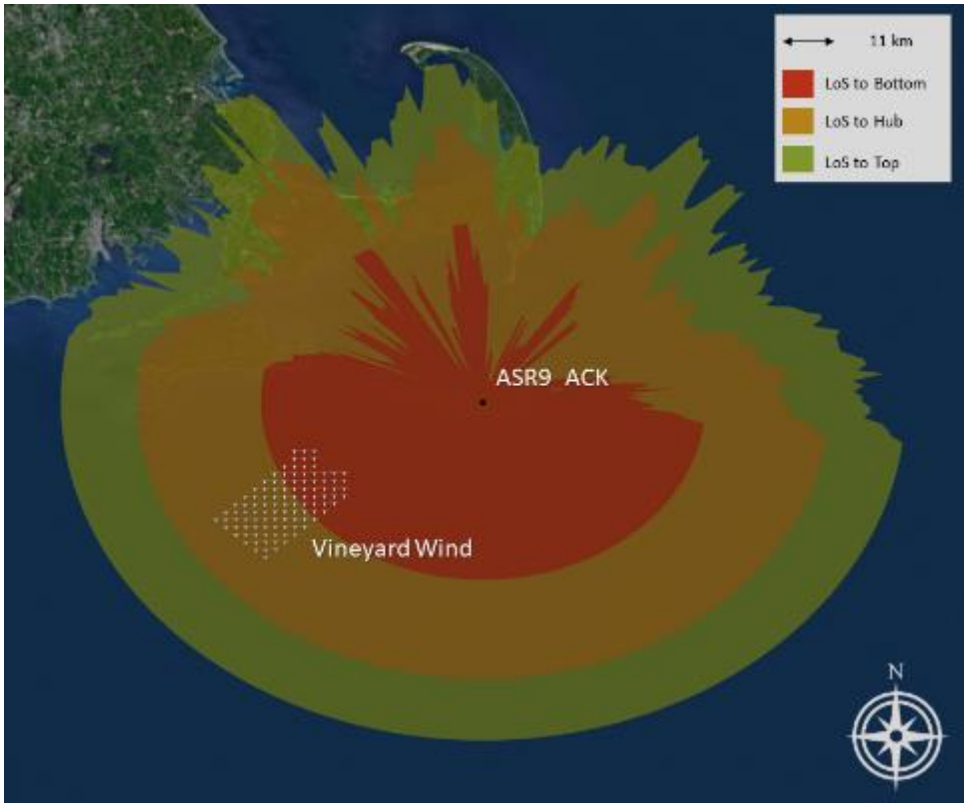

Figure 188 - Vineyard Wind, ASR-9, ACK

SeaSonde

Figure 189 - Vineyard Wind, SeaSonde, AMAG

Figure 190 - Vineyard Wind, SeaSonde, LPWR

Figure 191 - Vineyard Wind, SeaSonde, MVCO

Figure 192 - Vineyard Wind, SeaSonde, NANT

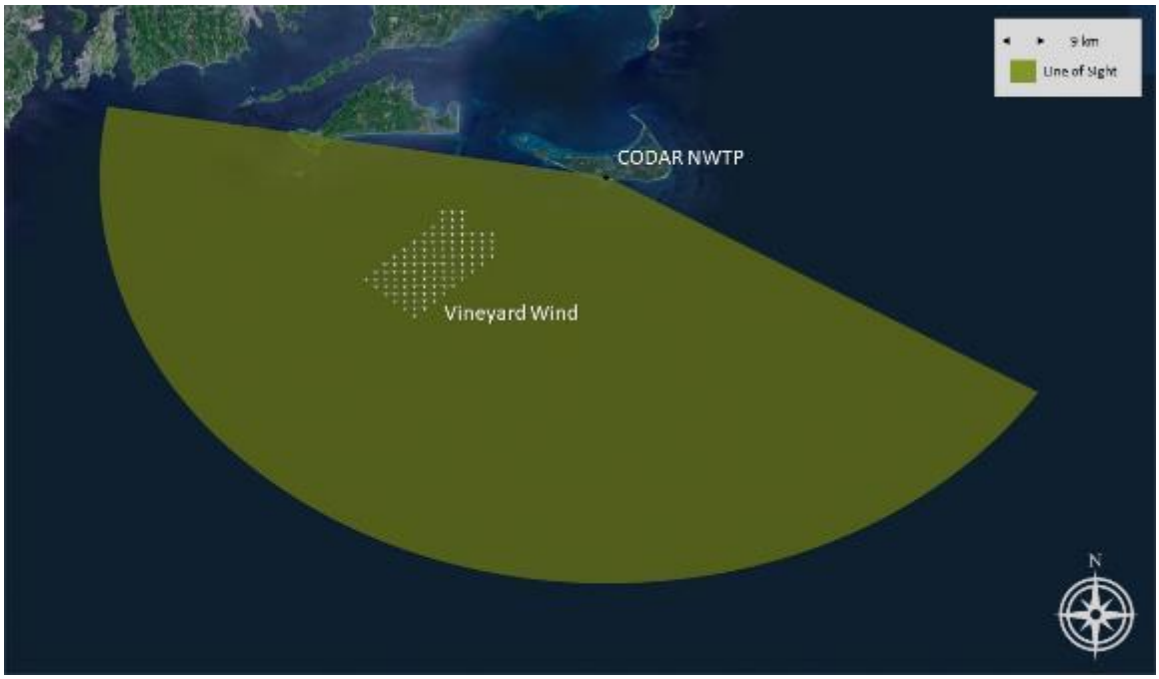

Figure 193 - Vineyard Wind, SeaSonde, NWTP

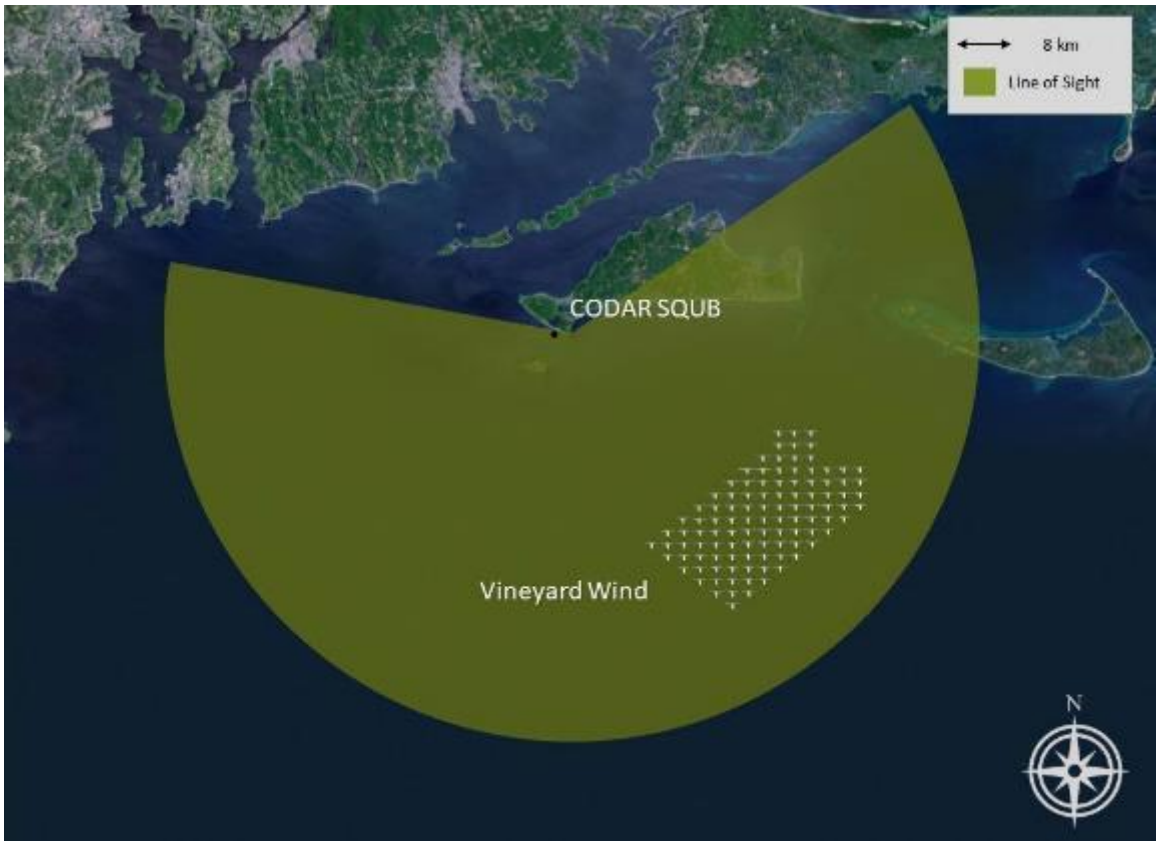

Figure 194 - Vineyard Wind, SeaSonde, SQUB

A.2 BAY STATE

ASR

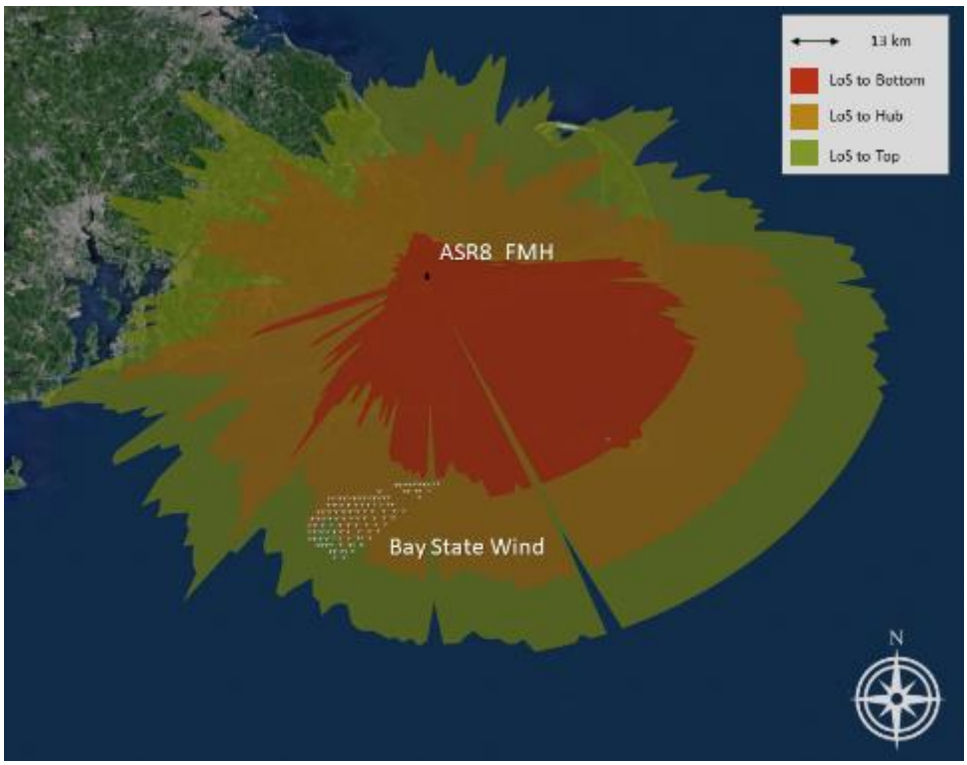

Figure 195 - Bay State, ASR-8, FMH

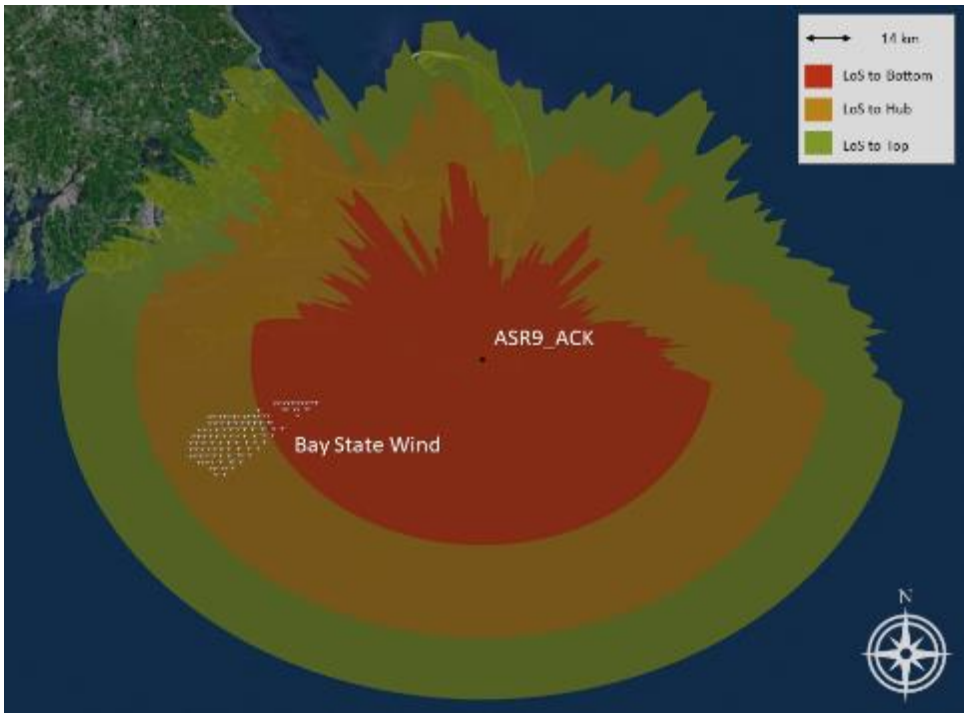

Figure 196 - Bay State, ASR-9, ACK

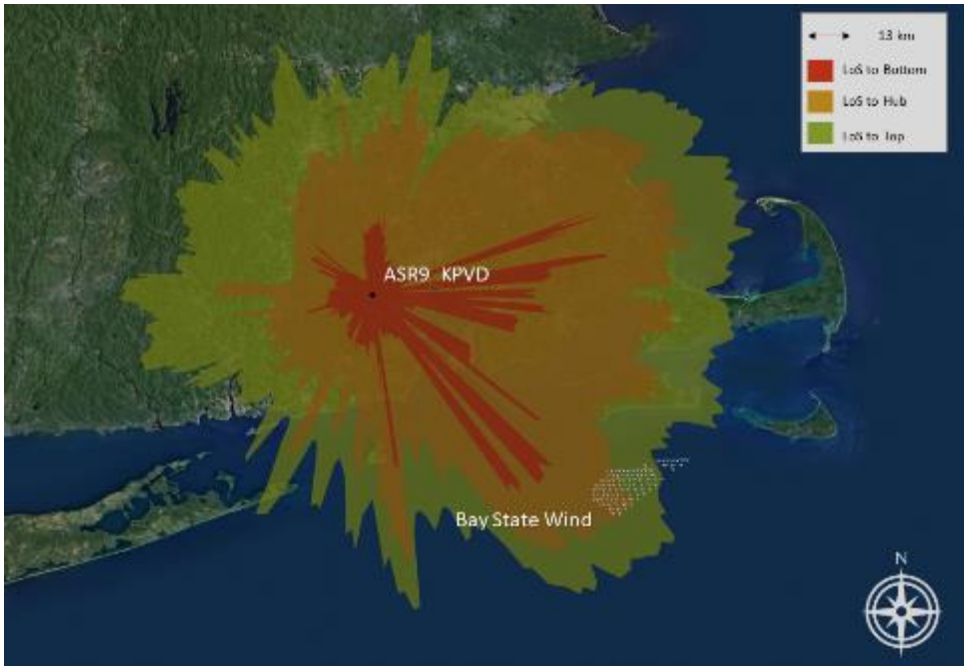

Figure 197 - Bay State, ASR-9, KPVD

SeaSonde

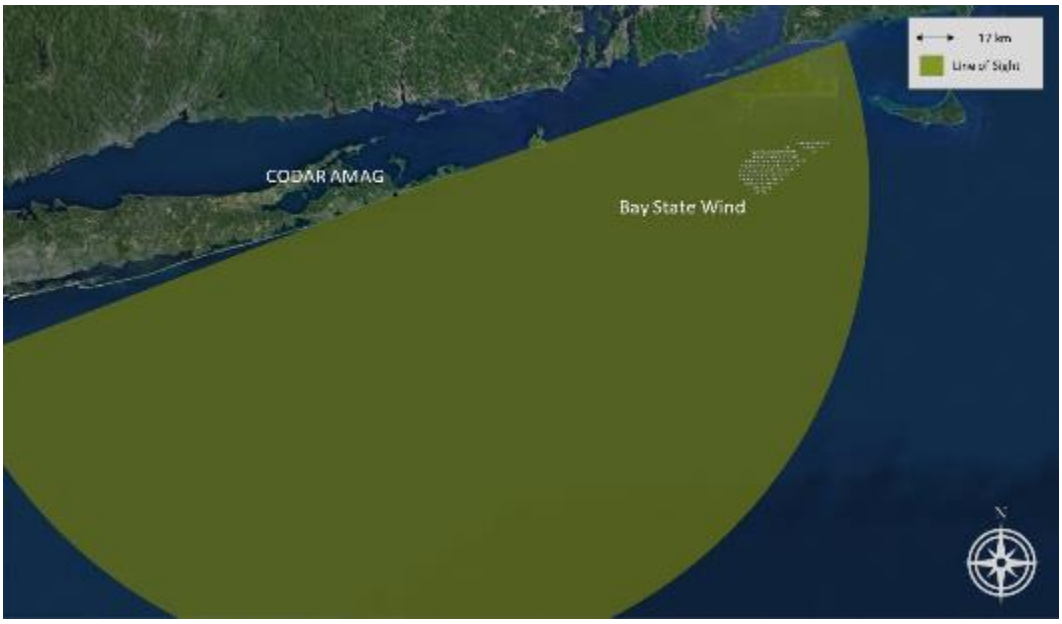

Figure 198 - Bay State, SeaSonde, AMAG

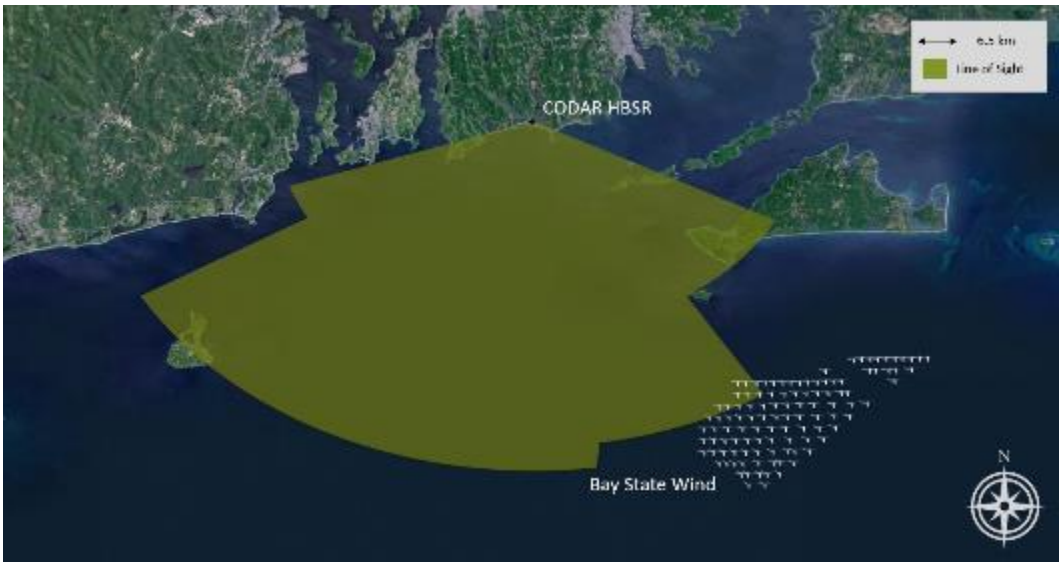

Figure 199 - Bay State, SeaSonde, HBSR

Figure 200 - Bay State, SeaSonde, LPWR

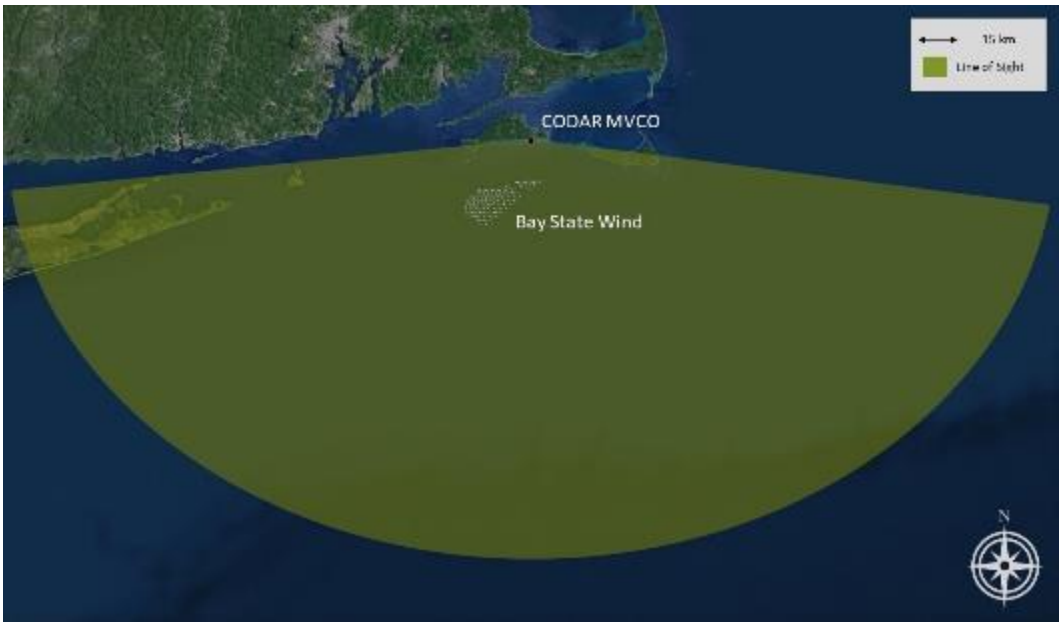

Figure 201 - Bay State, SeaSonde, MVCO

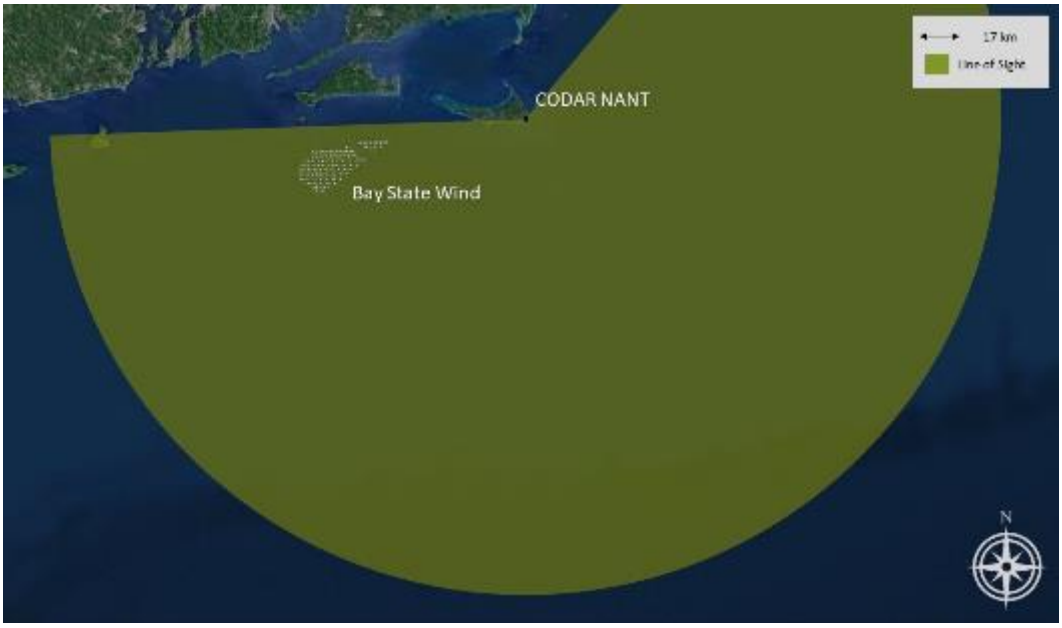

Figure 202 - Bay State, SeaSonde, NANT

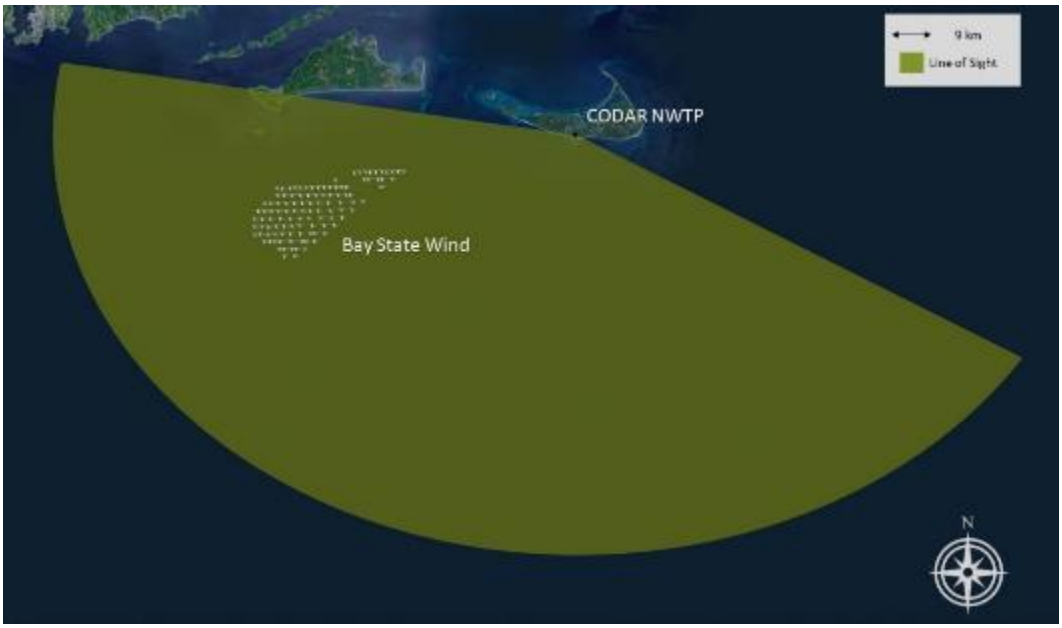

Figure 203 - Bay State, SeaSonde, NWTP

Figure 204 - Bay State, SeaSonde, SQUB

A.3 SOUTH FORK

ASR

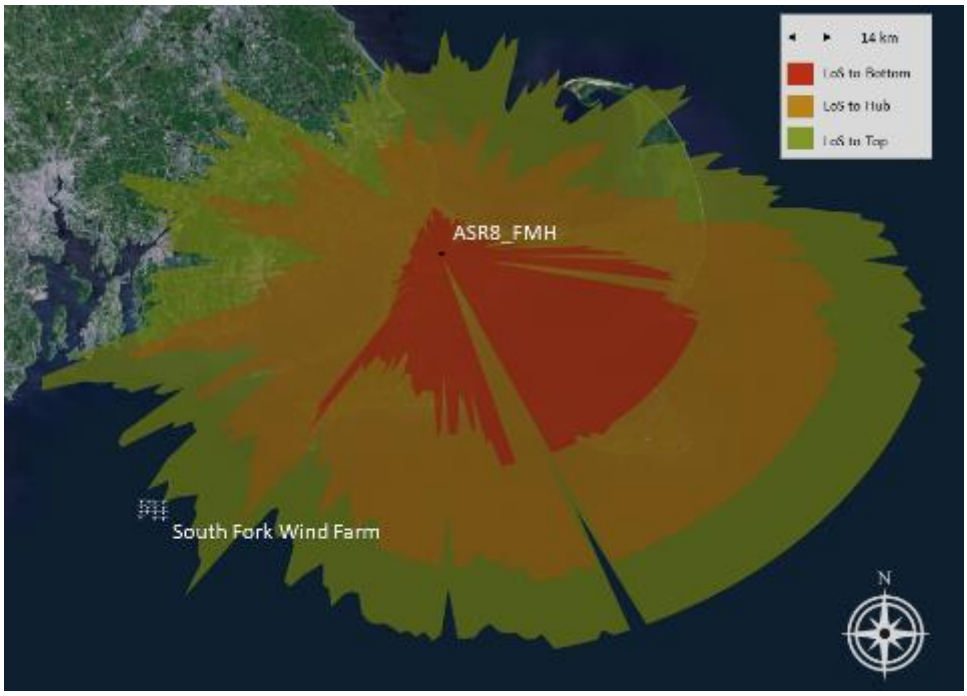

Figure 205 - South Fork, ASR-8, FMH

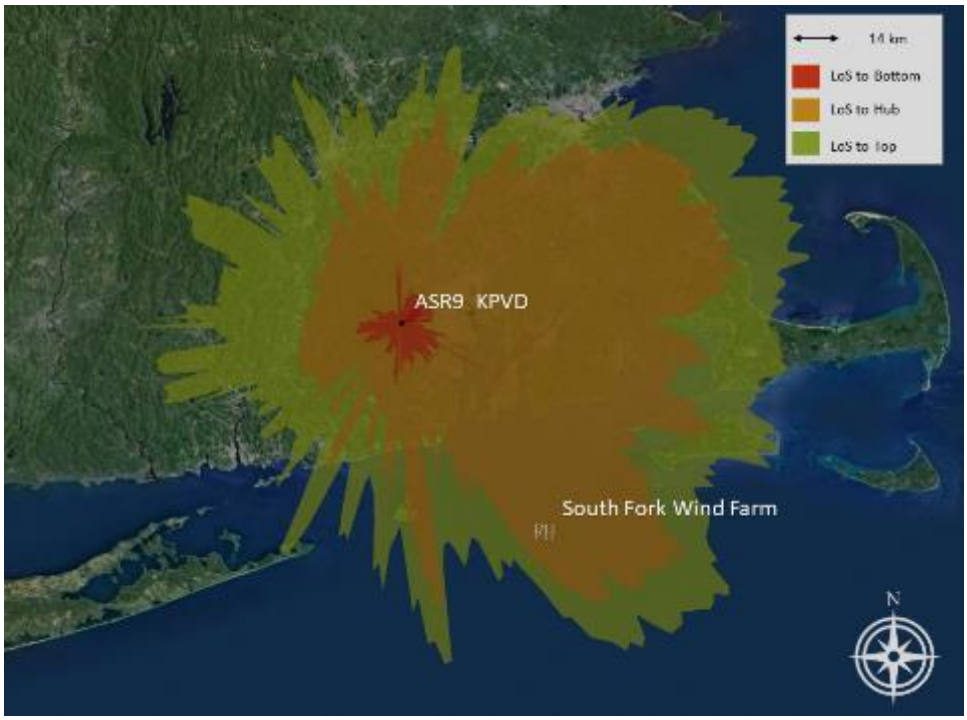

Figure 206 - South Fork, ASR-9, KPVD

SeaSonde

Figure 207 - South Fork, SeaSonde, AMAG

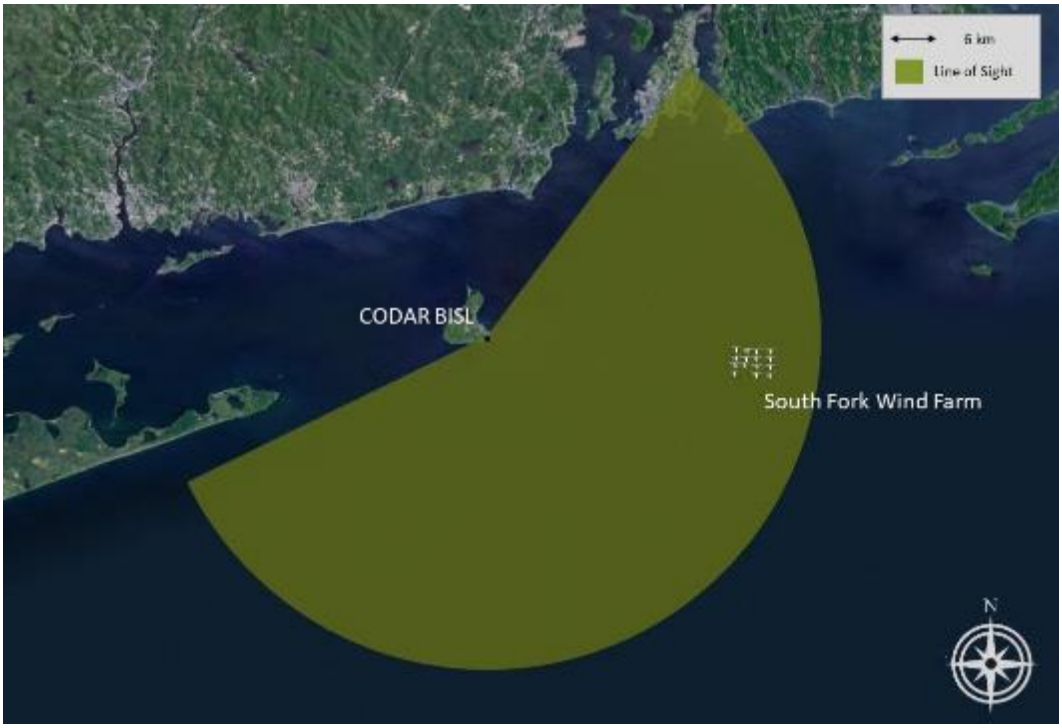

Figure 208 - South Fork, SeaSonde, BISL

Figure 209 - South Fork, SeaSonde, CPVN

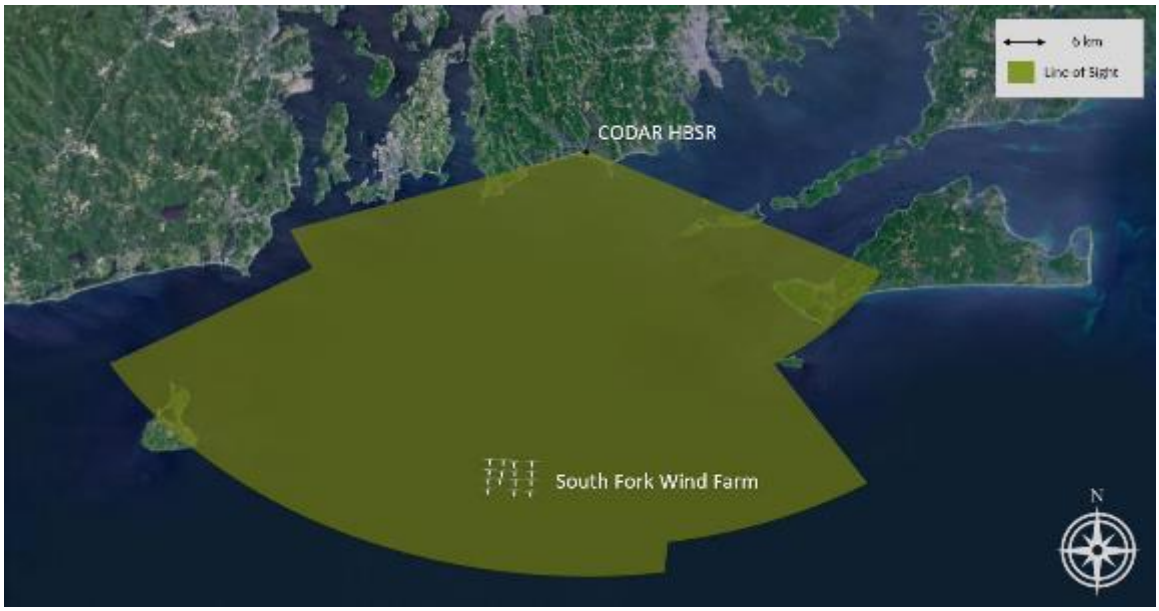

Figure 210 - South Fork, SeaSonde, HBSR

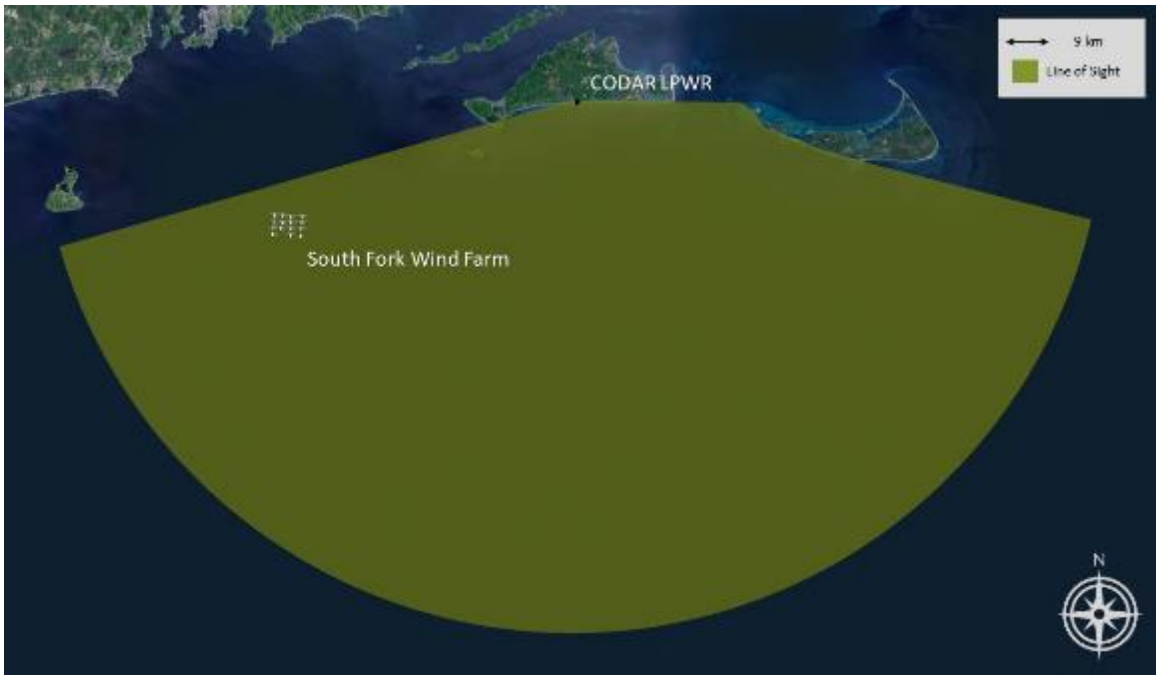

Figure 211 - South Fork, SeaSonde, LPWR

Figure 212 - South Fork, SeaSonde, MVCO

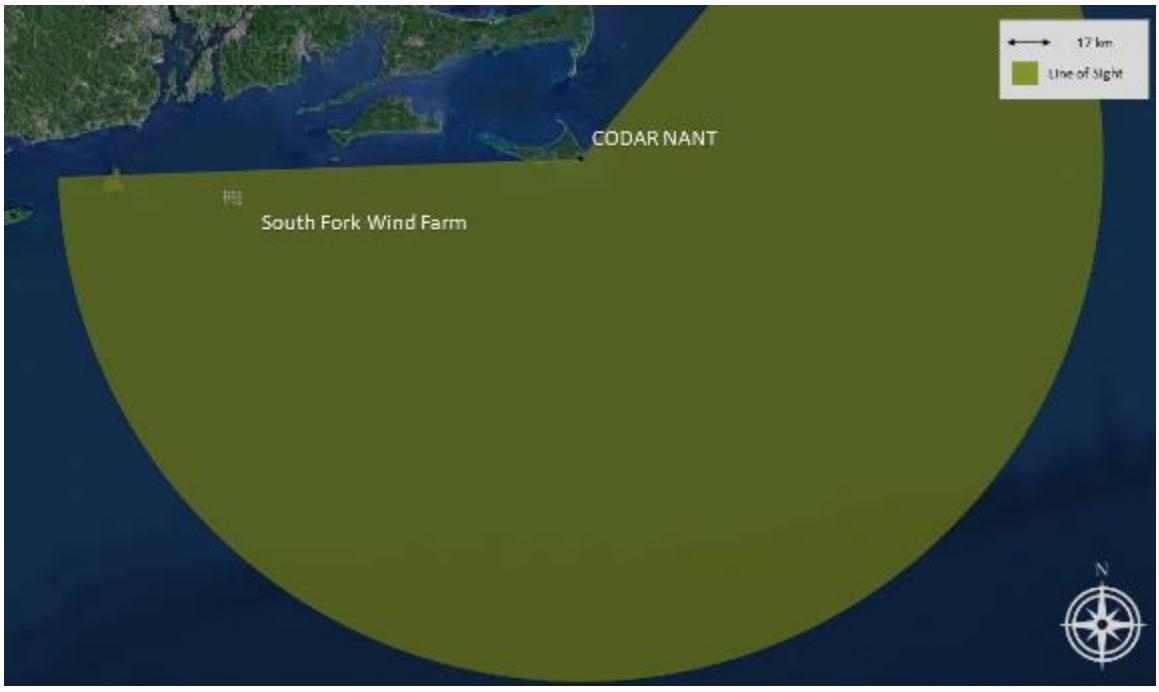

Figure 213 - South Fork, SeaSonde, NANT

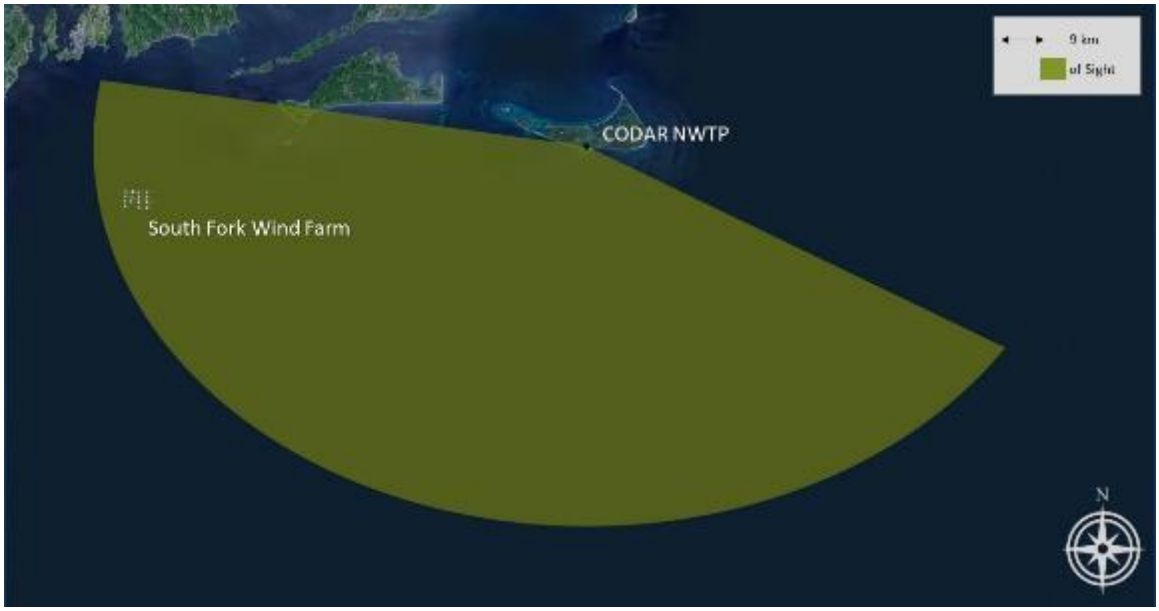

Figure 214 - South Fork, SeaSonde, NWTP

A.4 MAYFLOWER

ASR

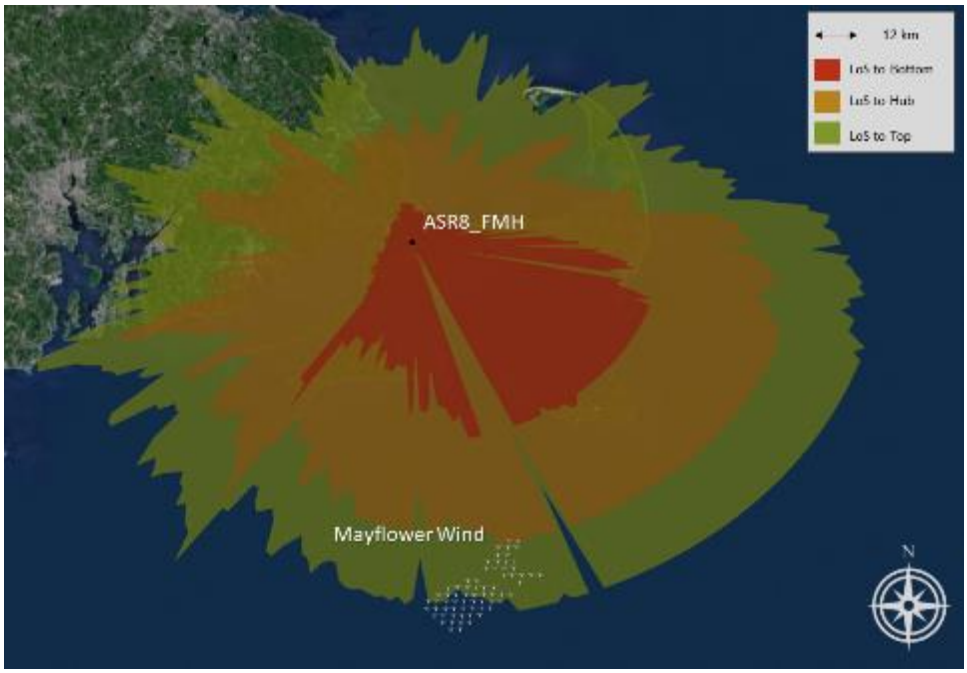

Figure 215 – Mayflower Wind, ASR-8, FMH

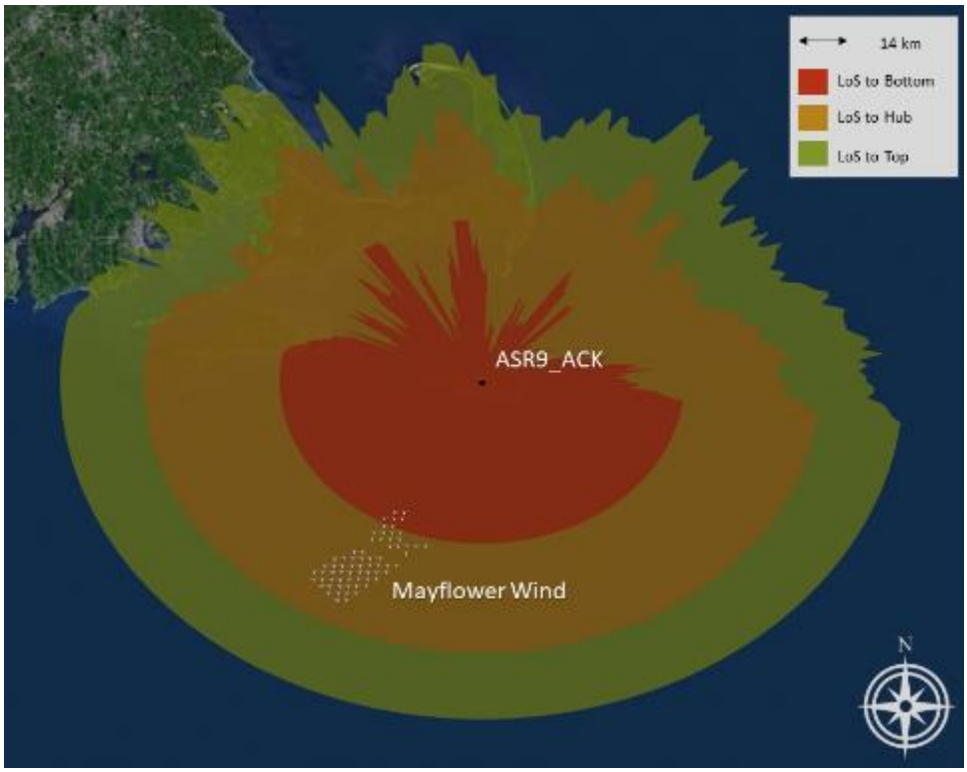

Figure 216 - Mayflower Wind, ASR-9, ACK

SeaSonde

Figure 217 - Mayflower Wind, SeaSonde, AMAG

Figure 218 - Mayflower Wind, SeaSonde, LPWR

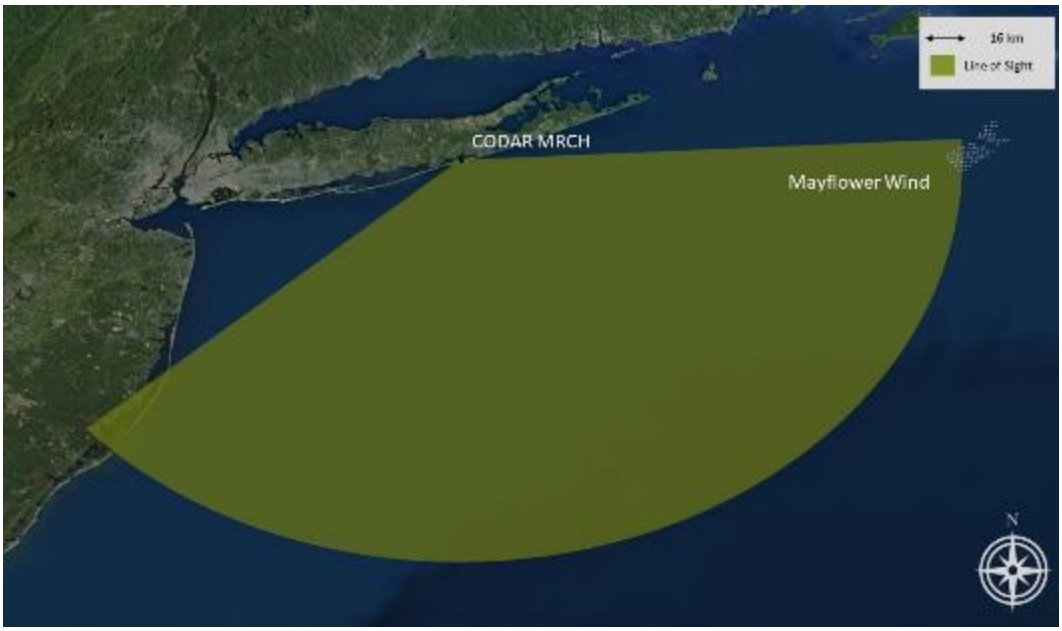

Figure 219 - Mayflower Wind, SeaSonde, MRCH

Figure 220 - Mayflower Wind, SeaSonde, MVCO

Figure 221 - Mayflower Wind, SeaSonde, NANT

Figure 222 - Mayflower Wind, SeaSonde, NWTP

A.5 RI/MA CUMULATIVE SCENARIO

ASR

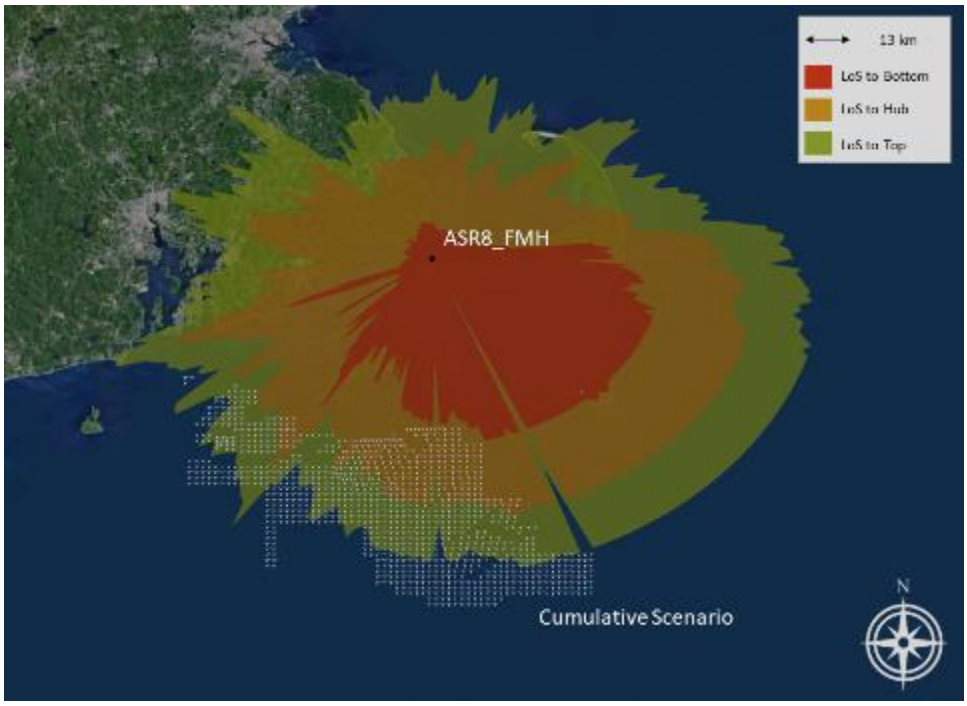

Figure 223 - RI/MA Cumulative Scenario, ASR-8, FMH

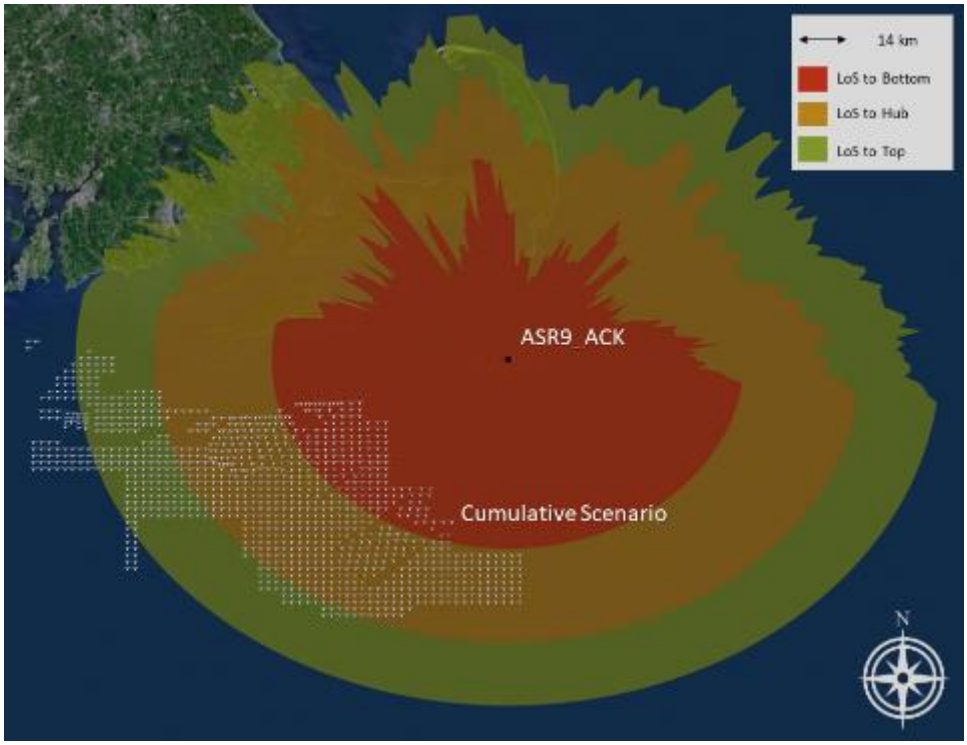

Figure 224 - RI/MA Cumulative Scenario, ASR-9, ACK

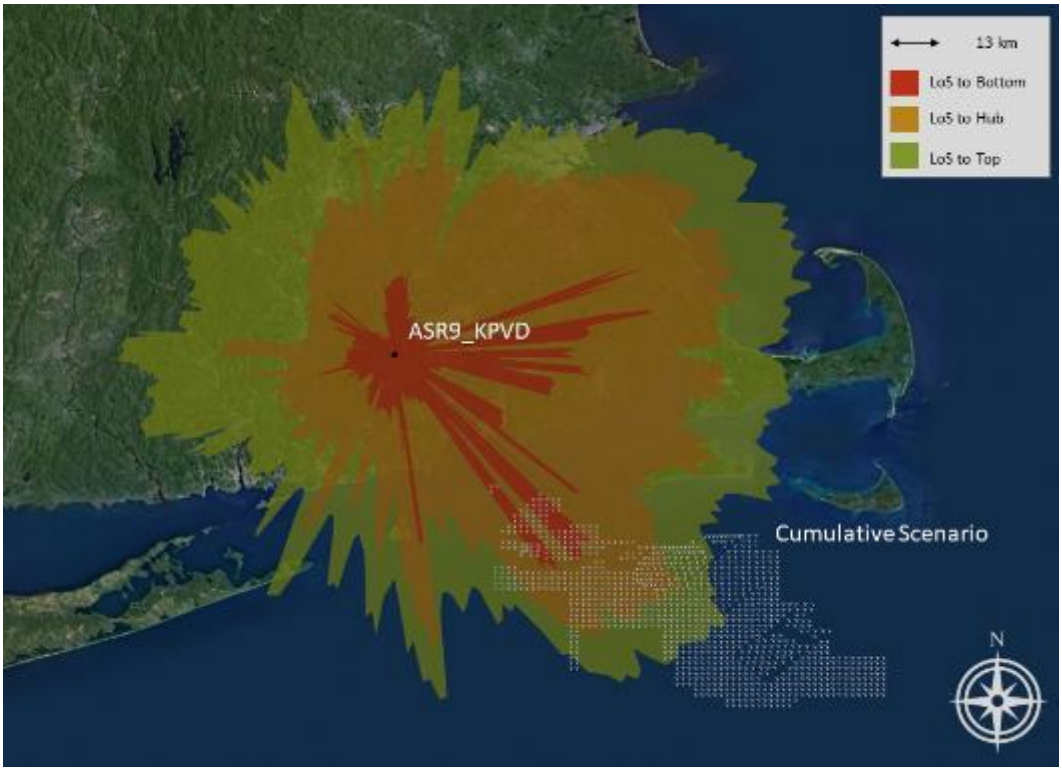

Figure 225 - RI/MA Cumulative Scenario, ASR-9, KPVD

SeaSonde

Figure 226 - RI/MA Cumulative Scenario, SeaSonde, AMAG

Figure 227 - RI/MA Cumulative Scenario, SeaSonde, BISL

Figure 228 - RI/MA Cumulative Scenario, SeaSonde, CPVN

Figure 229 - RI/MA Cumulative Scenario, SeaSonde, HBSR

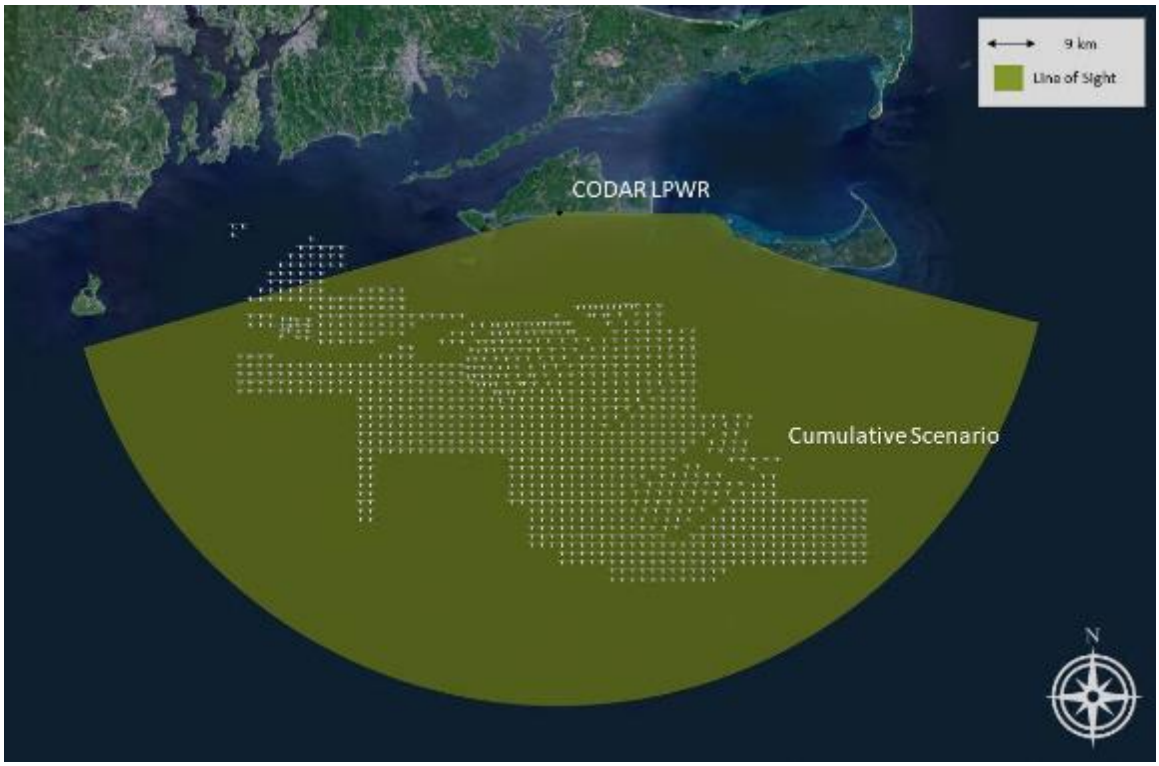

Figure 230 - RI/MA Cumulative Scenario, SeaSonde, LPWR

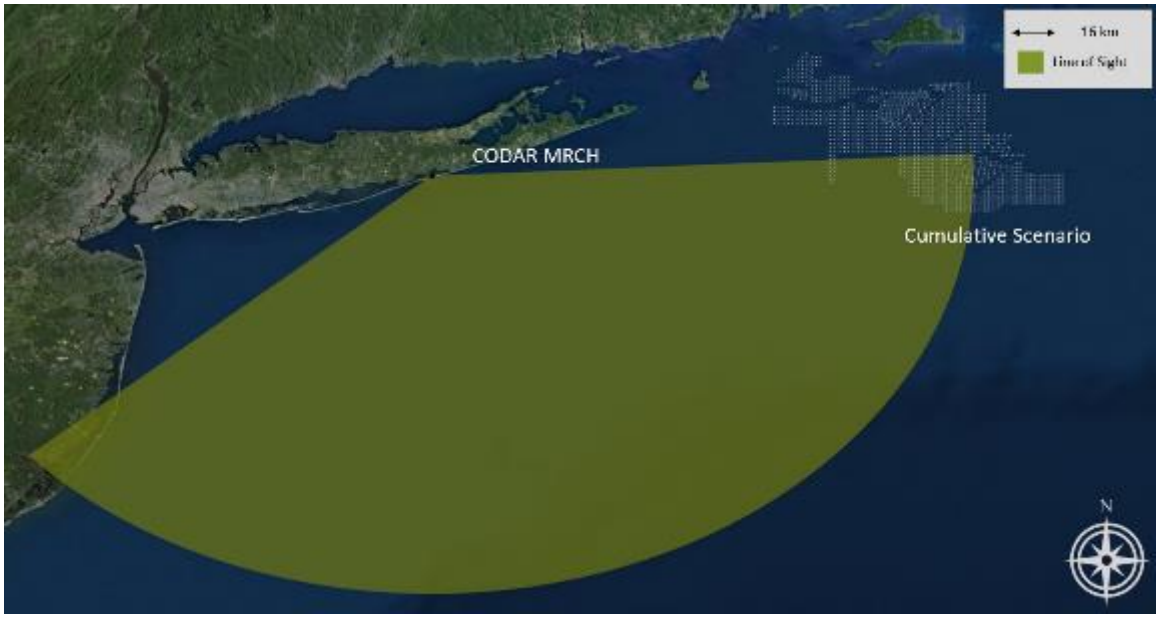

Figure 231 - RI/MA Cumulative Scenario, SeaSonde, MRCH

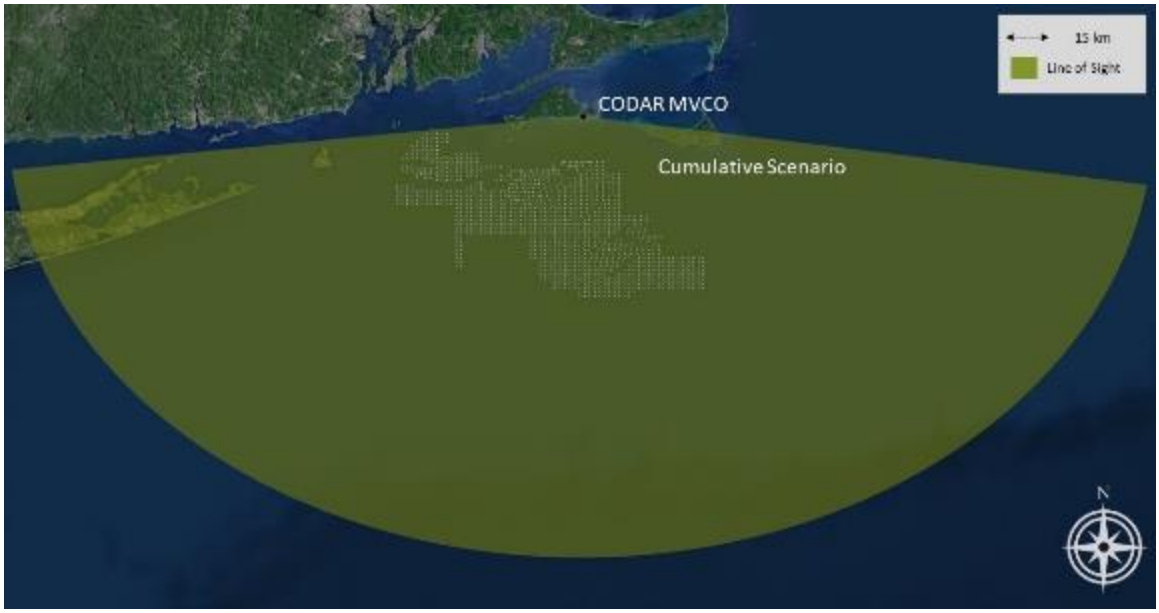

Figure 232 - RI/MA Cumulative Scenario, SeaSonde, MVCO

Figure 233 - RI/MA Cumulative Scenario, SeaSonde, NANT

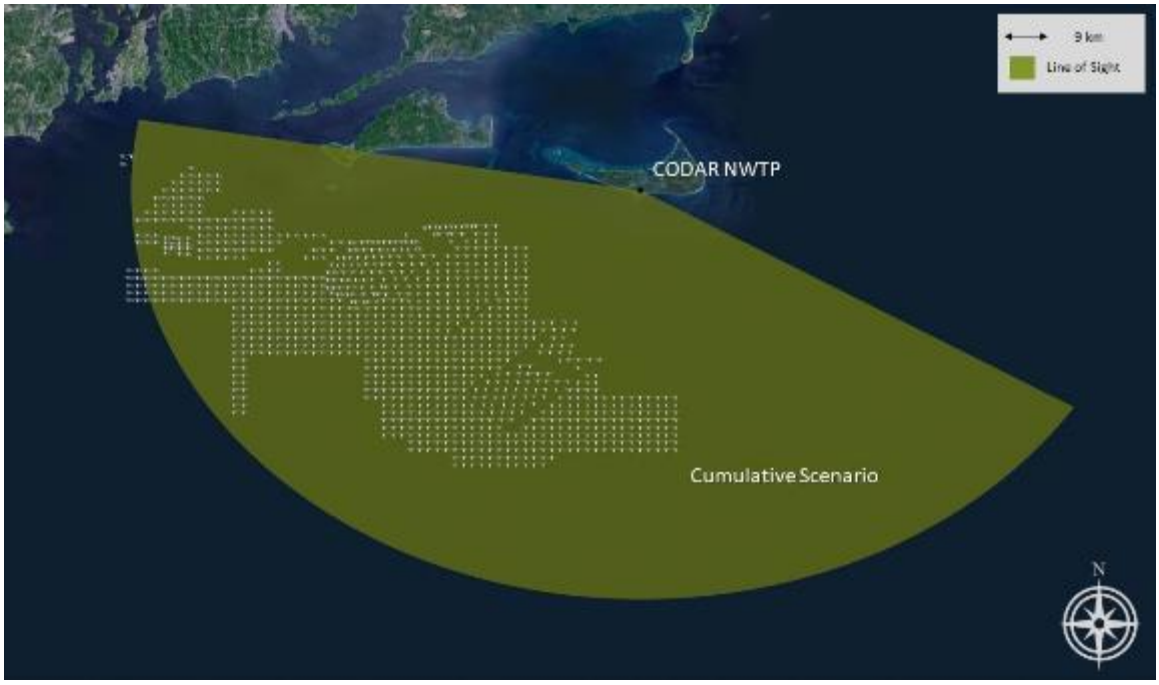

Figure 234 - RI/MA Cumulative Scenario, SeaSonde, NWTP

Figure 235 - RI/MA Cumulative Scenario, SeaSonde, SQUB

A.6 EMPIRE WIND

ARSR

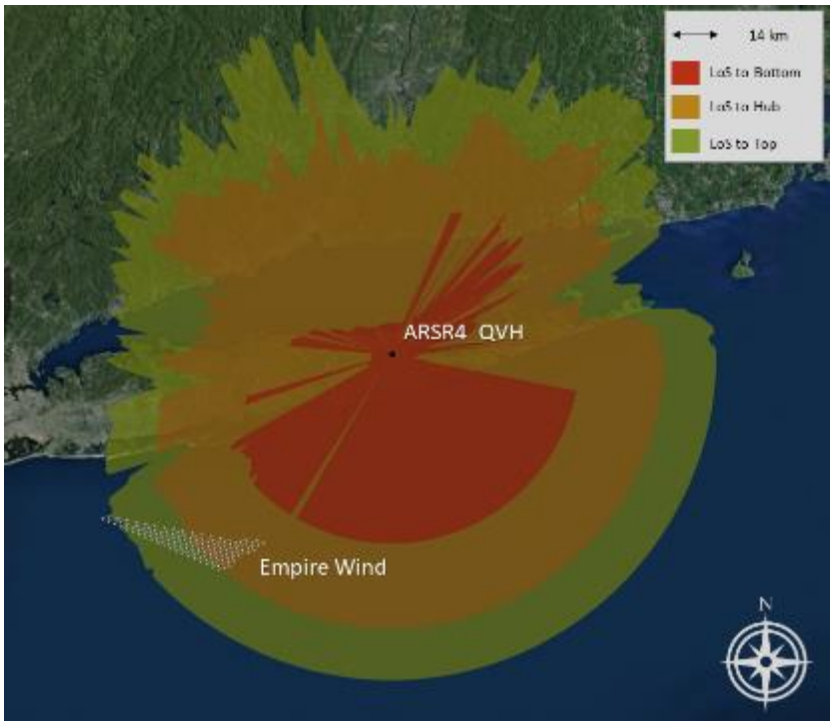

Figure 236 - Empire Wind, ARSR-4, QVH

ASR

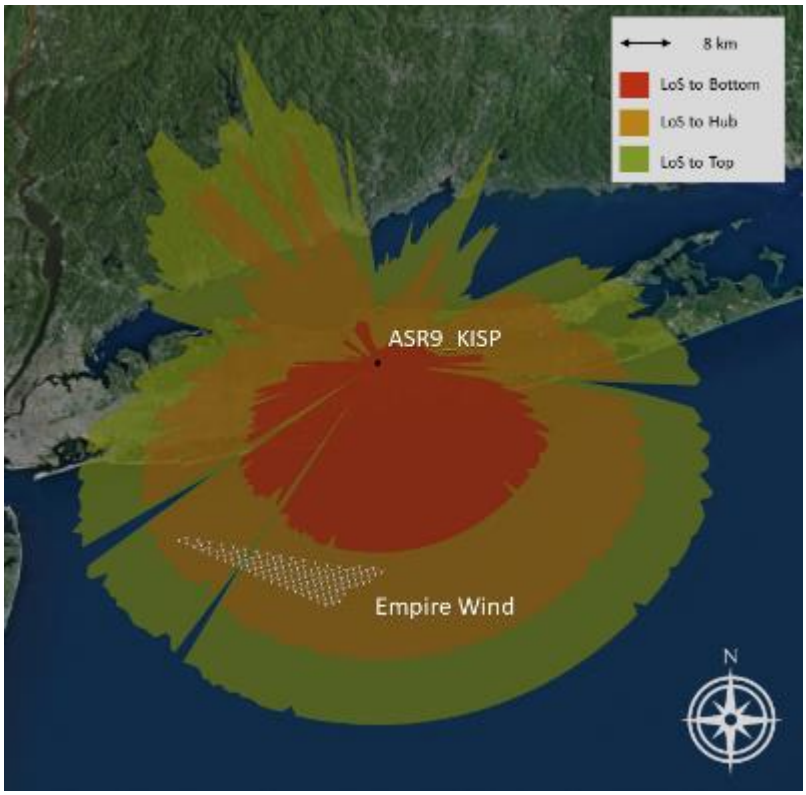

Figure 237 - Empire Wind, ASR-9, KISP

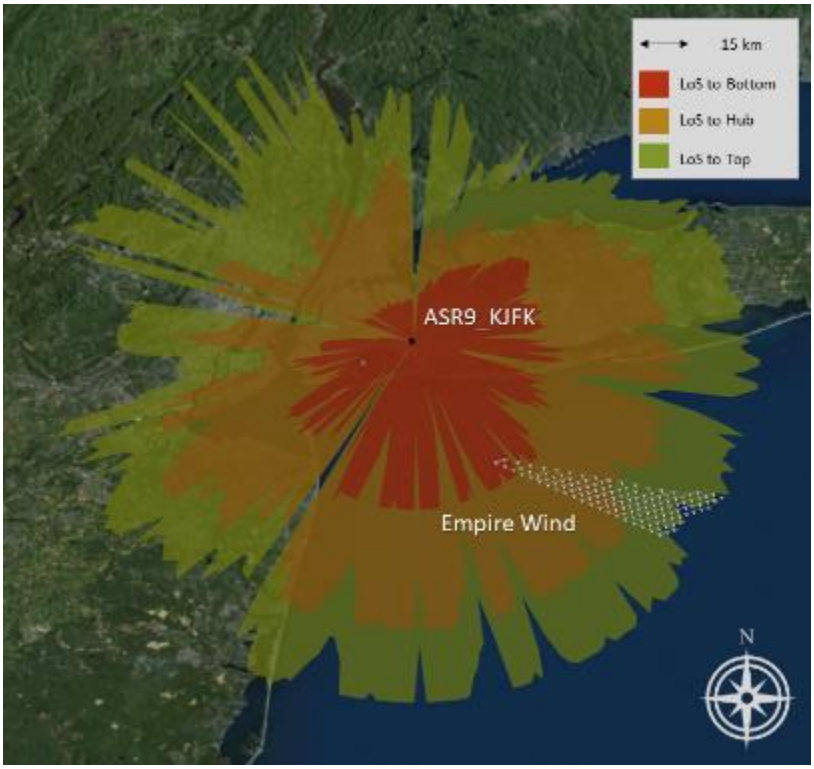

Figure 238 - Empire Wind, ASR-9, KJFK

SeaSonde

Figure 239 - Empire Wind, SeaSonde, AMAG

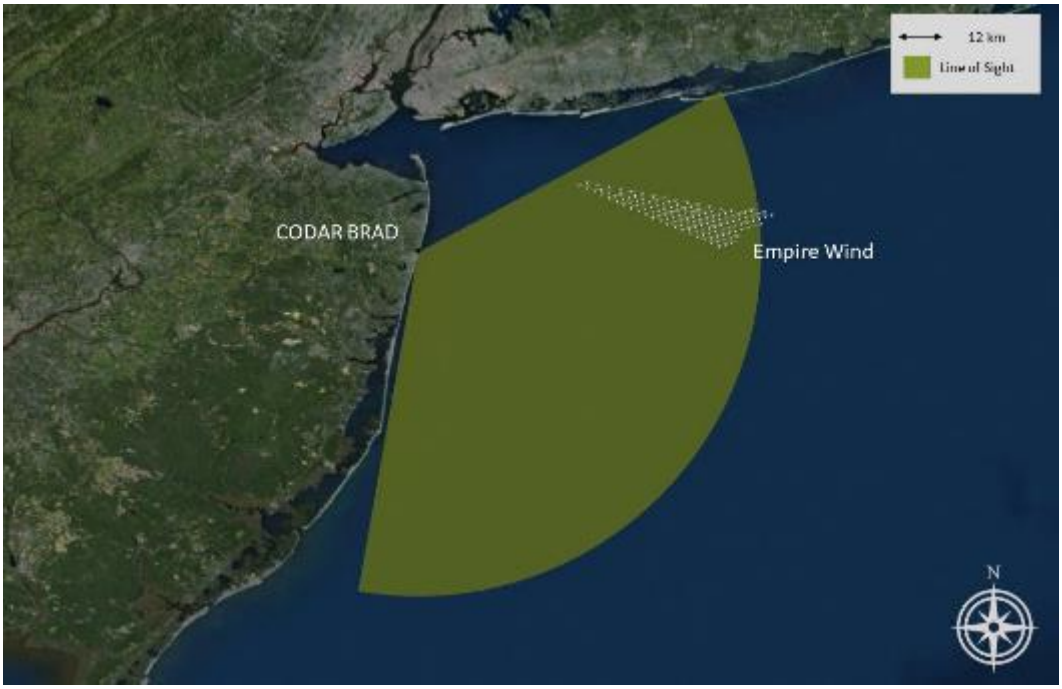

Figure 240 - Empire Wind, SeaSonde, BRAD

Figure 241 - Empire Wind, SeaSonde, HEMP

Figure 242 - Empire Wind, SeaSonde, HOOK

Figure 243 - Empire Wind, SeaSonde, LOVE

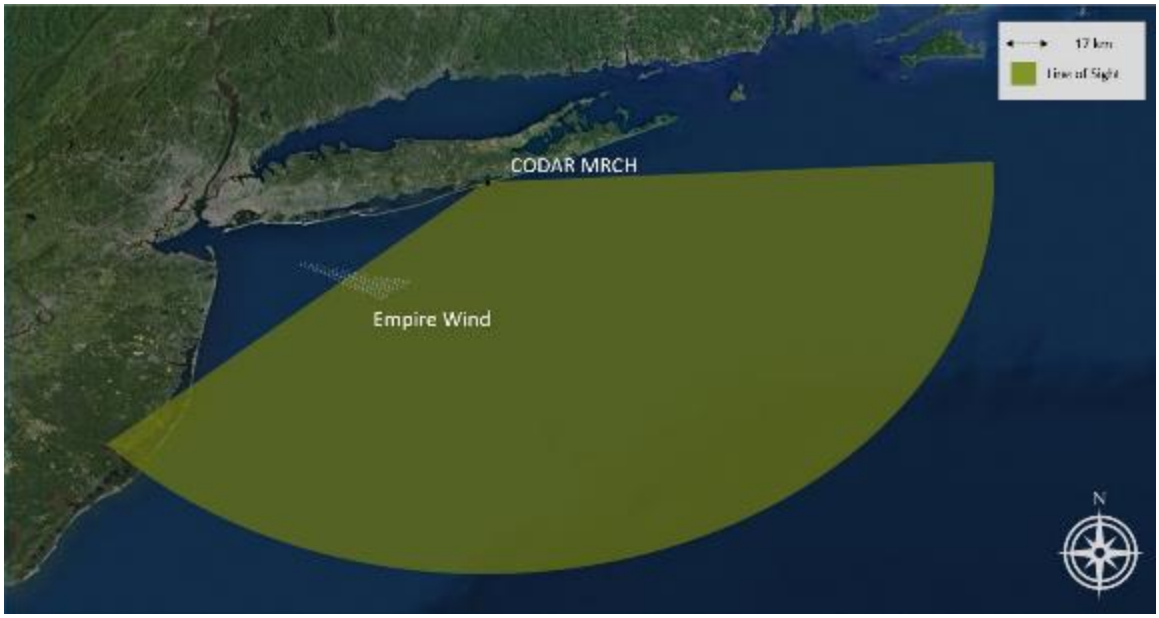

Figure 244 - Empire Wind, SeaSonde, MRCH

Figure 245 - Empire Wind, SeaSonde, SEAB

Figure 246 - Empire Wind, SeaSonde, SPRK

NEXRAD

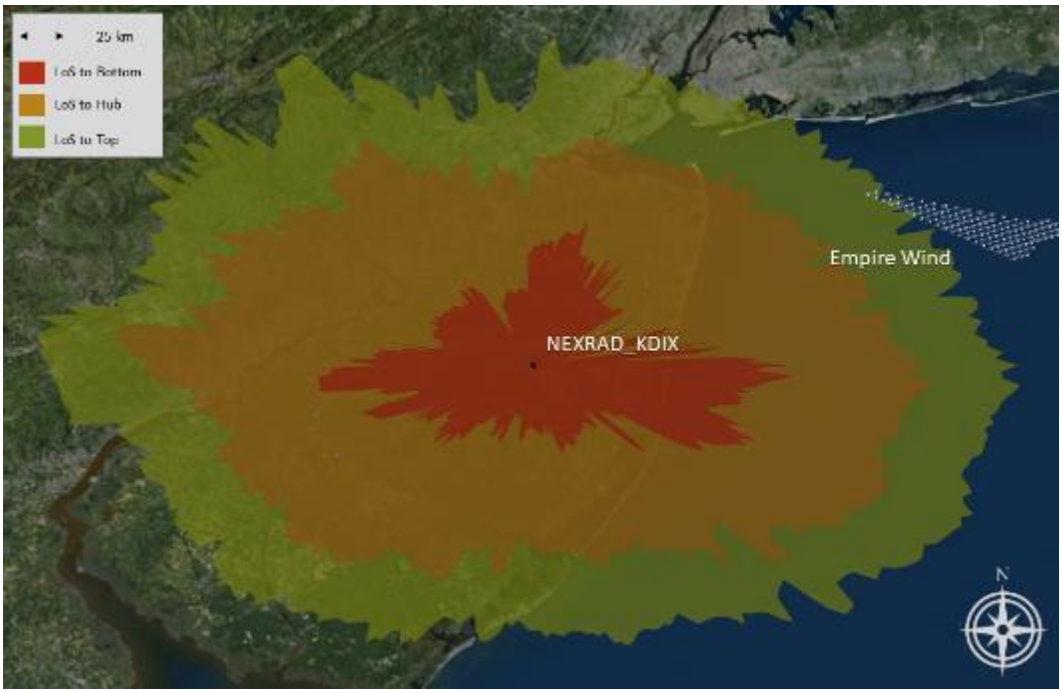

Figure 247 - Empire Wind, NEXRAD, KDIX

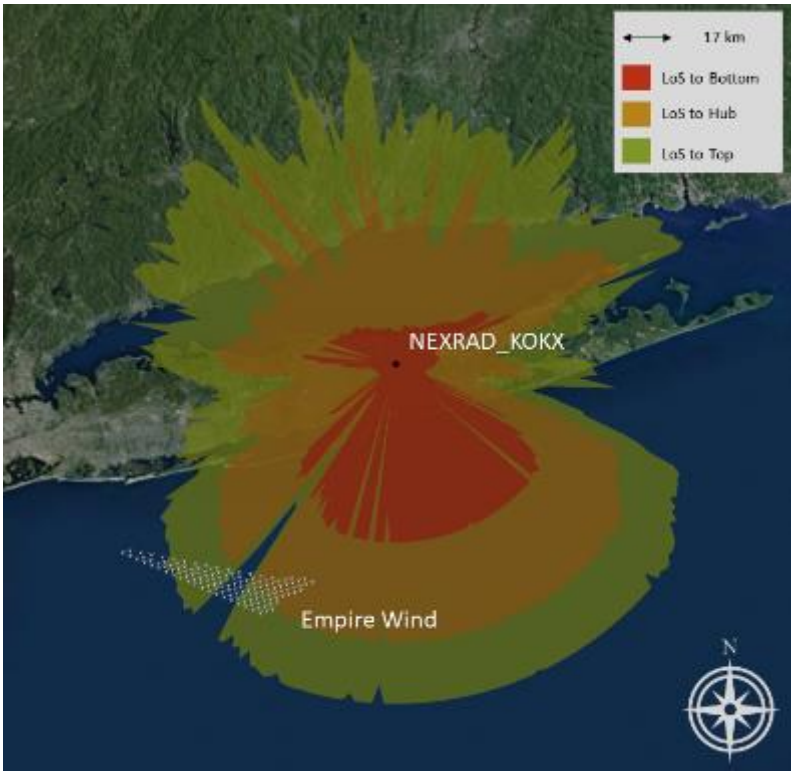

Figure 248 - Empire Wind, NEXRAD, KOKX

Terminal Doppler Weather Radar

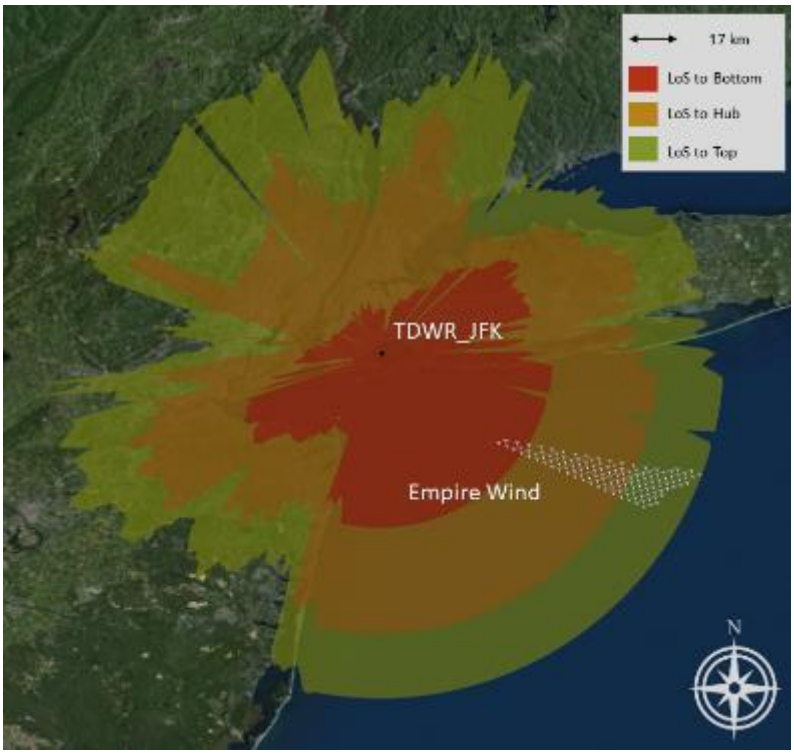

Figure 249 - Empire Wind, TDWR, JFK

A.7 OCEAN WIND

ARSR

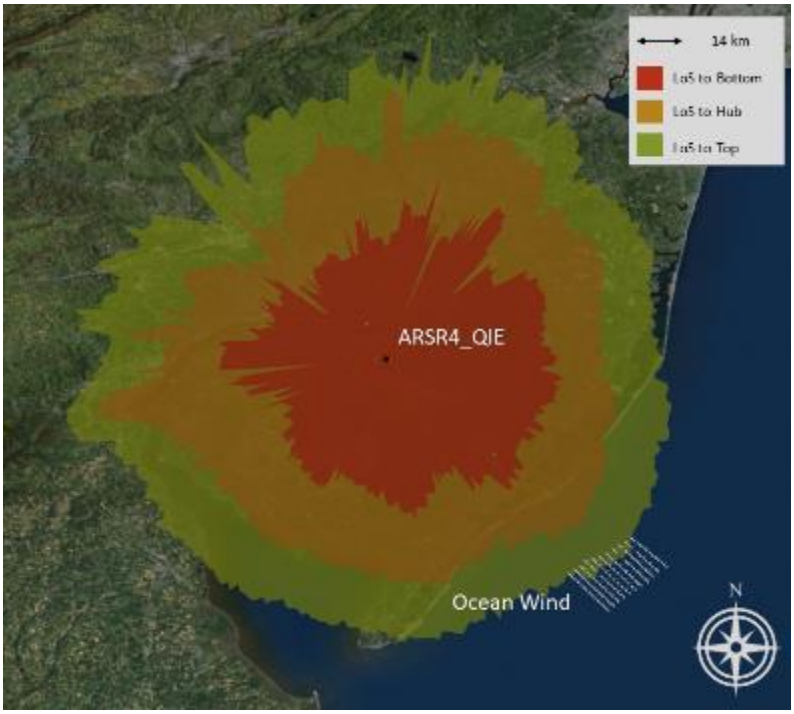

Figure 250 - Ocean Wind, ARSR-4, QIE

ASR

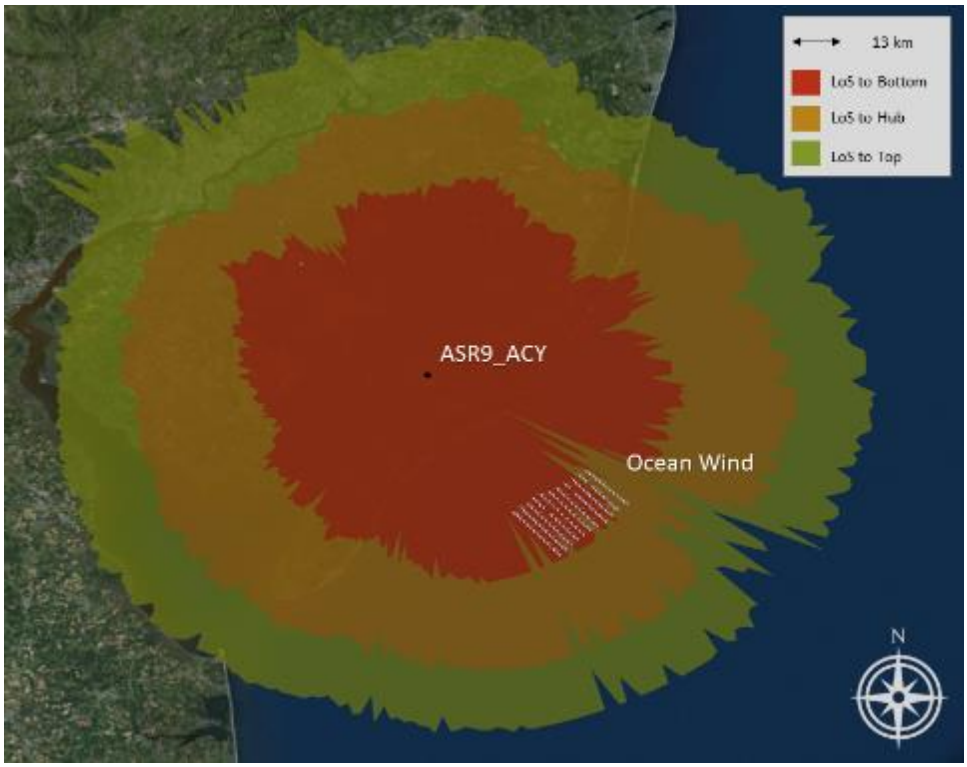

Figure 251 - Ocean Wind, ASR-9, ACY

SeaSonde

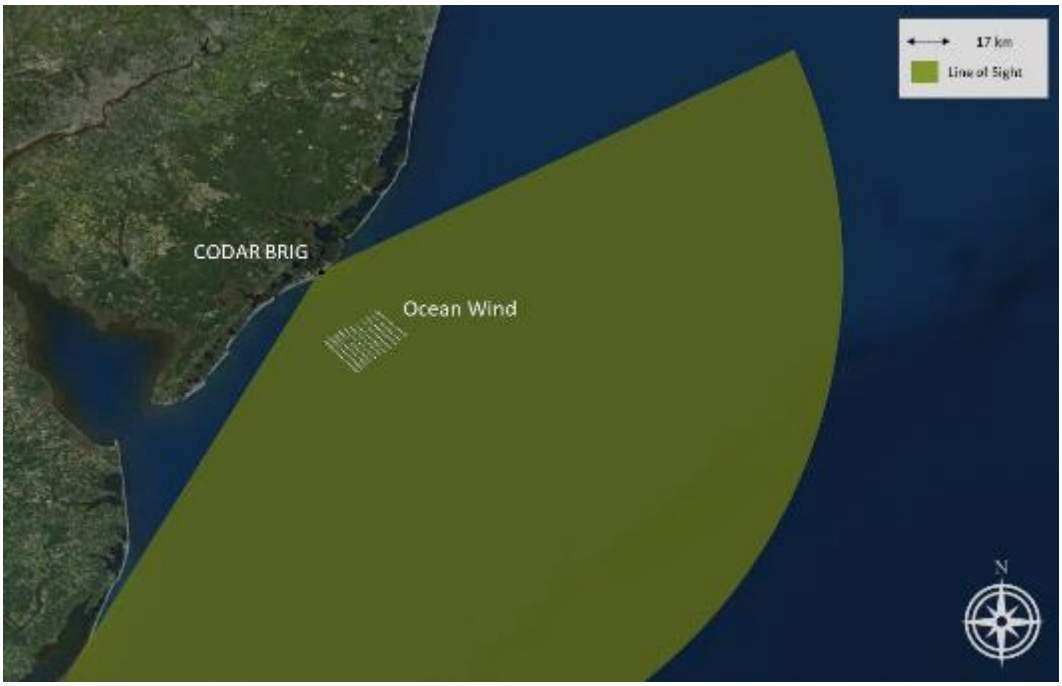

Figure 252 - Ocean Wind, SeaSonde, BRIG

Figure 253 - Ocean Wind, SeaSonde, BRNT

Figure 254 - Ocean Wind, SeaSonde, HEMP

Figure 255 - Ocean Wind, SeaSonde, LOVE

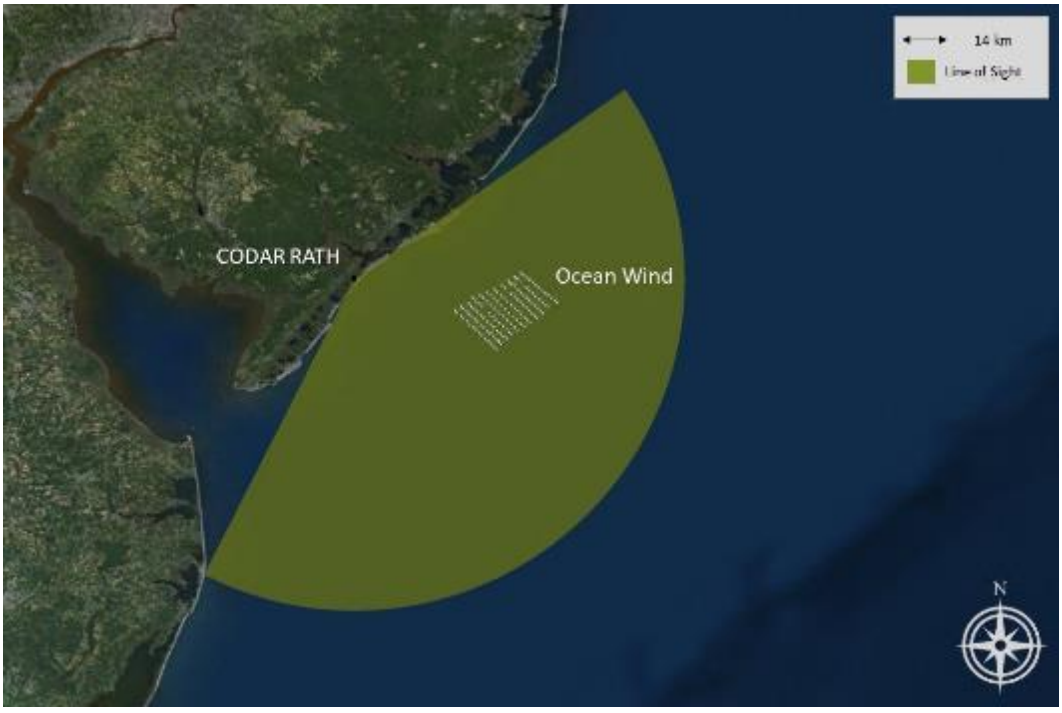

Figure 256 - Ocean Wind, SeaSonde, RATH

Figure 257 - Ocean Wind, SeaSonde, SPRK

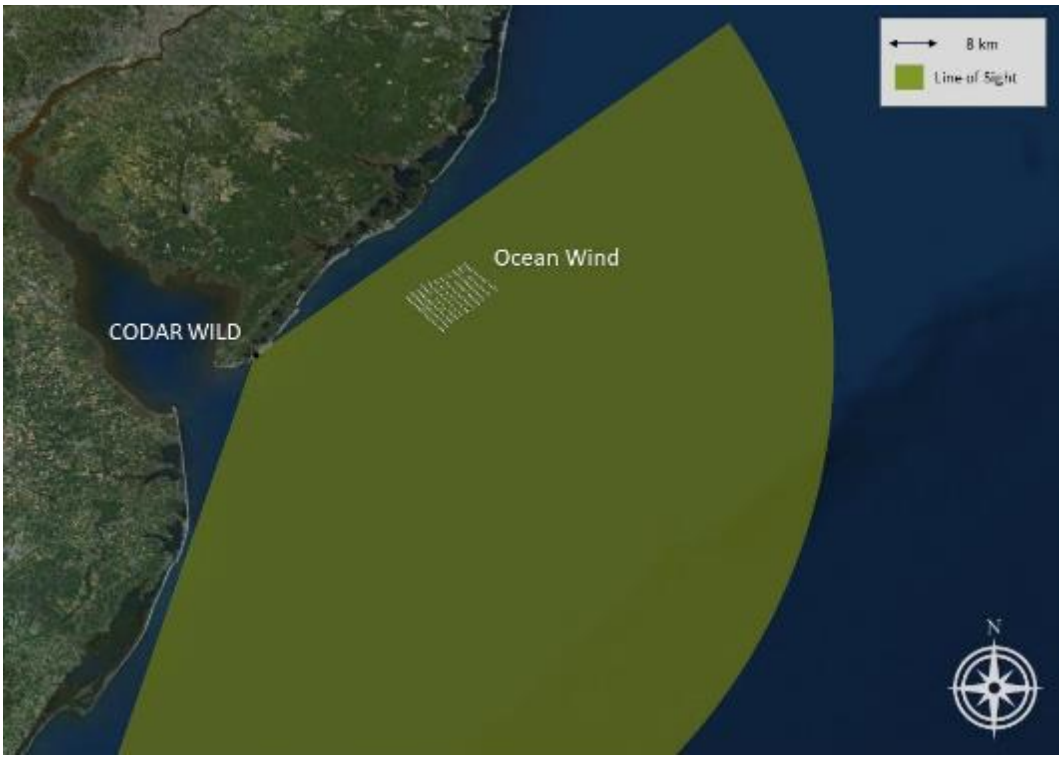

Figure 258 - Ocean Wind, SeaSonde, WILD

Figure 259 - Ocean Wind, SeaSonde, WOOD

A.8 SKIPJACK

ASR

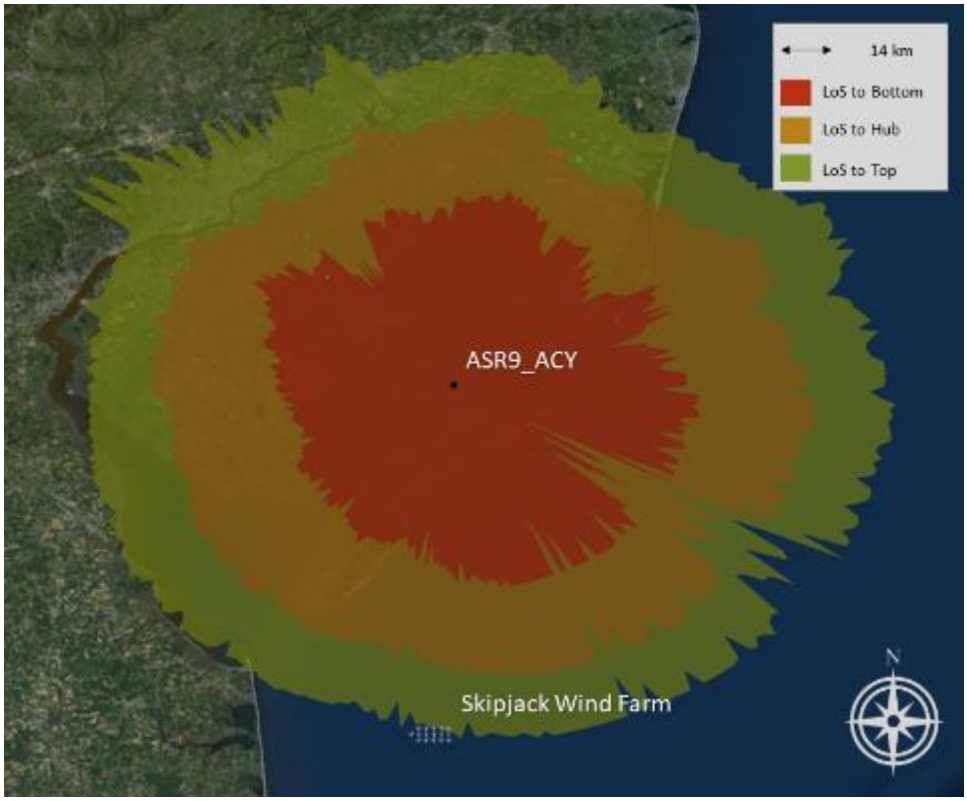

Figure 260 - Skipjack, ASR-9, ACY

SeaSonde

Figure 261 - Skipjack, SeaSonde, BRIG

Figure 262 - Skipjack, SeaSonde, CMPT

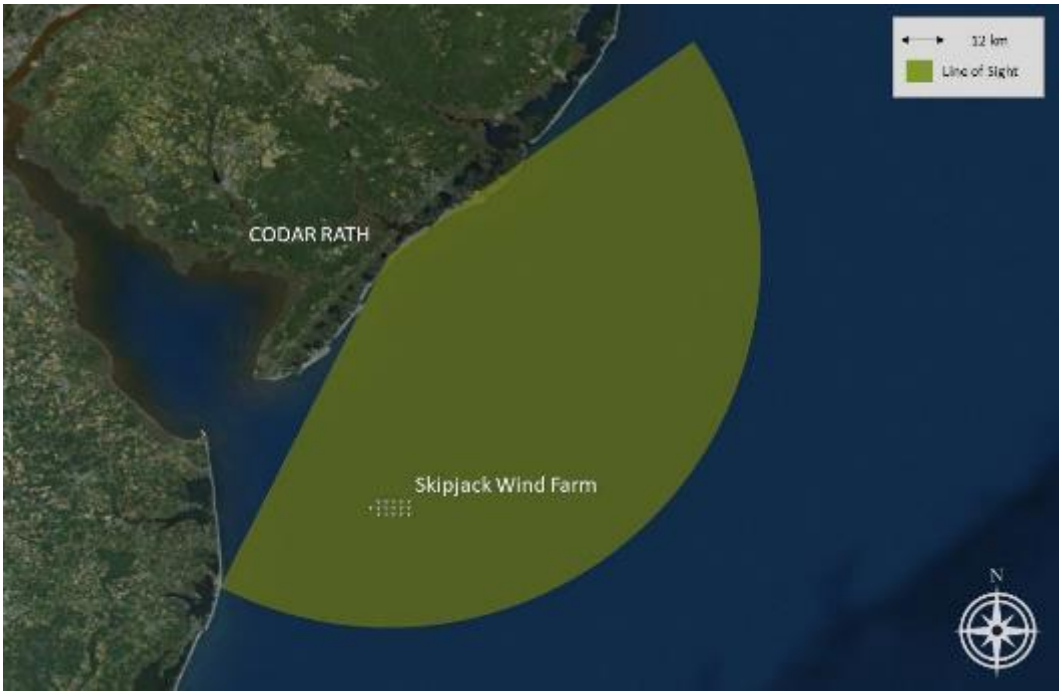

Figure 263 - Skipjack, SeaSonde, RATH

Figure 264 - Skipjack, SeaSonde, WILD

Figure 265 - Skipjack, SeaSonde, WOOD

NEXRAD

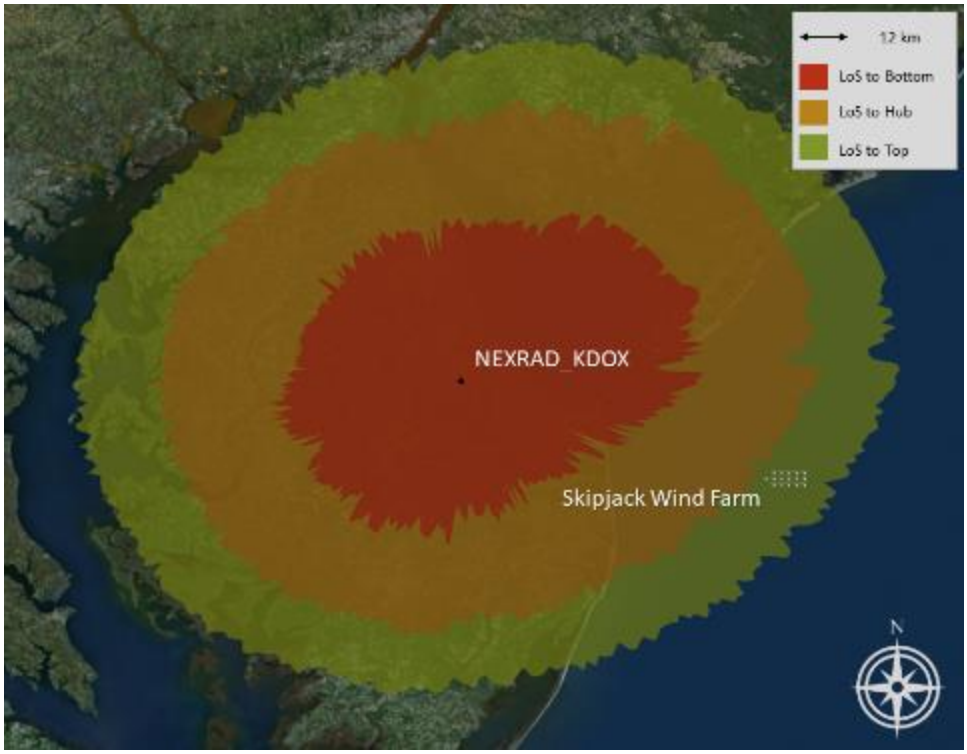

Figure 266 - Skipjack, NEXRAD, KDOX

A.9 GRAND STRAND

SeaSonde

Figure 267 - Grand Strand, SeaSonde, CSW

Figure 268 - Grand Strand, SeaSonde, GTN

Department of the Interior (DOI)

The Department of the Interior protects and manages the Nation's natural resources and cultural heritage; provides scientific and other information about those resources; and honors the Nation’s trust responsibilities or special commitments to American Indians, Alaska Natives, and affiliated island communities.

Bureau of Ocean Energy Management (BOEM)

The mission of the Bureau of Ocean Energy Management is to manage development of U.S. Outer Continental Shelf energy and mineral resources in an environmentally and economically responsible way.

BOEM Environmental Studies Program

The mission of the Environmental Studies Program is to provide the information needed to predict, assess, and manage impacts from offshore energy and marine mineral exploration, development, and production activities on human, marine, and coastal environments. The proposal, selection, research, review, collaboration, production, and dissemination of each of BOEM’s Environmental Studies follows the DOI Code of Scientific and Scholarly Conduct, in support of a culture of scientific and professional integrity, as set out in the DOI Departmental Manual (305 DM 3).